ESTUARINE HYDRAULICS IN A SHALLOW DELTAIC ESTUARY WITH REFERENCE TO THE KALI GARANG ESTUARY SEMARANG, INDONESIA

SURIPIN

ESTUARINE HYDRAULICS
IN A SHALLOW DELTAIC ESTUARY
WITH REFERENCE TO THE KALI GARANG ESTUARY
SEMARANG, INDONESIA

BY

©S U R I P I N.

A Thesis Submitted to the School of Graduate Studies

in Partial Fulfilment of the Requirements for

the Degree of Master of Engineering

FACULTY OF ENGINEERING AND APPLIED SCIENCE

MEMORIAL UNIVERSITY OF NEWFOUNDLAND

AUGUST, 1992

ST.JOHN'S NEWFOUNDLAND CANADA

ISBN 0-315-78099-1

Abstract

Most of the Indonesian rivers are characterized by the formation of deltas at the mouths. The estuaries are usually shallow and the longitudinal bed slope low. The rivers debouch into an ocean with low to moderate marine energy. The river flow fluctuates seasonally in accordance with the monsoon season. During the wet season, from November to April, floods may occur due to the intense rainfall. The river flow becomes quite small during the hot, dry seasons.

Naturally, the rivers bring a lot of sediments which originate from volcano ashes and erosion of the catchment basin. Most sediments flow down to the estuaries and near-shore areas during the high river flows of the rainy season. In most cases, many hydraulics structures have been built along the river systems. They are intended for sediment control, flow regulation and flood control.

The fluctuation of river flow is considered to be a major factor in determining estuarine circulation patterns and delta formation. Typically, the circulation pattern shifts from that of a highly stratified estuary during the high river flow of the rainy season to that of a well-mixed estuary during the low river flow of the dry season. Furthermore, the quantity and variation of discharge in association with wave effects results in various delta geometries ranging from river-dominated to wave-

dominated deltas. River-dominated deltas are characterized by highly irregular and protruding shorelines and by sediment bars deposited parallel to the direction of river flow. Wave-dominated deltas are characterized by straight shorelines with sediment barriers deposited parallel to the shorelines.

To understand the contribution of river flow and marine forces to the behaviour of estuaries and the geometry of deltas in Indonesia, the Kali Garang Estuary has been chosen as a subject of study. The Estuary consists of two branches: Kali Semarang, and the West Channel. Tidal excursion, salinity distribution and circulation patterns are used to represent the estuarine behaviour. The Discharge Effectiveness Index is used to evaluate the relative contribution of river flow versus marine forces to the development of deltas. Field observations of water level, salinity, temperature, currents, and sediments were made during the dry season of 1991. Existing data sets related to the study were also collated.

The study shows that the Kali Garang Estuary experiences a small-diurnal tide-range ($\approx$ 65 cm). In the manmade West Channel the tide propagates up the estuary as far as the weir. The tidal range decreases landward and the fresh water discharge flows seaward over the saline water that intrudes landward below it. In the Kali Semarang, the tide propagates as far as its mid length. Fresh water mixes directly with seawater, and a weak vertical stratification is experienced. The saline water moves up and down the estuary due to the flood and ebb tides.

The coast where the estuary discharges to the sea is subject to a very moderate wave climate. Maximum wave power occurs in phase with maximum river

discharge and this results in the formation of a wave-dominated delta. The high river sediment during the rainy season is spread out by waves generated by the west monsoon. This material is then redistributed along the shoreline by waves generated by the east monsoon during the low freshwater flow of the dry season.

Acknowledgements

I wish to express my gratitude to Dr. J.H. Allen and Dr. J.J. Sharp, my Supervisors, by whom the supervision of this thesis was carried out. Without their guidance, advice and encouragement this study would not have been accomplished.

I am greatly indebted to Dr. C.A. Sharpe, the Associate Dean of the School of Graduate Studies and to Dr. J.J. Sharp, the Associate Dean of Faculty of Engineering and Applied Science for the opportunity to study at Memorial University of Newfoundland.

My appreciation is due to Dr. Leonard M. Lye for his invaluable help and suggestion. I would also like to say special thank you to my parents for their blessing and love, and also to my wife and my daughter for their love, patience and encouragement.

Appreciation is also due to the staff of Memorial University of Newfoundland, Huntsman Marine Science Centre, Diponegoro University, colleagues and friends for their help and information.

SURIPIN
August, 1992

Contents

List of Figures

List of Tables

List of Symbols

Symbol	Description	Dimensions
A	Basin area	L^2
A	Cross section area	L^2
A	Dimensional longshore transport constant	L^2T/M
A_o	Advancing wedge constant	-
A_s	Surface Area	L^2
a	Tidal amplitude	L
B	Channel breadth	L
C	Chezy coefficient	$L^{1/2}/T$
C	Concentration of sediment	M/L^3
C	Wave celerity	L/T
C_g	Wave group celerity	L/T
C_B	Dimensional bedload coefficient	L^3/MT
C_S	Storage coefficient	-
D	Depth	L
d	Diameter of particle	L
d_{50}	Median diameter	L
E	Wave Energy	M/T^2
e	Porosity	-
F	Ratio of the sum of the amplitudes of the two main diurnal constituents (K_1 and O_1) to the sum of the amplitudes of the two main semi diurnal constituents (M_2 and S_2)	-
F	Functional constant	$L^{½}T^{½}$
F	Functional relation	-
F_r'	Densimetric Froude number	-
f	Frequency	-
g	Acceleration due to gravity	L/T^2
H	Water depth	L
H	Wave height	L
H_b	Wave height at breaker position	L
H_f	Wave height after undergoing frictional attenuation	L
H_g	Significant wave height obtained from gage record	L
H_o	Wave height at deep water	L
H_{rms}	Root mean square of wave height	L
H_s	Significant wave height	L

H'	Wave height after refraction	L
h_s	Water depth from bottom to interface layer	L
h'	Water depth from surface to interface layer	L
I	Rainfall intensity	L/T
I_e	Gradient energy	-
I_Q	Discharge effectiveness Index	LT^2
i	Subscript index number	-
j	Subscript index number	-
K	Flow ratio; the ratio of the volume of fresh water per tidal cycle to the volume of salt water in the flood tide	-
K_R	Refraction coefficient for waves	-
K_s	Shoaling coefficient for waves	-
$K_{s(b)}$	Shoaling coefficient for waves evaluated at the breaker position	-
$K_{s(g)}$	Shoaling coefficient for waves evaluated at the wave gage	-
K_x	Longitudinal dispersion coefficient	L^2/T
k	Wave number	-
L	Wave length	L
L_o	Length of advancing wedge	L
l	Length	L
M	Mean diameter	L
M_d	Median diameter	L
M_ϕ	Mean Phi diameter	-
m	Constant	
N	Number of station	-
n	Manning coefficient	-
P	Wave power	ML/T^3
P_l	Longshore component of wave power	ML/T^3
Q	Discharge	L^3/T
Q	Longshore transport sediment	L^3/T
Q_f	Fresh water discharge	L^3/T
Q_g	Gross longshore transport	L^3
Q_l	Longshore transport moves to the left side	L^3
Q_n	Net longshore transport	L^3
Q_p	Peak discharge	L^3/T
Q_r	Longshore transport moves to the right side	L^3
q	Discharge per unit width	L^3/LT
q_B	Bedload rate	L^3/LT
q_S	Suspended sediment rate	L^3/LT
R	Hydraulic radius	L
R_{avg}	Average rainfall depth	L
R_e	Reynolds number	-
S	Salinity	-
S_e	Estuarine number	-

S_o	Salinity at initial point (x = 0)	-
T	Return period	T
T	Tidal period	T
T_R	Tidal range	L
t	Time	T
t_c	Time of concentration	T
U	Mean tidal current	L/T
u	Velocity in x direction	L/T
u_r	Velocity of fresh water	L/T
$u\Delta$	Densimetric velocity	L/T
u_*	Shear velocity	L/T
V_T	Tidal volume	L^3
v	Velocity in y direction	L/T
w	Velocity in z direction	L/T
x	Linear measure	L
y	Linear measure	L
z	Linear measure	L
α_o	Angle between shoreline and wave crest in deep water	-
α_b	Angle between shoreline and wave crest in breaker zone	-
α_ϕ	Skewness	-
γ	Specific weight	M/L^2T^2
δ	Increment	-
η	Height of wave profile	L
ν	Kinematic viscosity of water	L^2/T
ρ	Mass density	M/L^3
ρ_f	Mass density of fresh water	M/L^3
ρ_m	Average density of fresh and saline waters	M/L^3
ρ_s	Mass density of sediment material	M/L^3
ρ_s	Mass density of saline water	M/L^3
σ	Standard deviation	-
σ	Specific density	-
σ	Wave frequency	-
τ	Shear stress	M/LT^2
τ_o	Bed shear stress	M/LT^2
τ_c	Critical shear stress	M/LT^2
ϕ	Latitude	-
Φ_s	Sediment transport parameter	-
Φ_{16}	The 16th percentile	L
Φ_{50}	The 50th percentile	L
Φ_{84}	The 84th percentile	L

Chapter 1

Introduction

Indonesia is an archipelago composed of five major islands; Java, Sumatra, Kalimantan (Borneo), Sulawesi (Celebes), and Irian Jaya (New Guinea); and thousands of small islands (Figure 1.1). The region extends along the equator (06°50'N to 11°60'S and 92°25'E to 141°30'E). Indonesia is bounded by two continents, Asia in the North and Australia in the South, and by two oceans, Indian in the West and Pacific in the East.

Geologically, most islands were formed during the Mio-pleocene or later periods accompanying a series of volcanic activity. Therefore, the islands are characterized by eolian and sedimentary formations of Neogene Tertiary together with andesitic, and basaltic rocks of volcanic origin. The eolian and sedimentary rocks of the Mio-pliocene are mostly derived from andesitic and basaltic rocks. Weathering processes have changed the rocks to fertile, soft soil. The landmasses are covered mainly by tropical forest.

Present-day formation of the Indonesian Islands occurred over the last 15,000 years during the Flandrian transgression which ended approximately 5000 years ago. Increasing sea levels, of approximately 100 meters during the Pleistocene Ice Age,

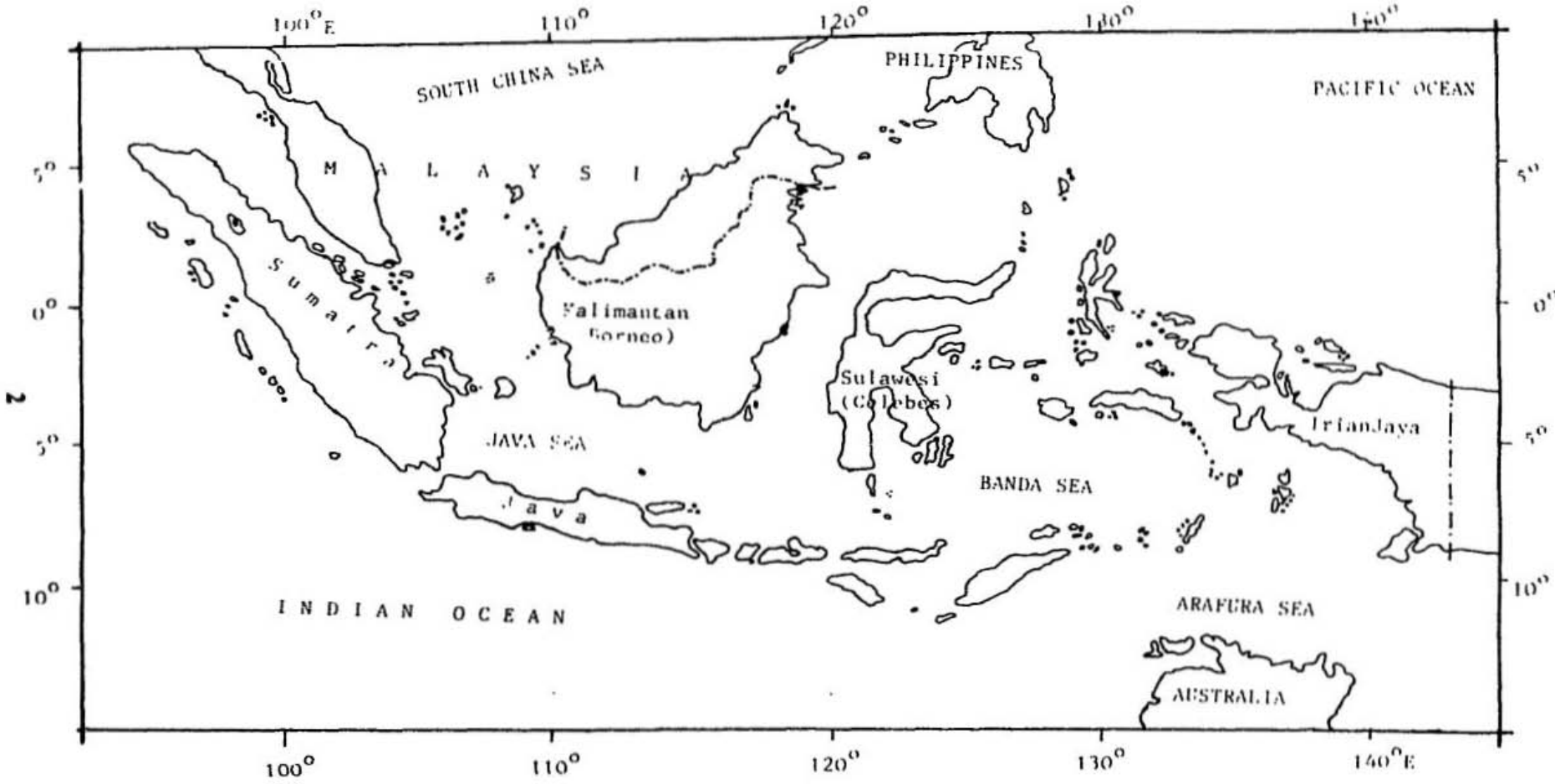

Figure 1.1 Location Map of Indonesia

inundated low lands and separated Indonesia from the Asian and Australian continents. Java, Sumatra, and Kalimantan were separated from Asia. Irian Jaya was separated from Australia, while Sulawesi remained the same as before.

During the subsequent rise in sea level, the river systems have fed a high rate of sediment continuously to the lower reaches and have built a thick sequence of deltaic sediments which developed seawards from the mouth.

As most river system in Indonesia debouch into an ocean with small to moderate marine forces, tidal action and wave effects, river-dominated deltas are usually developed. These deltas are characterized by the bifurcation of channels that form through the deposited sediment. The river flow is usually distributed between the various branches. However, in some cases where the marine forces become significant, the delta geometries are altered to either intermediate river-tide or river-wave deltas, or occasionally to a tide-dominated or wave-dominated delta.

Climatic conditions are dominated by the tropical monsoons. The east monsoon usually lasts from May to October and the west monsoon from November to April. The west monsoon brings considerable rain which causes heavy flooding all over the country.

The soil, geology, and climatic conditions mentioned above strongly influence the characteristics of the river systems. On a world scale, Indonesian river basins provide a high volume of natural sediment materials (Figure 1.2). Fresh water flows fluctuate seasonally. The flow is high during the rainy season and low during the dry season.

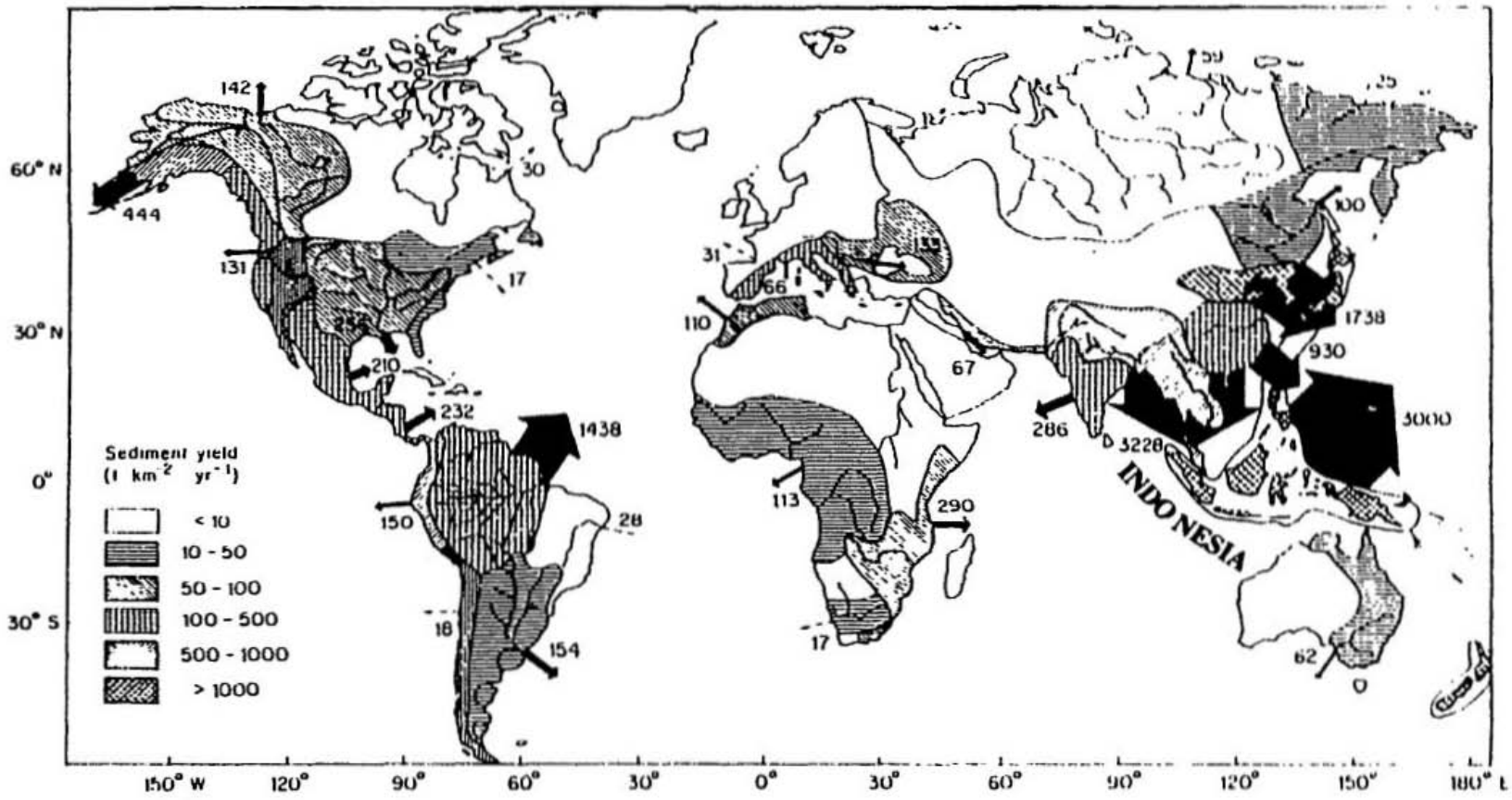

Figure 1.2 **Annual Discharge of Suspended Sediment from the Drainage Basin of the World. Number are Average Annual input in 10^6 tons (*After Milliman and Meade, 1983*)**

General problems related to the characteristics of the river systems mentioned above are flood, drought, erosion, and sedimentation. High river flows during the rainy season inundate low lying basins which usually consist of farmland and densely populated areas. In contrast, the low flow during the dry season provides insufficient water for agriculture and human use.

In response to public demand and protection, the Government of Indonesia has taken some countermeasures against those problems. These are focused on river basin and river course improvements. The first is aimed at reducing erosion, and the latter proposes to regulate river flow and increase river channel capacity in order to discharge floods.

As these measures have been introduced, some significant results have been obtained. Flood damage has been reduced while shortages of water during the dry season have been minimized. Moreover, the increasing availability of river water during the dry season has resulted in an increase of the annual rice yield.

On the other hand, modification of the natural cycle of rivers by construction of dams, training walls, bank protection and weirs has altered the natural movement of water and sediment. New areas of deposition and erosion together with areas of potential flooding are created. This is particularly true in the estuaries of many Indonesian rivers. Many of these estuaries are deltaic in nature.

This thesis will study the parameters involved in water and sediment movement using a smaller Indonesian Deltaic Estuary as a practical example. The estuary chosen is the Kali Garang Estuary which is located in Semarang, Central Java.

The estuary consists of two branches: the Kali Semarang and the manmade West Channel. This estuary provides a good illustration of the general characteristics of Indonesian estuaries, particularly those located in Java Island.

Chapter 2

Theoretical Background

2.1 Introduction

An estuary is defined as a transition zone where fresh water from land drainage mixes with and dilutes saline seawater. As such, the characteristics of any estuaries are affected by the river system characteristics and by the area of the ocean into which the estuary discharges.

The main factors, which play a crucial role in determining the characteristics of an estuary, are fresh water river discharge, tidal action, density difference between fresh and sea water, the estuary geometry, sediment transport, influence of winds and waves and, in some large estuaries, Coriolis effects.

Tidal action can displace considerable volumes of water within the estuary. In a shallow water estuary, tidal motion can be modified considerably. Range may be amplified or diminished depending on the topography. The shoreline and nature of the bottom can also strongly affect tidal currents by obstructing or constricting water flow, thereby altering the circulation pattern. Furthermore, the level of energy contained in tidal currents affects sediment transport. These currents can play a major

role in building tidal flats and deltas.

The rate of fresh water flow affects the water level and salt water penetration. Density of estuarine water is function of salinity, temperature, and sediment load. The density difference induced by intermingling of the two different waters drives water circulation and mixing processes.

Strong winds that blow along an estuary may cause an increase or decrease in water level up to several centimetres. These winds will also influence the mixing processes in the upper layers of water.

Ocean waves rework river sediments brought seawards by river discharge. The waves may then transport sediment back into the near-shore areas, moving them inshore or alongshore. Waves also provide marine sediments for the lower reaches of the estuary. These processes play a considerable role in development and formation of river deltas.

Additionally, in a wide, deep estuary, Coriolis effects play a considerable role in modifying the circulation patterns. In the Northern hemisphere, the effect of this force is to shift the seaward flowing fresh water and the landward flowing seawater layers to the right in the direction of flow. In the Southern hemisphere this force deflects these water masses to the left.

2.2 Classification of Estuaries and Their Relations to Sedimentation

Scientists have attempted to classify estuaries based on a number of

different scientific or professional viewpoints. Some of the common classifications that relate closely to sedimentation are based on, tidal range, sediment sources or water circulation patterns.

Tidal range.

Davis and Hayes (quoted in Kennish, 1986) developed a relationship between tidal range (TR) and estuarine type. They identified estuaries in terms of microtidal, mesotidal, and macrotidal systems. Microtidal estuaries have a small tidal range (TR $\leq$ 2 m). In such cases tides play a less dominant role in reworking the river sediments than do waves. These estuaries are usually characterized by sandy sediment river deltas or by wave built structures or spits aligned with the beach. Many Indonesian estuaries are in this group. Tidal action affects circulation significantly only during the dry season.

Mesotidal estuaries experience an intermediate tidal range (2 m $<$ TR $<$ 4 m). In this type, the distribution of sediment deposition is primarily influenced by tidal currents. As a result, tidal deltas and meandering tidal channels develop. Silt and clay materials collect on tidal flats and in salt marshes.

Macro tidal estuaries have a high tidal range (TR $\geq$ 4 m). Tidal currents completely dominate the distribution of sediments within the estuary and delta area. The estuaries are usually broad mouthed and funnel shaped. Sandy sediments are deposited in the central portion of the estuary and fine sediments accumulate on broad, tidal flats

or salt marshes.

Sediment sources.

The sediment sources of an estuary provide another possible method of classification. Based on it, Rusnak (quoted in Lauff, 1967, p. 180) classified estuaries into positive filled and inverse filled. In the first category, the sediments being deposited or moving through the estuary are dominated by river born sediments. Marine source sediments dominant in the second case. All Indonesian estuaries fall into the category of positive-filled basins, i.e estuaries in which river sediments are more important than marine sediments.

Water Circulation Pattern.

Classification based on the water circulation is the most widely used system. This system classifies estuaries based on the variation of river discharge and tidal range. Cameron and Pritchard (1963) described the relationship between fresh water discharge and tidal action, and classified estuaries into three classes or orders in accordance with the strength of river discharge relative to the tidal action. The classes are termed: (1) salt wedge estuary, which is highly stratified; (2) partially mixed estuary, which is moderately stratified; (3) vertically homogeneous estuary, with a lateral salinity gradient; and (4) sectionally homogeneous estuary, with a longitudinal

salinity gradient. In the highly stratified estuary, river discharge dominates strongly over a small tidal action. The less dense fresh water floats on top of denser seawater in a layer that thins in the seaward direction. The seawater intrudes into the estuary in a wedge shape that gets thinner as it moves landward (Figure 2.1a.). Sedimentary material in a stratified estuary accumulates at the limit of penetration of the salt wedge. Suspended material entering the salt wedge would be brought to the limit of penetration by tidal and/or density currents.

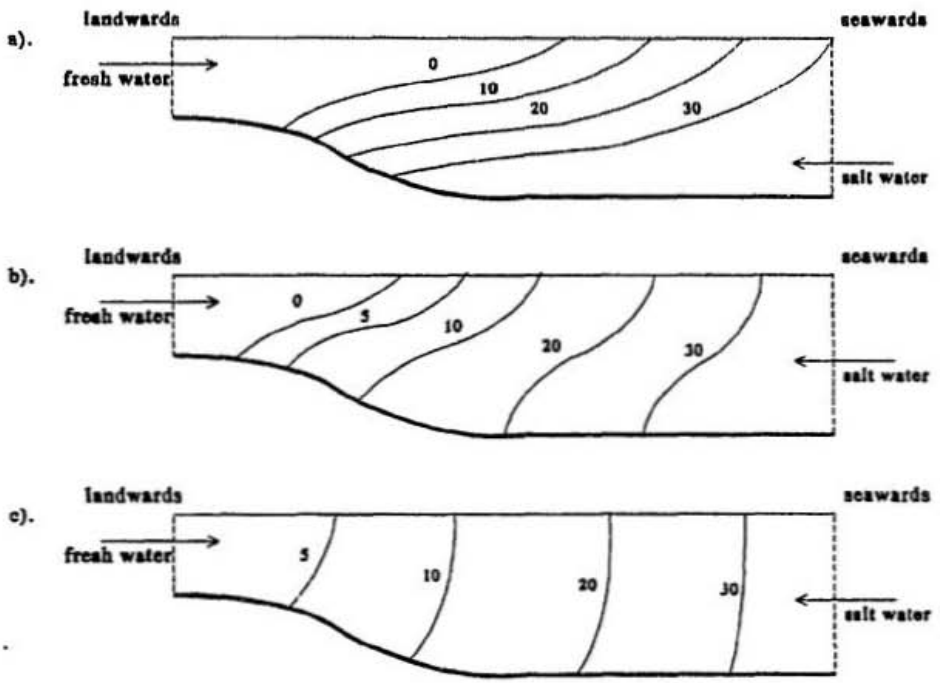

Figure 2.1 Classification of Estuaries Based on Water Circulation, *a) Highly Stratified, b) Partially mixed, c) Well mixed (After Pritchard, 1955).*

The presence of tidal motion within the estuary enhances vertical

turbulent mixing. Mixing increases as tidal action increases. When the estuary is completely homogeneous, the vertical salinity gradient disappears. Although lateral and horizontal salinity gradients remain, the estuary is known as vertically homogeneous (Figure 2.1c.). In an estuary which has a sufficiently small ratio of width to depth, the lateral salinity gradient can be broken by lateral frictional forces and the only salinity gradient retained is the longitudinal one. The estuary is then called sectionally homogeneous. Suspended material in the well-mixed estuary accumulates over a much longer length of channel than in a moderately stratified estuary and is confined mainly to the limit of penetration of salt water.

Between the highly stratified and well-mixed estuaries, there is a partially mixed estuary (Figure 2.1b.). Here, the tidal force is about equal to the fresh water flow in contributing to estuarine circulation. Material carried in suspension is deposited over the limits of the saline intrusion which may vary over several kilometres as the interface moves up and down due to the tide.

2.3 Fresh Water Discharge

Fresh water flow plays an important role in determining the salt water distribution, circulation pattern, and sediment transport. For this reason, it is very important to ascertain the fresh water flow entering the estuary at any time. Basically, there are two methods of estimating the fresh water flow: direct measurement of flow or the use of empirical formulae relating rainfall to run-off.

The first is the more accurate but it is a much more expensive undertaking and as a result data is sparse. In Indonesia the other method is often used in practice accompanied, perhaps, by occasional calibrations. The following section will deal with the relationship between rainfall and runoff, together with other factors related to it.

2.3.1 Rainfall

Rainfall is quantitatively described in terms of depth (millimetres) and duration (minutes or hours) (Roberson, et al., 1988). Depth is the total amount of rain to fall in a given time. Intensity is the rate of rainfall per unit time (mm/minutes or mm/hours). The rainfall varies significantly from place to place, even within a few square kilometres. It varies, not only in intensity, but also in time and duration.

Average rainfall.

Because rainfall varies spatially, the data of a single station may be significantly different from that of another station within the same catchment area. When several stations have recorded rainfall in a given catchment area, all data should be considered in determining the average depth of rainfall over the basin. The average amount can be calculated by using the following methods.

Station Average Method.

The data of all stations are simple averaged as

$$R_{avg} = \frac{\sum_{i=1}^{N} R_i}{N} \tag{2.1}$$

where R_{avg} is average rainfall depth over the basin, R_i is rainfall measured in station i, and N is number of stations.

Thiessen polygon method.

The rainfall measured at each station is assumed to be representative only of the area closest to it. The portion of the drainage area for each station is determined by drawing the Thiessen polygon (Figure 2.2a). The average rainfall is computed from

$$R_{avg} = \frac{\sum_{i=1}^{N} R_i . A_i}{\sum_{i=1}^{N} A_i} \tag{2.2}$$

where A_i is the area represented by station i.

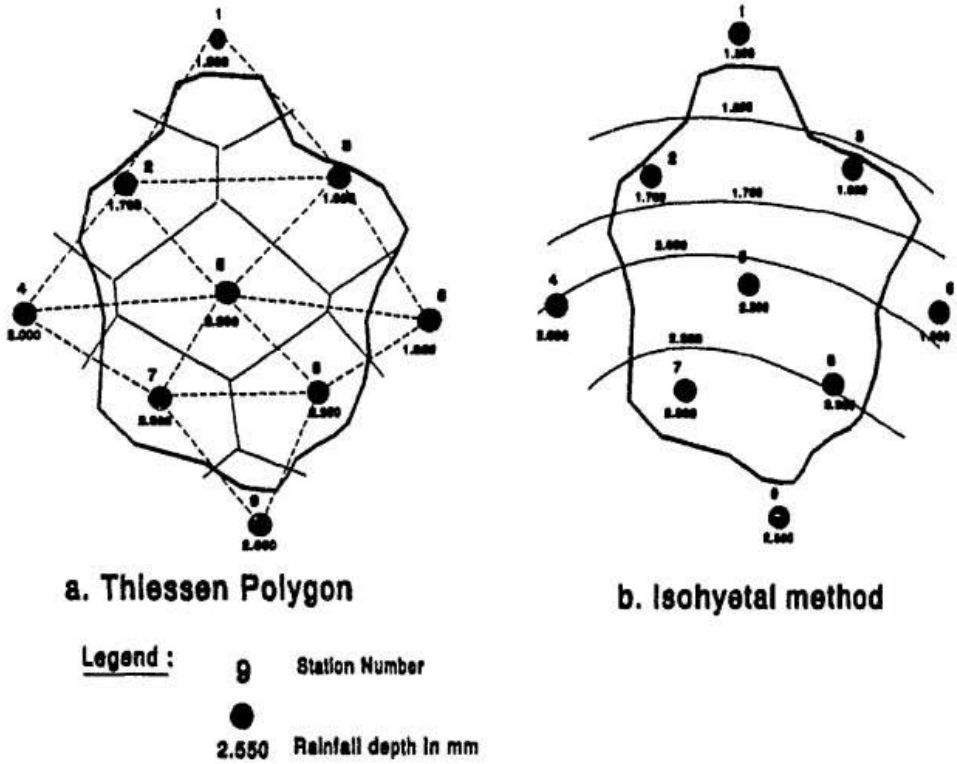

Figure 2.2 Averaging rainfall (a) Thiessen Polygon Method, and (b) Isohyetal Method

Isohyetal method.

The average rainfall is determined based on the isohyetal lines (i.e., lines of equal rainfall depth) which are constructed on the map of the catchment area (Figure 2.2b). The average rainfall is

$$R_{avg} = \frac{\sum_{j=1}^{m} A_j \cdot \frac{1}{2}(R_j + R_{j+1})}{\sum_{j=1}^{m} A_j} \qquad (2.3)$$

where R_j is the rainfall on isohyet j, A_j is area between isohyet j and $j+1$, and m is the number of intervals between isohyets.

Intensity-duration-frequency curves (IDF).

Naturally, the rainfall intensity has an inverse correlation with the duration; the higher the intensity, the shorter the duration, and vice versa. The maximum in a river basin flood may not be caused by the heaviest storm in a short duration but by the rainfall with a duration as long as the time of concentration, t_c. The time of concentration is defined as the time required for surface run-off to travel from the most remote part of the basin to the point at which the flood is to be estimated.

The occurrence of a given rainfall intensity is irregular. For these reasons, rainfall intensity-duration-frequency curves (IDF) are constructed to estimate the maximum run-off for a certain return period. The curve can be constructed by using the following steps

1. The maximum rainfall each year is selected for each considered duration.
2. The selected data are arranged orderly from the highest to the lowest data.

3. The return period is determined using Weibull's formula; T = (n+1)/m, where T is average return period in years, n is number of years of record, and m is rank of storm.
4. The rainfall intensities for each return period considered are then plotted in a table of plotting for an IDF curve.

Typical rainfall intensity-duration-frequency curves (IDF) are shown in Figure 2.3. This shows the curves for the cities of Surabaya and Jakarta (Indonesia).

2.3.2 Run-off

Surface run-off is affected by numerous hydrological factors such as rainfall intensity and duration, geologic structure, relief, plant cover of catchment area, and shape of basin. Analytical methods for computing runoff cannot yet relate all those factors in a rigorous fashion. However, many empirical methods have been developed which may give satisfactory results.

The most commonly used is the so-called the modified rational method. This is

$$Q_p = 0.278 . C . C_s . I . A \qquad (2.4)$$

where Q_p is peak discharge in m^3/s, C is a run-off coefficient, C_s is a storage coefficient, I is the mean rainfall intensity in mm/hour, and A is the drainage area in km^2.

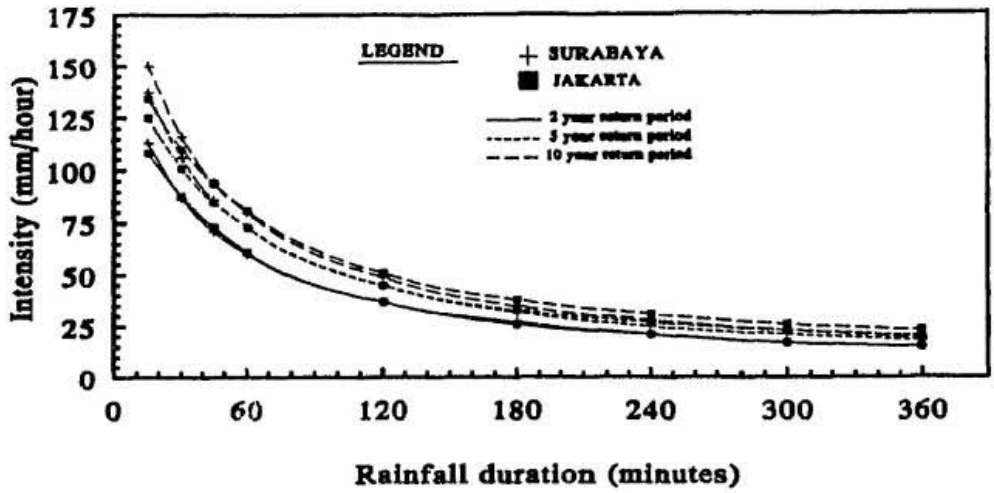

Figure 2.3 Intensity-duration-frequency (IDF) Curves for the Cities of Jakarta and Surabaya. (*Department of Public Works, Indonesia, 1961*)

Run-off coefficient (C).

The run-off coefficient C is a dimensionless constant that depends on texture, permeability and land use of the area. Table 2.1 lists values of C recommended for the modified rational method.

Storage coefficient (C_s).

The value of C_s depends on the drainage area. The larger the area the larger the effect of storage tends to be. The magnitude of C_s can be estimated by the following

relation

$$C_g = \frac{2\,t_c}{2\,t_c + t_d} \qquad (2.5)$$

where $t_c = t_o + t_d$, t_o is the time required the surface run-off from basin to nearest channel and t_d is the time needed to travel from the first channel to the point considered.

Table 2.1 Run-off Coefficients, C (*Source : Department of Public Work, Indonesia, 1982*)

Type of Area	Run-off Coefficient, C
Urban business	0.95
Commercial office	0.70
Residential development	
Scarce housing	0.50
Medium housing	0.65
Densely housing	0.75
Suburban residential	0.40
Apartments	0.70
School and mosques	0.80
Industrial	0.80 - 0.90
Parks, cemeteries	0.25
Rail-road yards	0.35
Unimproved grassland	0.35

Rainfall intensity, I.

Rainfall intensity, I, depends on t_c and IDF curve (Figure 2.3).

For the purpose of calculation of salinity, circulation pattern and sediment movement, the direct measured river discharge is used in this study.

2.4 Tides and Tidal Propagation in Estuaries

Tides are the rise and fall of water level generated by response to the attractive forces of the moon and sun, and by the rotation of the earth-moon system about its common centre of gravity. The earth-moon system revolves around its centre of mass with a period of 27.3 days. The combined gravitational effect between the sun and the moon is strongest when they are in alignment with the earth. Resulting tides are called spring tides. Spring tides occur every 14 days, just after the full or new moon. Conversely, when the sun and the moon are at right angles to the earth, the resulting tide is at a minimum. The tides are then known as neap tides and the moon is said to be in quadrature.

Although gravitational forces are responsible for the tides, many irregularities in the tidal cycle cannot be explained on this basis alone. There are many other factors influencing, modifying and controlling the tides which are initiated by gravitational forces. Some of these modifying factors are variable. Others are constant. The most noticeable of the variable influences are atmospheric pressure and wind action.

The constant factors result in a number of different tidal constituents. Doodson (1920) listed some 390 different partial-tide constituents which are all related to the sun-earth, moon-earth, or combined interactions. Table 2.2 lists the major tide-

force constituents, their periods and their contributions to tides relative to the principal component M_2. The basic strengths of the components listed in Table 2.2 are not the same for all places on the surface of the earth. They may vary strongly from one area to another depending on the local basin geometry. In Semarang-Indonesia for example, the dominant component is the Luni-solar diurnal (K_1), although this force contributes only 58.4 % of the principal component M_2.

Table 2.2 The Main Tide-force Constituents (*Source : Bearman, 1989*)

Name of Constituents	Symbol	Period, solar hours	Coefficient ratio, $M_2 = 100$
Semi-diurnal			
Principal lunar	M_2	12.42	100.0
Principal solar	S_2	12.00	46.6
Larger lunar elliptic	N_2	12.66	19.2
Luni-solar semi-diurnal	K_2	11.97	12.7
Diurnal			
Luni-solar diurnal	K_1	23.93	58.4
Principal lunar-diurnal	O_1	25.82	41.5
Principal solar diurnal	P_1	24.07	19.4
Larger lunar elliptic	Q_1	26.87	7.9
Long-Period			
Lunar fortnightly	M_f	327.86	17.2
Lunar monthly	M_m	661.30	9.1

Centrifugal acceleration and boundary irregularities modify the effects of gravity. Water particle centrifugal acceleration is induced by the earth's rotation and

causes moving water in the Northern hemisphere to deflect to the right. In the Southern hemisphere the centrifugal action turns moving particles to the left. This phenomenon is known as the Coriolis effect.

Finally, the boundary irregularities cause innumerable reflections of tidal propagation. These boundaries also introduce friction and dissipate the tidal energy.

2.4.1 Tidal Types

The principal basic tides can be classified by using a ratio (*F*), of the sum of the amplitudes of the two main diurnal constituents (K_1 and O_1) to the sum of the amplitudes of the two main semi-diurnal constituents (M_2 and S_2) (An Open University Course Team, 1986), thus

$$F = \frac{Amplitude\,K_1 + Amplitude\,O_1}{Amplitude\,M_2 + Amplitude\,S_2} \qquad (2.6)$$

A ratio *F* of 0 - 0.25 implies a semi-diurnal type; a ratio *F* of 0.25 - 1.50, a mixed-predominantly semi-diurnal type; a ratio *F* of 1.50 - 3.00, a mixed-predominantly diurnal; and a ratio of *F* greater than 3.00 refers to a diurnal tide.

The term semidiurnal tide is used for a tidal curve having two high waters (HW) and two low waters (LW) of about equal height during a tidal day (24 hours 50 minutes), see Figure 2.4a. A diurnal tide has only one high and low water during the same period (Figure 2.4c). In a mixed tidal type there are sometimes one high and one low water and sometimes two high and two low waters during a tidal day (Figure 2.4b).

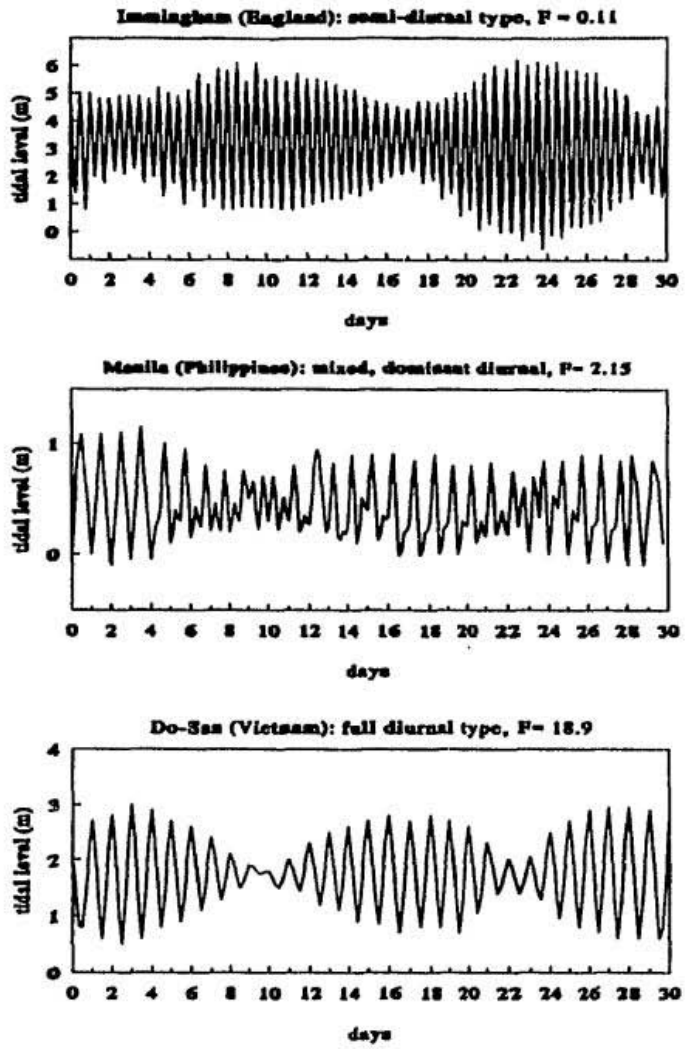

Figure 2.4 Examples of Different Tidal Types, (a) Semi-diurnal, (b) Mixed, Dominant Diurnal, and (c) Full Diurnal Type

The basic patterns identified by factor, *F*, can be modified by local effects, particularly the local effects of harmonics of the partial tides. Figure 2.5 shows a real tide as recorded in the field.

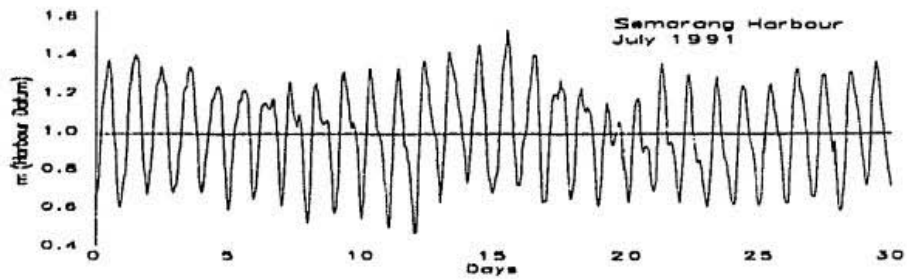

Figure 2.5 Examples of Recorded Tide in Semarang Harbour, Indonesia (F = 1.67, Dominant Component is K_1)

2.4.2 Tidal Propagation in Estuaries

Tidal energy in estuaries is derived from local ocean tides rather from than the direct action of astronomical forces. As ocean tides propagate into a shallow water estuary, their profile depends in part on the basin depth. When the water depth in the estuary does not appreciably exceed the tidal amplitude, the tide wave is propagated as a shallow water wave. Hence the speed C is given by

$$C=\sqrt{gh+\eta} \tag{2.7}$$

where h is the water depth; g is acceleration due to gravity; and η is the height of the water surface above mean tidal level. As the water depth decreases, η/h increases. Hence, the tidal wave speed decreases. Consequently, the tidal crest (HW) propagates faster than the trough (LW). Furthermore, there is an asymmetry in the tidal cycle,

with a relatively long time interval between high water and the succeeding low water, and a shorter interval between low water and the next high tide.

Tides in a river channel are also modified by varying degrees of interference between the wave which enters the estuary and reflection from the boundaries or from the estuary head, frictional dissipation, and decreasing channel cross section (Kennish, 1986). Depending on the geometry and associated resonance characteristics of the channel, the tides may behave as either progressive waves or as standing waves. Progressive waves usually occur in a wide and long (assumed of infinite length) estuary where the entering wave height is reduced significantly by bottom friction. Waves reflected by boundaries are smaller than entering waves. The important point in this type of wave is that the currents are in phase with the tide; i.e., the maximum currents occur near the time of high and low water. Minimum currents occur near mid-tide.

In an unrestricted estuary, where wave attenuation is small and the amplitude and period of the entering wave equal those of the reflected wave, a standing wave is experienced. Here, the tidal levels and velocities are out of phase by 90 degrees. The maximum amplitude occurs at the head of the estuary and at antinodes that are located at multiple distances of one half of the wave length (L/2) from the head. Nodal points of zero amplitude and of maximum velocity exist at L/4 and at odd multiples thereof. A well known example of this type is the Bay of Fundy (Canada) which has a length of about one quarter of the wavelength. The maximum tidal range at the head is some 15 m and the maximum tidal currents occur at about mid-tide.

In addition to the effects of the geometric factors discussed above, estuaries have special variable influences on tidal level. These are large freshwater inflow at the head, wind actions and atmospheric pressure. These three factors may significantly affect the water level.

2.4.3 Tidal Wave Entering A Channel Closed at One End

This case may be dealt with as one complete reflection of the entering progressive wave from the closed end. Thus two waves of equal amplitude a and period T are superimposed, one travelling in the positive and one in the negative x direction. In accordance with the definition on Figure 2.6 (Ippen and Harleman, 1966), then

$$\eta = 2a \cos\sigma t \cos kx \tag{2.8}$$

and

$$u = 2\frac{a}{h} C \sin\sigma t \sin kx \tag{2.9}$$

where σ = $2\pi/T = kC$,

k = $2\pi/L$,

T = tidal period (seconds),

L = wave length (m), and

C = wave celerity (m/s).

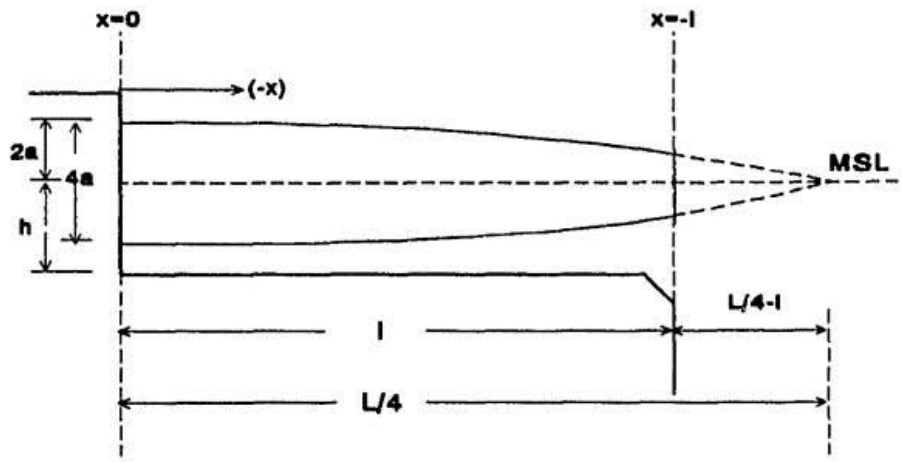

Figure 2.6 Wave Entering Channel of Finite Length with Reflecting End.

High water is obtained, therefore,

at the closed end : $x = 0$

Thus in equation 2.8 with $t = 0$

$\eta_{0max} = 2a$

at the open end : $x = -l$

Thus in equation 2.8 with $t = 0$

$\eta_{(-l)max} = 2a \cos kl$

The ratio of the maximum tide at the closed end to tide at the entrance is

$$\frac{\eta_{0max}}{\eta_{(-l)max}} = \frac{1}{\cos kl} \qquad (2.10)$$

This ratio is infinite if $kl = \pi/2$ *for* $l/L = 1/4$. Note that equation 2.10 applies only for one time.

2.5 Waves in Shallow Water

Waves are disturbances on the surface of a fluid. They usually occur on the interface between the air and the water body (surface waves), but may also occur on the interface between two different water masses (internal waves). In estuaries, waves may affect sediment movement directly or indirectly. In this section, wave means a wind generated wave. The size of a wind generated wave is controlled by three variables: (1) the fetch, which is the distance the wind blows over the water surface in a constant direction, (2) the duration with which the wind blows in one direction, and (3) the wind speed. Increasing these three factors results in increased wave heights.

The important variables in wave observation are wave height, wave period, and wave direction. The wave height and period may be recorded by using a wave gage recorder. Since the wave directions are difficult to measure they are usually assumed to have the same direction as the direction of the generating winds. In engineering applications the measured wave height is transferred into a significant wave height. Munk (1944) (quoted in U.S. Army CERC, 1984, p. 3-2) defined significant wave hight (H_s) as the average height of the one-third highest waves.

2.5.1 Wave Energy and Wave Power

The processes associated with wave energy have a significant effect on the distribution of river sediments, on the rate of longshore transport and on the

formation of deltas. For these, it is important to ascertain both the quantity and distribution of the wave energy at the delta zone.

The energy contained within a wave occurs in two forms: kinetic and potential. The total energy (E) in a wave per unit crest width is given by (U.S. Army CERC, 1984, p. 2-63)

$$E = \frac{\rho g H^2}{8} \tag{2.11}$$

where E is in Joule/m^2, ρ is the density of the sea water in kg/m^3, g is the acceleration due to gravity in m/s^2, and H is the wave height in metre.

Wave energy flux is the rate at which energy is transmitted in the direction of wave propagation across a vertical plane perpendicular to the direction of the wave advance and extending over the entire depth. The energy flux per unit length of wave crest is

$$P = EC_g = \frac{\rho g H^2}{8} C_g \tag{2.12}$$

where P is the energy flux that is frequently called the wave power (N/s = J/s-m), and Cg is the group velocity of the wave (m/s). This can be calculated from (Wiegel, 1964)

$$C_g = \frac{1}{2}\frac{L}{T}\left(1 + \frac{(4\pi d/L)}{\sinh(4\pi d/L)}\right) \tag{2.13}$$

In deep water (d/L $>$ 0.5), the group wave velocity is equal to one half of wave velocity, and in shallow water (d/L $<$ 0.05) the group velocity is equal to the wave

velocity and proportional to the root-square of the depth d, thus

$$C_{g\,(deep\ water)} = \frac{1}{2}C \tag{2.14}$$

$$C_{g\,(shallow\ water)} = C \approx \sqrt{gd} \tag{2.15}$$

For an oblique wave, the wave crest makes an angle, α with the shoreline. In that case the wave power becomes

$$P = \frac{\rho g H^2}{8} C_g Cos\alpha \tag{2.16}$$

and the longshore component (P_l) is given by

$$P_l = \frac{\rho g H^2}{8} C_g Sin\alpha\, Cos\alpha \tag{2.17}$$

2.5.2 Energy Dissipation and Wave Attenuation

When waves travel from deep water to shallow water, wave energy will be dissipated. Based on theory and field measurements, Bretschneider and Reid (1954) have derived equations to estimate the reduction of wave height due to bottom friction. The wave height, H_f, after undergoing frictional attenuation over a distance x is given by

$$H_f = \frac{H'}{\left(\frac{f H'^2 \phi \cdot x}{K_s \cdot T^4} + 1\right)} \tag{2.18}$$

where H' is the wave height after refraction, f is the friction coefficient (for low roughness bottom, eg. silt and clay the value is 0.02, Wright and Coleman, 1973), T is the wave period, K_s is the shoaling coefficient, and ϕ is given by

$$\phi = \frac{64\pi^3}{3g}\left(\frac{K_s}{\sinh 2\pi\left(\frac{d}{L}\right)}\right)^3 \qquad \textbf{(2.19)}$$

The shoaling coefficient K_s is calculated from the relation

$$K_s = \frac{H}{H_o'} = \sqrt{\frac{1}{\tanh\left(\frac{2\pi d}{L}\right)}\,\frac{1}{\left(1+\frac{(4\pi d/L)}{\sinh(4\pi d/L)}\right)}} \qquad \textbf{(2.20)}$$

where d is the water depth (m), and L is the wave length (m), H is the wave height (m) at the depth d, and H_o' is the wave height in deep water (m) if the wave is not refracted.

The energy flux in the near-shore can be obtained by substituting H_f into the energy flux equation to replace H.

The annual wave power can be obtained from the expression

$$P = \sum_{j=1}^{N} (f_j P_j) \qquad \textbf{(2.21)}$$

where N is a number of wave-class characteristics, j refers to the particular set of wave characteristics, and f_j is the percentage frequency of the wave set j.

2.6 Salinity Distribution and Circulation Pattern in Estuaries

Estuarine water consists of a combination of freshwater and seawater. Freshwater originates from land drainage, and saltwater intrudes from the ocean. The salt penetrates up the estuary by advection and diffusion. The salinity in estuarine water varies gradually in space and time. It is different between lower and upper parts. It changes seasonally, daily, and throughout a tidal cycle.

The salinity intrusion and circulation pattern in estuaries are functions of freshwater flow, tidal action, the estuary geometry, wind influence, Coriolis effects, and the density difference between fresh and salt water. Patterns are directed by the strength of each factor relative to the others. As the significance of one factor is often dependent on the relative weakness of one or more of the others, a measure of the interaction between the different factors is extremely difficult to obtain. Hence the determination of the salinity distribution and circulation patterns in estuaries are complex problems.

2.6.1 Salinity Distribution in Well-mixed Estuaries

Salinity distribution and estuarine circulation patterns are non linear. There are a number of important independent or interdependent variables that vary spatially and temporally. Quantitative treatment of both phenomena can be represented theoretically by three well known laws of mechanics; conservation of momentum,

conservation of mass, and continuity.

In a well mixed estuary, salt transport can be described by a conservation of mass or by an advection-dispersion equation (Helder and Ruardij, 1982). Consider a Cartesian system with coordinates; x, y, and z, where x and y are the horizontal and sectional coordinates, respectively, and z is the vertical coordinate measured downwards from the mean water surface. The three-dimensional advection-dispersion equation can be written as

$$\frac{DS}{Dt} = \frac{\partial}{\partial x}\left(K_x \frac{\partial S}{\partial x}\right) + \frac{\partial}{\partial y}\left(K_y \frac{\partial S}{\partial y}\right) + \frac{\partial}{\partial z}\left(K_z \frac{\partial S}{\partial z}\right) \tag{2.22}$$

where

$$\frac{DS}{Dt} = \frac{\partial S}{\partial t} + u\frac{\partial S}{\partial x} + v\frac{\partial S}{\partial y} + w\frac{\partial S}{\partial z} \tag{2.23}$$

and where S is salinity, K is the dispersion coefficient, g is the acceleration due to gravity, t is time and u, v and w are the x, y, and z component of velocity.

In narrow, well-mixed estuaries the major spatial variability occurs along the estuary axis and transport of salt can be treated as a one-dimensional process. A one dimensional treatment may also provide a very useful result for estimating the cross-sectionally averaged quantity of salinity intrusion in a partly mixed estuary (Ucles and Stephens, 1990).

Consider a river channel with fresh water discharge Q_f and width B. Salinity is nearly constant in the ocean and approaches zero at the upstream. Equation 2.23 can be rewritten as

$$B\left(\frac{\partial S}{\partial t}+u\frac{\partial S}{\partial x}\right) = \frac{\partial}{\partial x}\left(BK_x\frac{\partial S}{\partial x}\right) \tag{2.24}$$

for stationary conditions, where $\delta S/\delta t = O$, equation 2.24 becomes

$$Bu\frac{dS}{dx} = \frac{d}{dx}\left(BK_x\frac{dS}{dx}\right) \tag{2.25}$$

or

$$Q_f\frac{dS}{dx} = \frac{d}{dx}\left(BHK_x\frac{dS}{dx}\right) \tag{2.26}$$

where H is the depth of the estuary.

For Q_f constant, a single integration of equation 2.26 gives

$$S = S_o\exp\int_{x_o}^{x}\frac{Q_f}{BHK_x}\,dx \tag{2.27}$$

where S_o is the salinity at $x = x_o$.

For a given value of K_x, the longitudinal salinity distribution can be predicted.

Dispersion coefficients (K_x)

For a one-dimensional method can be estimated from the longitudinal distribution of salinity, the estuarine cross-sectional area and the river flow (Helder and Ruardij, 1982). Therefore, the longitudinal dispersion coefficient can be estimated by

integrating and rearranging equation 2.26 to

$$K_x = \frac{Q_f \cdot S_x}{A_x \cdot \frac{dS}{dx}} \qquad (2.28)$$

where K_x is longitudinal dispersion coefficient (m^2/sec), Q_o is fresh water flow (m^3/sec), S_x is salinity (ppt), A_x is cross-sectional area (m^2), x is distance (m) along the longitudinal axis of estuary.

Salinity distributions along the channel for different conditions, either of fresh water flow or tide or of both, can be estimated from knowledge of the dispersion coefficient in each cross section.

2.6.2 Salinity Distribution in A Salt Wedge Estuary

Keulegan (1966) stated that the intrusion of salt in a river opening to a sea with low tidal action is affected by the upstream movement of a definable and limited saline layer underlying the fresh water. The length of an advancing wedge (L_o) is a function of the densimetric Reynolds number (Re), densimetric velocity (u_Δ), and the velocity of fresh water opposing the advancing wedge (u_r), see Figure 2.7. The relation is given as

$$\frac{L_o}{H} = A_o \, R_e^m \left(\frac{2 u_r}{u_\Delta} \right)^{-\frac{5}{2}} \qquad (2.29)$$

where the Reynolds number, R_e is quantified by

$$R_e \cdot\cdot u_\Delta \frac{H}{\nu} \tag{2.30}$$

and the densimetric velocity, u_Δ is expressed as

$$u_\Delta = \sqrt{\frac{\Delta \rho}{\rho_m} gH} \tag{2.31}$$

and where $\Delta\rho$ is the density difference between fresh and saline water (kg/m^3), ρ_m is the average density of the two waters (kg/m^3), and H is the depth of the river (m). The value of the constant, A_o, varies with H/B and with R_e and the value of constant, m, with R_r only (Keulegan, 1966).

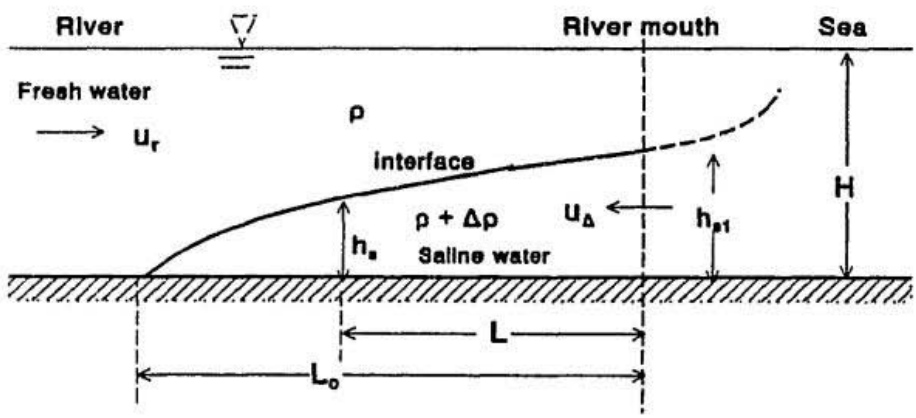

Figure 2.7 Schematic Chart of Saline Wedge

The vertical salinity distribution in the salt wedge estuary depends on the densimetric Froude number, F_r . This is given by

$$F_r = \frac{u}{\sqrt{\sigma g h'}} \tag{2.32}$$

where u is the mean velocity of the upper layer (m/s), h' is the depth of the density interface (m), g is the acceleration due to gravity (m/s^2), and the specific density, σ, is given by

$$\sigma = \frac{\rho_s - \rho_f}{\rho_s} \tag{2.33}$$

where ρ_f and ρ_s are the fresh water and sea water densities respectively (kg/m^3),

As the value of Fr' increases the mixing process becomes more intense, and the salinity of the upper layer increases. Farmer and Morgan (1953) found that if $Fr' > 1.0$ an internal wave is formed. Further increases in velocity cause this wave to break and start interfacial mixing. Hence the local vertical salinity gradient decreases.

2.6.3 Circulation Patterns

Circulation patterns in an estuary are largely controlled by the strength of the river flow relative to the strength of tidal currents in combination with the geometrical configuration of the estuary. Circulation patterns range from those experienced in salt wedges to those of well mixed estuaries (see section 2.2).

The competing effects of fresh water discharge and tidal currents may be quantified through the estuarine stratification number, S_e. This can be used to roughly predict the circulation pattern in the estuary. Pickard (1975) attempted to quantify an estuarine number, $S_.$, in his formula

$$S_e = \frac{U^3 B}{g Q_f} \tag{2.34}$$

where U is the mean tidal current, B is the width of estuary, g is gravity, and Q_f is fresh water discharge. A small value of S_e would lead to a stratified estuary, and a large value would be associated with a well mixed estuary. The transition occurs in the range 0.03 to 0.3. The mean current, U, is related to the tidal prism, that is the volume of water entering the estuary or passing a given cross section on the flood tide. The mean tidal current can be estimated from the following relation

$$U = \frac{2 T_R A_s}{B H T} \approx \frac{2 V_T}{A T} \tag{2.35}$$

where U is given in m/s, T_R is tidal range (m), A_s is surface area (m^2) , B and H are width and depth of channel, respectively (m), V_T is tidal volume (m^3), A is cross section area (m^2), and T is tidal period (seconds).

In a different way, Simons (1969) (quoted in Silvester, 1974) proposed quantifying the degree of mixing by a flow ratio (K), which is the ratio of the volume of fresh water per tidal cycle to the volume of salt water in the flood tide.

Then for :

$K \geq 0.7$	the estuary is highly stratified,
$0.7 > K > 0.1$	the estuary is partially mixed, and
$K \leq 0.1$	the estuary is well mixed.

Based on either the estuarine number (S_e) or the flow ratio (K), estuaries may change their classification from stratified to well mixed due to the reduction of the fresh water flow and change from well mixed to stratified by increasing in fresh water inflow. Similar changes may result from the increase and/or decrease in tidal ranges from neap to spring and/or vice versa.

2.7 Sedimentation and the Movement of Sediments

The main sources of natural sediment entering an estuary are the catchment area of the river system (river-borne), the ocean (marine sources), and a small fraction which originates in the estuary from biologically and chemically in situ precipitated materials.

In the complexity of an estuarine environment, sediment usually experiences a variety of physical, biological, and chemical processes that go on independently or in combination. The sediments pass through repeated cycles of erosion, transportation, deposition, and re-suspension prior to being deposited permanently or being lost to offshore areas.

2.7.1 Characteristics of Sediment

Sediments in estuaries can range in size from gravels and coarse sands to clay and flocculating silt. The sediments consist of the products of the weathering,

disintegration, and decomposition of pre-existing rocks and sediments and therefore contain many of the rock forming minerals. They also include organic matter and solid materials biologically and chemically precipitated from waters within the basin. Sediments can be described in terms of their chemical or physical properties.

This section deals with the physical properties of particles which are closely related to the sediment movement; i.e., the grain size distribution of sediment material. Knowledge of the grain size distribution is important in determining the origin and the manner of sediment movement. The size of sedimentary grains is usually expressed in either a metric or logarithmic scale, in which a continuous range of sediment sizes is subdivided into classes or grades. There are two common size scales used today: the Unified Soil Classification (USC) and the Wentworth's modified scales. These two scales have different limits of the class sizes. The USC boundaries correspond to the US Standard Sieve Size. The Wentworth classification differentiates between sediments using limits which are always expressed in the form of 2^n mm, where n can be any integer, i.e 2, 4, 6, 8 etc., or 0,5, 0.125, 0.062, 0.031, etc. The Wentworth scale was modified by Krumbein (1936) by transforming the millimetre scales to a phi unit scale based on the definition

$$\phi = -\log_2 d \tag{2.36}$$

where the diameter, d, is in millimetre. The Wentworth and Phi unit scale are given in Table 2.3.

Table 2.3 Classification of sediment according to size (Wentworth's modified scale)

Nomenclature	Diameter	
	Millimetres	Phi (ϕ)
Very large boulders	4,000 - 2,000	- 12 - - 11
Large boulders	2,000 - 1,000	- 11 - - 10
Medium boulders	1,000 - 500	- 10 - - 9
Small boulders	500 - 250	- 9 - - 8
Large debris	250 - 130	- 8 - - 7
Small debris	130 - 64	- 7 - - 6
Very coarse gravel	64 - 32	- 6 - - 5
Coarse gravel	32 - 16	- 5 - - 4
Medium gravel	16 - 8	- 4 - - 3
Fine gravel	8 - 4	- 3 - - 2
Very fine gravel	4 - 2	- 2 - - 1
Very coarse sand	2.000 - 1.000	- 1 - 0
Coarse sand	1.000 - 0.500	0 - 1
Medium sand	0.500 - 0.250	1 - 2
Fine sand	0.250 - 0.125	2 - 3
Very fine sand	0.125 - 0.062	3 - 4
Coarse silt	0.062 - 0.031	4 - 5
Medium silt	0.031 - 0.016	5 - 6
Fine silt	0.016 - 0.008	7 - 8
Very fine silt	0.008 - 0.004	8 - 9
Coarse clay	0.004 - 0.002	9 - 10
Medium clay	0.002 - 0.001	10 - 11
Fine clay	0.001 - 0.0005	11 - 12
Very fine clay	0.0005 - 0.0002	12 - 13

Naturally, since the finer sediment grains are more mobile than the coarser ones, a large amount of information concerning movement can be obtained from a study of the grain size and distribution in different size fractions. From the distribution data, the grain size accumulation curve can be described. Furthermore, the

range of grain size may reflect some part of the variability of the forces causing movement.

Grain size distribution is commonly determined by mechanical analysis using a either sieve analysis or a hydrometer analysis. The first is used for coarse particles. The size of grain is expressed as a sieve hole diameter. The latter is used for the fine particles. Particle diameter is indirectly determined based on Stokes Law. The basic formula of Stokes law (single particle) is

$$Size(in\ 10^{-6}\ m) = F\sqrt{\frac{D}{t}} \tag{2.37}$$

where D is depth of the sampling in cm, t is time in minutes, and F is a dimensional constant which has a value 12.99 at 24°C, 13.30 at 22°C and 13.6 at 20°C.

Within the framework of Stokes law, however, many interacting variables, such as particle shape, concentration, and density influence the manner in which particles settle in a column of standing water. Hence, the equation 2.37 cannot be applied directly. In the hydrometer analysis, rate of particle settling is expressed in the change of density of the suspension as a measure of its content of solids. Variations of fluid density are reflected in the depth at which the hydrometer floats below the fluid surface. The relationship between the density of suspension, fall velocity and grain diameter is then determined using a table or monogram. Wide variety of opinion related to the sample concentration, Dyer (1979) recommended the use of 10 g and certainly no more than 20 g of sample in 1000 ml of water.

Grain size distribution data (either from sieve analysis or hydrometer

analysis) are illustrated graphically by means of histograms and cumulative curves. These two graphs provide a visual indication of the size fractions that compose the particular sediment material.

A sample is usually described as well sorted if all particles have sizes that are close to the typical size. If the particles are distributed over a wide range of size, the sample is said to be well graded. A well graded sample is poorly-sorted and a well sorted sample is poorly-graded. This nature of the sample can be identified from various statistical parameters or from graphic measures.

Median diameter (M_d)

Mean diameter, M_d, is the most common measure used in engineering, i.e

$$M_d = d_{50} \tag{2.38}$$

where d_{50} is the size in millimetres that divides the sample so that half the sample, by weight, has particles coarser than the d_{50} size. In the phi unit distribution it is termed as $M_{d\phi}$.

Mean diameter (M).

Inman (1952) proposed the average of the size of the 84th and 16th

percentiles as measure of the mean.

$$M_\phi = \frac{\phi_{16} + \phi_{84}}{2} \tag{2.39}$$

Standard deviation (σ)

Standard deviation, σ, is a measure of the degree to which samples spread out around the mean. Inman (1952) proposed that the standard deviation could be calculated from

$$\sigma_\phi = \frac{\phi_{84} + \phi_{16}}{2} \tag{2.40}$$

where ϕ_{84} and ϕ_{16} are the sediment sizes, in phi units, finer than 84 percent and 16 percent by weight of the sample, respectively.

Skewness (α_ϕ)

Skewness, α_ϕ, is the measure of the degree to which the phi unit departs from symmetry; Inman (1952) proposed

$$\alpha_\phi = \frac{\phi_{84} + \phi_{16} - 2\phi_{50}}{\phi_{84} - \phi_{16}} \tag{2.41}$$

The sample is called well sorted if the value of σ value is less than 0.5, and it is called poorly sorted if the σ value is greater than 1.00.

2.7.2 The movement of Sediment.

A sediment particle will move whenever the force of flowing water (buoyancy and drag forces) over it is able to overcome the resistance force (gravity and friction forces) of the grain. A certain velocity at which the combined drag and lift forces is sufficient to dislodge particles from their equilibrium position is called the critical or threshold velocity. A small increment of velocity will cause motion, but the motion will die away after a time and particles will come to rest in a new equilibrium position. With further increase in velocity, movement will become more general and prolonged. Particle movement, therefore gradually changes from saltation-dominated to suspension-dominated with increasing force of the flowing water.

Sediments are commonly divided into bed load, suspended load, and wash load. Bed load comprises grains which are rolling, sliding, or occasionally jumping along the bed. Suspended load includes particles which are moving with the water, about the same velocity, and which are supported by turbulence. These grains settle toward the bed when the flow diminishes. Wash load comprises particles which are transported and perpetually in suspension, even when the fluid has been flowing at low velocity for some time. Since the wash load is usually lost into the offshore zone and does not significantly affect the configuration of the channel, it will not be discussed further.

2.7.3 Sediment Discharge From River

Essentially , the sediment transport rate is the total weight of grains passing through a section per unit time, per unit area. Thus, the volume of river sediment entering the estuary can be estimated by using the sediment carrying capacity, that is the total weight of grains passing through a section per unit time, per unit width of channel. Calculation of the river sediment discharge rate is usually divided into bedload and suspended load rates.

Many sediment transport formulae have been proposed. Since each formula was derived for a specific circumstance, the use of them should be suited to the field observations. In this study the formulae derived by Sato, et. al., and Kalinske (quoted in Bogardi, 1978) will be used to estimate the bed load and suspended load rates, respectively. These two formulae have been examined in the Brantas River, East Java-Indonesia (Department of Public Works, 1966).

Bed-load rate.

The first attempt to obtain a theoretical understanding of bed load movement was made by Du Boys (1879) (quoted in Dyer, 1986). He proposed that the bed load moves in layers so that the top layer of a thickness about the same as the particle diameter d is transported at the highest velocity, with the velocity decreasing linearly with the depth to zero at the bottom. The relation developed was

$$q_b = C_B \tau_o (\tau_o - \tau_c) \qquad (2.42)$$

where q_b is the rate of transport (kg/sec m), τ_o, and τ_c are the actual and the critical shear stress, respectively (kg/m^2), and C_B is a dimensional coefficient (m^3/kg sec).

Based on field data, Sato, et. al. (1958) formulated a relation between bedload rate and the factors aforementioned. After certain simplifications confirmed by experiments, Sato, et. al. (quoted in Bogardi, 1974, p. 255 - 258) were able to show that

$$\Phi_s = \frac{q_b(\frac{\rho_s}{\rho_w} - 1) \cdot g}{u_*^3 \cdot F\left(\frac{\tau_o}{\tau_c}\right)} \qquad (2.43)$$

or

$$q_b = \Phi_s \frac{u_*^3 \cdot F\left(\frac{\tau_o}{\tau_c}\right)}{(\frac{\rho_s}{\rho_w} - 1) \cdot g} \qquad (2.44)$$

where : q_b = bed load per unit time per unit width of section (m^3/s-m)

u_* = critical velocity near bed

= $(gRI_e)^{1/2}$ (m/s),

where R = hydraulic radius (m),

I_e = energy gradient (m/m)

τ_c = critical shear stress on bed (N/m^2);

τ_o = shearing stress on bed (N/m^2);

$= \rho g R I_e$,

ρ_s = density of sediment material (kg/m^3)

ρ_w = density of water (kg/m^3)

Φ_s = f(n), n is Manning's coefficient,

The value of Φ_s depends on Manning's resistance coefficient and varies as shown below :

$n \geq 0.025, \quad \Phi_s = 0.623$

$n < 0.025, \quad \Phi_s = 0.623\ (40\ n)^{-3.5}$

The function $F(\tau_o/\tau_c)$ depends on the ratio actual to critical shear stress and is shown in Figure 2.8

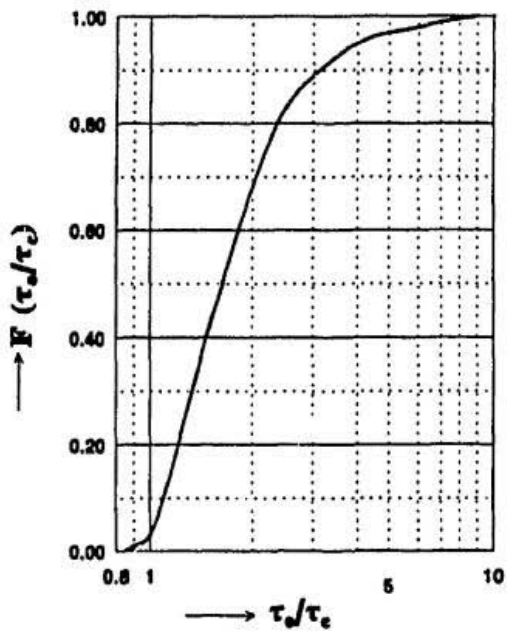

Figure 2.8 Relation Between $F(\tau_o/\tau_c)$ and (τ_o/τ_c)

Friction velocity (u_*), and critical shear stress (τ_c) can be calculated by using the following equations

$$u_* = \sqrt{\frac{\tau_o}{\rho}} \tag{2.45}$$

or

$$u_* = \sqrt{gRI_e} \tag{2.46}$$

where ρ is water density (kg/m^3), g is gravitational acceleration (m/s^2), R is hydraulic radius (m), and I_e is energy gradient (m/m).

The critical shear stress has been derived from basic experiments carried out Shields who found (Chadwick, and Morfett, 1986, p. 250) that

$$\tau_c = 0.056\,(\rho_s - \rho)\,g\,d_{50} \tag{2.47}$$

where τ_c is given in N/m^2, ρ_s and ρ in kg/m^3, g in m/s^2, and d in m.

Suspended load transport rate.

Generally, the suspended sediment transport rate, q_s, can be expressed as

$$q_s = \int_0^h uC\,dz \tag{2.48}$$

where q_s is the suspended transport rate in kg/s-m, u is the flow velocity in m/s, and C is the concentration in mg/l.

Since the mean velocity is usually at about 0.6 of the depth measured from

the bottom, while the mean concentration is within the bottom few centimetres of the flow, the velocity-concentration cannot be integrated analytically. Some advanced formulae have been developed based on theory or measurement. In general the variables involved are critical velocity (u_*), water density, and size and density of material. The first two factors represent the flow condition, and the last two variables represent sediment characteristics. Kalinske (quoted in Bogardi, 1974) has tried to relate these factors in his formula

$$q_s = A_s \left(\frac{u_*^2}{(\frac{\rho_s}{\rho_w} - 1) \cdot g \cdot d_{50}} \right)^p \cdot u_* \cdot d_{50} \qquad (2.49)$$

where d_{50} = median diameter of particle (m),

A_s, p = constant

Based on the examination of the Brantas River, East Java-Indonesia (Department of Public Works, 1966), it was found that the constant factors A_s and p in equation 2.49 were 4.0514 and 2.135 for A_s and p respectively. Thus,

$$q_s = 4.0514 \left(\frac{u_*^2}{(\frac{\rho_s}{\rho_w} - 1) \cdot g \cdot d_{50}} \right)^{2.135} \cdot u_* \cdot d_{50} \qquad (2.50)$$

2.7.4 Tidal Response on Sediment Movements

The vertical water movements associated with the rise and fall of the tide are accompanied by horizontal water motion termed tidal currents. In the open ocean

or near an unbounded body of water these currents are rotary in nature, changing speed and direction throughout all compass directions during a tidal cycle. The rotation is mainly due to the Earth's rotation. In the Northern hemisphere the rotation is in a clockwise manner.

In narrow channels or estuaries, tidal currents are restricted to flow essentially along one path in a reversing direction: landward currents during flood tide and seaward currents during ebb tide. These currents are responsible for resuspending and removing sediment either up or down the estuary. In the case of a symmetrical tide the net resulting transport may be insignificant. When the tide is asymmetric the volumetric difference between the upward and downward transports can be considerable.

In the case of asymmetric tides, the flood period is always shorter than the ebb period, and flood currents become stronger than ebb currents. Consequently there is a great movement of sediment landwards. The longer slack water at high water (than that at low water) enables a greater proportion of the material to settle to the bed. Thus the combination of the greater velocity on the flood tide and the settling at high water produces considerable deposition along the estuary. Part of this deposited material is resuspended and transported back downstream by ebb currents.

Normally the vertical distribution of velocity of the ebb current is high near the surface in the upper layer and low near the bottom. In contrast the flood current is high near the bottom and low at the upper layer. Currents near the bottom are responsible for picking bottom particles up into suspension. As a result, the

concentration of sediment is higher during the flood tide than during the ebb tide.

Wright, et.al. (1973) has examined tide-dominated estuaries where standing waves are usually developed. In this case, the currents are maximum at mid-tide and slack at high and low waters. Consequently, when the water levels are highest and inundate the widest surface area, currents are weak. In the Ord River (Australia) this effect resulted in an extensive deposition of silts and clays from suspension along the higher levels of the river banks (Wright et. al., 1975).

As the currents within the estuaries are derived from both tidal and non tidal currents (current generated fresh water flow and density currents), it is difficult to determine the sediment transported by the tide only. However, if the non tidal currents are minor, the tidal transport can be estimated from the direct measurement of sediment concentration in association with the water level during a tidal cycle for a certain tidal range.

Another way of estimating the tidal effect on sediment movement is by measuring the estuarine currents directly since the movement of sediment is a function of current speed. Bed material will move whenever the critical current exceeds the velocity of erosion U_e. The material will settle whenever the critical velocity for deposition U_d is achieved. Based on limited field data, Dronkers (1986) found that these velocities, U_e and U_d, are about 0.5 m/s and 0.2 m/s, respectively. Although these values are still questionable whenever they are used in different situations and circumstances, the values can be used to estimate whether or not the observed estuarine currents affect the sediment movement.

2.7.5 Wave Effects on Sediment Movements

When a deep-wave approaches a shoreline at an oblique angle it generates two different currents: longshore and rip currents. These two currents are responsible for transporting sediment within the surf zone. Sediment which is usually moved parallel to the shoreline is termed longshore transport. At present, two basic methods have been developed to estimate the amount of longshore transport in relation to the wave climate: an Energy Flux Method and an Empirical Method (U.S. Army CERC, 1984, p. 4-91 to 4-108).

In the energy flux method, the rate of longshore transport Q is assumed to be dependent on the longshore component of energy flux in the surf zone. The longshore energy flux in the surf zone is approximated by assuming conservation of energy flux in shoaling waves, using small amplitude theory, and then evaluating the energy flux relation at the breaker position. The approximation for the longshore component of energy flux at the breaker line (P_{lb}) is given by (U.S. Army CERC, 1984, p. 4-93)

$$P_{lb} = C_b \left(\frac{\rho g H_b^2}{8}\right) \sin\alpha_b \cos\alpha_b \qquad (2.51)$$

where H_b is the wave height, C_b is the wave speed at the break points, and α_b is the angle between the advancing wave crest and the shore line at the break point, ρ is seawater density, and g is acceleration due to the gravity.

Equation 2.51 is valid only for a single wave train with one period and one

height. Most ocean wave conditions are characterized by a variety of heights that are distributed in a Rayleigh distribution (U.S. Army CERC, 1984, p. 4-93). The correct height to use in equation 2.51 is the root-mean-square height, H_{rms}, that is defined by

$$H_{rms} = \sqrt{\frac{1}{N}\sum_{j=1}^{N} H_j^2} \tag{2.52}$$

where H_j is the height of successive individual waves, N is the total number of the recorded waves. However, most wave data are available as significant heights H_s , and coastal engineers are used to dealing with H_s rather than H_{rms}. Therefore the value of H_s may be substituted into equation 2.51 to produce the longshore component of energy flux (P_{ls}). Thus

$$P_{ls} = \frac{\rho g H_s^2}{8} C_g \sin\alpha\cos\alpha \tag{2.53}$$

The value of P_{ls} computed using significant wave height is approximately twice the value of the exact energy flux for a sinusoidal wave height with a Rayleigh distribution. This means that P_{ls} is proportional to energy flux but not equal to it. Therefore P_{ls} is termed the longshore energy flux factor (U.S. Army CERC, 1984, p. 4-93). Galvin and Schweppe (1980) (U.S. Army CERC, 1984, p. 4-93 to 4-94) derive some variations of energy flux (P_l) and longshore energy flux factor (P_{ls}), depending on wave data available. In the case where the wave climate in deep water is available, the energy flux factor is given by

$$P_{ls} = 0.05\rho g^{\frac{3}{2}} H_o^{\frac{5}{2}} (\cos\alpha_o)^{\frac{1}{4}} \sin 2\alpha_o \tag{2.54}$$

where H_o is the deep water wave height and α_o is the angle between the incoming wave crest and shoreline.

Longshore transport (Q_{α_o, H_o}) can be estimated from the relation given by (U.S. Army CERC, 1984, p. 4-101)

$$Q_{\alpha_o, H_o} = (f A P_{ls})_{\alpha_o, H_o} \tag{2.55}$$

where f is the percentage wave frequency, and A is a dimensional constant. For metric units A = 1290 (m^3 s/N yr), so that

$$Q_{\alpha_o, H_o} = 2.03 \cdot 10^6 f H_o^{\frac{5}{2}} F(\alpha_o) \tag{2.56}$$

where

$$F(\alpha_o) = \left[(\cos \alpha_o)^{\frac{1}{4}} \sin 2\alpha_o \right] \tag{2.57}$$

The value of $F(\alpha_o)$ is calculated as an average value for waves coming from a sector generally 45° or 22.5° (U.S. Army CERC, 1984, p.4-103).

In the Empirical Method the longshore transport rate is assumed to depend partly on breaker height, since as breaker height increases, more energy is delivered to the surf zone, and the surf zone through which sediment moves is widened. Galvin (1972) showed that the relationship between average breaker height, H_b, during a one year period and Gross Longshore Transport Q may be written as

$$Q = 1.646 \times 10^6 H_b^2 \tag{2.58}$$

where Q is given in M^3/year and H_b in metres. H_b can be calculated from the following relation

$$H_b = \sum \frac{(K_s)_b}{(K_s)_g} f H_g \qquad (2.59)$$

where $(K_s)_b$ is the shoaling coefficient evaluated at the breaker position and $(K_s)_g$ is the shoaling coefficient evaluated at the wave gage, f is the percentage frequency of the wave heights, and H_g is the significant height obtained from gage records and assumed to correspond to the height obtained by visual observers.

2.7.6 Estuarine Sediment Budget

As mentioned earlier, sediment entering an estuary typically originates from river borne and marine sources. The sediments are distributed either along the estuary or in the near shore area and/or in the ocean. Calculation of the amounts of sediment moving, remaining, or taken from the estuary is usually called the sediment budget. It includes estimation of transportation, deposition, and erosion processes of sediment materials within the area considered.

The residual in the sediment budget can be estimated by balancing sources and sinks. A source is any process that increases the quantity of sediment material within the estuary. Conversely, a sink is that which decreases sediment material. A schematic of sediment budgeted in an estuary is shown in Figure 2.9.

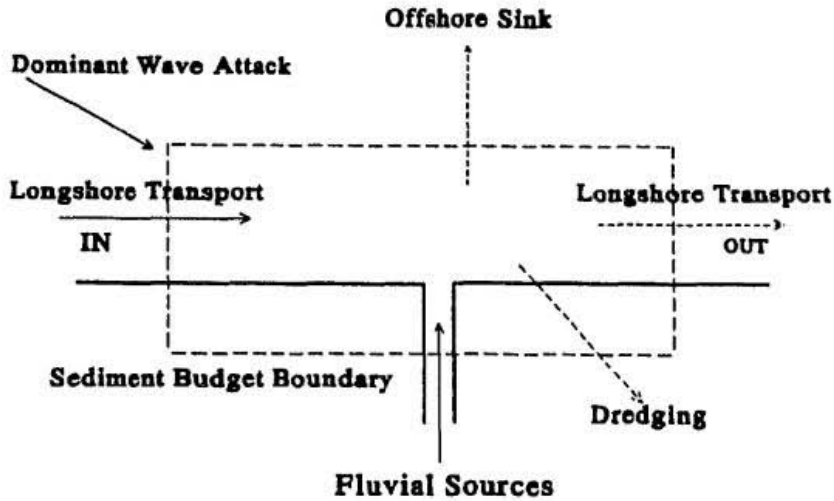

Figure 2.9 Schematic of Sediment Budget in Estuary

In the complete estuary sediment budget, the difference between the sediment gained from all sources and the loss of sediment to all the sinks should be zero. In some cases, the sediment budget is used to estimate the unknown erosion and/or loss of material to the sea or deposition within the estuary. The total budget is

Total sources - total sinks = 0

or Total sources - total sinks = unknown

The main sources are river-borne and littoral transport. Sinks occur because of dredging or mining or by sediment being lost to an offshore area. The volume of river-borne sediment and the littoral transport can be estimated by using sediment carrying capacity, and longshore transport rates, respectively as discussed in the preceding sections. Dredging and/or mining can be determined from records.

2.8 River Deltas

Deltaic estuaries develop wherever a river, particularly one that carries substantial quantities of sediment, debouches into a receiving basin through several mouths.

The term delta was first used by the Greek historian, Herodotus, in approximately 450 BC to describe the triangular deposition of sediments at the mouth of the Nile River which, being triangular, resembled the Greek capital letter delta, Δ (Bearman, 1989, p. 129). In general, deltas can be defined as coastal areas or near shore features developed from river-borne sediments such as river mouth bars, tidal flats, tidal ridges, beach dune complexes, swamps, marshes, and evaporite flats.

2.8.1 The Structure of Deltas

A delta plain generally consists of a subaerial delta and a subaqueous delta. Figure 2.10 illustrates the major components of a delta plain. The subaerial delta is the portion of the delta plain above the low tidal limit. This portion typically consists of a lower delta plain and an upper delta plain. The lower delta plain lies within the region of river-marine interaction and extends landward to the limit of tidal influence. The upper delta plain is the older portion of the subaerial delta and exists above the area of significant tidal or marine influence. The subaerial delta is dominated by river processes.

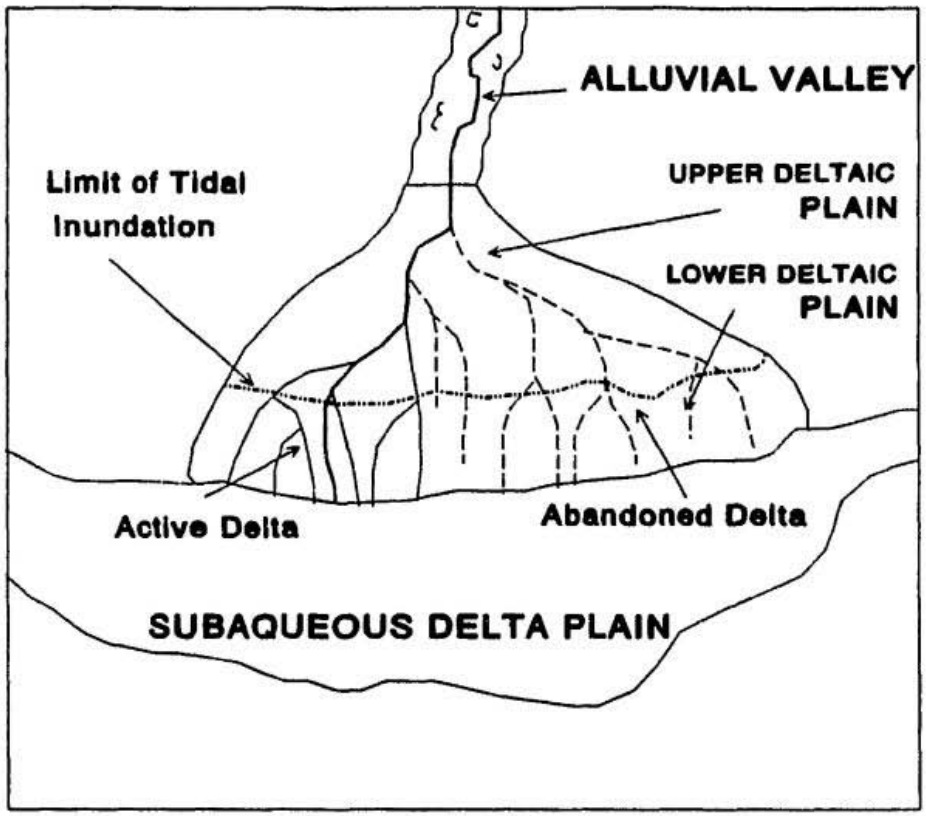

Figure 2.10 Components of a Delta Plain (*After Coleman, 1982*)

The subaqueous delta is the portion of the delta plain that lies below the low-tide water level. The subaqueous delta plain consists of the delta front and the prodelta. The delta front is the segment that is adjacent to and seaward of the lower delta plain. It is composed in part of bed load and may contain coarse material such as sand and gravel. The prodelta is the most seaward part of the subaqueous delta and is composed of the finest material (clay and silt) deposited from the suspension.

Both the subaqueous and subaerial deltas may consist of active and

abandoned deltas. The active delta plain is the growing portion occupied by functioning distributary channels. An abandoned delta plain develops when the lower course changes its direction to a shorter or more efficient route to the sea.

2.8.2 Deltaic Processes

The deposition, orientation, and morphologic patterns and sedimentary sequences of a delta are produced by a complexity of interaction among numerous fluvial and coastal processes. Wright (1977) identified the processes that strongly influence the formation of various types of deltas. These are, the discharge regime and sediment load of the associated river; the nature of the river mouth processes; the relative magnitude of marine forces, particularly tides, waves and their modification near shore, and the receiving basin geometry. Figure 2.11 illustrates schematically the major factors and their contributions to the delta formation. The following section will briefly review the contributions of the fresh water flow and wave effects to the development and formation of deltas.

The general configuration of a delta depends on the relative degree of the contribution between wave energy flux adjacent to the shore and river discharge (Wright and Coleman, 1972). If the effects of the river discharge and sediment load are high in comparison with the effects of the wave energy flux, sediments will be deposited just beyond the river mouth and the adjacent coast and protruding deltas are developed. In contrast, if river sediment discharge is relatively small and wave energy

high, the wave will quickly rework the river-borne sediments into a marine-dominated delta configuration.

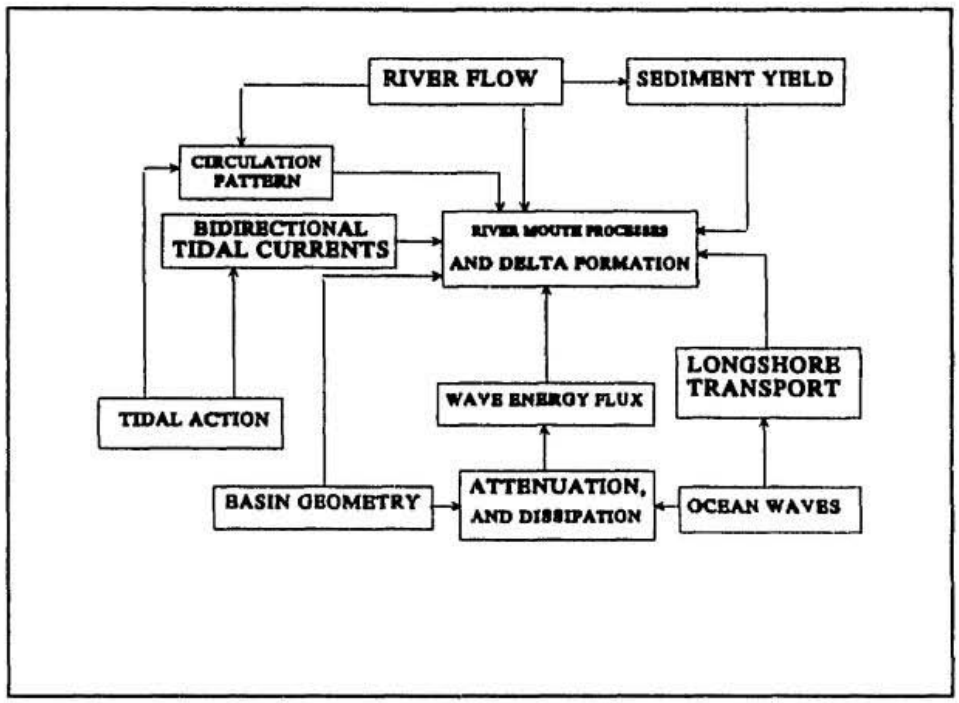

Figure 2.11 Major Factors Control on a Delta Formation

The preceding basic concept is insufficient to completely explain the effects of the strength of the river discharge relative to that of the wave force. Variation in discharge throughout the hydrologic year is the most important flow characteristic which exerts great influence on deltas geometries.

If the discharge peaks coincide with the times of greatest wave energy, the increased river sediment supply may be balanced by the capacity of waves to redistribute the sediment. This situation tends to give a regular and smooth progradation

of the delta shoreline. If, on the other hand, discharge and wave-energy maxima are out of phase, then the river outflow may dominate for part of the year, and this will be followed by a period of intense reworking by the waves. In this condition, spits and barrier beaches along the coast flanking the river mouth will likely be developed.

A number of experts such as Davies (1958), Jennings (1955) and Wright and Coleman (1971) have tried to quantify the relationship between discharge-wave power and delta geometry. In this thesis, the discharge effectiveness index, I_Q, proposed by Wright and Coleman (1971, 1972, 1973) will be used to identify the degree to which delta morphology is wave dominated or river-dominated. This index is the ratio of discharge per unit width of river mouth to the near shore wave power per unit length of wave crest. Thus

$$I_Q = \frac{q}{P} \qquad \textbf{(2.58)}$$

where q is river discharge per unit width of river mouth and P is the near shore wave power per unit length of wave crest.

A low value of the index, I_Q, relates to a wave-dominated delta which exhibits wave straightened shorelines and abundant beach ridges. A high index relates to a river-dominated delta with sand bodies deposited at high angles to the shoreline.

Observation of seven deltas made by Coleman and Wright (1972) may be used as a standard. The results of the work of Coleman and Wright represent a spectrum of deltas types reflecting processes ranging from river dominated, low wave energy to wave dominated, low fluvial influence, as presented in Table 2.4 below.

Table 2.4 Mean Annual Summaries of Discharge/Wave Power Climate and Attenuation Ratios of Seven Deltas (*After Wright and Coleman, 1972*)

Delta	Mean Annual Wave Power(J/s-m)		Mean Discharge 10^3 m^3/s	Mean Annual Discharge Effectiveness Index	Mean Annual Attenuation Ratio
	Deep water	Near shore			
Mississippi	106.0	0.013	17.69	5477.0	7913.3
Danube	23.0	0.014	6.29	1171.0	2585.0
Ebro	72.8	0.051	0.55	267.8	1299.5
Niger	67.6	0.659	10.90	4.4	102.8
Nile	136.0	3.210	1.47	3.2	42.5
Sao Francisco	371.0	9.970	3.12	1.3	37.2
Sinegal	156.0	37.700	0.77	0.3	4.2

2.8.3 Deltaic Geometries

Delta geometries are controlled by a number of factors that vary broadly between one delta and another. As result each delta has its own individual attributes that set it apart from the others. Depending on the magnitude of the three major controlling factors: river process, tide, and waves, deltas can be grouped into three major shapes: river dominated deltas, tide dominated delta, and wave dominated delta. In some cases the three factors work together, and other factors must also be taken into account. Coleman and Wright (1973) concluded that deltas are be classed into six general types. These six types of deltas are illustrated in Figure 2.12.

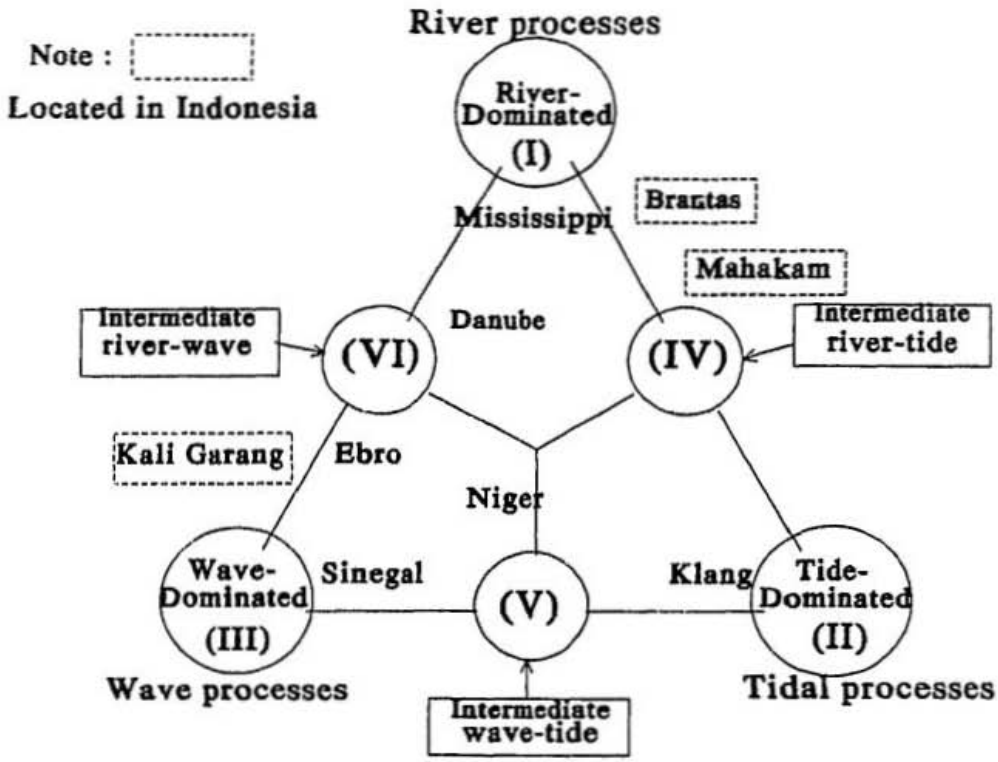

Figure 2.12 The Classification of Various Delta Morphologies Based on the Relative Strength of River, Tidal and Wave Processes.

Chapter 3
Indonesian Estuaries and Deltas

Nearly all Indonesian estuaries are drowned river valleys, also known as coastal plain estuaries or rias. They were formed within the last 15,000 years during the Flandrian transgression which ended approximately 5,000 years ago. A rise in sea level of 100 to 130 m subsequent to the Wiscosin glaciation inundated river valleys, creating these estuaries. They are being progressively infilled with sediment. The natural sediment discharge from these rivers is high and limited wave and tidal action leads to the estuaries being rapidly filled. As a result, deltas soon develop seaward of the river mouths.

This chapter deals with general characteristics of estuaries and deltas in Indonesia and major factors related thereto. Two river-delta systems; the Mahakam and Brantas Deltas, have been chosen to represent the formation of deltas with different river characteristics. Figure 3.1 shows the location of these two deltas.

It is known that numerous factors determine and affect the characteristics of a river system. Figure 3.2 illustrates the various components of a river system and major factors that control each part. The major factors affecting the river system are climate, geology, morphology and other hydrological factors, tides, waves, and winds.

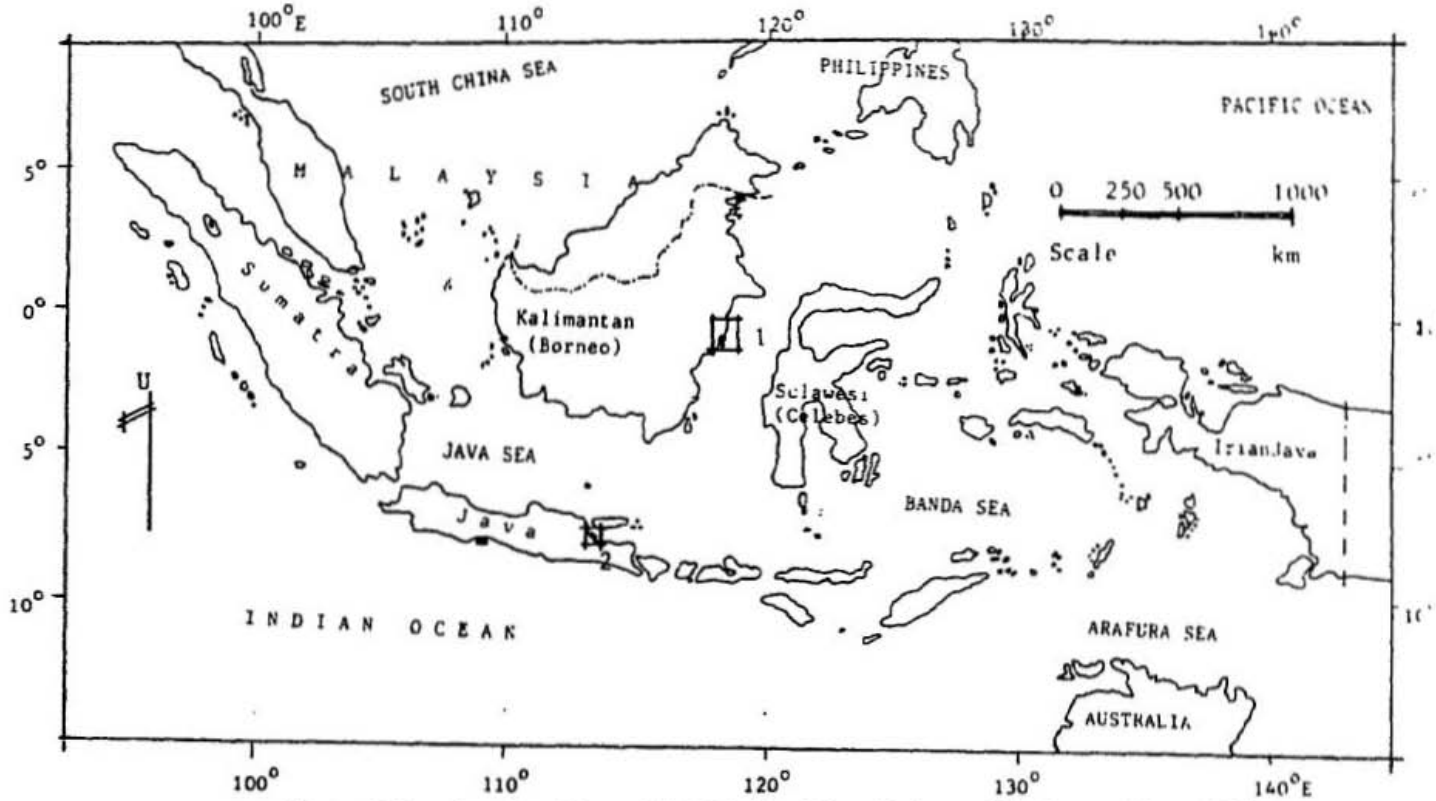

Figure 3.1 Location Map of *1*) Mahakan River Delta and *2*) Brantas River Delta

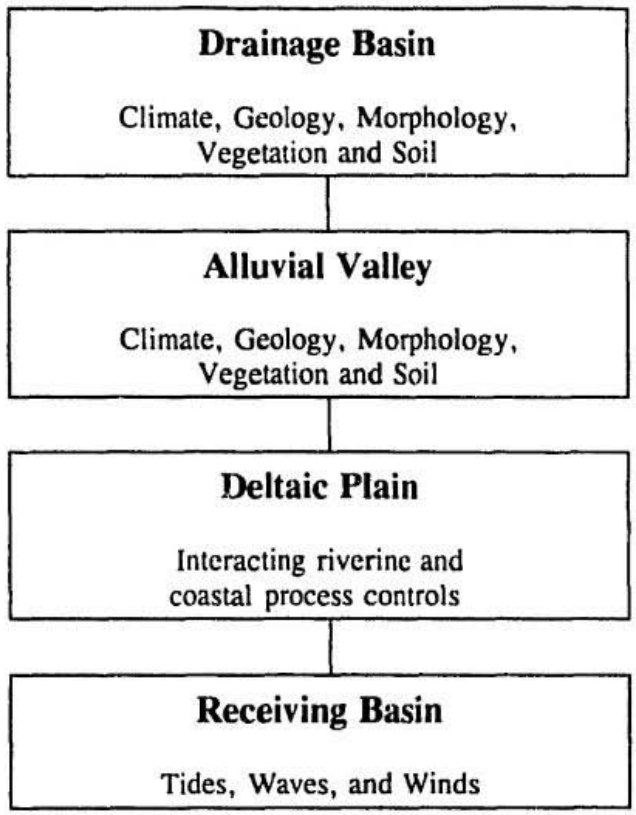

Figure 3.2 Components of River System and Major Process Controlling Each Part.

3.1 Topography and Geology

Indonesia is an archipelago composed of five major islands; Java, Sumatra, Kalimantan (Borneo), Sulawesi (Celebes), and Irian Jaya (New Guinea). It is located along the equator between 06°50'N and 11°60'S and between 92°25'E and 141°30'E. It is bounded by two continents, Asia in the North and Australia in the

South, and two oceans, the Indian ocean in the West and the Pacific in the East. All major islands, except Kalimantan, are laid over the earthquake epicentre of the Circum-Pacific belt. Therefore there are many either active and non active volcanoes. This situation causes the features of Kalimantan Island to be different from the others. The general topographic and geology of the main islands can be described as follows.

Java Island.

Java Island is a long island, extending in a west-east direction. The land features are mountainous with a number of volcanoes. Some are active while other are not. There are at least thirty mountains that lie on south-side along Java Island. Their elevation ranges from 1,750 m to 3,416 m above sea level. The coastal plain extends along the north side of the island. Java is the most densely populated island. About 60 % of the total population of Indonesia (180 million) lives on Java, which is only 1/15 of the total area. As a result of the high population, much of the tropical forest that originally covered the land has been changed to settlement areas or to farmland.

The main river systems of Java Island are the Brantas, the Solo, and the Citarum Rivers. These rivers originate from hilly areas and flow down through low lying, densely populated areas before they debouch into the ocean. The Brantas River debouches into the Madura Strait and the other two into the Java Sea.

All over the island, a large scale upheaval took place in Mio-pleocene or later periods accompanying a series of volcanic eruptions having an east-west trend.

The geology of the island, therefore, is characterized by eolian and sedimentary formations of Neogene Tertiary and andesitic and basaltic rock of volcanic origin.

Sumatra, Sulawesi, and Irian Jaya.

Topographically these three islands are almost the same as Java Island. Sumatra is a long island extending in the southeast-northwest (SE-NW) direction. A series of mountains and volcanoes lies on the southwest-side of the island. The northeast side consists of lowland, marshes and coastal plain. Sumatra has an area some three times that of Java Island. The main streams of Sumatra are the Musi, Batang Hari, and Batang Indragiri Rivers. These three rivers originate from the mountains and flow northeastwards through the lowland. Sulawesi has no big river, since the island is convoluted and no part is more than 150 km from sea. Irian Jaya is a mountainous island. It contains the highest mountain in Indonesia (i.e., Puncak Jaya; 5,020 m above sea level). The Memberomo River is the major river of Irian Jaya. The coastal plain is mainly laid on the south side of the island. These three islands are less populated than Java. Only about 30% of the total Indonesia population lives there.

Kalimantan (Borneo).

Kalimantan is the biggest Island among the Indonesian Islands. Its area is about three and a half times that of Java Island. Kalimantan is located on the equator.

The land features are less hilly, and it is mountainous only in the middle of the island with the highest elevation being about 2,988 m above sea level. Most of the land consists of lowland and coastal plain and is covered by tropical forest. The population is only about 10% of the total Indonesian population. People live primarily on low lying land near a river course where most cities developed.

The main rivers in Kalimantan are the Mahakam, Barito, and Kapuas Rivers. These rivers are characterized by a very small slope, particularly in the lower reaches. In consequence, the river water is almost stagnant during low river discharge. This causes the flushing time to increase and, since the rivers are used both as water supply and for sewage disposal, the water quality decreases accordingly.

3.2 Climate

Climatic conditions are affected by monsoons. The east monsoon usually lasts from April to November and the west monsoon from December to March. Figures 3.3 and 3.4 show the general directions of the east monsoon and the west monsoon, respectively. The west monsoon brings considerable rain and causes heavy floods all over the country. However the east monsoon is dry and rainfall is sparse. Therefore the river discharge fluctuates seasonally with the maximum occurring during January-February and the minimum during July-August. The annual rainfall ranges from 1,600 mm to 2,500 mm.

The region is entirely within the tropics, so that there is little variation

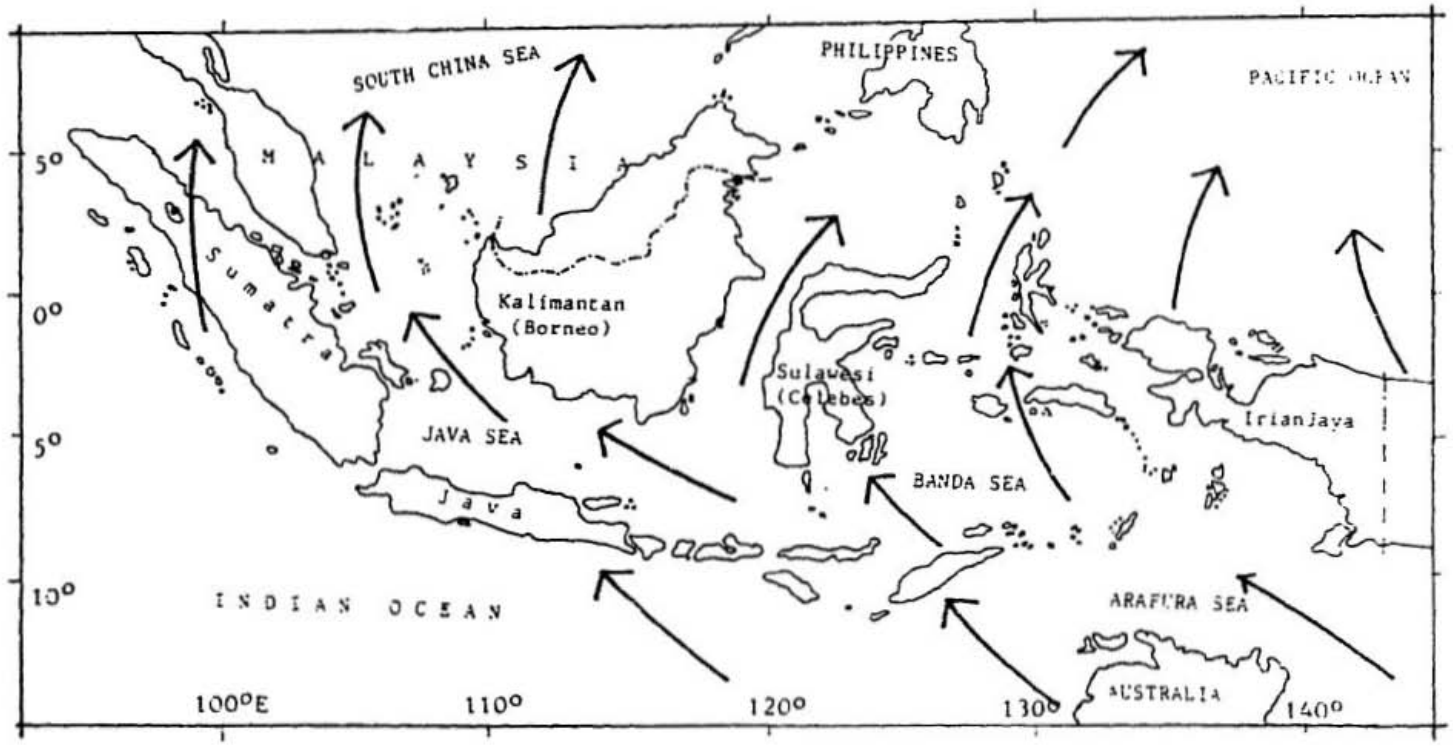

Figure 3.3 Generalized Direction of the East Monsoon Over Indonesia, April to November

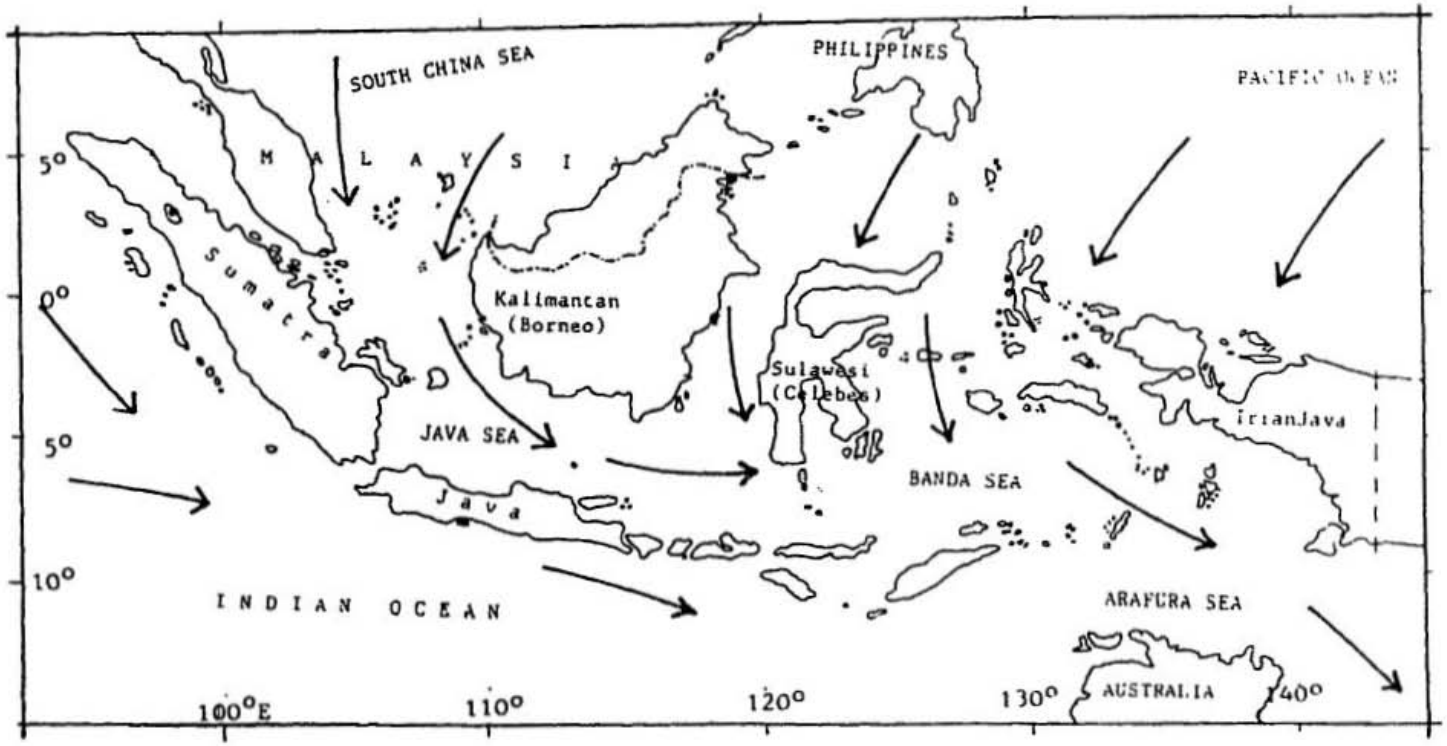

Figure 3.4 Generalized Direction of the West Monsoon Over Indonesia, December to March

in air temperature throughout the year. The monthly mean temperature ranges from 23°C to 30°C. Humidity all around the area is relatively high. Yearly mean relative humidity varies from 80% to 90%, while the monthly mean relative humidity ranges from 60% to 90%. Daily evaporation varies from 1.4 mm/day to 6.5 mm/day with maximum evaporation in August to September and minimum in January to February. This humid tropical condition led to lands originally covered by tropical plants and grasses. The tropical environments are also conducive to the production and preservation of organic material and peat deposits.

3.3 River Sediments

The main source of sediment entering Indonesian estuaries is via the fresh water flowing in at the head of the estuary. Amounts of sediment supplied from the drainage basin are dependent upon its various hydrological factors but normally greatest transport occurs at maximum storm run off.

The monsoon, tropical, areas of Indonesia have a naturally high rate of sediment potential. Materials originate from the erosion of the drainage basin and from material of volcanic eruption. Volcanic material is dominant in a number of Javanese rivers. Most of the sediment flows down into the estuary during high precipitation during rainy season.

3.4 Waves

Wind generated waves which affect the Indonesian coasts are mainly those associated with the west monsoon and the east monsoon. Waves may occur due to submarine earthquakes or under water volcanoes but these are a rare occurrence. There are no storm waves directly associated with tropical hurricanes since the region is out of the tropical cyclone area. Exposed Indian coast sectors in the south of Java and northwest of Sumatra, and the exposed Pacific coast of north Irian Jaya are typically subjected to high wave regimes. Therefore, there are steep, sandy coasts. Other coasts are generally subjected to low to moderate wave regimes. These coasts are subjected to seasonally altered longshore drift directions although the eastern drift component appears to dominate (Silvester, 1974).

3.5 Tides

There have been relatively few tidal studies in Indonesia other than the published tide tables in some main harbours. However, several generalizations may be made from available information. Basically, most of the coasts are mesotidal coasts (tidal range 2-4 m) except the north-coast of Irian Jaya and northwest-coast of Sumatra which are microtidal coasts (tidal range < 2 m).

3.6 The Mahakam River Delta

The Mahakam River (Figure 3.1) is located on the east coast of Kalimantan (Borneo) between 0°21' and 1°10' southern latitude and between 117°15' and 117°40' eastern longitude. The river debouches into a restricted basin of Makassar Strait. The drainage basin of the river covers almost one third of the island of Kalimantan. The monsoon-tropical climate in the drainage basin results in discharge with an average discharge of 1,500 m^3/s, but with high fluctuation (Dutrieux, 1990). Tides along this portion of the Kalimantan coast are semi-diurnal with an average range of 2.5 m.

Large quantities of sediment (160 mg/l) are transported by the Mahakam River. The delta plain comprises some 1,500 km^2 and consists of numerous bifurcating distributaries (Figure 3.5). Channels form a divergent network of variably important rivers. The delta plain has a very flat topography (0.1 % slope) and is covered by an extremely dense vegetation, particularly mangroves.

The important factors affecting the Mahakam River Delta are river processes and tidal action. High river flow, particularly during rainy season, is restricted by shallow water beyond the river mouth. River mouth processes, however, are dominated by frictional forces. Consequently, the high sediment load of fine-grained deposits from upstream are spread laterally over a large area seaward of the river mouths. The wide, lateral, distribution of this sediment builds an unstable platform across which some distributaries developed. Decreasing river flow during the dry

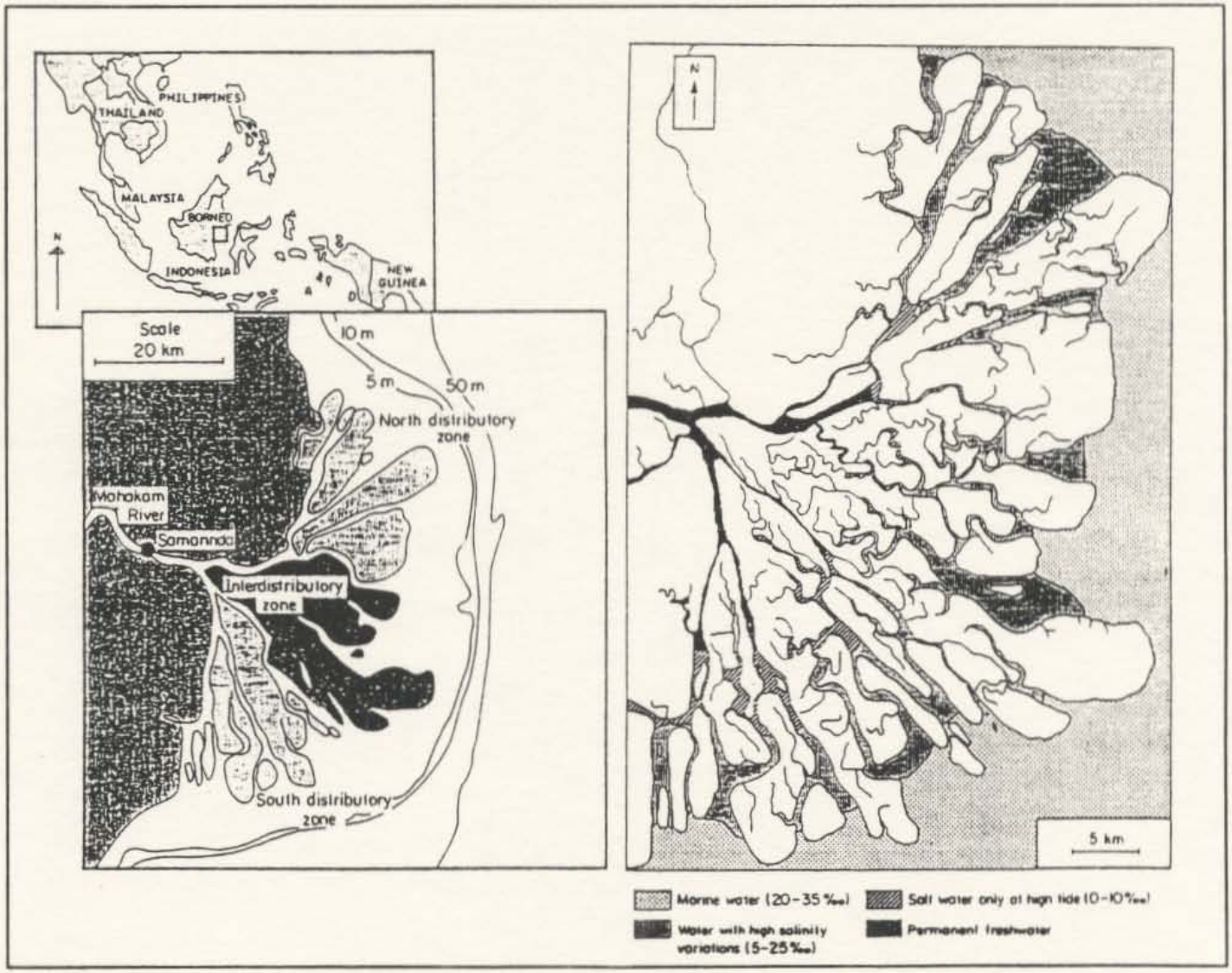

Figure 3.5 The Mahakam River Delta, Kalimantan-Indonesia

season causes the effect of tidal currents to become significant. During the spring tide the sea water intrudes as far as 25 km landwards of the distributary mouth (Dutrieux, 1990). Sea water inundates almost all parts of the delta plain. Slack flood water occurs during high water and the sediment load which is resuspended by tidal currents is deposited in the form of levees. The ebbing water flows over the delta plain and forms a numerous of crevasses.

3.7 The Brantas Delta

The Brantas River (Figure 3.1) is located in east Java between 07°01' and 08°15' southern latitude and between 110°30' and 112°55' eastern longitude. The river debouches onto the close-end, narrow basin of Madura Strait. An area of 12,000 km^2, consisting of a series of hills and volcanoes, form the drainage basin. The monsoon, tropical, climate in the drainage basin results in discharges with considerable fluctuation. Average discharge is about 200 m^3/s but daily flows vary from 60 m^3/s to 1,600 m^3/s. Tides around the coast in this area are mixed, dominant semi-diurnal with an average range of 2.0 m.

The Brantas River transports large quantities of sediment that originate mainly from the eruption of Kelud volcano and a small part from the erosion of the catchment basin. The annual fluvial load is some 11.2 x 10^6 m^3. In it lower reaches, the river splits into two branches. These are the Surabaya and Porong man-made branches. The delta, which is river dominated, develops seawards of the mouth of the

Porong branch where most river flow has been directed. Delta growth is about 300 m seawards per annum. The delta plain has a very flat topography (0.1 % slope) and is mainly used as shrimp pond.

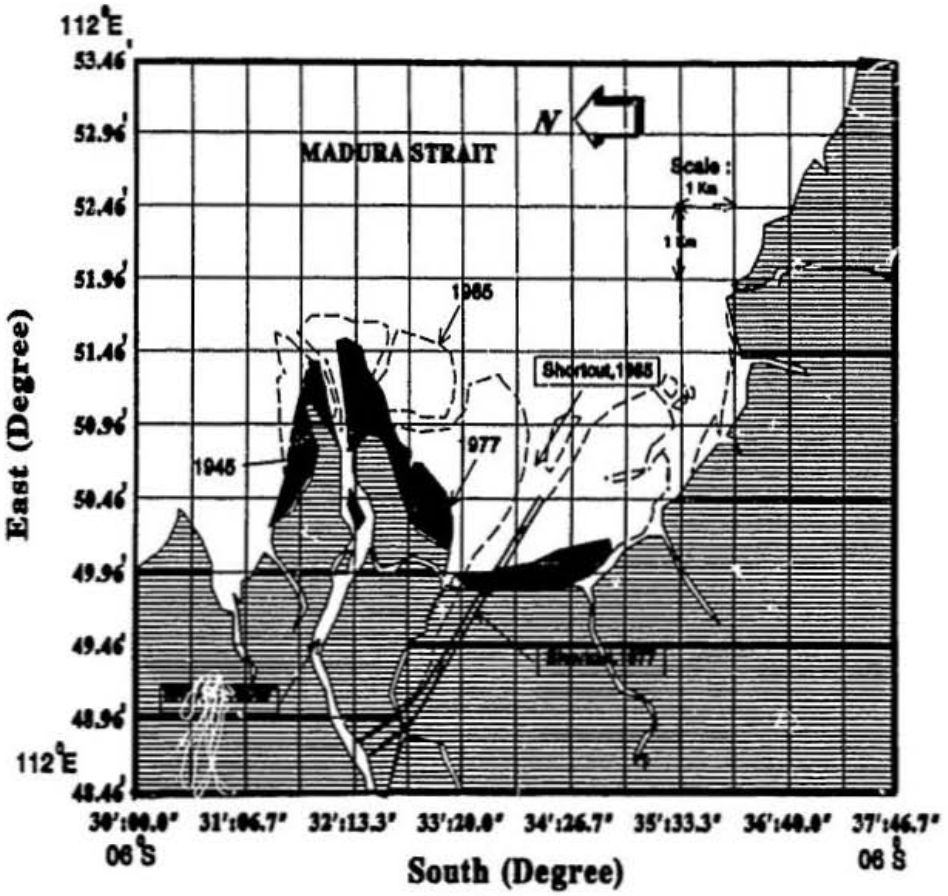

Figure 3.6 Schematic of the Brantas Delta, East Java-Indonesia.

The important factors affecting the Brantas River Delta are river processes and tidal action. A high river flow during the rainy season dominates the

processes within the delta region. Decreasing water flow during the dry season allows tidal action to play a significant role in redistributing the river delta. Also, coastal waves mainly arise from the east, since those from the other directions are fetch limited either by Java or Madura Islands. Waves are generated by the east monsoon. Thus the wave power and the maximum river discharge are out of phase. The near-shore wave power is small due to the dissipation of a very gentle slope of the receiving basin. As a result the delta shoreline is irregular and is composed from fine grained sediment.

Chapter 4

The Estuary of The Kali Garang

4.1 General Characteristics

The Kali Garang (Figure 4.1) is situated in Semarang, Central Java, between 6°50' and 7°10'S and between 109°50' and 109°35E. The river originates from the Ungaran Mountain and flows into the Java Sea. It is formed by the confluence of three tributaries; the Upper Kali Garang, Kali Kreo, and Kali Kripik. The three tributaries flow parallel northward and join to form the main channel of the Kali Garang about 9 km south-southwest and upstream of Semarang city and about 5 km upstream of Simongan Weir. The weir splits the river flow into two branches; Kali Semarang and West Channel. The weir also controls the flow in both branches which debouch into the Java Sea.

The Kali Garang has a total catchment area of 196 km^2 which consists of the basin of the Upper Kali Garang (67.95 km^2), the basin of the Kali Kreo (34.58 km^2), the basin of the Kali Kripik (61.84 km^2), and the lower basin (31.63 km^2). Administratively, the area includes the municipality of Semarang, Semarang regency, and Ungaran regency. With a total population of about 1.1 million in 1987, the maximum

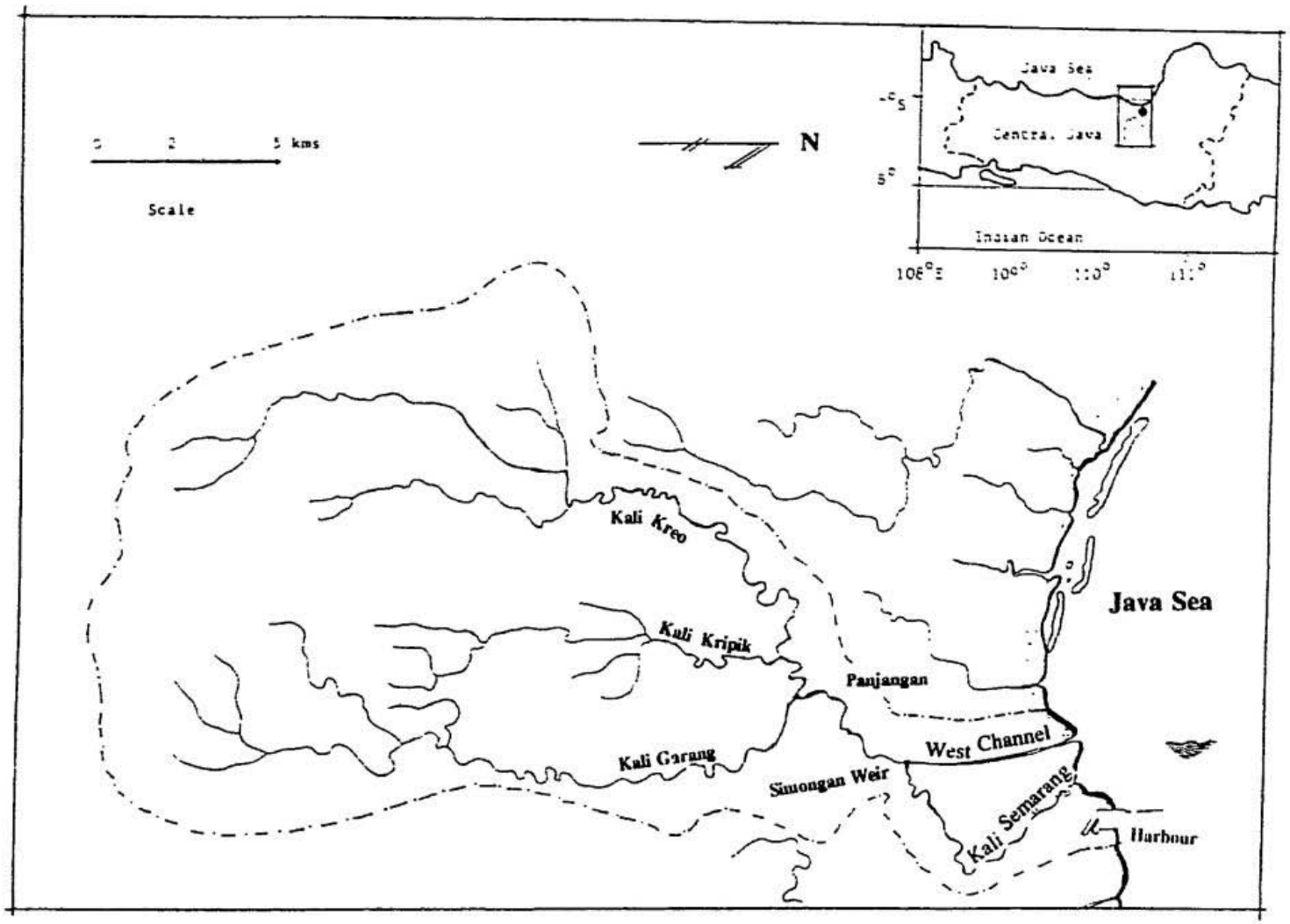

Figure 4.1 Location Map of the Kali Garang River System

density was 25,100 people per square kilometre in the lower basin, and a minimum density was 5,000 people per square kilometre at the upper basin.

Present land use consists of paddy fields (16.57 %), upland fields (27.44 %), marsh and swamp (5.90 %), forest (4.50 %) plantation (2.60 %), urban settlement (32.00 %), and others (10.99 %).

4.1.1 Topography

Kali Garang river basin can be considered in two parts: upper and lower. The upper part is situated on the hilly area of the Ungaran mountain on the South side, and has a slope of 15 to 40%. With an average elevation of about 50 to 125 m above sea level, the land consists mainly of upland field with irregular plants cover, plantation, and a small part of forest. The lower part, that extends along the seashore at the South side, has a slope of 0 to 2 %, and an elevation about 5 m above sea level. It consists of settlement areas, paddy fields, marshes and swamps.

4.1.2 Geology

Geologically, the upper basin of the Kali Garang is generally volcanic rock, volcanic breccia, and sandy rock all of which derive from volcanic eruptions. The lower basin is formed from the alluvial material deposited by the Kali Garang and its tributaries. This is mostly from clay, silt and sand.

In general, the drainage basin has a high erosion rate. Annual soil loss ranges from 5 mm (high erosion rate) to 2 mm (low erosion rate) (Department of Public Works, 1982).

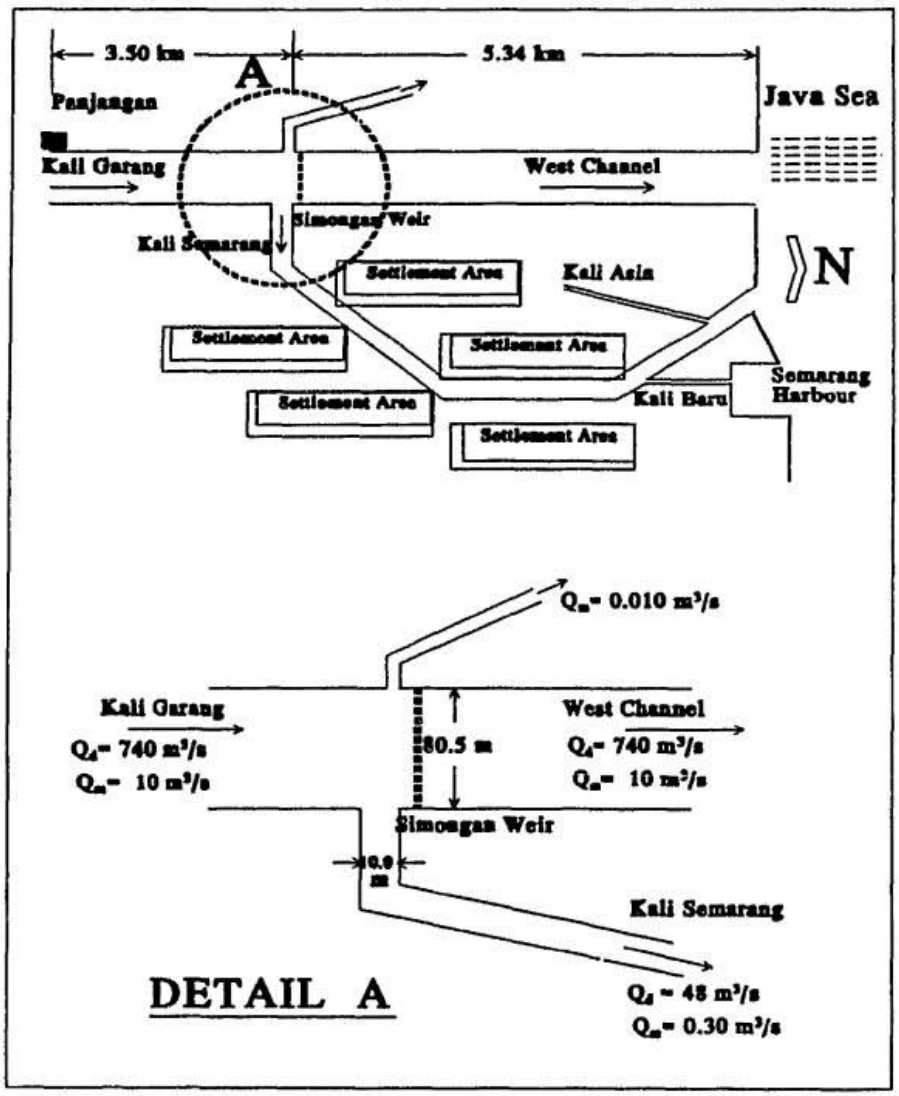

Figure 4.2 Sketch chart of the Kali Garang Estuary and the Simongan weir

4.1.3 The Simongan Weir

The Simongan weir as well as the West Channel is a part of the flood control system of Semarang city that was built by the Dutch during the Colonial period in the 1900's. The weir is located about 5 km downstream of the confluence of the tributaries and splits the Kali Garang into two branches; the Kali Semarang and the West Channel. Freshwater flows into both branches are controlled by the weir. During the dry season the freshwater discharge released by the weir into the Kali Semarang is maintained at 0.20 m^3/sec. No freshwater is released during the rainy season. In times of fresh water flood, however, the excess discharge is directed by the weir through the West Channel.

Weir dimensions can be summarized as follow. The weir crest is 64.60 m long. Two sluice gates, each 2.60 m wide are located at both sides of the weir. The weir crest and downstream elevation are + 5.60 m and + 1.40 m, respectively. The bed elevation upstream of the weir is +3.70 m. Flow into the Kali Semarang passes through seven gates each 1.80 m wide. The base elevation of each gate is +4.00 m.

4.1.4 The Kali Semarang Channel

The Kali Semarang Channel is the original lower reach of the Kali Garang. It flows through the densely inhabited area of Semarang city and extends north-eastward from the Simongan weir with a north-west turn about four kilometres from

Java sea. The total length is 8,240 m.

Today the Channel is used as a drainage and flushing channel for Semarang city. The gate that connects the Channel to the Kali Garang is closed throughout rainy season, and is only opened during the dry season.

In 1984, the river channel was improved by The Committee of Normalisation of Kali Semarang. Its course was realigned and its banks were protected by constructing vertical walls. The river width varies from 42 m at the mouth to 10 meters towards the weir, with bed slopes varying from about 0.0002 to 0.0007.

Various current feature of the Kali Semarang and the design discharge at several points along the channel are summarized in Table 4.1 and Figure 4.3 below.

Table 4.1 The present feature of the Kali Semarang

Section	Distance from the weir (m)	Bed Elevation (m)	Width (m)	Design discharge (m^3/s)
Gate (Simongan)	0	+ 4.00	10.0	0.0
Gajah Mada	2,701	+ 2.16	14.0	2.9
Sebandaran bridge	3,517	+ 1.60	14.0	12.4
Kapuran bridge	3,739	+ 1.46	20.0	20.9
Johar	4,709	+ 0.95	20.0	37.7
Berok bridge	5,113	+ 0.76	30.0	39.6
Kali Baru	5,749	+ 0.45	34.0	33.0
Boom Lama	6,439	+ 0.28	40.0	32.5
Kali Asin	7,630	+ 0.00	42.0	31.7
Mouth	8,240	- 0.50	42.0	47.3

Suspended sediments derived from the surrounding area amount to 13,000 m^3/year (Department of Public Works, 1982). About 90 % of this load was

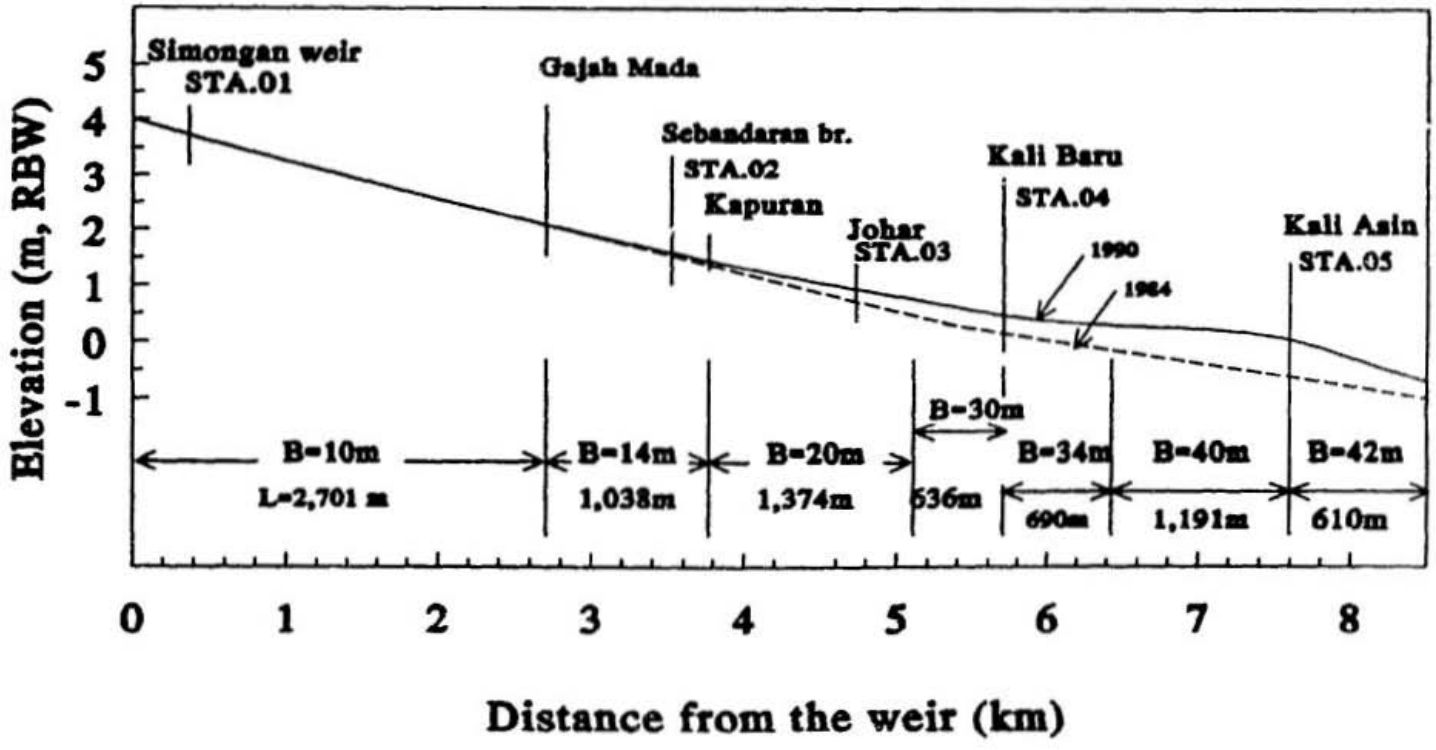

Figure 4.3 Longitudinal Section of the Kali Semarang

deposited within the channel, particularly in the lower reach. This estimation was based on the potential erosion of the river basin.

4.1.5 The West Channel

The West Channel (Figure 4.4) was built at the same time as the Simongan weir and is intended to accommodate flood water directly to the Java Sea rather than through the Kali Semarang. The channel extends straight northward for about 5,340 m. Based on the latest measurement, which was taken in 1990, its width varies from 340 m at the mouth to about 100 meters just below the weir. Depths vary from 5 to 2 m and the average bed slope is 0.0004. Bed elevations decrease seawards from about -1.0 m to -3.0 m.

A masonry levee was built in 1982. The levee extends along both banks from about the middle to the mouth (3 km) and was designed to avoid overflow during the rainy season.

4.1.6 The Delta of Kali Garang

Historically the lower part of Semarang city is situated on alluvial material deposited by from the Kali Garang and its tributaries. Burns and Mc Donnell (1976) found that the shore line within the West Channel mouth extends seawards about 10.5 m/year.

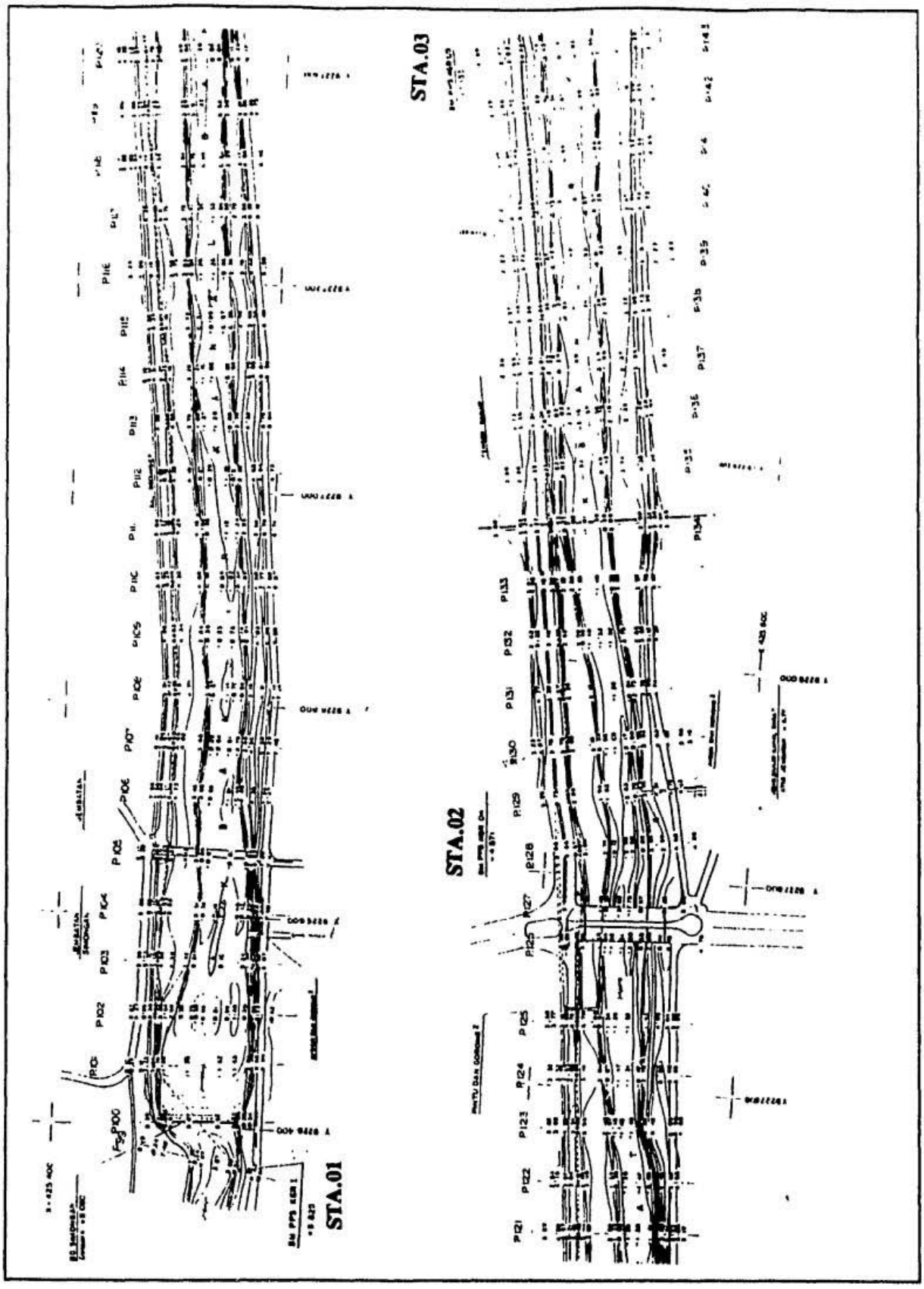

Figure 4.4 Plan View of the West Channel (1/3)

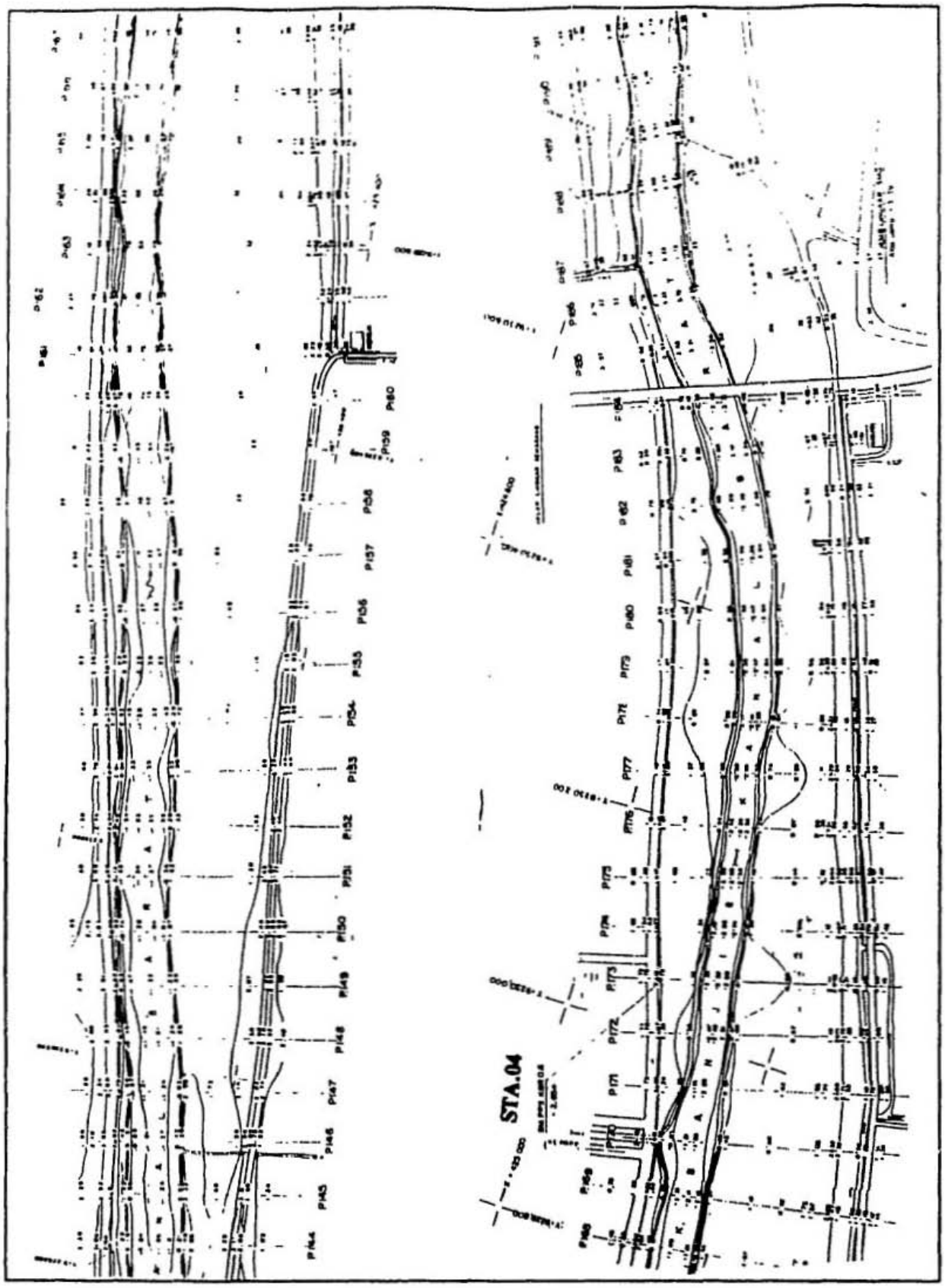

Figure 4.4 Plan View of the West Channel (2/3)

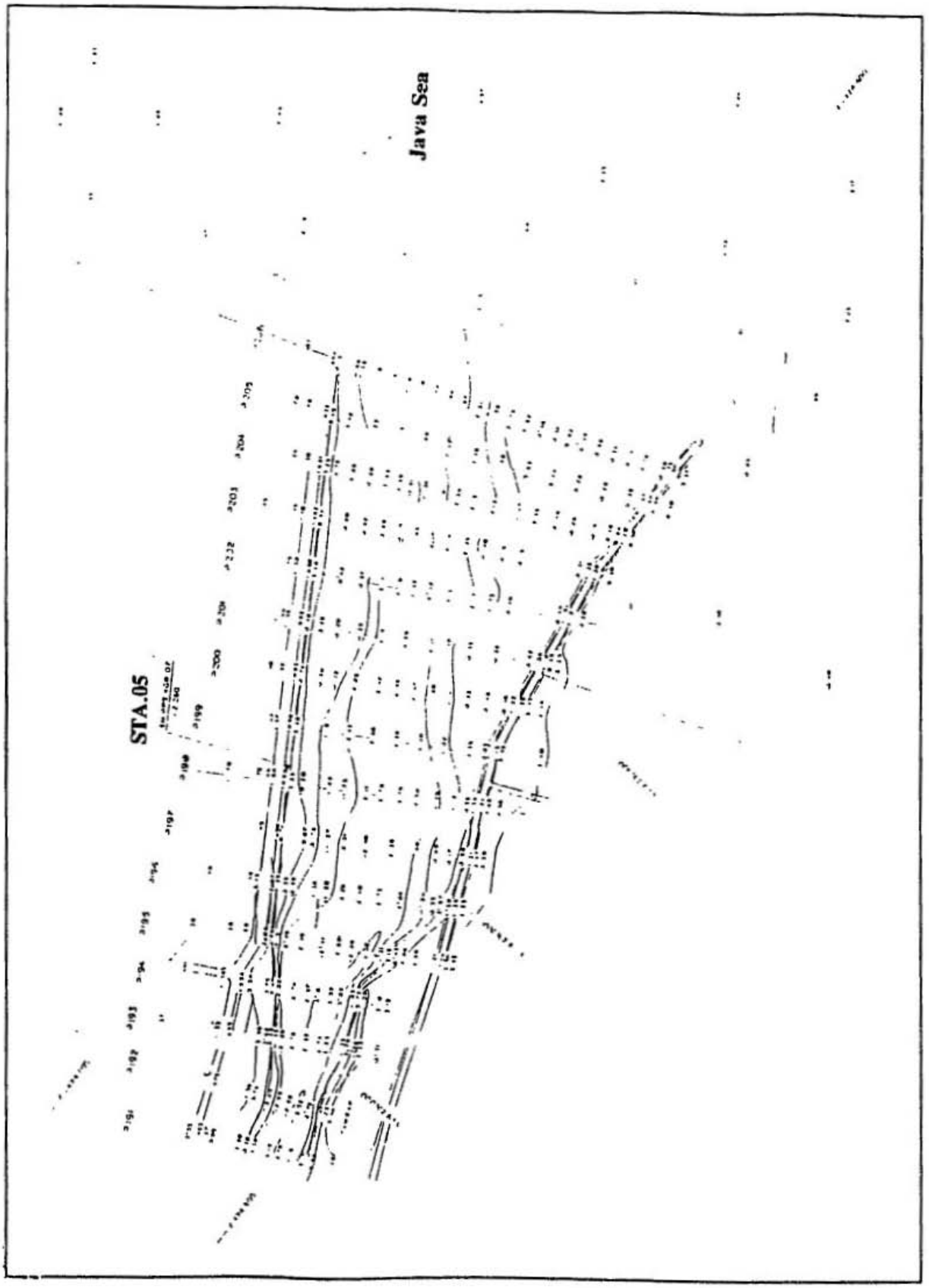

Figure 4.4 Plan View of the West Channel (3/3)

The present condition of the Kali Garang Delta can be seen in Figure 4.5. The West Channel mouth protrudes about 400 m seawards from the shoreline. Westwards of the mouth there are some bar islands that extend parallel to the shoreline. The islands have a straight shoreline facing the sea and are composed of fine sand and silt.

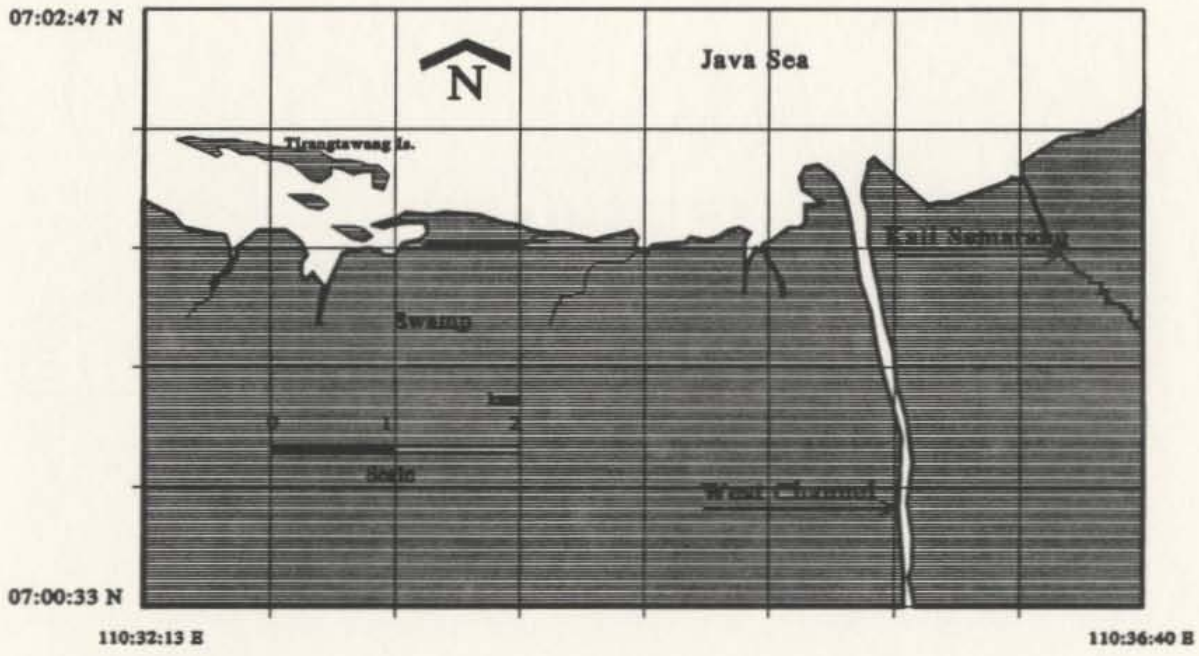

Figure 4.5 The Kali Garang Delta

4.2 Existing Data and General Analysis

Existing data were collated from a number of government offices. Data include hydrology, water flow, tide, waves, and winds.

4.2.1 Hydrological Data

The basin of the Kali Garang is located in the tropical zone. It has two seasons: dry and rainy. During the dry season, May to October, winds are dominated by the east monsoon. In the rainy season, November to April, winds are affected by the west monsoon.

Meteorological data such as rainfall, temperature, relative humidity, and evaporation were obtained from Semarang Meteorological Station. General hydrological conditions during 1990 are summarized in Table 4.2.

Rainfall.

The average annual rainfall is about 2,750 mm. The monthly average rainfall for the January 1990 to December 1990 period is 241 mm with the maximum at 667 mm in January. Daily rainfall intensity varies considerably as presented graphically in Figure 4.6.

Evaporation.

An annual evaporation is about 1,640 mm and varies from 182.5 mm in October to 87.4 mm in January. Monthly evaporation is presented in Table 4.2. Daily evaporation varies from 6.4 mm to 3.5 mm with the average being 4.5 mm/day. Figure 4.7 shows variation of monthly evaporation during 1990.

Table 4.2 Hydrological Data, 1990

Month	Monthly average temperature ° C	Monthly average humidity %	Monthly average evaporation mm/day	Monthly precip-itation mm
January	26.1	87.2	2.8	667
February	26.3	88.2	4.5	662
March	26.9	83.5	3.5	300
April	28.2	78.9	4.6	119
May	27.8	80.2	3.9	98
June	27.7	74.6	4.4	139
July	27.2	74.3	4.6	186
August	27.4	74.5	4.7	172
September	27.8	71.1	5.7	150
October	28.7	69.3	5.9	17
November	28.7	73.3	5.7	121
December	26.8	64.0	3.5	265
Average	27.5	78.3	4.5	241

Temperature.

The average monthly temperature ranges from 26.1°C in January to 28.7°C with an average annual value of 27.5°C (see Table 4.2). The daily maximum and minimum temperature are 36°C and 23°C, respectively.

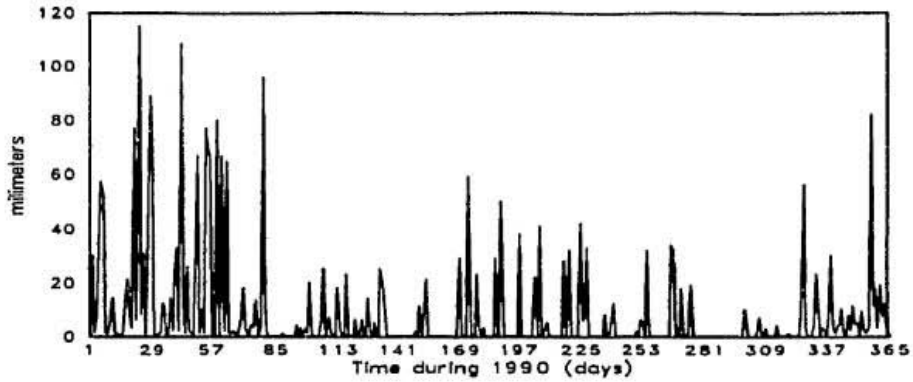

Figure 4.6 Daily Rainfall Variation During 1990

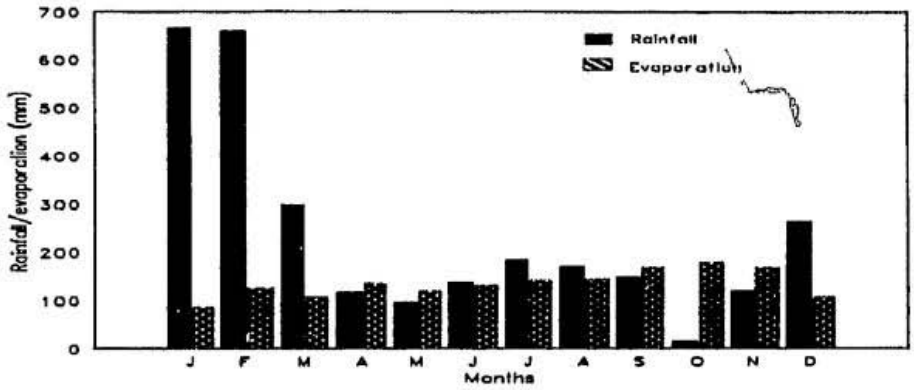

Figure 4.7 Monthly Rainfall and Evaporation, 1990.

Relative Humidity.

The average annual relative humidity is 78.3 % and the average monthly varies from 88.2 % in February to 64.0 % in December as presented in Table 4.2. Daily humidity varies from 84% to 35 %.

4.2.2 Fresh Water Discharge

The salinity at any point in the estuary and at any particular depth depends on the amount of fresh water present at that point at that time. It was, therefore, very important to ascertain the fresh water flow entering the estuary at any time. The amount of fresh water flow can be estimated by direct measurement of flow or by the use of empirical formulae relating rainfall to run-off (see section 2.3)

Measured Fresh Water.

The amount of fresh water flowing in the Kali Garang was gauged at Panjangan located about 3.5 km upstream of the Simongan weir (Figure 4.2) by the Directorate General of Water Resource, Department of Public Work. The gauge records flow from about 178 km^2 (88%) of the total drainage area.

During the period of April 1986 to December 1989, the maximum average daily flow was 187 m^3/s and occurred on February 5, and 22, 1989. The minimum flow was about 0.30 m^3/s. Figure 4.8 shows the variation of daily fresh water flow during the period January to December 1989.

Maximum flood occurred in January 26, 1991. The water elevation at the time was +9.40 m (3.80 m above weir crest). River discharge was estimated about 1,000 m^3/s. The same flood happened in 1963.

Table 4.3 Monthly Fresh Water Flow of the Kali Garang at Panjangan from April, 1986 to December 1989.

Month	Monthly fresh water flow (m^3/s)			
	1986	1987	1988	1989
January	-	22.18	12.73	9.89
February	-	29.72	19.50	48.39
March	-	24.85	15.96	15.12
April	29.77	12.05	10.45	13.16
May	5.76	6.38	7.49	5.91
June	8.57	5.05	2.75	8.56
July	5.88	3.49	2.46	2.82
August	4.12	2.46	1.70	2.26
September	4.36	1.88	1.77	1.94
October	3.50	2.08	3.64	3.32
November	8.21	3.82	3.90	3.52
December	6.99	8.91	27.53	6.34

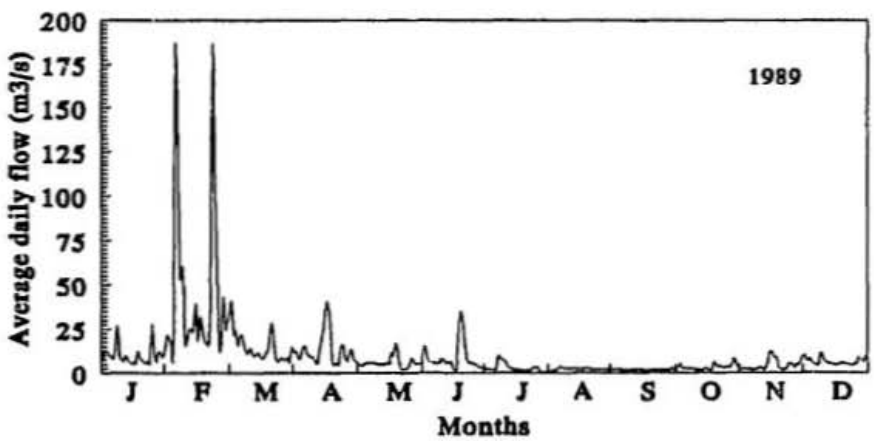

Figure 4.8 Variation of Average Daily Flow of the Kali Garang at Panjangan, During 1989.

Runoff.

Runoff calculations in the drainage basins of the Kali Garang and its tributaries were obtained from the Design of Drainage System of Semarang City, 1989 (Bappeda Kotamadya Dati II Semarang, 1989). The procedure and result are summarized in the following section.

The peak discharge, Q_p.

Peak Discharge, Q_p, was calculated by using the modified rational formula (equation 2.4). *The run-off coefficients, C*, used are given in Table 2.1. *The storage coefficient, C_s,* for the Kali Garang basin was estimated at 0.8 (Bappeda Kotamadya Dati II Semarang, 1989). *Time of concentration, t_c,* was estimated based on the equation 2.5, where t_o was obtained from Figure 4.9.

Rainfall intensities, I.

Rainfall intensities I, were estimated based on 13 years data and are shown in Table 4.4. Rainfall intensity for each duration and different frequency were calculated by Weibull's formula as mentioned in section 2.3, and presented graphically in Figure 4.10.

Table 4.4 Maximum Rainfall (*Source : Department of Public Works, 1982*)

	Rainfall duration (minutes)									
Year	5	10	15	30	45	60	120	180	360	720
1959	20.0	25.0	30.0	50.0	53.0	53.4	53.4	54.6	54.6	54.6
1960	18.2	22.0	32.1	45.9	46.0	47.0	51.2	57.0	67.4	71.0
1961	20.6	25.7	27.8	40.1	42.7	43.5	50.0	65.6	87.0	115.8
1962	10.8	20.0	25.2	30.2	35.0	37.5	45.2	51.5	72.6	75.9
1963	12.2	20.0	24.9	38.2	39.5	40.3	44.0	61.5	69.7	117.5
1964	20.8	31.2	41.6	62.4	77.6	80.0	89.1	91.4	97.7	100.0
1965	11.0	14.6	18.3	28.3	38.3	39.6	41.1	43.8	90.8	124.9
1966	26.5	29.6	34.2	42.8	50.0	53.6	71.9	80.0	90.0	91.0
1976	17.0	20.0	33.2	42.8	59.0	74.9	106.5	106.5	134.6	182.6
1978	17.0	24.5	36.0	60.0	72.1	84.5	97.7	102.0	114.6	114.9
1979	15.2	23.5	29.1	36.9	50.1	55.6	98.7	98.7	126.0	126.0
1980	13.8	27.9	62.0	62.0	81.6	91.0	175.3	184.9	191.6	191.6
1981	20.0	40.0	50.0	65.0	70.0	80.0	112.6	120.0	174.0	180.4

Calculations of peak discharges were carried out for each tributary and for the main channel. The results are summarized in Table 4.5.

Table 4.5 Runoff of the Kali Garang and its tributaries

Basin	Area (km^2)	Q_p (m^3/sec.)
Kali Kreo	61.84	306.84
Kali Kripik	34.58	285.72
Upper Kali Garang	65.77	402.74
West Channel (weir)	177.55	695.11
Kali Semarang (mouth)	10.25	30.07

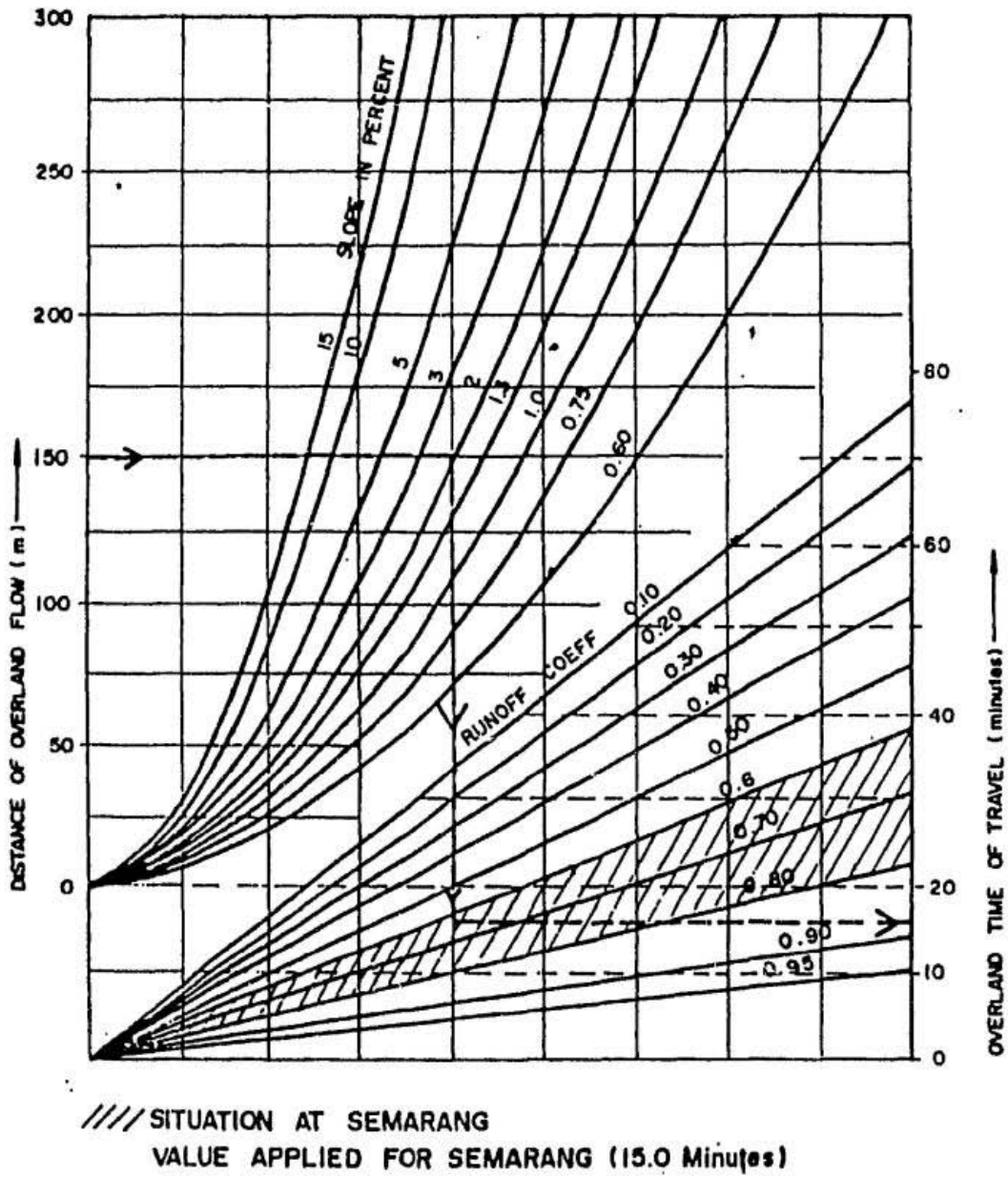

Figure 4.9 Design Chart for Estimation of Overland Time of Flow (*Source: Department of Public Works, 1982*)

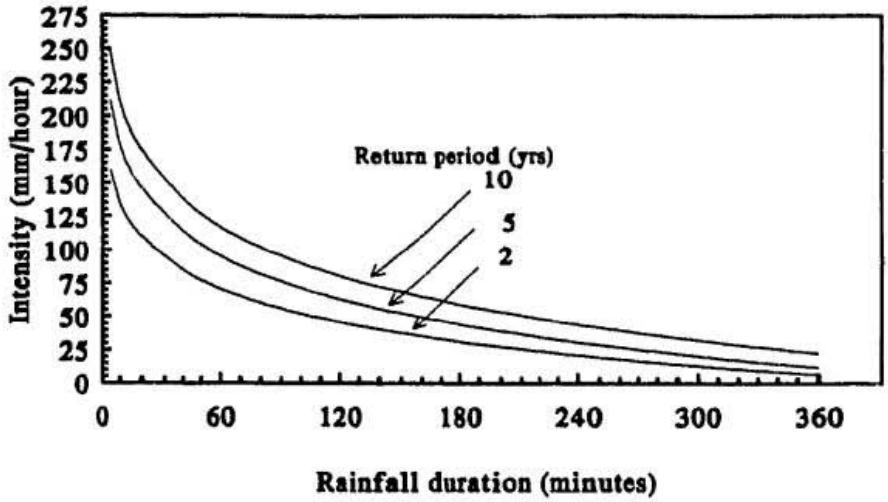

Figure 4.10 Intensity-duration-frequency (IDF) Curves.

4.2.3. Tidal data

Direct measurements of the tide at the Kali Garang Estuary have never been made. Instead, tidal information is derived from Semarang Harbour which is located about 2 km and 3 km East from the Kali Semarang and the West Channel mouths respectively (Figure 4.11).

Based on the tidal constituents which influence the Semarang region, the tidal type is a mixed, predominantly diurnal tide with an "F" ratio of 1.67. The Luni-solar diurnal (K_1) component is dominant (Table 4.6). Thus the mean tidal period is 23.93 hours.

The Tide at the Semarang Harbour.

Tides have been recorded since 1985 by using an Automatic Water Level Recorder (AWLR) located at the wharf facing the harbour channel (Figure 4.11).

Table 4.6 Tidal Constituents in Semarang *(Source: Department of Fisheries and Oceans, Canada)*

Constituent	Period lunar hrs.	Amplitude cm.	Phase, degree
M_2	12.42	10	286.00
S_2	12.00	8	187.20
N_2	12.66	5	249.70
K_2	11.97	4	229.80
K_1	23.93	22	8.90
O_1	25.82	8	246.10
P_1	24.07	7	12.30
Q_1	26.87	2	154.80

The instrument consists of a vertical tube open to the sea through a small orifice near the bottom. Inside the tube, a float sits on the water surface. A wire joins the float to a recording mechanism where the wire is connected to a counterbalance weight. Water levels are recorded by a pen moved across the recorder paper which is secured around a drum rotated by clockwork. Water level is recorded against time in form of graphic output.

This recorder has been operating since 1985, and original records have been tabulated hourly for every month. These data were analyzed to determine the tidal range, duration of rise and fall, type of tide, and water level distribution.

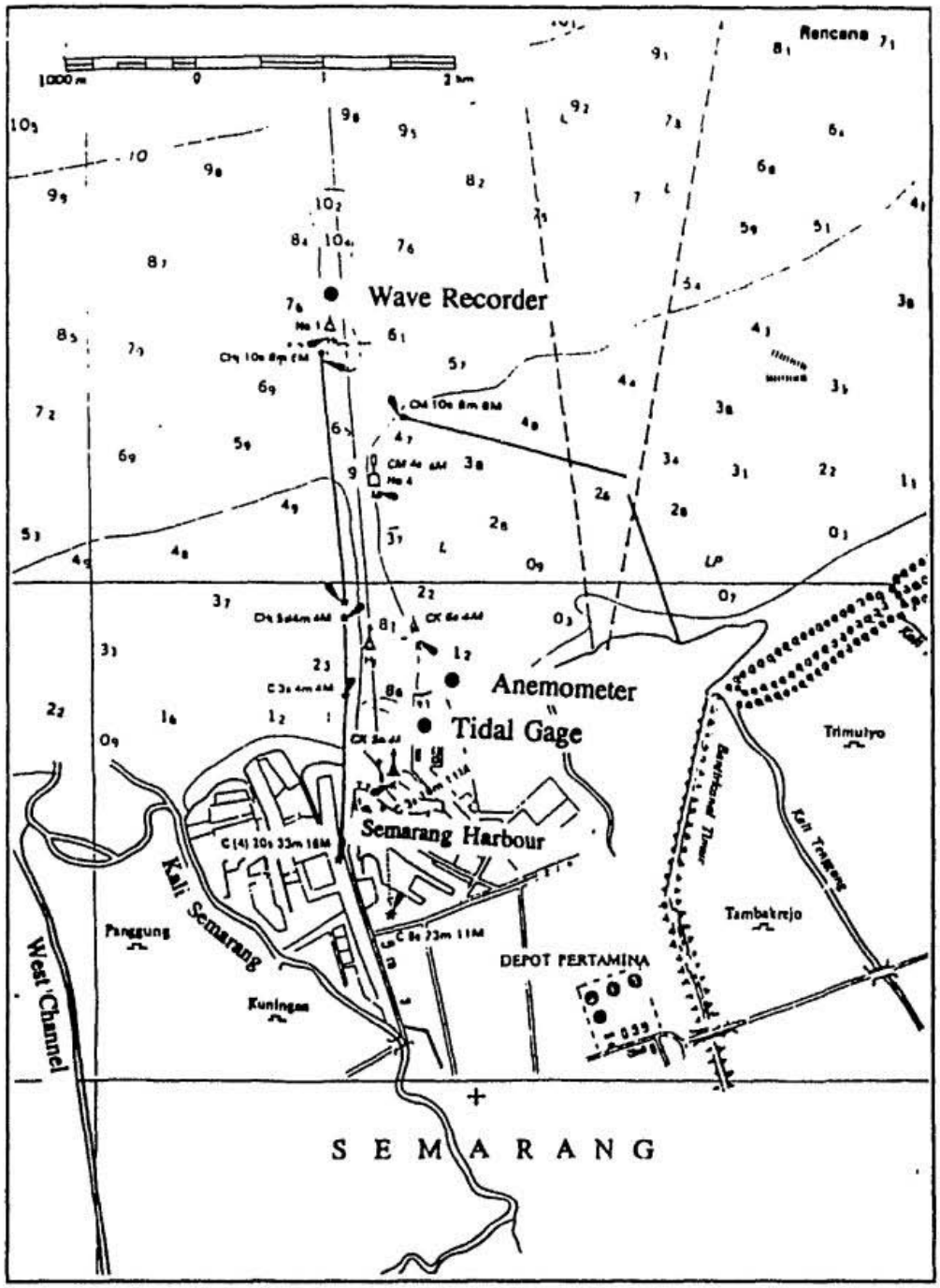

Figure 4.11 Lay Out of Semarang Harbour, Showing the Location of Tidal Gage, Wave Recorder and Anemometer

The tidal range, duration of rise and fall and mean tidal level (MTL), were obtained from tabulation of the elevation and time of each high and low water for the whole of 1990 and for three months in 1991. Results for 1991 are presented in Table 4.7. Figure 4.13 shows the results for 1990.

During the three month period, May 1st to July 31st, 1991, the tide was dominated by diurnal tides although an unequal semi-diurnal tide occurred for a few days around neap tide. During this period, the maximum tidal range was 1.09 m and the average was 0.57 m. Mean Tidal Level was 0.72 m above the Kali Garang Datum (RBW[1]).

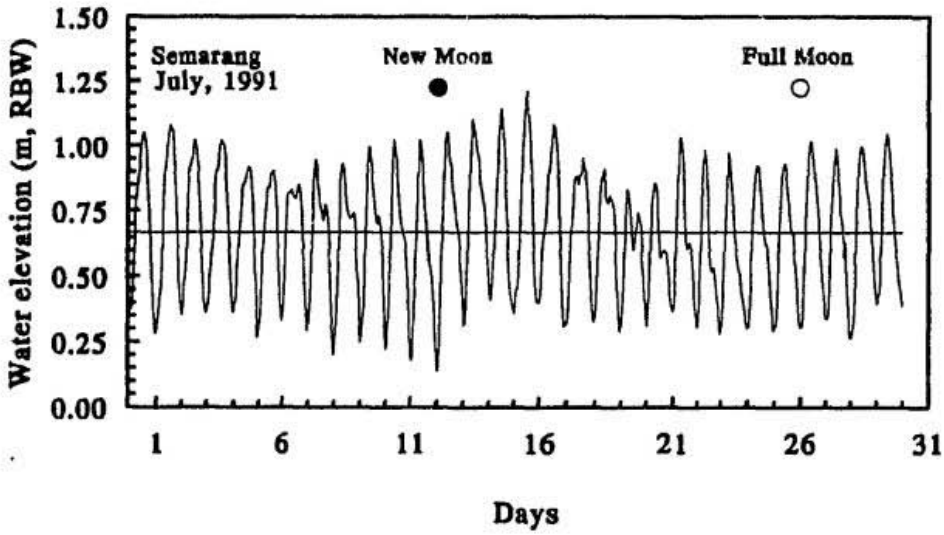

Figure 4.12 Tide in Semarang Harbour, July 1991.

[1] RBW is the datum used by the Government of Indonesia in the Kali Garang

Table 4.7

Analyses of
Tidal data of Semarang Harbour
Record from May 1st to July 31st, 1991
Elevation is given in cm, RBW

Date		High Water Time (hrs)	High Water Hght (cm)	Low Water Time (hrs)	Low Water Hght (cm)	Duration Fall (hrs)	Duration Rise (hrs)	Range Fall (cm)	Range Rise (cm)	Mean Level (cm)	Mean Level (cm)
May	1	14.30	104	23.10	42	8.40	14.50	62	62	73	73
	2	14.00	104	24.00	37	10.00	16.15	67	66	73	70
	3	16.15	103	22.30	46	8.15	17.30	57	69	75	81
	4	16.00	115	23.30	43	7.30	17.10	72	79	79	83
	5	16.40	122	0.30	57	7.50	6.45	65	28	90	71
	6	7.15	85	9.15	80	2.00	6.45	5	38	83	99
		16.00	118	22.30	43	6.30	16.45	75	82	81	84
	7	15.15	125	23.30	34	8.15	7.10	91	44	80	56
	8	6.40	78	8.15	75	1.25	7.45	3	44	77	97
		16.00	119	23.50	28	7.50	8.00	91	53	74	55
	9	7.50	81	9.50	73	2.00	6.10	8	41	77	94
		16.00	114	0.40	30	8.40	6.20	84	54	72	57
	10	7.00	84	9.40	77	2.40	6.40	7	46	81	100
		16.20	123	23.50	29	7.30	7.10	94	56	76	57
	11	7.00	85	9.30	75	2.30	7.00	10	41	80	96
	12	16.30	116	0.30	35	8.00	6.30	89	59	76	65
		7.00	94	11.00	78	4.00	6.15	16	31	86	94
	13	17.15	109	0.15	45	7.00	7.45	64	56	77	73
		8.00	101	12.10	85	4.10	4.50	16	10	93	90
	14	17.00	95	0.45	41	7.45	8.25	54	57	68	70
		9.10	98	14.00	80	4.50	4.30	18	15	89	88
	15	18.30	95	2.00	46	7.30	8.50	49	59	71	76
	16	10.50	105	1.30	49	14.40	10.00	56	66	77	82
	17	11.30	115	2.45	49	15.15	9.45	66	71	82	85
	18	12.30	120	2.50	58	14.20	11.00	62	69	89	93
		13.50	127	23.00	59	9.10	3.00	68	8	93	63
	19	2.00	67	4.30	61	2.30	9.15	6	70	64	96
		13.45	131	23.40	53	9.55	14.50	78	78	92	92
	20	14.30	131	23.10	28	8.40	15.50	103	101	80	79
	21	15.00	129	23.15	29	8.15	16.45	100	97	79	78
	22	16.00	126	0.15	17	8.15	7.15	109	68	72	51
	23	7.30	85	9.00	80	1.30	6.40	5	39	83	100
	24	15.40	119	0.30	25	8.50	6.45	94	70	72	60
		7.15	95	9.40	78	2.25	7.35	17	28	87	92
	25	17.15	106	0.45	31	7.30	6.55	75	62	69	62
		7.40	93	11.00	76	3.20	6.15	17	16	85	84

continued (2/3)

Table 4.7 (continued 2/3)

Date		High Water Time (hrs)	High Water Hght (cm)	Low Water Time (hrs)	Low Water Hght (cm)	Duration Fall (hrs)	Duration Rise (hrs)	Range Fall (cm)	Range Rise (cm)	Mean Level (cm)	Mean Level (cm)
	26	17.15	92	0.30	41	7.15	8.00	51	55	67	69
	27	8.30	96	1.45	46	17.15	7.45	50	56	71	74
	28	9.30	102	0.30	49	15.00	9.30	53	60	76	79
	29	10.00	109	1.15	46	15.15	10.45	63	63	78	78
		12.00	109	24.00	45	12.00	11.40	64	68	77	79
	30	11.40	113	23.00	43	11.20	13.10	70	72	78	79
	31	12.10	115	23.30	41	11.20	16.00	74	71	78	77
June	1	15.30	112	0.15	41	8.45	14.45	71	71	77	77
	2	15.00	112	1.30	39	10.30	12.45	73	79	76	79
	3	14.15	118	22.40	43	8.25	10.00	75	52	81	69
	4	8.40	95	21.00	36	12.20	13.10	59	79	66	76
	5	10.10	115	0.30	31	14.20	14.15	84	80	73	71
	6	14.45	111	22.40	27	7.55	16.50	84	84	69	69
	7	15.30	111	23.30	31	8.00	15.45	80	72	71	67
	8	15.15	103	0.50	23	9.35	10.40	80	85	63	66
	9	11.30	108	22.30	28	11.00	8.20	80	59	68	58
	10	6.50	87	11.00	67	4.10	5.30	20	18	77	76
		16.30	85	24.00	29	7.30	7.30	56	73	57	66
	11	7.30	102	13.00	89	5.30	3.30	13	2	96	90
		16.30	91	24.00	31	7.30	8.30	60	71	61	67
	12	8.30	102	1.00	31	16.30	8.45	71	74	67	68
	13	9.45	105	0.45	32	15.00	9.45	73	72	69	68
	14	10.30	104	2.10	41	15.40	9.30	63	77	73	80
	15	11.50	118	23.10	37	11.20	1.40	81	4	78	39
	16	0.50	41	3.10	39	2.20	10.40	2	81	40	80
		13.50	120	1.10	39	11.20	1.20	81	3	80	41
	17	2.30	42	3.50	39	1.20	8.10	3	80	41	79
		12.00	119	23.00	33	11.00	14.30	86	92	76	79
	18	13.30	125	22.30	36	9.00	15.30	89	80	81	76
	19	14.00	116	23.00	26	9.00	17.30	90	86	71	89
	20	16.30	112	23.50	37	7.20	17.40	75	65	75	70
	21	17.30	102	24.00	33	6.30	7.00	69	58	68	62
	22	7.00	91	11.30	82	4.30	6.45	9	4	87	84
		18.15	86	24.00	30	5.45	8.00	56	67	58	64
	23	8.00	97	13.30	83	5.30	3.00	14	2	90	84
		16.30	85	21.15	37	4.45	9.15	48	61	61	68
	24	6.30	98	23.30	29	17.00	8.30	69	69	64	64
	25	8.00	98	24.00	31	16.00	8.00	67	72	65	67
	26	8.00	103	24.00	32	16.00	10.00	71	72	68	68
	27	10.00	104	0.10	35	14.10	10.00	69	70	70	70
	28	10.10	105	23.10	33	13.00	12.20	72	68	69	67

continued (3/3)

Table 4.7 (continued 3/3)

Date		High Water Time (hrs)	High Water Hght (cm)	Low Water Time (hrs)	Low Water Hght (cm)	Duration Fall (hrs)	Duration Rise (hrs)	Range Fall (cm)	Range Rise (cm)	Mean Level (cm)	Mean Level (cm)
	29	11.30	101	24.00	31	12.30	12.00	70	76	66	69
	30	12.00	107	23.30	31	11.30	13.00	76	74	69	68
July	1	12.30	105	23.00	28	10.30	13.30	77	80	67	68
	2	12.30	108	24.00	35	11.30	13.00	73	67	72	68
	3	13.00	102	23.00	37	10.00	14.00	65	66	69	69
	4	13.00	102	23.00	36	10.00	14.00	66	56	69	64
	5	13.00	92	23.00	27	10.00	16.30	65	73	60	64
	6	15.30	100	23.00	33	7.30	10.00	68	51	66	58
	7	9.00	83	12.30	80	3.30	10.00	3	5	82	83
		15.45	85	23.15	29	7.30	3.15	56	65	57	62
	8	6.30	94	13.00	73	6.30	2.30	21	4	84	75
		15.30	77	23.15	20	7.45	7.45	57	73	49	57
	9	7.00	93	14.30	72	7.30	3.00	21	2	83	73
		17.30	74	24.00	25	6.30	7.30	49	74	50	62
	10	7.30	99	15.00	70	7.30	1.50	29	3	85	71
		16.50	73	24.00	22	7.10	7.00	51	80	47	62
	11	7.00	102	0.30	17	17.30	8.00	85	84	60	59
	12	8.30	101	1.30	15	17.00	9.30	86	90	58	60
	13	11.00	105	2.15	35	15.15	6.45	70	74	70	72
	14	9.00	109	6.50	35	21.50	5.10	29	33	95	97
	15	12.00	113	23.40	35	11.40	12.20	78	86	74	78
	16	12.00	121	22.15	40	10.15	14.30	81	68	81	74
	17	12.45	108	23.30	20	10.45	13.30	88	75	64	57
	18	13.00	95	22.30	31	9.30	9.00	64	60	63	61
	19	7.30	91	10.40	78	3.10	2.50	13	4	85	80
		13.30	82	23.00	29	9.30	7.00	53	54	56	56
	20	6.00	83	11.30	60	5.30	4.30	23	14	72	67
		16.00	74	13.00	57	21.00	3.00	17	3	66	59
		16.00	60	23.50	37	7.50	6.50	24	68	48	70
	22	6.40	104	13.50	61	7.10	1.10	44	3	82	62
		15.00	63	23.00	31	8.00	8.00	33	62	47	61
	23	7.00	92	14.00	52	7.00	3.00	41	12	72	57
		17.00	63	23.15	28	6.15	7.55	35	69	46	63
	24	7.10	97	23.50	30	16.50	8.40	67	63	64	62
	25	8.30	93	23.10	29	14.40	9.30	64	64	61	61
	26	8.40	93	23.00	31	14.20	9.45	62	71	62	66
	27	8.45	102	0.15	34	15.30	9.15	68	65	68	67
	28	9.30	99	24.00	27	14.30	9.00	72	72	63	63
	29	9.00	99	24.00	39	15.00	9.30	60	66	69	72
	30	9.30	105	0.40	39	15.10		-	66	-	72
Average :			**100**		**44**	**9:24**	**9:16**	**57**	**57**	**72**	**72**

Distributions of tidal range and water level were also analyzed for the 1990 period. The distribution of tidal range was obtained by tabulating a vertical distance between a high water and consecutive low water. Results are presented graphically in Figure 4.13. During 1990 the tidal range varied from 0.13 m to 1.05 m with an average of 0.65 m.

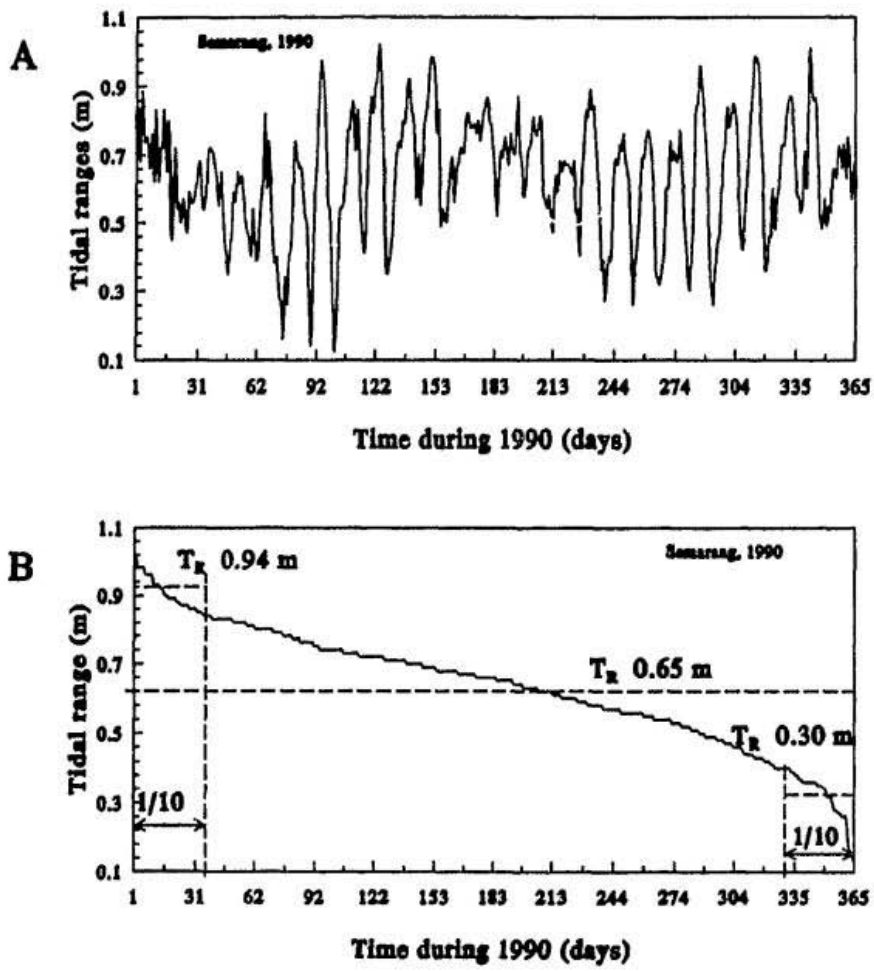

Figure 4.13 Daily Variation of Tidal Ranges in Semarang During 1990 (A), Distribution of Tidal Range (B).

The average tidal range of the one-tenth highest tides is 0.95 m, and the average tidal range of the one-tenth lowest is 0.35 m. These values will be used hereafter as mean spring and mean neap tides, respectively.

The distribution of water level was found by tabulating an hourly water level during a one year period. Data were classed in 5 cm increments. The frequency of occurrence for each class of water level was then calculated to determine the percentage of occurrence. Figure 4.14 shows the sea water distribution during 1990. The mean sea water level (MSL) is 0.74 m, RBW, the high-high water level (HHWL) and the low-low water level (LLWL) are 1.35 m and 0.15 m, respectively. The average of the one-fourth highest water levels is 1.06 m, and the average of the one-fourth lowest water levels is 0.42 m. Here and after, these two values are used to represent the low water level (LWL) and the high water level (HWL), respectively.

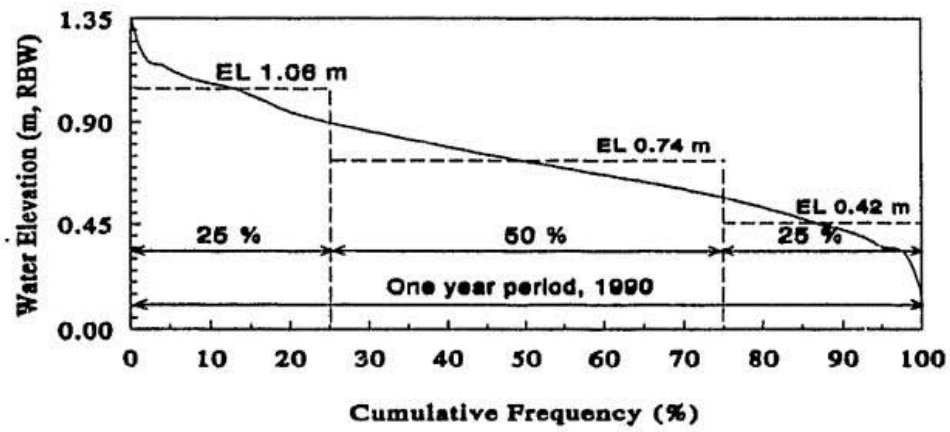

Figure 4.14 Distribution of Water Elevation in Semarang Harbour, 1990

4.2.4 Wind and Wave

Wind and wave data were obtained from the Directorate General of Marine Transportation, Section of Tanjung Emas Harbour, Semarang.

Wind Data.

The wind measurement station was located within the harbour area at the tip of the wharf (see Figure 4.11) with the anemometer placed at a height of 11 m above the harbour datum. Winds were recorded continuously in both velocity and direction. Data were averaged and presented hourly, so there were 24 data for each day. Distribution of wind directions during 1989 period is summarized in Tables 4.7 and 4.8.

During a year, the wind blows primarily from east, east-south-east, and south-east (E + ESE + SE = 45.6 %). This wind blows from April to October and is called the east monsoon. The other prevailing wind blows from west, west-south-west, and south-west (W + WSW + SW = 22.4 %). This wind blows during November to March and is called the west monsoon.

Table 4.8 Wind Data , 1989

LOCATION SEMARANG, INDONESIA
LAT.006:56 S, LONG. 110:25 E
PERIOD JANUARY 01, 1989 TO DECEMBER 31, 1989

Frequency

Direction	JAN	FEB	MAR	APR	MAY	JUN	JUL	AUG	SEP	OCT	NOV	DEC	YEAR	Direction
N	36	4	44	43	79	60	45	59	70	55	76	39	610	N
NNE	3	6	10	14	8	18	11	9	7	4	9	7	106	NNE
NE	15	5	19	34	25	25	12	14	18	15	20	18	220	NE
ENE	7	7	14	13	24	20	23	25	21	16	16	15	201	ENE
E	40	24	68	58	78	85	121	128	120	98	86	63	969	E
ESE	64	17	64	104	154	128	182	224	162	156	114	74	1443	ESE
SE	69	36	103	128	216	157	197	178	144	147	112	89	1576	SE
SSE	17	12	17	17	30	32	17	10	8	23	18	24	225	SSE
S	31	27	35	38	22	30	12	12	14	19	30	37	307	S
SSW	15	12	12	13	10	25	9	7	6	2	20	21	152	SSW
SW	71	28	35	32	28	16	15	4	11	23	24	48	335	SW
WSW	52	85	35	20	5	22	5	6	9	18	7	38	302	WSW
W	127	213	90	35	10	17	21	21	23	31	16	113	717	W
WNW	107	128	90	45	2	14	22	6	29	21	25	55	544	WNW
NW	66	65	78	94	17	36	34	22	51	73	79	83	698	NW
NNW	24	3	30	32	36	35	18	19	27	43	41	20	328	NNW
Total	744	672	744	720	744	720	744	744	720	744	693	744	8733	Total

Wave Data.

A wave recorder, which has been operated since 1987, was located about 3 km seaward from the shoreline or about 300 m north of the tip of the west breakwater, where the water depth is approximately 10 m (Figure 4.11). The site is open to WNW to NNE winds. From other directions, the fetch is limited by Java Island.

The recorder provides information about the sea surface elevation which is recorded for a 20 minute period every hour by pen on paper chart rolls. Sea state

parameters (H_s and T_s) are derived from these chart records.

Table 4.9 Wind Data in 1989 (in percent)

LOCATION SEMARANG, INDONESIA
LAT.006:56 S, LONG. 110:25 E
PERIOD JANUARY 01, 1989 TO DECEMBER 31, 1989

Percentage frequency (%)

Direction	JAN	FEB	MAR	APR	MAY	JUN	JUL	AUG	SEP	OCT	NOV	DEC	YEAR	Direction
N	4.8	0.6	5.9	6.0	10.6	8.3	6.0	7.9	9.7	7.4	11.0	5.2	7.0	N
NNE	0.4	0.9	1.3	1.9	1.1	2.5	1.5	1.2	1.0	0.5	1.3	0.9	1.2	NNE
NE	2.0	0.7	2.6	4.7	3.4	3.5	1.6	1.9	2.5	2.0	2.9	2.4	2.5	NE
ENE	0.9	1.0	1.9	1.8	3.2	2.8	3.1	3.4	2.9	2.2	2.3	2.0	2.3	ENE
E	5.4	3.6	9.1	8.1	10.5	11.8	16.3	17.2	16.7	13.2	12.4	8.5	11.1	E
ESE	8.6	2.5	8.6	14.4	20.7	17.8	24.5	30.1	22.5	21.0	16.5	9.9	16.5	ESE
SE	9.3	5.4	13.8	17.8	29.0	21.8	26.5	23.9	20.0	19.8	16.2	12.0	18.0	SE
SSE	2.3	1.8	2.3	2.4	4.0	4.4	2.3	1.3	1.1	3.1	2.6	3.2	2.6	SSE
S	4.2	4.0	4.7	5.3	3.0	4.2	1.6	1.6	1.9	2.6	4.3	5.0	3.5	S
SSW	2.0	1.8	1.6	1.8	1.3	3.5	1.2	0.9	0.8	0.3	2.9	2.8	1.7	SSW
SW	9.5	4.2	4.7	4.4	3.8	2.2	2.0	0.5	1.5	3.1	3.5	6.5	3.8	SW
WSW	7.0	12.6	4.7	2.8	0.7	3.1	0.7	0.8	1.3	2.4	1.0	5.1	3.5	WSW
W	17.1	31.7	12.1	4.9	1.3	2.4	2.8	2.8	3.2	4.2	2.3	15.2	8.2	W
WNW	14.4	19.0	12.1	6.3	0.3	1.9	3.0	0.8	4.0	2.8	3.6	7.4	6.2	WNW
NW	8.9	9.7	10.5	13.1	2.3	5.0	4.6	3.0	7.1	9.8	11.4	11.2	8.0	NW
NNW	3.2	0.4	4.0	4.4	4.8	4.9	2.4	2.6	3.8	5.8	5.9	2.7	3.8	NNW
Total	100	100	100	100	100	100	100	100	100	100	100	100	100	Total

The wave climate throughout 1989 is summarized in Table 4.9 below. Waves with H_s higher than one metre usually occur during November to March. During the other months, the sea is dominated by calm waves and the wave height is less than 0.50 m.

Table 4.10 Wave climate

STATION C-3
SEMARANG HARBOUR, INDONESIA
JANUARY 01, 1989 TO DECEMBER 31, 1989

H_s (m)	1	2	3	4	5	6	7
2.5							
2.0						1	
1.5				12	13		
1.0			14	97	67	5	1
0.5		35	179	246	88	9	
0.0	577	1252	921	401	111	18	1

Peak period in seconds

Chapter 5

Field Observation and Analysis

The problem was to determine the tidal propagation, salt water intrusion and circulation pattern together with the distribution of sediment transport and deposition along the two channels of the Kali Garang Estuary, and formation of delta seawards of the river mouth. The parameters considered were tidal action at the mouth of the estuary, river discharge, estuarine geometry, winds, waves and density variation between fresh and saline waters.

To understand the problems mentioned, some field measurements and observations were taken during May to August 1991. The initial step was to determine the location on survey cross sections and instrumentation. Locations of survey cross sections are shown in Figure 5.1 and described in Tables 5.1 and 5.2.

5.1 Water Level Measurement

Water levels were measured by using a pole marked in metres and millimetres. This is usually known as a Visual Tidal Scale. Poles were installed vertically at the river bank in such a way that it was still possible to obtain readings

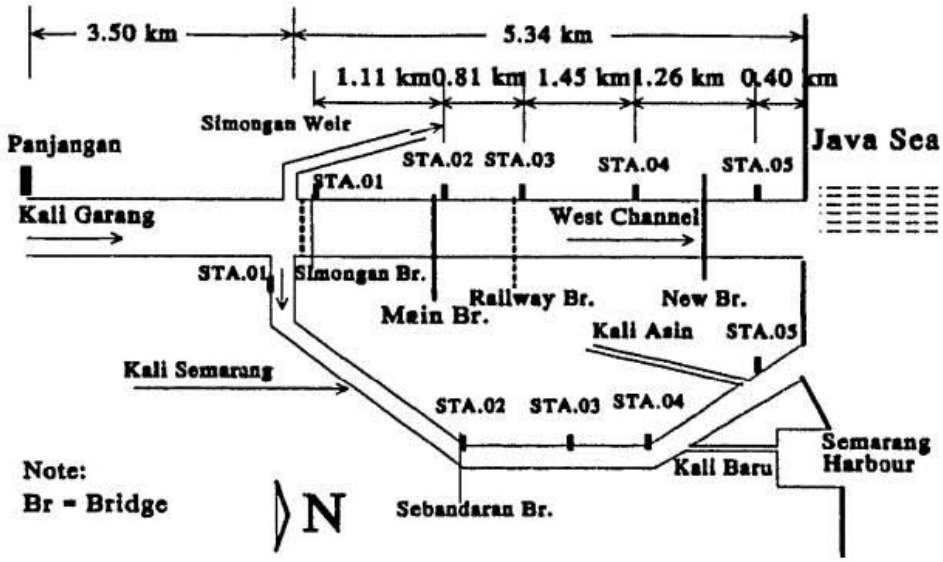

Figure 5.1 Sketch Chart of the Kali Garang Estuary Showing the Observation Stations.

Table 5.1 Survey Cross Sections at the West Channel

Survey Section Number	kms from weir	kms apart	Description
-	0		Simongan weir
		0.310	
01	0.310		Simongan bridge
		1.112	
02	1.422		BM.PPS.KGR.04
		0.810	
03	2.232		BM.PPS.KGR.05
		1.450	
04	3.682		BM.PPS.KGR.06
		1.255	
05	4.937		BM.PPS.KGR.07
		0.400	
-	5.337		Java sea

even at the lowest low water. The levelling system was based on the Kali Garang Datum (RBW). Three poles were installed at each branch, at stations 01, 03, and 05 for the West Channel, and stations 02, 04, and 05 for the Kali Semarang (Figure 5.1).

Table 5.2 Survey Cross Sections at the Kali Semarang

Survey Section Number	kms from weir	kms apart	Description
-	0		Simongan weir
		0.150	
01	0.150		Kalisari Gate
		3.367	
02	3.517		Sebandaran Br.
		1.192	
03	4.709		Johar
		1.040	
04	5.749		Kali Baru
		1.832	
05	7.581		Kali Asin
		0.650	
-	8.231		Java sea

Readings were taken simultaneously at three stations, at one hour intervals over one tidal period (about 24 hours) both during spring and neap tides. The aim of these measurements was to estimate the type of tidal propagation along the channel (tidal curves), longitudinal water profiles and tidal volumes.

As mentioned in section 4.2, the tide at the Semarang Harbour is predominantly a diurnal tide. Normally the difference between spring and neap tide is small, unless there is an unequal-semidiurnal tide. Measurements of water level show that the tides at the West Channel and the Kali Semarang are similar to those at the

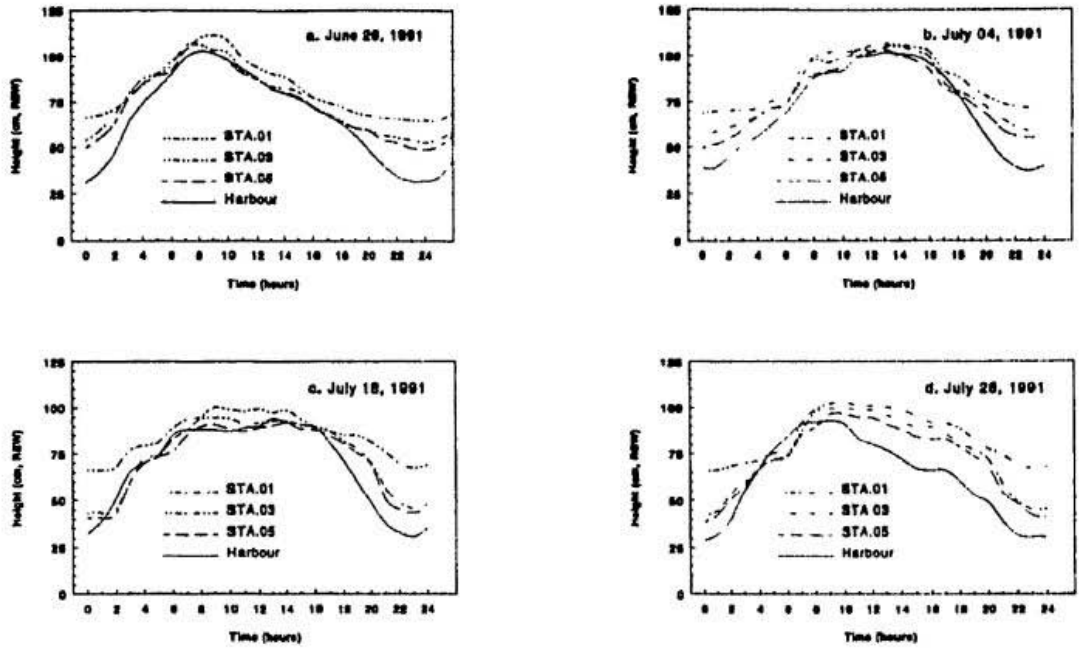

Figure 5.2 Tidal curves in the Semarang Harbour and three stations in the West Channel on *a)* June 26, 1991, *b*) July 04, 1991, *c)* July 18, 1991, and *d)* July 26, 1991.

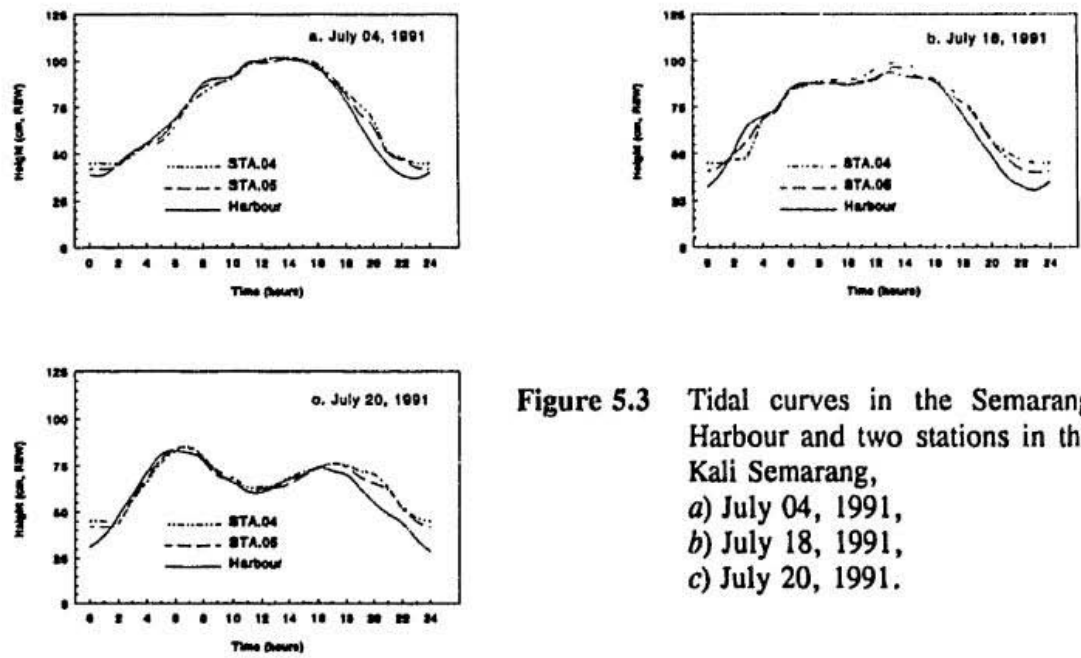

Figure 5.3 Tidal curves in the Semarang Harbour and two stations in the Kali Semarang,
a) July 04, 1991,
b) July 18, 1991,
c) July 20, 1991.

Harbour. The tidal range decreases gradually up the estuary. Figures 5.2 and 5.3 show the tidal curves found during measurements at the West Channel and the Kali semarang, respectively.

In the West Channel, the tide propagates upstream as far as the weir. The tide reaches the weir in less then one hour. Tidal range just below the weir was about 75 % of that at the river mouth. Theoretically the channel should experience a standing wave. Since the length of the channel is far less than one quarter of the wave length (diurnal L $\pm$ 95 km), the standing tide in the channel is not apparent.

In the Kali Semarang, the tide propagates to about the mid length of the channel (between Sebandaran bridge and Johar). The maximum tidal limit is at Sebandaran Bridge (3,517 m from the weir). During the observations, the fresh water flow was almost zero. The channel was dry, except for the lower part of the Kali Asin. During flood tides the channel was inundated but it dried out again during the ebb tides.

5.1.1 Tidal Curves and Longitudinal Water Profiles

Typical raw data obtained from the water level measurement is given in Appendix A, Table A.1. Data from each station were plotted against time and tidal curves for each station were obtained by connecting the hourly water level data. The longitudinal water level profiles were obtained by plotting both the maximum and minimum water level from each station against distance. If there was a different time in reaching either HW or LW at each station, the time at the mouth was used as

reference. The results are given in Figures 5.4 and 5.5, respectively, for the West Channel and the Kali Semarang.

General water profiles (during low discharge) can be estimated by averaging the water surface gradient found during observation. The gradient was taken at both high water and low water.

Table 5.3 Water Surface Gradient at the West Channel

Date	Gradient at HW I_{HW} (10^{-5})		Gradient at LW I_{LW} (10^{-5})	
	Upper part (STA.01-03)	Lower part (STA.03-05)	Upper part (STA.01-03)	Lower part (STA.03-05)
June 26	1.0309	0.0348	2.8076	1.3928
July 04	0.3948	0.3480	2.9170	2.0891
July 18	1.2280	1.2187	5.0450	0.9057
July 26	0.6361	1.0446	4.8910	1.7409
Average	0.8225	0.6615	3.9150	1.5321

Table 5.3 shows that the average of the water surface gradients in the West Channel during low water (LW), I_{LW}, is higher than that during high water (HW), I_{HW} (i.e., I_{LW} is three times as high as I_{HW}). Another feature of interest is that the water surface gradient at the upper part (i.e., STA.01-03) is higher than that at the lower part (i.e., STA.03-05). This indicates that seaward velocities in the upper reach are higher than those in the lower reach.

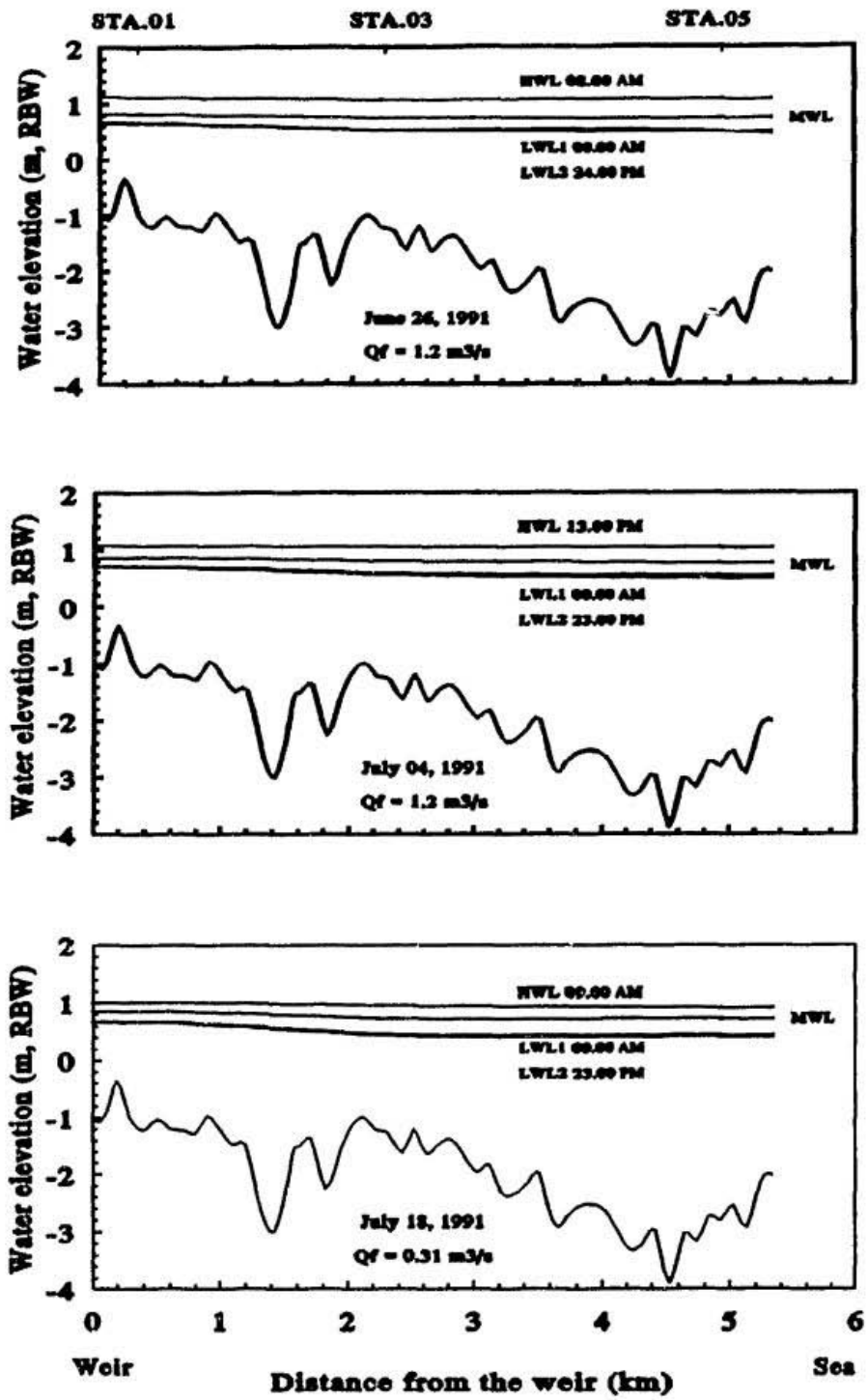

Figure 5.4 Water Profiles at the West channel.

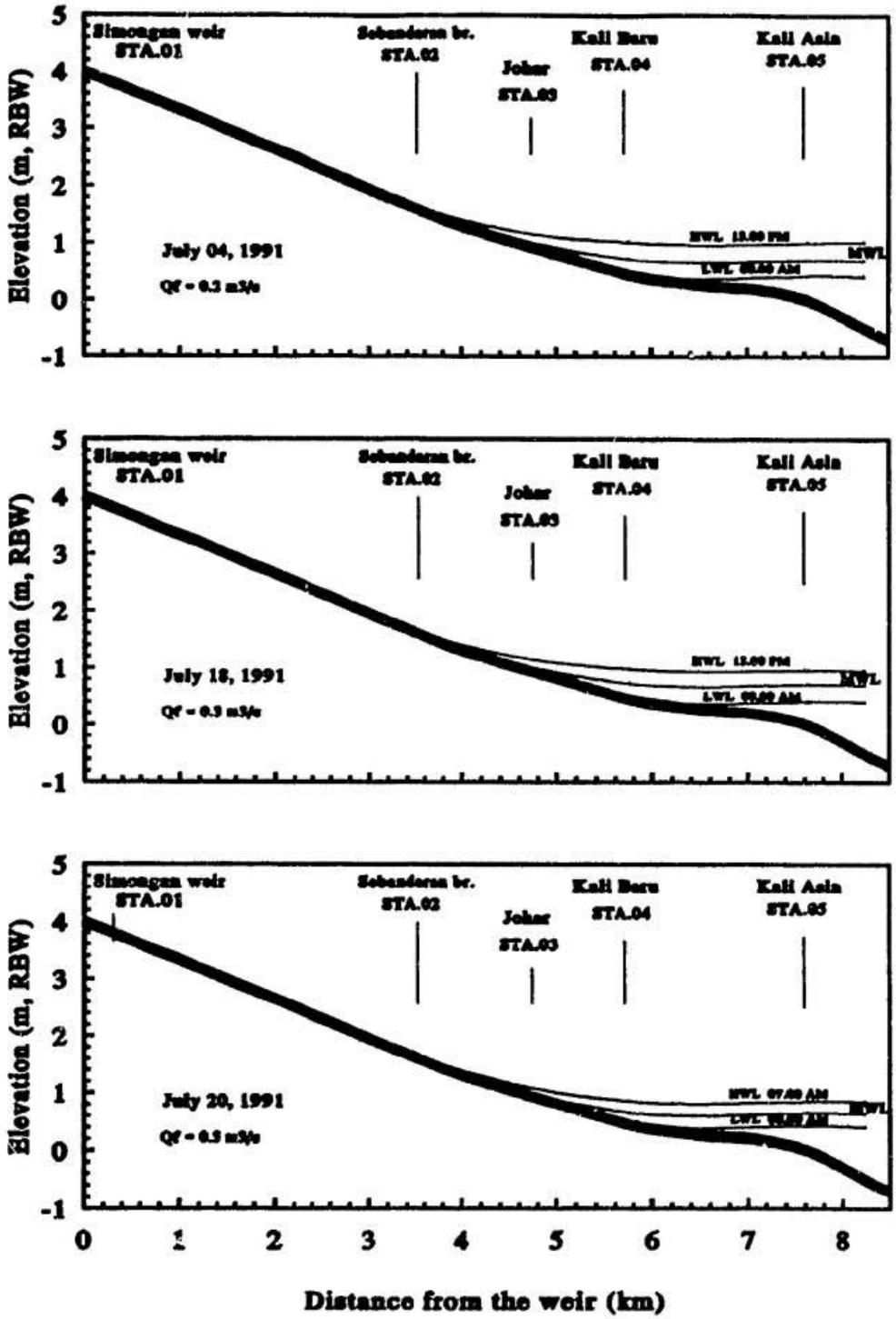

Figure 5.5 Water Profiles at the Kali Semarang.

Table 5.4 Water Surface Gradient at the Kali Semarang

Date	Gradient at HW I_{HW} (10^{-4})		Gradient at LW I_{LW} (10^{-4})	
	Upper part (STA.02-04)	Lower part (STA.04-05)	Upper part (STA.02-04)	Lower part (STA.04-05)
July 04	3.1100	0.0224	6.140	0.1344
July 18	3.2690	0.1389	6.140	0.2016
July 20	4.0138	0.0403	6.140	0.1344
Average	3.4642	0.0677	6.140	0.1561

In the Kali Semarang, I_{LW} is about twice I_{HW}. In the upper part of the estuary (i.e STA.02-04) the values of I_{HW} and I_{LW} are both much higher than the values in the lower part of the estuary (i.e STA.04-05). This phenomena might be due to the variation of the tidal limit. In table 5.4 above, the tidal limit was assumed to be constant and to be located at STA.03. In fact, the location of the tidal limit varies with the tidal level at the mouth.

5.1.2 Estimation of Tidal Volume in the West Channel

The tidal volume was estimated for three different tidal conditions: spring tide (tidal range of 0.94 m), mean tide (tidal range of 0.65 m), and neap tide (tidal range of 0.30 m), see Figure 4.13. The mean water level at the mouth was found to be 0.74 m. The water profile depends on the water elevation at the mouth and the water surface gradient as calculated in Table 5.3 above. When the water profile was obtained

the corresponding areas below the various water levels could then be calculated. The volumes between the sections were calculated by averaging the two areas concerned and multiplying by the centre line distance between the sections. The tidal volume was obtained by subtracting the water volume below high water (HW) and water volume below low water (LW).

The calculation was facilitated by the EL-A curves shown in Figure 5.6 and water surface profiles. The EL-A curve is the relation between water level and cross section area. Curves were calculated for five stations in the West Channel. The relationship between elevation and area is expressed in a polynomial equation as presented in Figure 5.6.

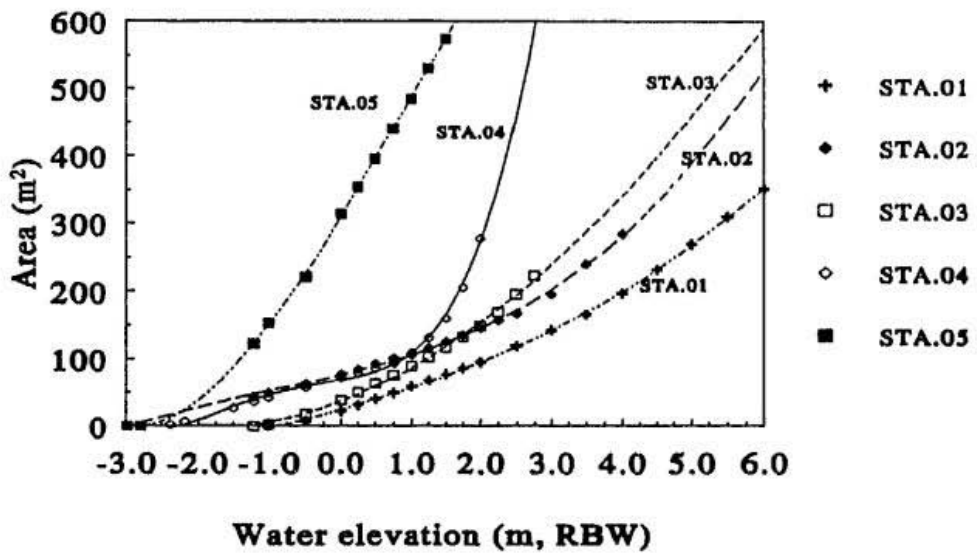

Figure 5.6 Elevation-Area (EL-A) Curves at Five Stations of the West Channel

$A_{STA.01} = 25.1259 + 30.0944\,X + 1.867\,X^2 + 0.3705\,X^3$

$A_{STA.02} = 76.5707 + 25.7555\,X + 2.6061\,X^2 + 0.9404\,X^3$

$A_{STA.03} = 37.2935 + 40.8725\,X + 9.1158\,X^2 - 0.0095\,X^3$

$A_{STA.04} = 69.235 + 19.466\,X + 5.1433\,X^2 - 11.563\,X^3 + 3.195\,X^4$

$A_{STA.05} = 309.0575 + 171.8912\,X + 9.645\,X^2 - 4.458\,X^3$

Water surface profiles were derived from the average water surface gradient as calculated in section 5.1.1, Table 5.3. The initial water elevation at the mouth was taken as mean sea level (MSL) plus or minus tidal amplitude for high water (HW) and low water (LW), respectively. The results are tabulated in Table 5.5.

Table 5.5 Tidal Volume in the West Channel

Station	Distance from the weir (m)	Volume Below High Water (HW)			Volume Below Low Water (LW)			Volume Between HW and LW		
		Spring 100 cm	Mean 64 cm	Neap 28 cm	Spring 100 cm	Mean 64 cm	Neap 28 cm	Spring 100 cm	Mean 64 cm	Neap 28 cm
WEIR	-	-	-	-	-	-	-	-	-	-
STA.01	310	20602	18509	16653	10179	11937	13742	10423	6572	2911
STA.02	1442	63697	60042	56780	46207	48993	51916	17491	11049	4864
STA.03	2232	42428	36818	32643	19381	22806	26469	22047	14013	6173
STA.04	3682	94969	82254	72651	53938	57496	62146	41030	24758	10505
STA.05	4937	323726	304284	284661	214868	234357	254005	108858	69927	30656
Total	4937	544422	501906	463387	344573	375588	408278	199850	126319	55109

5.1.3 Discussion on Tidal Propagation in the West Channel

Tides around the coast of Semarang are mixed, diurnal, with an average tidal range of 0.65 m. The Kali Garang estuary, therefore, experiences a microtidal action. Observation of the water level in the West Channel (section 5.1) shows that tides propagate up the estuary to the Simongan weir. The tidal range decreases gradually from the mouth to the weir. At slack water during a flood tide, the water level is almost horizontal along the estuary. The slope is about 0.00007 m/m. At slack water during ebb tide, the water slope is about 0.00026 m/m.

Configuration of the West Channel can be expected to affect the tidal

propagation. The narrow, relatively uniform, channel (average width at normal discharge is 50 m) causes boundary dissipation to be higher than the effect of convergence. Another feature of importance is the presence of the Simongan weir. The weir stops tides propagating further upstream. Theoretically, the channel should experience a standing wave, with an incoming wave reflected by the weir. As mentioned in section 2.4, the length of the channel plays a major role in determining the mode of the water profile when there is a standing wave. Here, the channel is 5.35 km long with an average river depth of about 2.0 m. The luni-solar diurnal (K_1) component is dominant. Hence the tidal period is 23.93 hours. Therefore the wave celerity (C) is given by

$$C = \sqrt{9.81 \times 2.0}$$

$$= 4.41 \text{ m/s}$$

and the wave length (L) is

$$L = 4.41 \times 23.93 \times 3{,}600$$

$$= 379{,}913 \text{ m}$$

and the time needed to travel from the mouth to the weir (t) is

$$t = (5.35 \times 10^3)/(4.41 \times 60)$$

$$= 20 \text{ minutes.}$$

The length of the channel is far less than one fourth of the wave length (5,350 m $<<<$ 94,978 m). Therefore there is no node point within the channel. If

the channel was frictionless and the convergency factor was negligible, the tidal range should be same throughout the channel.

The travel time (t) is small in comparison with the tidal period. There is practically no difference in time between the occurrence of high water at the mouth and high water at the head(i.e., at the weir). The incoming wave reaches the head before one fourth of wave length completely enters the mouth. Therefore the interference between incoming and reflecting waves is not apparent along the channel.

Finally, tidal propagation is affected by the obstruction of bridge piers. The high water is lowered at the upstream end and the low water is lowered at the downstream end. Consequently the tidal range upstream is smaller than that downstream of the piers. Overall, the tidal range along the West Channel decreases in a landward direction.

5.2 Measurements of Salinity, Temperature, and Currents in the West Channel.

In the West Channel, salinity, temperature, and current measurements were taken simultaneously. The salinity and temperature readings were obtained by using an STC-2D Salinometer. Current speed was measured using a currentmeter (Type C 10.150). Both instruments were calibrated before the survey. The relationship between velocity and the number of revolutions, n, is :

$$\text{for n} < 0.69, \quad v = 0.2375\, n + 0.016 \tag{5.1}$$

$$\text{for n} > 0.69, \quad v = 0.2535\, n + 0.005 \tag{5.2}$$

where n is number of revolution per second, and v is water velocity in metres per second.

The measurements were taken at about mid channel at each station. Readings were made at depths of 10 cm, 25 cm, 50 cm, 100 cm, 150 cm, 200 cm, 250 cm, and about 20 cm above the bottom for each station. The salinity and temperature were read directly from the salinometer.

The currentmeter was carefully positioned parallel to the flow direction, and away from obstacles which might affect the propeller rotation. Readings were taken during one minute for each interval depth.

These measurements were used to determine the longitudinal profile of salinity taken at particular times relative to the tidal cycle, density distribution, circulation patterns, and variation of salinity and velocity in relationship to water elevation. Variation of water density with salinity and temperature is determined by the equation of state (quoted in Thomann, and Mueller, 1987, p. 102) as

$$\rho_{s,t,o} = 1+(10^{-3}\,[(28.14-0.0735\,T-0.00469\,T^2) + (0.802-0.002\,T)\,(S-35)]) \tag{5.3}$$

where $\rho_{s,t,0}$ is the density at salinity S in parts per thousand (ppt), temperature, T, in °C and atmospheric pressure. Furthermore, the density is quantified in the form of *sigma-t* (σ_t) as

$$\sigma_t = (\rho_{s,t,o} - 1).1000 \tag{5.4}$$

5.2.1 Longitudinal Salinity Distribution

Longitudinal measurements of salinity, temperature and currents were taken on June 15, June 19, and June 26, 1991. The average fresh water flow during those dates was 1.6 m^3/s. Tides were diurnal with ranges at the mouth equal to 67, 70, and 58 cm on June 15, June 19, and June 26, respectively. The observation was started from the head of the estuary (weir) to the mouth. Time difference between one station and the next station was about one hour. The field data obtained from the measurements are given in Appendix A, Tables A.3-1 to A.3-4.

Salinity information at each station was plotted against distance for every depth measured using the poles that were installed at every station. The longitudinal bed profile was determined based on the latest measurement (1990) taken by the Directorate General of Water Resources.

When the measurements from each profile had been plotted, the data were contoured to develop lines of equal salinity. Figure 5.7 shows the longitudinal distribution of salinity in the West Channel. Referring to Pritchard and Cameron's classification (see section 2.2), the West Channel can be classified as a highly stratified estuary.

The results shown in Figure 5.7 indicate that sea water intrudes into the West Channel at the bottom of the channel. Fresh water flows downstream over saline water. The fresh water layer is thinner at the seaward end due to the widening of the

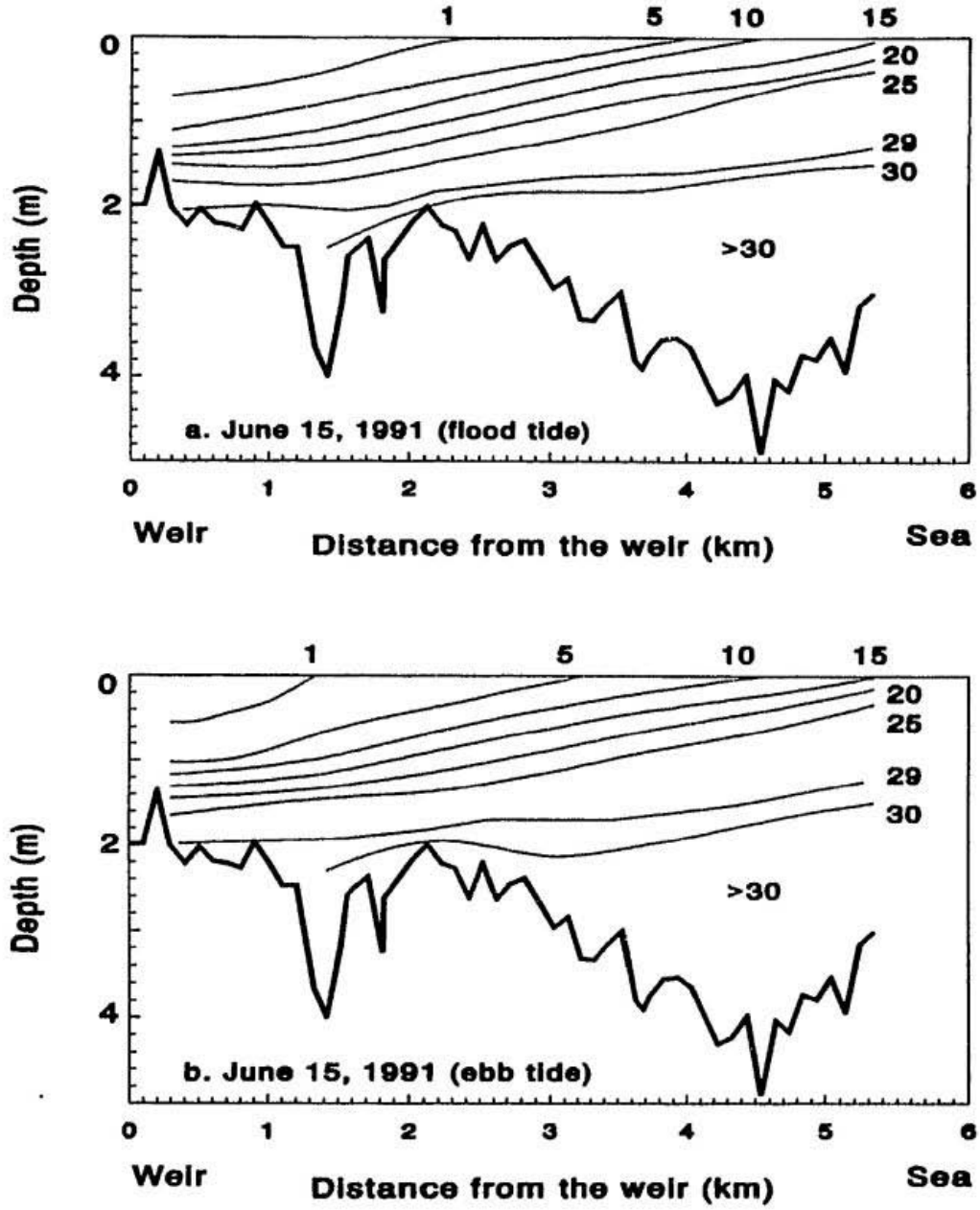

Figure 5.7 Salinity distribution in the West Channel (unit ppt), *a), b)* and *c)* $Q_f = 1.6$ m^3/s, and *d)* $Q_f = 3.5$ m^3/s.

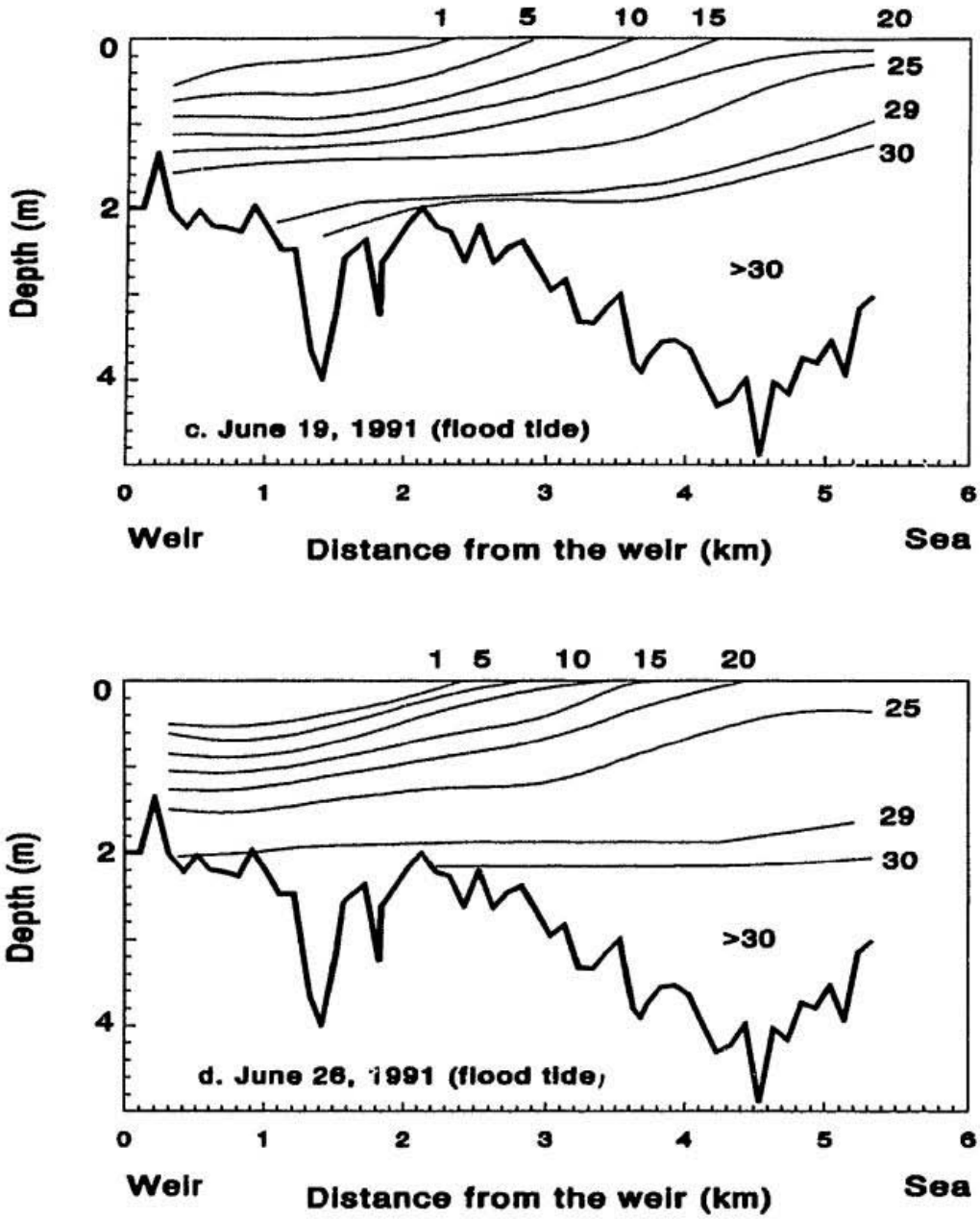

Figure 5.7 Salinity distribution (continued 2/2)

channel. Its average salinity increases seawards. Near the mouth the water column is only moderately stratified. Wind and waves from the sea accelerate the mixing process near the mouth so that the thin layer of fresh water is almost completely mixed with the sea water seawards of the mouth. The saline water in the lower layer was almost motionless during the measurement. Increasing salinity in the upper layer is caused more by vertical dispersion rather than by internal mixing. Further discussion on this matter is given in section 5.2.5.

5.2.2 Density and Circulation

Based on the salinity and temperature data the value of *sigma-t* (σ_t) at each point can be calculated using equations 5.3 and 5.4. The value of σ_t at each depth can then be plotted against distance to obtain the density distribution. Figure 5.8 shows the density and velocity distribution along the West Channel. Closely spaced contour indicate an interfacial layer, which is defined as a position at which the vertical density gradient, $d\rho/dh$, is a maximum. As the position of the halocline is known, the circulation patterns along the channel can be analyzed by calculating the densimetric Froude number, Fr' (equation 2.32). The water depth, h', is measured from the surface to the middle of the interfacial layer and the velocity is taken by averaging velocities over the upper layer. The calculation of Fr' was made at each station for each measurement period.

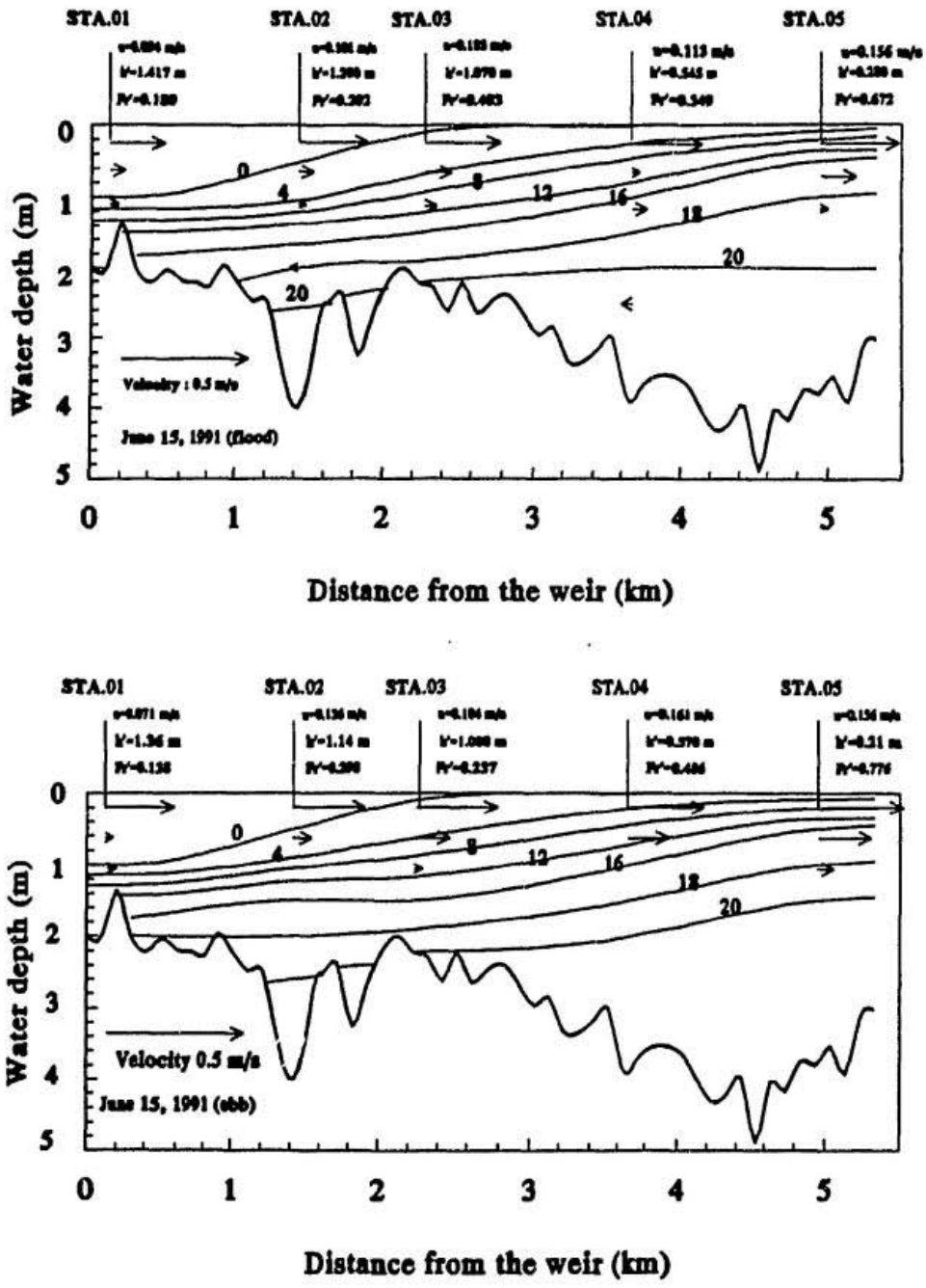

Figure 5.8 Distribution of Density (σ_t) and Flow Structure Along the West Channel, Based on Observations of June 15, 1991 (*Fr'= Densimetric Froude Number*).

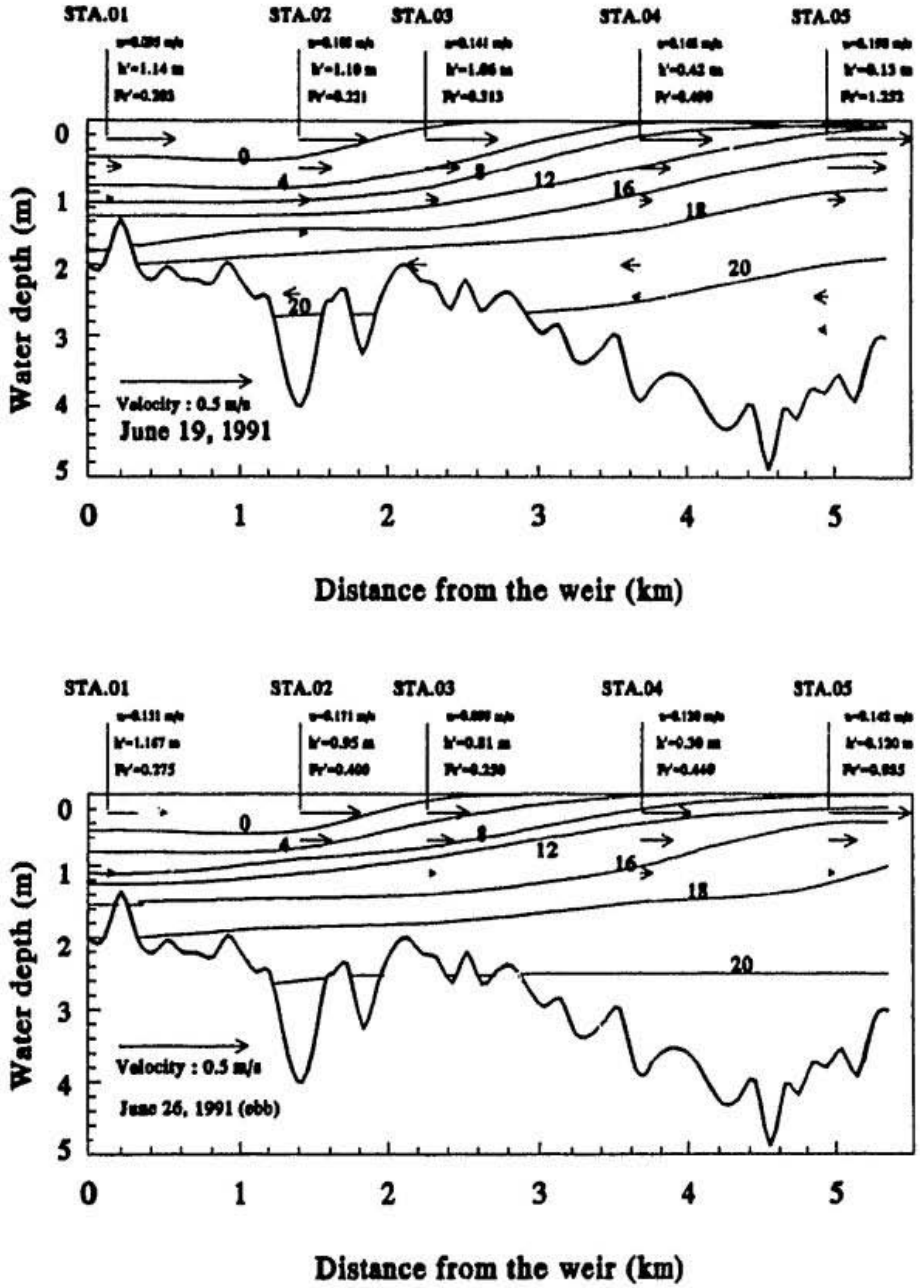

Figure 5.8 Distribution of Density (σ_t) and Flow Structure Along the West Channel, Based on Observations of June 19, 1991 (above) and June 26, 1991 (below), (continued 2/2)

The results (Figure 5.8) show that the value of *Fr'* increases seawards due to the decreasing thickness of the upper layer. Landwards of the mouth the value of *Fr'* is always less than 1.0. This means that there are no internal waves (Farmer and Morgan, 1953). The very low difference in velocity between the two water layers is unable to generate internal stresses. Mixing processes occurred in one direction only, that is from the lower layer to the upper one. The volume of the upper layer increases seawards.

The presence of wind action seawards of the mouth appreciably affects the circulation pattern. The thin surface layer of fresh water is easily disturbed by winds which generate small waves and break the stratification. The salinity survey implies that the water column seawards of the mouth is only slightly stratified.

5.2.3 Salinity and Velocity Variation

The effect of tidal variation on the salinity and velocity was measured at STA.03. Measurements were taken on July 15 and July 18, 1991. On these date, the fresh water flows were 1.6 m^3/s and 0.6 m^3/s, respectively. Tides were diurnal with a range of 68 cm on July 15 and 60 cm on July 18. On July 15, the measurements were started at 8.00 AM and were carried out until 3.00 PM (LW at 1.00 AM and HW at 12.00 noon). On July 18, the observations were made from 6.00 AM to 5.00 PM (LW at 00.00 midnight and HW at 1.00 PM). Readings were taken hourly at depths of 10, 25, 50, 100, 150 cm below the surface, and 20 cm above the bottom. Observed data

are given in Appendix A, Tables A.4-1 to A.4-4.

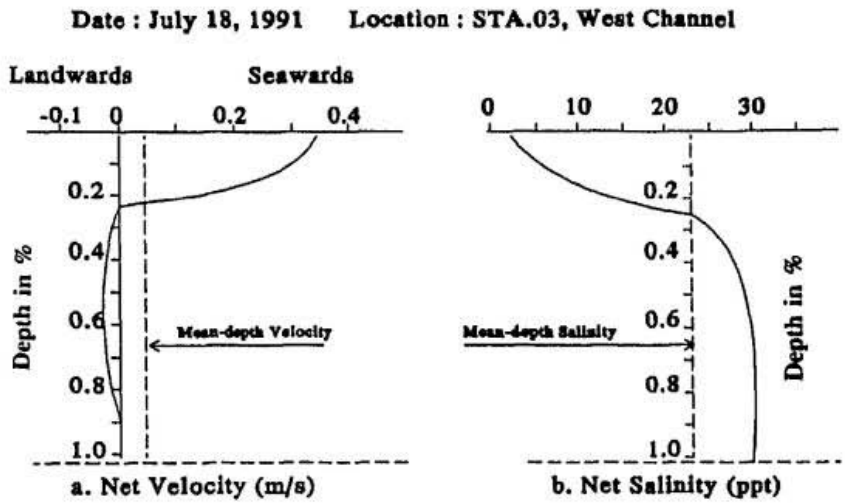

Figure 5.9 Typical Net Movement at STA.03, West Channel: Depth is given in percent.

Measurements showed that the salinity in the lower layer was almost constant with a variation smaller than 2%. The salinity of the upper layer was slightly affected by the water level giving higher salinity during high water than during low water.

Currents in the upper layer always flow downstream during both flood and ebb tides and increase after the high water is reached. In the lower layer, the currents flow landward during the flood tide until about high water, and then there is no flow during the ebb tide. Figure 5.9 shows net salinity and net velocity during a tidal cycle at STA.03 of the West Channel. These typical profiles were derived from data taken on July 18, 1991.

5.2.4 Length of Saline Wedge

The length of salt intrusion in a salt wedge estuary can be determined by using equation 2.29 (see section 2.6.2). Measurements of longitudinal salinity distribution, Figure 5.7, and density and circulation, Figure 5.8, show that the penetration of salt water in the West Channel was limited by the weir. Because of this, the length of the salt wedge could not be found from the measurement. An indirect determination was then made by relating the height of the wedge h_s at each point to the depth of the river mouth H and the distance L of the corresponding point in terms of H. In other words, the relationship is

$$\frac{h_s}{H} = f\left(\frac{L}{H}\right) \tag{5.4}$$

The measured values of L/H and h_s/H (Figures 5.7 and 5.8) are given in Table 5.6.

Table 5.6 Shape of Saline Wedge *(A) June 15 (flood), (B) June 15 (ebb), (C) June 19, and (D) June 26, 1991*

Station	L/H (km/m)	h_s/H (m/m)			
		June 15 (flood)	June 15 (ebb)	June 19	June 26
01	1.493	0.25	0.26	0.35	0.33
02	1.134	0.38	0.38	0.39	0.44
03	0.873	0.48	0.48	0.46	0.54
04	0.404	0.73	0.73	0.77	0.81
05	0	0.93	0.91	0.96	0.96

The values of h_s/H in Table 5.6 were plotted against L/H to obtain the shape of salt wedge. The curve was fitted by using a polynomial relation. Results are presented in Figure 5.10.

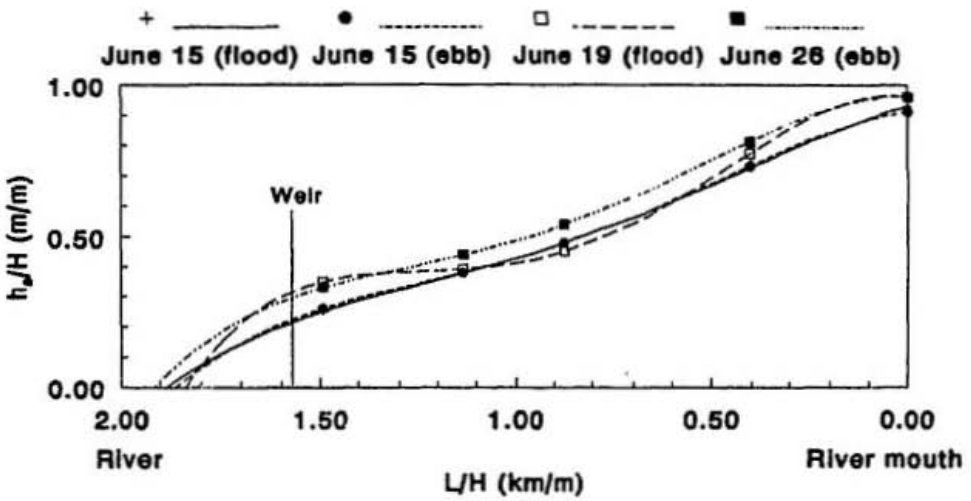

Figure 5.10 Form of Saline Wedge in the West Channel

Figure 5.10 shows that the average value of L/H is 1.9 km/m or 1,900 m/m. This value was substituted into equations 2.29 to 2.31 obtain the coefficient A_o. For the readers' convenience equations 2.29 to 2.31 are repeated here as equations 5.5, 5.6 and 5,7, respectively

$$\frac{L_o}{H} = A_o R_e^m \left(\frac{2\,u_r}{u_\Delta}\right)^{-\frac{5}{2}} \qquad \textbf{(5.5)}$$

$$R_r = u_\Delta \frac{H}{\nu} \tag{5.6}$$

$$u_\Delta = \sqrt{\frac{\Delta \rho}{\rho_m} gH} \tag{5.7}$$

Here $\Delta\rho$ = 20 kg/m^3, ρ_m = 1,010 kg/m^3, g = 9.81 m/s^2, H = 3.1 m, thus from equation 5.7 the densimetric velocity, u_Δ = 0.778 m/s. The kinematic viscosity ν = 0.818 10^{-6} m^2/s. Reynolds number, R_e, is obtained from equation 5.6, that is 2.9 10^6. Current velocity, u_r was obtained from the average of the four measurement given in Figure 5.8, that is 0.098 m/s. The value of m is taken at 0.25 (between 0.25 to 0.5, Keulegan, 1966). Hence from equation 5.5 the value of the constant A_o is 1.46. Thus

$$\frac{L_o}{H} = 1.46\left(\frac{u_\Delta H}{\nu}\right)^{0.25}\left(\frac{2\,u_r}{u_\Delta}\right)^{-2.5} \tag{5.8}$$

As this equation (equation 5.8) was derived during the low fresh water flow, its use may be limited and further study is suggested to obtain a better relationship.

5.2.5 Discussion

Figures 5.7 and 5.8 show that the West Channel is highly stratified with regard to salinity distribution and water density during the period of low fresh water flow in the dry season. The effect of the stratification is to distort the normal vertical

velocity profiles into profiles typified by that shown in Figure 5.9. Fresh water flows downstream on the top of the seawater throughout tidal period, while a tidal density current moves up slowly only at the beginning of flood tide. The salt water rests on the bottom as an almost motionless layer. As a result, the net water movement after a tidal cycle of 23.93 hours shows the surface water to be moving seawards and the bottom layer to have a net landwards movement.

Stratification during the time of observation was examined by calculating the estuarine number, S_e, (equations 2.34 and 2.35). The calculation was undertaken at STA.01, STA.03, and STA.05. Results are presented in Table 5.7.

Table 5.7 Estuarine Number, S_e, of the West Channel

Date	Tidal range at the mouth (cm)	Fresh water flow (m^3/s)	Estuarine Number, S_e		
			STA.05	STA.03	STA.01
June 26, 91	58	1.60	$2.13\ 10^{-5}$	$1.51\ 10^{-5}$	$2.55\ 10^{-8}$
July 04, 91	50	1.60	$1.57\ 10^{-5}$	$1.03\ 10^{-5}$	$1.41\ 10^{-8}$
July 26, 91	55	0.65	$2.09\ 10^{-5}$	$1.43\ 10^{-5}$	$1.06\ 10^{-8}$

A cursory glance at the values of S_e in Table 5.7 shows that, according these estuarine numbers, the West Channel during low fresh water flow was highly stratified ($S_e < 0.03$). To confirm this result, the effects of fresh water discharge and tidal action on the degree of stratification were examined by using a flow ratio, K, suggested by Simons (1969) (quoted in Silvester, 1974, see section 2.6.3). In Table 5.8

this ratio has been calculated for various river discharges and for three tidal ranges in the West Channel.

Again, according to the Table 5.8, the West Channel is highly stratified throughout the year. These ratios are too high when applied in this estuary. This may be because of the presence of the weir beyond which the tide can not propagate. In fact, the tidal range downstream of the weir is still significant in comparison to that at the mouth. Therefore, the tidal effects due to the volume of salt water entering the estuary during a tidal cycle are not represented in the normal wedge.

Table 5.8 Values of flow ratios, *K*, for the West Channel

Fresh water flow in (m^3/s)	No. of daily avg. flow Jan'87-Dec'89	Ratio (K) for		
		Spring tide T=23.93 h.	Mean tide T=18.50 h.	Neap tide T=12.42 h.
2.00	307	0.8621	1.0545	1.6227
3.00	139	1.2932	1.5817	2.4340
5.00	205	2.1553	2.6362	4.0567
10.00	178	4.3106	5.2724	8.1133
15.00	91	6.4660	7.9086	12.1700
20.00	55	8.6213	10.5447	16.2266
25.00	58	10.7766	13.1809	20.2833
50.00	40	21.5532	26.3619	40.5666
100.00	6	43.1064	52.7237	81.1332
> 100.00	9	> 43	> 52	> 81

Despite this fact, it is very relevant to put forward Pritchard's statement about the parameter affecting the degree of estuarine stratification. Pritchard (1955) states that "other things being kept equal, an estuary tends to drift from highly stratified through moderately stratified to vertically homogeneous" with (1) decreasing river flow,

(2) increasing tidal range, (3) increasing width, and (4) decreasing depth. The effect of changing the values of these parameters can be evaluated as follows.

If the width, depth and tidal range are assumed to remain constant the effect of variation of river flow can be considered. Increasing river flow induces increasing stratification and the estuary changes from well mixed to a salt wedge estuary.

Variation of tidal range with constant river flow, width and depth can be easily examined. The tideless estuary would be highly stratified with fresh water flowing over seawater. As the tidal range increases, tidal currents and tidal flow increases, thus reducing the degree of stratification. The estuary changes from a salt wedge to well mixed with increasing tidal range.

The variation of width of an estuary while keeping the other variables constant affects the ratio between the tidal volume and the river volume. Increasing width increases the cross sectional area. Consequently, the tidal volume increases, while the velocity of the fresh water flow decreases. Therefore, increasing width decreases the stratification.

Increasing depth decreases the influence of bottom stress on the mixing process. As result, the stratification increases.

Referring to the fact that in the West Channel there is very low tidal density current, the only possible mixing is that created by molecular diffusion. Weak tidal action enables the establishment of a two layer flow. In the lower zone the salinity is practically constant and the water is almost motionless. Turbulence inherent in the

flow is insufficient to overcome the stabilizing gravitational effect. These cases are illustrated in section 5.2.1, Figure 5.7. A weak tidal action therefore only results in a horizontal motion of the salt water to and fro. There is very little salt water movement and the bottom salty layer is relatively stable. The fresh water flows down over it but it is not mixed into the bottom layer. The mixing is entirely upwards. Thus, the bottom layer has a fairly constant salinity along its length but loses salt gradually into the surface layer. This loss is replaced by a slow salt water flow at the beginning of the flood tide.

Fresh water velocity in the upper layer increases and its thickness decreases seaward, which has been illustrated by means of density distribution and flow structure in section 5.2.2, Figure 5.8. Here the flow just below the interface is in the same direction as that of the fresh water. In the region close to the bottom the motions are reversed. This is particularly true during the early stages of the flood tide.

The value of flow ratio, K, listed in Table 5.8 indicates that the river discharge has a very pronounced effect on the water movement in the estuary. The surface layer that flows downstream throughout the tidal cycle may be increased with increasing river flow, and the salt water may be swept completely out of the estuary during very high river flows.

The length of the salt penetration can be estimated by using equation 5.5. For example, assuming the river discharge is 25 m^3/s, the tidal level is + 0.74 m (MSL), the cross section area is 170 m^2, $\Delta\rho/\rho_m$ is 0.0198, and ν is 0.818 10^{-6} m^2/s, equation 5.8, gives an estimation of wedge length equal to 2.13 km. In the same way

it can be shown that, at a fresh water discharge of 75 m^3/s, the saline water is almost completely swept out from the estuary ($L_o \approx 125$ m).

5.3 Water Analysis

In the Kali Semarang, salinity was measured by titration. Samples were taken from the mid depth of the river at each station by using a water sampler. These samples were then stored in two-litre bottles. The sample was titrated with silver nitrate to obtain the chlorinity (*Cl*), that is the total weight of chloride, plus a chloride equivalent of bromide and iodine in a one kilogram water sample. The salinity was determined by using equation

$$S(‰) = 1.80655 \text{ X } Cl(‰) \qquad (5.9)$$

Dissolved Oxygen (DO), Biological Oxygen Demand (BOD), and the pH of the samples were also analyzed.

Sampling water for the analysis was taken during high water.on July 15, and July 19, 1991. The results of the water analysis are presented in Table 5.9. The distribution of salinity in the Kali Semarang was obtained by plotting data from each station against distance for every sampling period. The longitudinal bed profile was determined based on data obtained from the Committee of Normalisation of Kali Semarang and it was adjusted to the present condition. The plotted data were then contoured. Results are presented graphically in Figure 5.11.

Table 5.9 Water Analysis in the Kali Semarang, July 15, 1991 (above), and July 29, 1991 (below).

Station	Parameters				
	DO (ppm)	BOD (ppm)	pH	Conductivity (mV)	Salinity (ppt)
STA.01	6.13	3.20	8.3	133.4	0.21
STA.02	0.00	13.87	7.5	- 46.0	0.20
STA.05	1.70	27.00	7.4	92.2	19.69
STA.02	0.05	114.49	7.9	- 68.8	0.17
STA.04	4.91	*)	7.5	33.0	0.14
STA.04	0.00	247.04	7.7	12.6	7.15
STA.05	4.96	131.34	7.1	13.8	22.86

*Note *) undetected*

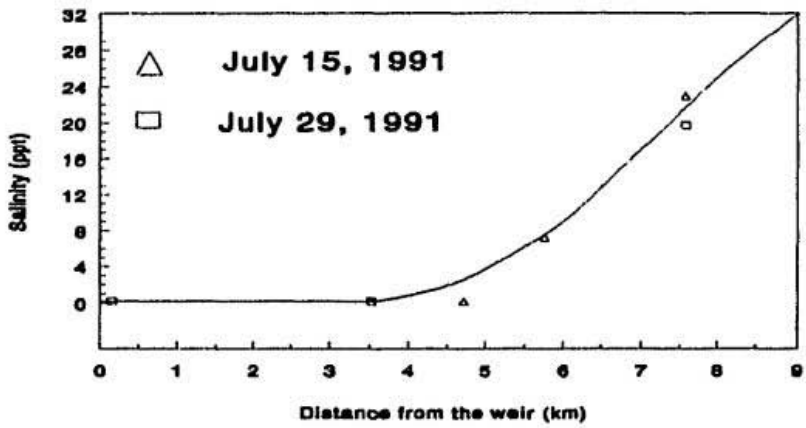

Figure 5.11 Longitudinal Salinity Profile in the Kali Semarang.

The result shows that the salinity in the Kali Semarang intrudes about 3.5 km upstream from the river mouth. This point is the furthest upstream to which the saline water intrudes. Its limit moves downstream during the ebb tide (low water) as far as the Kali Asin (about 600 m from the mouth). The variation of salinity is

completely dominated by tidal action at the mouth. This is true during a period of measurement at which the fresh water flow is very low.

The same analysis was also done for samples taken from the West Channel. The samples were taken on July 15, 1991 at STA.01, STA.03, and STA,05. Results are listed in Table 5.10 following.

Table 5.10 Water Analysis in the West Channel, Based on observations of July 15, 1991.

Station	Parameters				
	DO (ppm)	BOD (ppm)	pH	Conductivity (mV)	Salinity (ppt)
STA.01	6.36	2.45	8.2	148.6	1.71
STA.02	5.21	3.52	7.8	122.4	14.36
STA.05	5.69	1.36	7.8	115.4	27.23

Further discussion about water analysis and water pollution in estuaries is given in chapter 7.

5.4 Float Tests

Float tests were used to determine the speed and direction of the currents, and their effects on sediment movement. The float consisted of wooden cross with vanes 20 cm deep and 20 cm long from centre to tip. The cross was attached to a small bamboo with a small flag on top. The float was suitably weighted to keep the bamboo more upright and to keep the vane at the correct depth.

5.4.1 Currents in the West Channel

Float tests in the West Channel were undertaken at STA.03 on July 19 and July 25, 1991. The river flow during those periods was 0.5 m^3/s. Tidal influence was semidiurnal with a range of 55 cm on July 19, and was diurnal with a range of 64 cm on July 25. The float was centrally situated in the estuary. The vane was placed at about the mid depth of 2.0 metres average water depth (1 m below the surface). Time

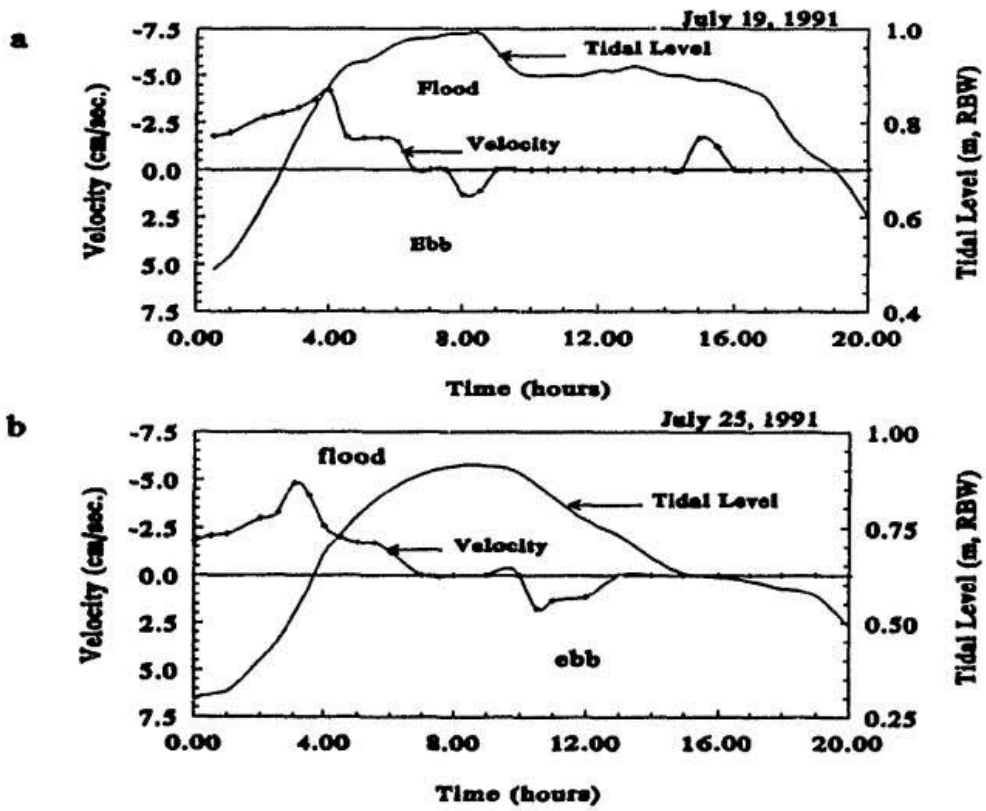

Figure 5.12 Measurements of Current Speed at STA.03 of the West Channel; *Measurement was taken by using float test, 100 cm below water surface in 200 cm of average depth.*

required to travel a distance of 20 m was recorded for each measurement. Floats were released at one half hour interval. Direction of the float movement was also observed. Data obtained are shown in Appendix A, Tables A.5-1 to A.5-4. Results show that the effects of Coriolis' force to the direction of the water movement were not apparent. The float always moved in the middle of the channel, where the float was released. It should be noted that the flow is low (maximum velocity measured was 5 cm/s), the channel is narrow, and it is located at the low latitude (equator). Figure 5.12 shows the quantitative-variation of current speed at STA.03, West Channel.

Flood currents are strongest three to four hours after the beginning of the rising tide, and are zero at mid-tide (slack water). The slack-flood occur for two to four hours. During strong flood currents, however, water on the upper layer still flows seawards. The ebb currents occur one or two hours after high water. The magnitude of the ebb current is lower than that of the flood current. Figure 5.13 shows the comparison between measured and calculated tidal currents taken in June 25, 1995. The current was calculate by using equation 2.9, where a = 0.30 m, h = 2.00 m, C = 4.41 m/s, L = 380 km, T = 23.50 hours, and x = 2.23 km.

As the theoretical values are based on an assumption that the tides are sinusoidal waves, the results are slightly different in the shape of the curve. The maximum flood current calculated is as the same as that measured, but the ebb current calculated is significantly higher. This is caused by the difference in duration between flood and ebb. The flood period is about 8.50 hours and the ebb period is about 15 hours.

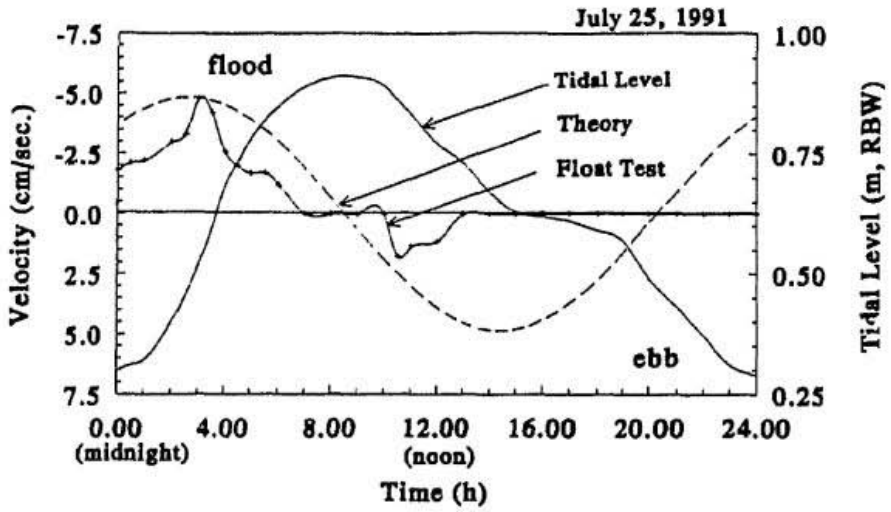

Figure 5.13 Comparison Between Calculated and Measured Tidal Currents at STA.03, West Channel, July 25, 1991.

5.4.2 Currents in the Kali Semarang

In the Kali Semarang, float tests were done on July 20 and July 26, 1991. The fresh water flow and tidal range on July 20 were 0.30 m^3/s and 52 cm, respectively. On July those were 0.40 m^3/s and 61 cm. The float was released at STA.05 (Lower area of the Kali Asin), where the channel at that location is straight and is as long as 200 m both in the upstream and downstream direction. The average depth is about 1.00 m. The float was therefore 50 cm below the surface. However the float did not flow smoothly due to the shallow water. The experiment was then done using a bottle. The bottle was 40 cm long. It was filled with water to keep it vertical and at

the correct depth. A small flag was attached on a piece of stick and put on the top of the bottle. The measurement was similar that taken with the float in the West Channel. Measured data is shown in Appendix A, Tables A.6-1 and A.6-2.

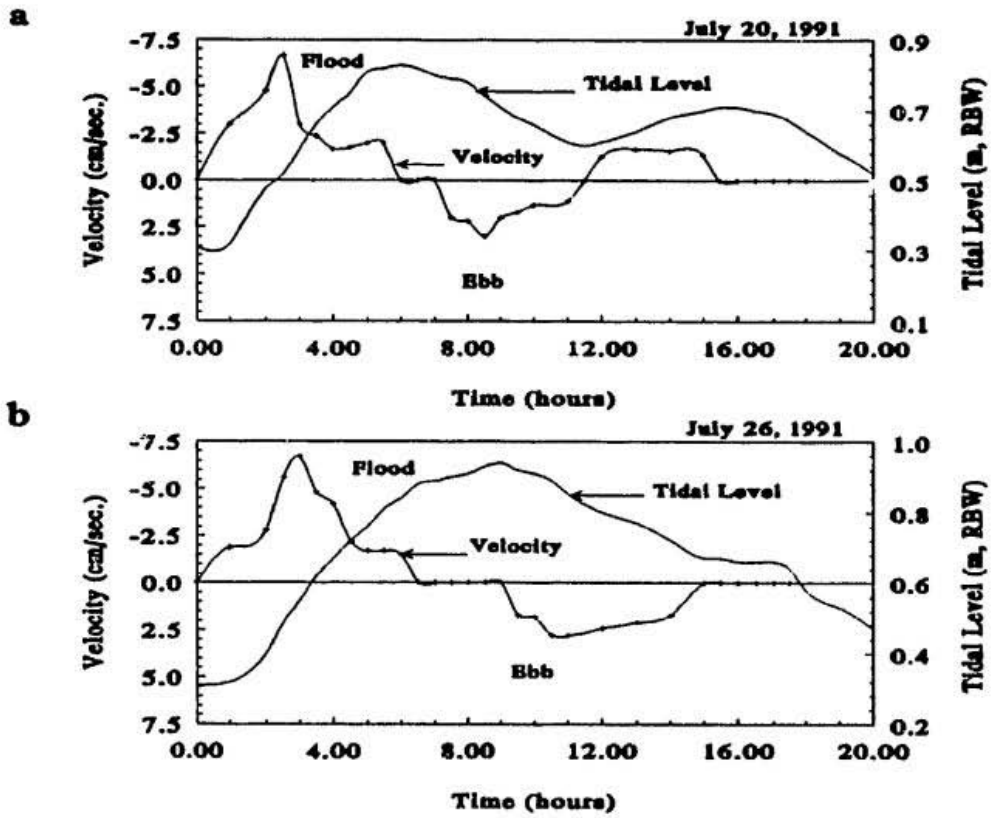

Figure 5.14 Measurements of Current Speed at STA.05 of the Kali Semarang; *Measurement was taken by using float test (Bottle), 40 cm below water surface in 100 cm of average depth.*

Currents move landwards during the flood tides and seawards during ebb tides (Figure 5.14). The current was faster about two hours after the beginning of the flood and ebb tides. The slack water between flood and ebb tide is as long as one to three hours. During that time the float moved up and down very slowly. This character

of tidal currents indicate that there is a standing wave. The incoming tidal wave is reflected by the bottom channel between STA.02 and STA.03.

For a comparison, the average maximum tidal currents in the Kali Semarang can be estimated by using (Thomann, 1987, p. 93)

$$\overline{U_{max}} = \frac{\pi X_{te}}{T_{K_1}} \qquad (5.10)$$

where x_{te} is the distance of tidal excursion, in this case the value is 3.51 km, and T_{K1} is period of dominant constituent, for K_1 the value is 23.93 hours. Thus from equation 5.10 U_{max} = 0.128 m/s.

5.5 Sediment Analysis

Sampling of bottom sediments were carried out using a simple coring device. The corer consists of a metal tube 10 cm in diameter, 50 cm long. Samples were taken during low water. A tube was inserted into the river bed manually until it was nearly full of soil and then pulled up slowly to keep the soil in the core. The soil was then kept in a plastic bag for further analysis. Samples were taken at STA.01, STA.03, and STA.05 in the West Channel; and at STA.01 in the Kali Semarang.

5.5.1 Particle Size Analysis

The purpose of this section is to determine the grain size distribution and

quality of the bed sediment along the estuary, and to trace the movement of the sediment. Samples were analyzed using sieve-analysis. The weight retained on each mesh was logged. This was then converted to a percentage of the total weight of sediment analyzed. The data obtained are presented in Table 5.11.

Table 5.11 Grain size analysis of bed-load sediment samples, *(1) frequency weight in %, (2) cumulative frequency weight in %.*

Diameter (ϕ)	West Channel						Kali Semarang STA.01	
	STA.05		STA.03		STA.01			
	1	2	1	2	1	2	1	2
-3	0.0	0.0	0.0	0.0	0.0	0.0	0.0	0.0
-2	0.0	0.0	0.0	0.0	0.5	0.5	0.0	0.0
-1	0.0	0.0	0.0	0.0	3.0	3.5	0.0	0.0
0	0.0	0.0	0.0	0.0	1.5	5.0	0.5	0.5
1	1.5	1.5	1.0	1.0	2.0	7.0	1.5	2.0
2	12.0	13.5	2.5	3.5	5.5	12.5	5.0	7.0
3	31.5	45.0	11.0	15.0	10.0	22.5	13.0	20.0
4	21.0	66.0	16.0	31.0	14.0	36.5	13.5	33.5
5	11.5	77.5	25.5	56.5	22.5	59.0	20.0	53.5
6	12.0	89.5	28.5	85.0	16.0	75.0	26.5	80.0
7	9.5	99.0	9.0	94.0	5.5	80.5	11.5	91.5
8	1.0	100.0	5.0	99.0	6.5	87.0	5.5	97.0
9	0.0	100.0	1.0	100.0	5.0	92.0	3.0	100.0
10	0.0	100.0	0.0	100.0	5.0	97.0	0.0	100.0
11	0.0	100.0	0.0	100.0	3.0	100.0	0.0	100.0

Tabulated data are also presented in graphical form as histograms. A histogram is a bar graph based on continuous data and shows the weight percentage of sediment in each size class. The independent variable is grain size, as horizontal axis, and the dependent variable is the weight percentage, as a vertical axis. The cumulative frequency curve is also used. In this case the vertical axis is laid off in divisions from 0 to 100 % and the horizontal axis retains its size scaling.

The percentage weight retained on the coarsest sieve is plotted at the relevant diameter. The sum of the sediment weight percentage in the coarsest two sieves is plotted above the next finer sieve mesh size. Then the sum of the residue on the coarsest three sieves above the third value, and so on, until the entire sediment distribution has been accounted for at the cumulative value of 100 %. Figure 5.15 shows the grain size analyses of the bed-sediments.

Table 5.12 Descriptive character of sediment samples

Class (size ϕ)	West Channel			Kali Semarang (Upper)
	Upper part	Middle part	Lower part	
Sand (-1.0 - 4.0)	66.0 %	30.0 %	36.5 %	20.0 %
Silt (4.0 - 8.0)	34.0 %	68.0 %	51.5 %	70.0 %
Clay (8.0 - 12.0)	0.0 %	2.0 %	12.0 %	10.0 %

Based on the Wentworth Classification (Table 2.3), sediment samples can be divided naturally into three different size groups or modes, namely sand, silt and clay. The percentage of each group of each sample is summarized in Table 5.12. The table shows that the distribution of sediment material along the West Channel decreases in diameter from the lower part to the middle and then increases in the upper part. In the upper part, the sediment is composed of sand (66 %) and silt (34 %). The percentage of sand decreases in the middle (30.0 %) but increases again in the

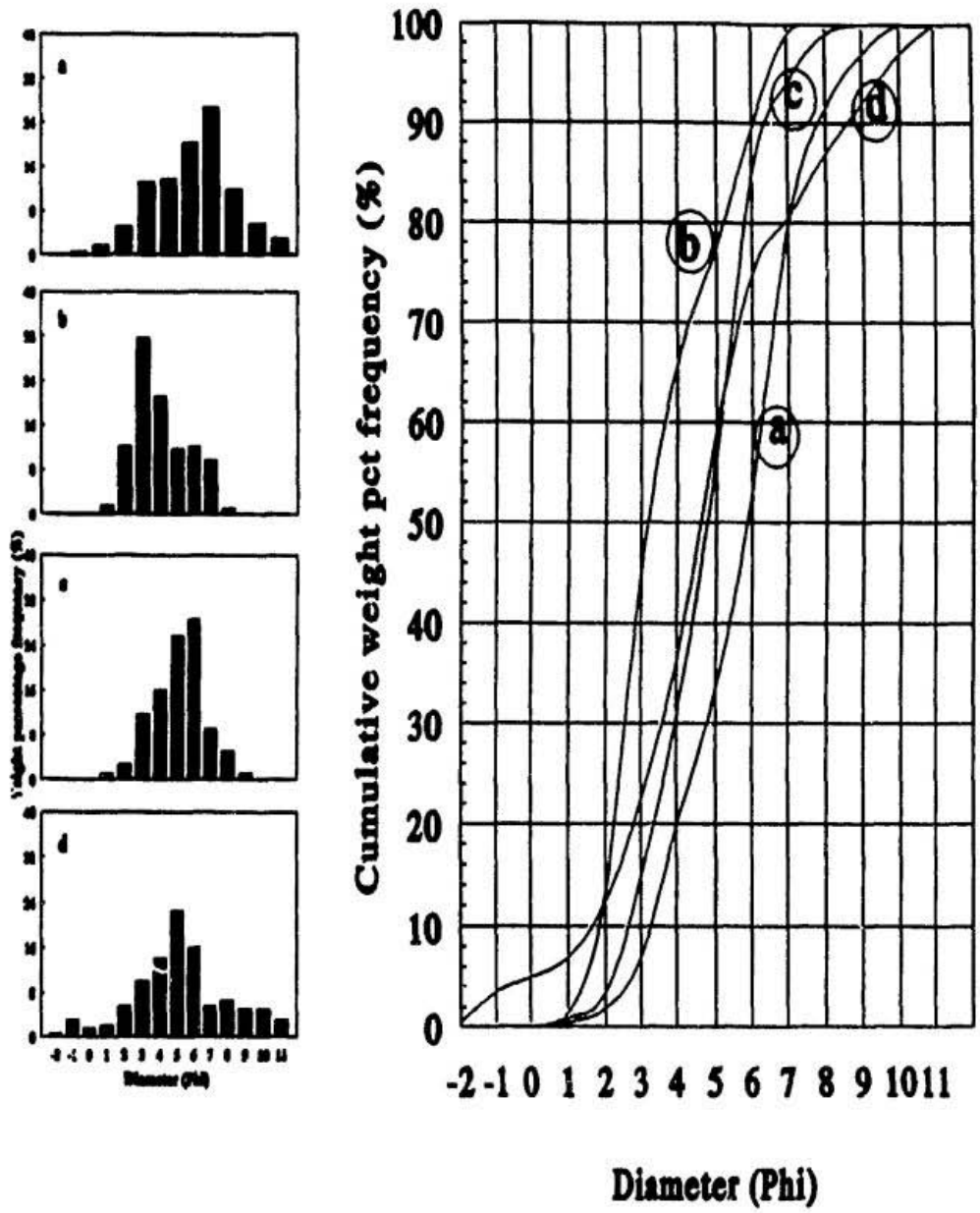

Figure 5.15 Grain Size Analyses; Plot of Frequency by Weight Percentage Against Grain Diameter (*left*), Plot of Cumulative Percentage Frequency by Weight Against Grain Diameter (*right*). *a)* Upper part of the Kali Semarang , *b)* STA.01, *c)* STA.03, and *d)* STA.05 of the West Channel.

lower part (36.5 %). Conversely, the percentage of silt increases in the middle (68.0 %) and decreases in the lower part (51.5 %). The percentage of clay increases seawards along the Channel. The original river sediment that is represented by the sample taken upstream of the weir, is dominated by silt (70.0 %). Sand and clay are only (20.0 %) and (10.0 %), respectively.

5.5.2 Measures of Size Distribution

The size distributions were described qualitatively using median diameter (M_d), mean diameter (M_ϕ), standard deviation (σ), and skewness (α_ϕ). The values of these parameters were calculated using equations 2.38 through 2.41 and were facilitated by the cumulative curve, Figure 5.15. Results are summarized in Table 5.13.

Table 5.13 Qualitative description of bed-load distribution

Measures	West Channel			Kali Semarang ϕ
	Upper Part ϕ	Middle ϕ	Lower Part ϕ	
$Md = \phi_{50}$	3.25	4.80	4.90	4.90
M_ϕ	3.80	4.55	4.90	4.75
σ_ϕ	1.60	1.25	2.40	1.85
α_ϕ	-0.31	-0.20	0.17	0.30

Based on Table 5.13, the sediment in all parts of the estuary can be seen to be distributed asymmetrically with a skewness value varying from -0.31 to 0.30. Sediments in the lower part have a better distribution than those from the other parts. The sediments are poorly sorted ($\sigma_\phi > 1$).

5.5.3 Discussion

Distribution of bed sediment samples indicate that the speed of the river current decreases as the water flows over the weir. The channel can be regarded as a settling basin for a large quantity of material supplied by fresh water. Coarser material settles first just downstream of the weir. The finer grains are still in suspension but gradually settle further downstream.

Both theoretical and observed tidal currents (Fig. 5.13) indicate that they are too small to either initiate sediment movement or to increase sediment concentration in the water. Thus settling is unaffected by tidal currents. The distribution of sediments along the channel disagrees with the idea that suspended sediments in the salt wedge estuary accumulate at the limit of penetration of the salt wedge. In fact, the salt water penetrates to the weir but the tidal currents are zero at this point due to reflecting waves.

In the lower part of the estuary, wave effects are believed to be important in returning sand back from the surf zone or surrounding area to the mouth, so that there is a higher percentage of sand there than that in the middle reaches.

Chapter 6

Sediment Budget and Delta Formation

No direct observations of sediment budget and delta formation were made. The only observations taken were samples of bottom sediment, water profiles, and tidal currents. The following sections deal with estimates of the sediment budget and delta formation. These estimates are based mainly on the theory related to the available basic data, such as river discharge, wind and wave data, tidal data, bathymetry, and geometry. A sediment budget was estimated from the rate of river sediment load and the rate of longshore drift. The delta formation was examined by using the discharge effectiveness index, I_Q.

6.1 Wave Energy Flux

Wave energy flux was calculated for waves of different periods separately and then was added together to get the total wave energy flux. The calculation was made at the subaqueous limit, where the depth is about 30 feet (9.0 m) (Wright and Coleman, 1972) and in the nearshore area (river mouth). In the present

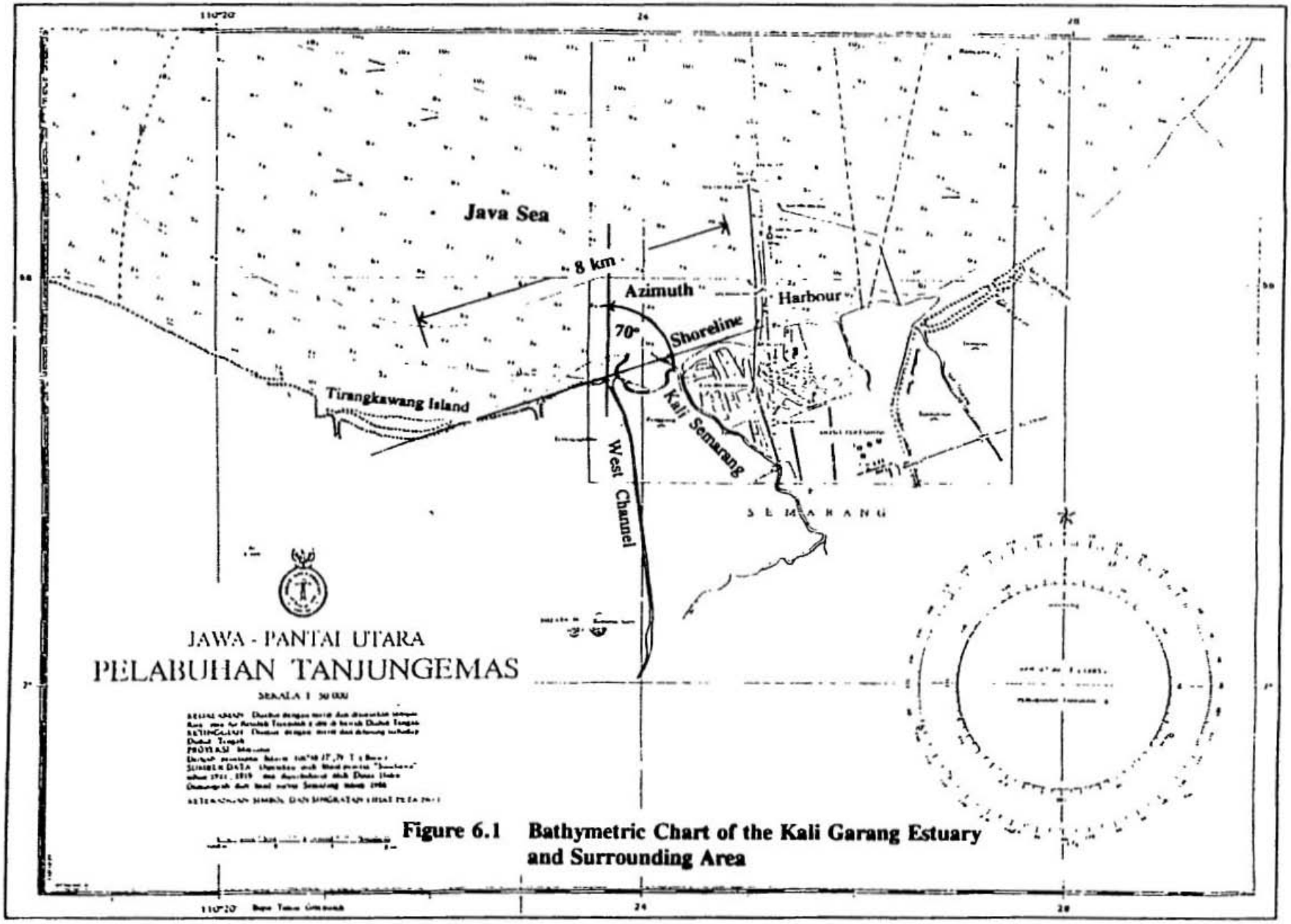

Figure 6.1 Bathymetric Chart of the Kali Garang Estuary and Surrounding Area

case the subaqueous limit is 4,000 m seawards of the shoreline (see Figure 6.1). The depth of the nearshore water is 1.70 m.

The first step was to determine the azimuth of the shoreline. Azimuth is the orientation of the shoreline with respect to north. In this case the azimuth was 70° (Figure 6.1). Hence the winds from a 180° seawards sector was taken as the winds generating wave energy within the delta area.

Percentages of occurrence of different wave heights were obtained from the wave hindcast given in Table 4.10. As waves are assumed to be derived solely from wind action, the percentage occurrence of wave direction will be the same as the wind direction at the location as given in Table 4.9. The wave energy was then calculated by using equations 2.12 to 2.21 (see section 2.5.1). The angle α_o is the angle between the wave crest and the shoreline or the angle of the wind direction with respect to a normal to the shoreline. Sea water density (ρ) was 1020 kg/m^3, g = 9.91 m/s. The calculation of deep wave energy flux is presented in Appendix B.

Near shore wave energy flux was calculated at the depth of 1.70 m. This depth was based on the mean depth of the river mouth. The shoaling coefficient, *Ks*, wave group celerity, *Cg*, and other wave variables were taken from Table C-1 in the U.S. Army (1984) (see Appendix H). Calculations of near shore wave energy flux are given in Appendix C. The summary of wave energy climate is shown in Table 6.1. Figure 6.2 shows the distribution of monthly wave energy flux during 1989.

Table 6.1 Wave-energy Flux and Wave Attenuation of the Kali Garang River Delta in 1989.

Months	Wave energy flux in deep water (J/m-s)	Wave energy flux in nearshore (J/m-s)	Wave attenuation
January	35.42	4.31	8.22
February	43.93	5.46	8.04
March	34.55	4.14	8.35
April	29.45	3.49	8.44
May	18.65	2.18	8.57
June	21.62	2.59	8.34
July	17.27	2.02	8.56
August	16.36	1.91	8.54
September	23.56	2.76	8.53
October	23.94	2.84	8.25
November	27.98	3.26	8.57
December	32.24	3.88	8.30
Average	27.08	3.24	8.37

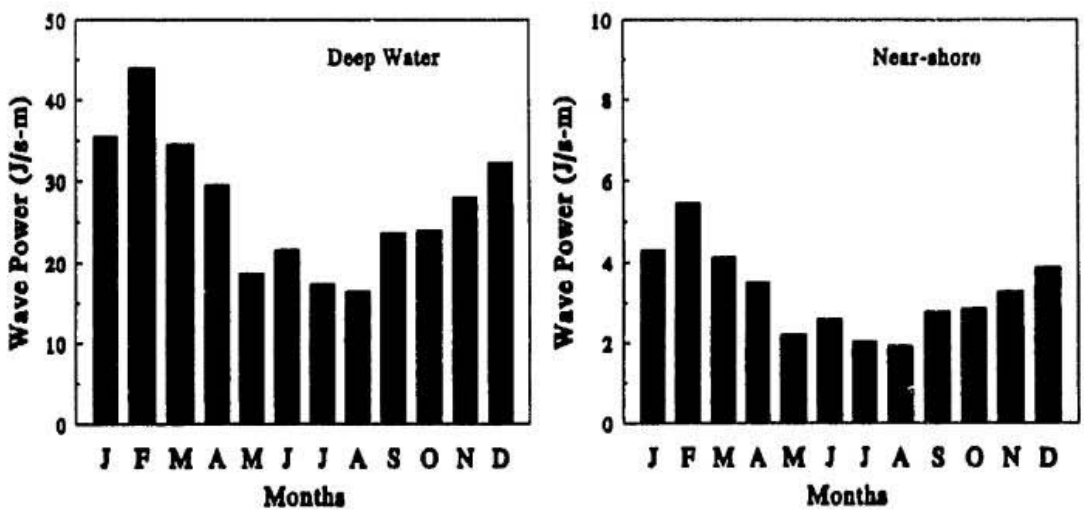

Figure 6.2 Distribution of Monthly Wave Energy Flux Climate During 1989

The result shown in Table 6.1 and Figure 6.2 indicate that the wave energy flux is high during the rainy season, October to April, with a maximum in February. This energy is mainly generated by the west monsoon which blows from the sector between West and North-west (onshore winds). The east monsoon that blows during the dry season (May to September) generates less energy flux, because a large part of this wind blows from the sector between East-south-east and South-south-east (offshore winds). This type of energy distribution will further affect the distribution of the longshore transport and the sediment originating from the river (see section 6.6).

6.2 River Sediment Load

Sediment entering the estuary from river sources was estimated using the sediment carrying capacity (see section 2.7.3). Suspended load was estimated using Kalinske's equation (equation 2.50) and the bedload using Sato's equation (equation 2.44). Ideally, these formulae should be examined with the field condition. Unfortunately, no measurements were taken at the Kali Garang River. However formulae have been developed for the Brantas River (Department of Public Work, 1966) which is in the same geographical area and, in the absence of any other information, these were applied to the Kali Garang.

6.2.1 Computations of Water Surface Profiles

As the observation of water elevation did not cover all conditions of river discharge and tidal level, the water surface profiles used in the sediment calculation are those obtained from the observation supported by those calculated using the standard step method (Chadwick, and Morfett, 1986) which is given in Appendix D. The calculation was done at three different tidal levels; 0.42, 0.74, and 1.06 m, and at eight (8) different river discharges; 5, 10, 15, 20, 25, 50, 75 and 100 m^3/s. Tidal levels were based on the water level distribution given in Figure 4.14. Water slope used for each stage of flow was an average of water slope obtained from three different tidal levels.

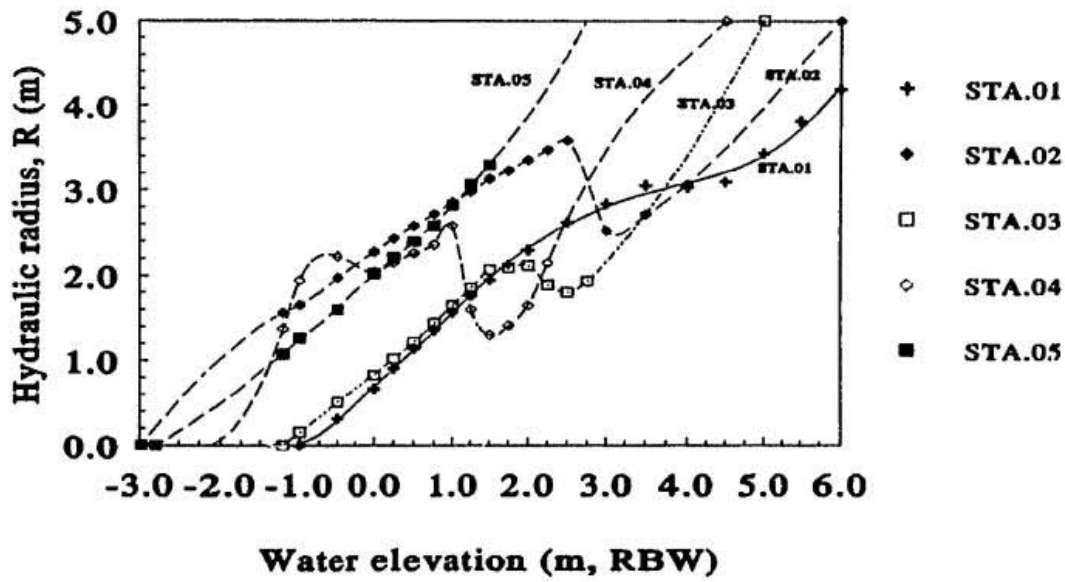

Figure 6.3 Elevation-Hydraulic Radius (EL-R) Curves at Five Cross Sections in the West Channel.

Calculation of water profiles utilized the EL-A (Figure 5.6) and EL-R curves (Figure 6.3). The calculated values obtained from the computation of water profiles are shown in Appendix E, and a summary is given in Figure 6.4.

6.2.2 Computation of Sediment Rates

In the calculation of sediment load (suspended and bed loads) the West Channel was divided into four sections, section I to section IV. Section I represents a region between STA.01 and STA.02. Section II represents a region between STA.02 and STA.03, and so on. Calculation was made for different water flows at different water slopes. Water flows were classified into eight (8) cases: 5.0, 10.0, 15.0, 20.0, 25.0, 50.0, 75.0 and 100.0 m^3/s.

Equation 2.50 was solved utilizing the EL-A, EL-R curves mentioned previously together with values given in Table 6.2. In this table the size of the sediment, d_{50}, represents measured sizes, ρ_s is an assumed value and τ_c was calculated from equation 2.47.

Table 6.2 Characteristics of Sediments

Section	d_{50} (mm)	τ_c (N/m^2)	ρ_s (kg/m^3)
I	0.105	0.0952	2,650
II	0.071	0.0639	2,650
III	0.035	0.0315	2,650
IV	0.034	0.0304	2,650

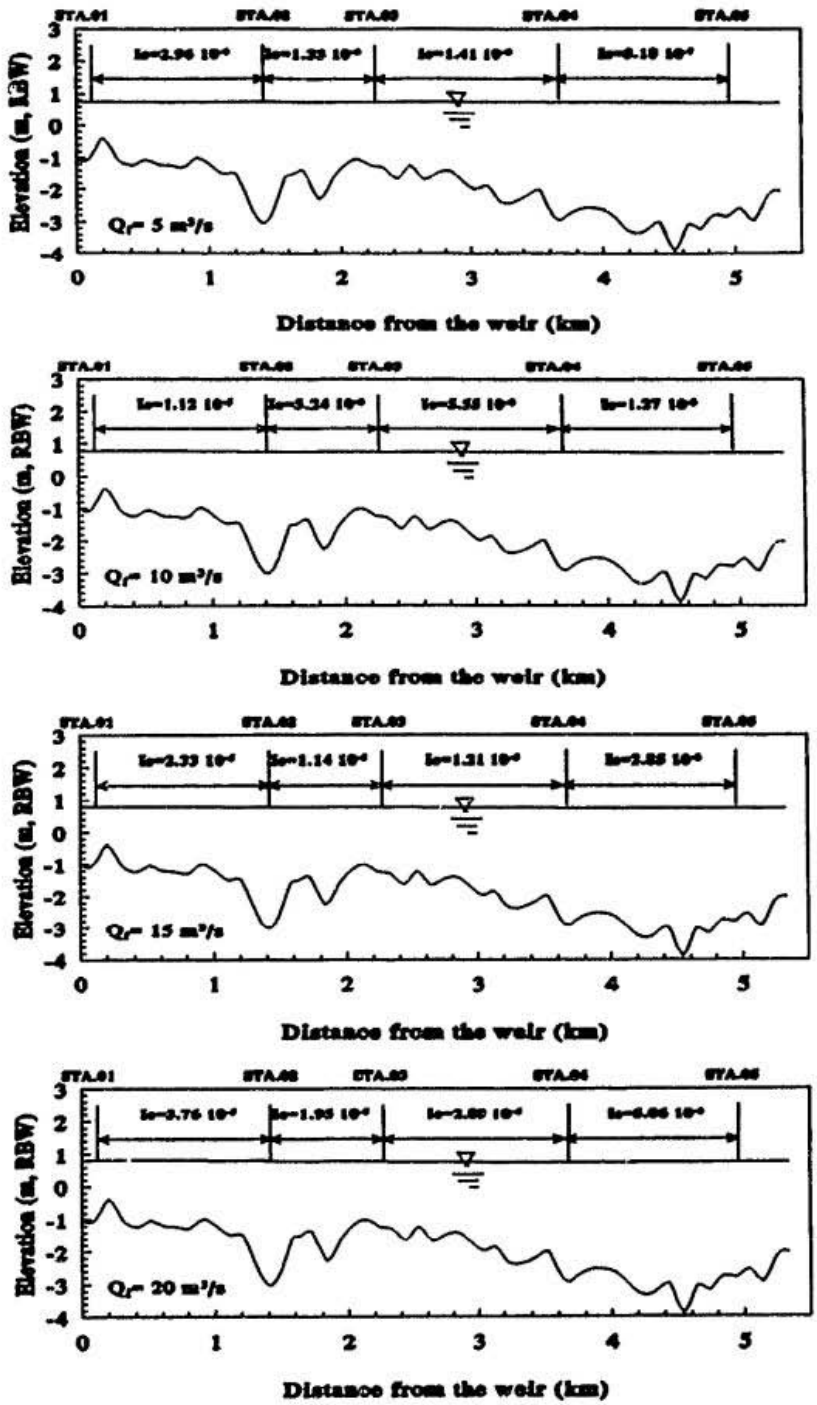

Figure 6.4 Water Profiles of the West Channel at Different River Flow and Tidal Level (1/2)

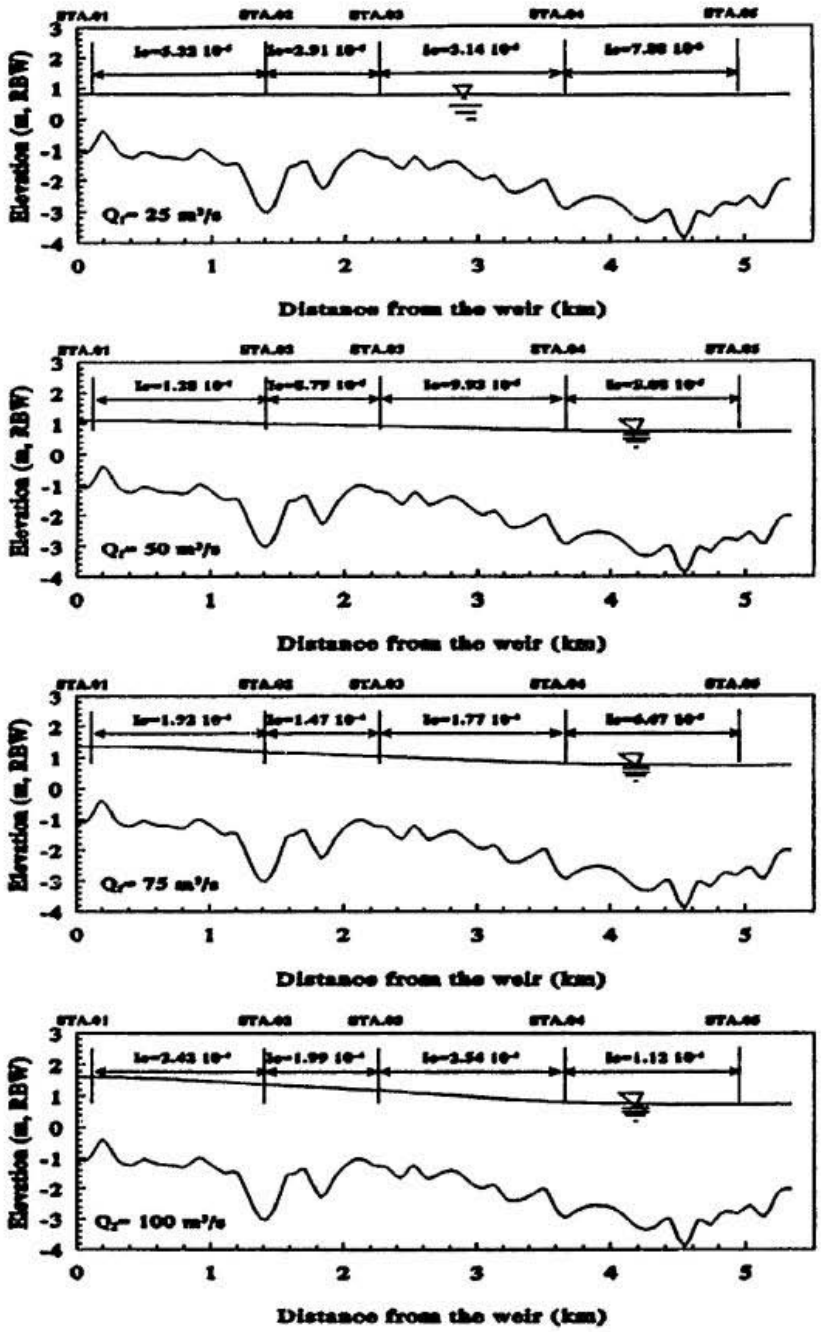

Figure 6.4 Water Profiles of the West Channel at Different River Flow and Tidal Level (continued 2/2)

The calculated values of suspended load and bedload rates at each section in the aforementioned river discharge are listed in Appendices E and F for suspended and bedload, respectively.

The results giving details of sediment rates at each section were then plotted to obtain the relationship between river discharge and sediment discharge. In this case both suspended load and bedload were approached by using a power or linear logarithmic relationship. Figure 6.5 presents the graph obtained. The relation between Q_s, Q_b, and Q_f are listed in Table 6.3, where Q_s and Q_b are suspended load and bed-load, respectively, given in 10^{-3} m^3/s, and Q_f is the river discharge in m^3/s.

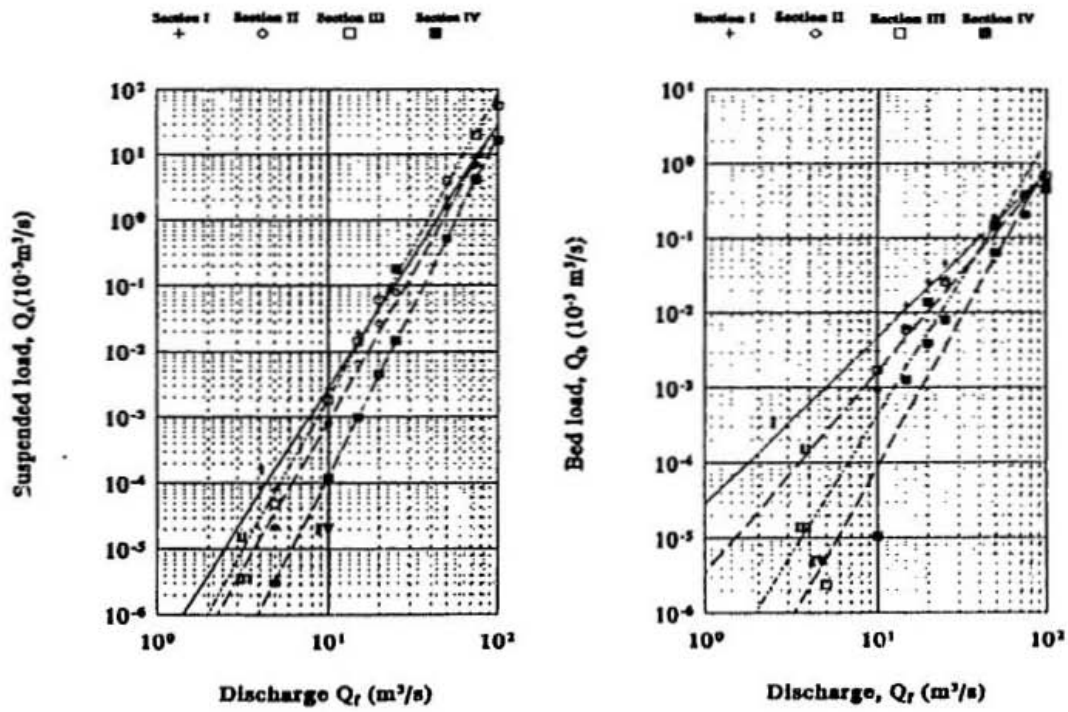

Figure 6.5 Relation Between Q_f and Q_s (left), and Q_f and Q_b (right)

Table 6.3 Relation between Q_f and Q_s, and Q_f and Q_b

Section	Relation between Q_f and Q_s	Relation between Q_f and Q_b
I	$LogQ_s=4.031LogQ_f-6.607$	$LogQ_b=2.206LogQ_f-5.549$
II	$LogQ_s=4.544LogQ_f-7.623$	$LogQ_b=2.662LogQ_f-5.460$
III	$LogQ_s=4.656LogQ_f-7.392$	$LogQ_b=3.366LogQ_f-7.044$
IV	$LogQ_s=5.183LogQ_f-9.104$	$LogQ_b=4.003LogQ_f-8.065$

6.2.3 Annual Sediment Discharge

Annual river sediment load is found by summating a daily sediment load during the whole of the year, where the daily river sediment load was calculated by substituting the average daily river flow into the equation listed in Table 6.3 and multiplying by a day's duration (86,400 seconds). Thus the result is in units of 10^3 m^3/day. The average daily river discharge is taken during a three year period; 1987 to 1989. The calculation of sediment load are summarized in Tables 6.4 to 6.6.

Table 6.4 Sediment Load at Each Section Along the West Channel in 1987

Months	Section I (STA.01-STA.02)		Section II (STA.02-STA03)		Section III (STA.03-STA.04)		Section IV (STA.04-STA.05)	
	Suspended load (m^3)	Bedload (m^3)	Suspended load (m^3)	Bedload (m^3)	Suspended load (m^3)	Bedload (m^3)	Suspended load (m^3)	Bedload (m^3)
January	775	108	520	68	1355	23	196	24
February	13523	231	15748	298	46317	204	11843	411
March	9136	289	9505	255	27257	157	6178	279
April	55	25	27	11	65	3	7	2
May	2	5	1	1	1	0	0	0
June	1	2	0	1	0	0	0	0
July	0	0	0	0	0	0	0	0
August	0	0	0	0	0	0	0	0
September	0	0	0	0	0	0	0	0
October	0	0	0	0	0	0	0	0
November	1	1	0	1	1	0	0	0
December	21	13	10	5	23	1	2	1
Total	23512	673	25810	640	75020	388	18256	716
Bulk Volume	39187	1122	43017	1067	125033	646	30376	1194

Table 6.5 Sediment Load at Each Section Along the West Channel in 1988

Months	Section I (STA.01-STA.02)		Section II (STA.02-STA03)		Section III (STA.03-STA.04)		Section IV (STA.04-STA.05)	
	Suspended load (m^3)	Bedload (m^3)	Suspended load (m^3)	Bedload (m^3)	Suspended load (m^3)	Bedload (m^3)	Suspended load (m^3)	Bedload (m^3)
January	49	26	23	12	56	2	6	2
February	19864	318	23182	378	69763	285	18074	602
March	372	54	426	32	697	11	108	12
April	21	16	9	7	21	1	2	1
May	11	9	4	4	10	1	1	0
June	0	0	0	0	0	0	0	0
July	0	0	0	0	0	0	0	0
August	0	0	0	0	0	0	0	0
September	0	0	0	0	0	0	0	0
October	8	4	4	2	10	0	1	0
November	1	1	0	0	0	0	0	0
December	9194	249	9917	232	28670	151	6758	280
Total	29519	679	33847	665	99226	451	24948	897
Bulk Volume	49199	1128	56411	1109	165376	751	41581	1495

Table 6.6 Sediment Load at Each Section Along the West Channel in 1989

Months	Section I (STA.01-STA.02)		Section II (STA.02-STA03)		Section III (STA.03-STA.04)		Section IV (STA.04-STA.05)	
	Suspended load (m^3)	Bedload (m^3)	Suspended load (m^3)	Bedload (m^3)	Suspended load (m^3)	Bedload (m^3)	Suspended load (m^3)	Bedload (m^3)
January	31	16	15	7	37	2	4	1
February	73171	196	99687	940	302953	873	89875	2201
March	167	45	96	23	239	6	29	5
April	143	35	84	19	213	5	27	5
May	3	5	1	2	3	0	0	0
June	67	18	38	9	95	3	11	2
July	0	1	0	0	0	0	0	0
August	0	0	0	0	0	0	0	0
September	0	0	0	0	0	0	0	0
October	0	0	0	0	0	0	0	0
November	1	2	0	1	1	0	0	0
December	2	4	1	1	1	0	0	0
Total	73586	923	99921	1003	303541	889	89947	2214
Bulk Volume	122643	1538	166535	1672	168206	1481	149911	3691

The annual river sediment load at every section along the West Channel can thus be presented in Figure 6.6. The unit of sediment load in Tables 6.4 to 6.6 and in Figure 6.6 is bulk volume (m^3), assuming the porosity, $e = 0.4$

$$Porosity\ e = 1 - \frac{volume\ of\ particles}{bulk\ volume}$$

The results (Figure 6.6) show that the amount of sediment increases from section I to III and then decreases in section IV. The highest sediment quantity is in section III. As sediment supply from upstream (sections I and II) is less than the amount of sediment transported in section III, there must be scouring in the last part of section

II and the first half of section III. Part of the sediment starts to deposit after the mid point of the section III and throughout section IV. In fact, the deepest part is at about mid of section IV. This means that deposition may occur as the flow enters the river mouth. The most significant feature of this estimation is that the sediment load is very sensitive to the river discharge. During 1989 the load was very high, as there was a big storm; i.e., the biggest discharge during the three year period was in February 5, and February 27, 1989. The daily average discharge at those days was 187 m^3/s. The average discharge during this three year period was 8.5 m^3/s.

According to this estimation, the West Channel supplies about 76,000 m^3 of river load each year to the adjacent coastal area.

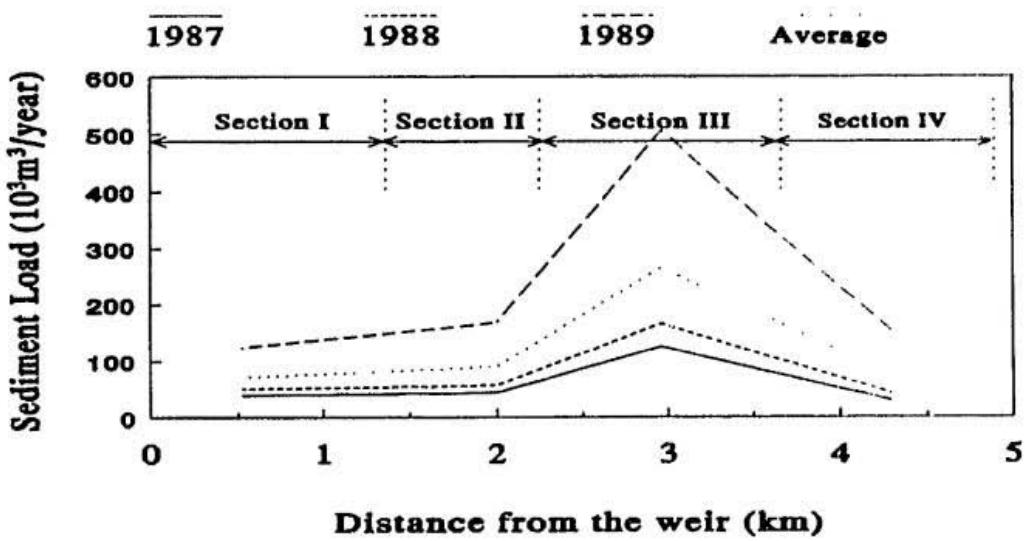

Figure 6.5 Sediment Load at Every Section Along the West Channel

6.3 Sedimentation Along the Kali Semarang

The amount of material deposited or eroded at each section along the Kali Semarang can be easily estimated based on the change of bed elevation between 1984 (just after improvement) and 1990. Based on data described in section 4.1.4, Table 4.1 and Figure 4.3 the volume of deposited or scoured material can be estimated as shown in Table 6.7 following.

Table 6.7 Deposited Material Along the Kali Semarang During a Period of 1984 to 1990.

Section	Distance from the weir (m)	Bed Elevation (m)		Width (m)	Deposition or Accretion (m^3)
		1984	1990		
Weir	0	4.00	4.00	10	-
Gajah Mada	2,701	2.16	2.16	14	0
Sebandaran	3,517	1.60	1.62	14	110
Kapuran	3,739	1.42	1.46	20	115
Johar	4,709	0.80	0.95	20	172
Berok	5,113	0.52	0.76	30	1,654
Kali Baru	5,749	0.10	0.45	34	6,074
Boom Lama	6,439	-0.10	0.28	40	9,350
Kali Asin	7,630	-0.45	0.00	42	20,307
Mouth	8,240	-0.65	-0.50	42	7,686
Total Deposition During 6 years (1984-1990)					45,468

At the upper reach, from the weir to Sebandaran Bridge (STA.02), there is neither deposition nor erosion. Below this point material starts to settle. Further down the deposited material is thicker until it reaches its maximum at the Kali Asin (see Figure 4.3), then decreases seawards. This pattern of deposition is probably related to tidal propagation, bed slope, and water pollution. Indeed, the tidal limit is about the Sebandaran bridge. The fresh water velocity slows down as it enters the tidal limit, particularly during flood tide. Velocity is further reduced by decreasing bed slope from 0.0007 at the upper part to 0.0003 at the lower part. Decreasing deposition downstream of the Kali Asin may relate to the discharge from the Kali Asin that is able to flush part of the sediment down to the sea, particularly during high flows in the rainy season. The effect of water pollution on sedimentation is to accelerate flocculation which results in an increase in settling velocity.

Potential erosion of the river basin suggests that the Kali Semarang receives 13,000 m^3/annum and 90 % of it is deposited within the channel (Department of Public Works, 1982). Based on values listed in Table 5.7 above, the annual deposition of material is 45,468/6 = 7,578 m^3/year. This large difference between predicted and actual values indicates the need for monitoring sediment movement at the channel to obtain a better estimation of sediment entering and leaving the channel.

Despite the large difference between the two values, the quantity of sediment supplied by the Kali Semarang to the surf zone is small in comparison to that supplied by the West Channel or littoral drift. Therefore, it will not be considered in the calculation of the sediment budget.

6.4 Longshore Transport

The longshore transport was calculated using the energy flux method (see section 2.7.5). The azimuth, α_o, and wave and wind data used are the same as those used in the calculation of wave energy flux. The average depth was 5.00 m (see Figure 6.1).

In this calculation of longshore transport, movement from the right to left side of the observer standing on the shore looking out to sea is indicated by the subscript *"l"* (Q_l) and is given a negative value. Movement towards the observer's right is indicated by the subscript *"r"* (Q_r) and is given a positive value. In this case the shore line runs East-West, so the movement from the East-north to the West is negative, and from the North-west sector to the East is positive.

The gross longshore transport rate (Q_g) and net longshore transport rate (Q_n) are defined, respectively, as

$$Q_g = Q_r - Q_l \tag{6.2}$$

$$Q_n = Q_r + Q_l \tag{6.3}$$

The longshore transport rate was calculated by using equation 2.56, where the directional term $F(\alpha_o)$ is calculated as an average between a sector of 22°30'. The calculation is presented in Appendix G.

A summary of the calculations of the longshore transport is given in Table 6.8 following.

Table 6.8 Longshore Transport at the Kali Garang River Delta in 1989

Period, T seconds	Q_l (m^3/yr)	Q_r (m^3/yr)	Q_g (m^3/yr)	Q_n (m^3/yr)
2.5	- 1,872	4,060	5,932	2,118
3.5	- 4,001	8,680	12,681	4,679
4.5	- 9,538	20,688	30,225	11,151
5.5	- 6,134	13,306	19,440	7,172
6.5	- 602	1,307	1,909	705
7.5	- 49	107	156	156
Total	- 22,196	48,148	70,344	25,952

The monthly distribution of the longshore transport should be proportional to the distribution of the wave energy flux. Accordingly, the distribution can be calculated based on the wind climate. Table 6.9 shows the distribution of longshore transport in 1989. The quantity of longshore transport in each direction per month is obtained by multiplying the percentage of yearly wind in the appropriate direction and month, and the annual-rate of longshore transport in that direction. The monthly longshore transport is then obtained by summating the longshore transport from all directions considered on the corresponding month.

The maxima of both gross and net transports occur in February. The minima (absolute value) of those are on August and July, respectively. Winds from northwest and west-northwest generate the highest longshore transport rate.

Table 6.9 Monthly Distribution of Longshore Transport, Q, During 1989

Month	Longshore Transport (m^3/year)								Monthly	
	ENE	NE	NNE	N	NNW	NW	WNW	W	Qn	Qg
January	-43	-290	-92	-755	70	1640	3195	2154	5875	8241
February	-48	-102	-206	-95	9	1787	4215	3993	9553	10454
March	-91	-377	-298	-932	88	1934	2685	1524	4532	7928
April	-86	-681	-436	-948	96	2413	1398	617	2374	6676
May	-153	-493	-252	-1675	105	424	67	164	-1814	3332
June	-134	-507	-573	-1312	107	921	421	302	-774	4278
July	-148	-232	-344	-948	523	847	666	353	246	3590
August	-163	-275	-275	-1248	57	553	177	353	-822	3101
September	-139	-362	-229	-1533	83	1308	887	403	419	4945
October	-105	-290	-115	-1169	127	1805	621	529	1404	4762
November	-110	-420	-298	-1738	129	2100	799	289	751	5884
December	-96	-347	-206	-823	59	2063	1642	1914	4207	7150
Total/dir	-1316	-4378	-3324	-13178	984	17796	16773	12595	25952	70344

6.5 Sediment Budget

Burns and Mc Donnell (1976) found that the delta growth in the vicinity of the West Channel mouth was about 10.5 metres per year. Unfortunately, there is no detailed information about the delta and detailed chart of the area is not available. In order to illustrate the sediment budget, a rough estimation of deposited material has been made based on the bathymetric chart, Figure 6.1, assuming that the fluvial sediment was distributed along the shoreline between the Semarang Harbour (east) and the tip of the Tirangkawang Island (west). Hence the length of shoreline is 8 km. An average depth at the nearshore area is about 1.5 m. Thus the volume of material

deposited should be 8.000 x 1.5 x 10.5 = 126.000 m^3/year. If this material was supplied by the river alone it would result in the average concentration being

$$\frac{126{,}000 \times 0.6 \times 2{,}650 \times 10^6}{10 \times 24 \times 60 \times 60 \times 10^3} = 635 \text{ ppm}$$

where the porosity, $e = 0.4$, sediment density, $\rho = 2{,}650$ kg/m^3 and average river discharge, $Q_f = 10$ m^3/s.

This value of concentration is likely to be higher than one would expect from a fresh water river, and it is thought that material must be transported from marine sources by longshore currents associated with waves.

Based on the previous sections, a theoretical estimation of the sediment movement and deposition in the vicinity of the Kali Garang Delta can be made. Figure 6.7 schematically illustrates the sediment budget during 1989. In that year, the river discharged 149,910 m^3 of suspended load and 3,690 m^3 of bed-load (Table 6.6). Gross longshore transport accounted for 70,344 m^3 with a net of 25,952 m^3 (Table 6.8). The gross total entering the deltaic zone was therefore 223,944 m^3. The net material is then 175,553 m^3. Based on this period the quantity of fluvial load alone has been greater than that deposited. It is thought that some of the suspended material sinks into the offshore area.

A more general estimation of estuarine budget can be made from the three year calculation (1987-1989) of river load (Table 6.4, 1/3 to 3/3). The average of fluvial load per annum during this period is (from Tables 6.4 to 6.6)

$$\frac{31,570 + 43,076 + 153,600}{3} = 76,082 \text{ m}^3$$

Thus the gross and net sediment budgets are 146,426 m^3 and 102,034 m^3, respectively.

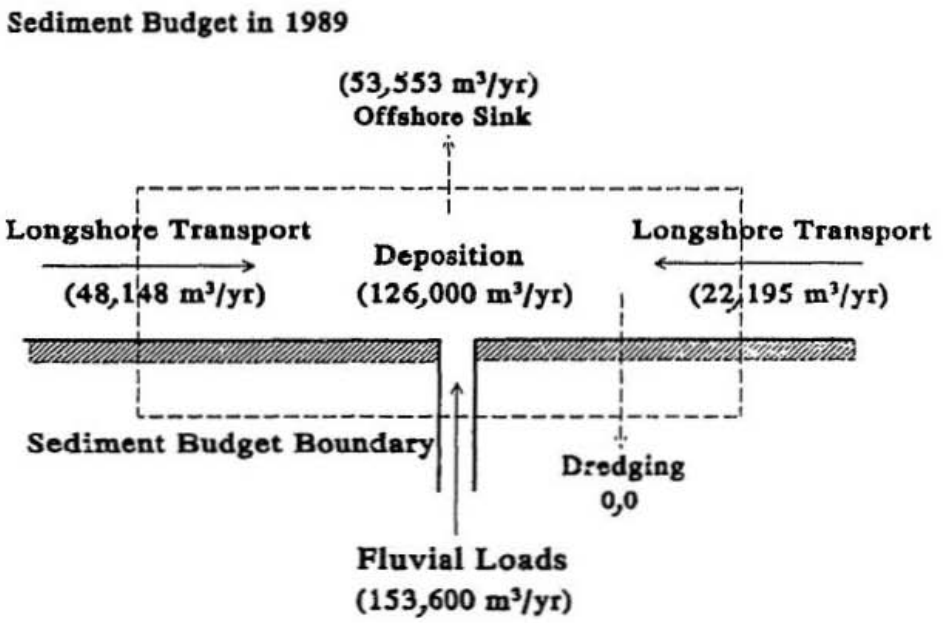

Figure 6.7 Schematic Chart of Sediment Budget in the Vicinity of the Kali Garang Estuary

Other simple estimations of fluvial load can be made based on the general chart of annual discharge of suspended sediment from the drainage basins, Figure 1.2. Here, Indonesia falls into the category of the highest sediment rate area. The rate is more than 1,000 tons per square kilometre per annum. Thus the suspended load

by 196 km^2 of the drainage basin of the Kali Garang River is more than 196 x 1,000 x 10^3 = 1,96 10^8 kg or equal to 123,270 m^3 (bulk material). Hence the gross and net sediment budgets are 193,270 m^3 and 149,220 m^3, respectively.

Although there is a discrepancy between sediment load calculated by one method and the others, the statement made in the first paragraph of this section, namely that the deposited material within the delta region of 126,000 m^3, is reasonable (average net sediment budget is ½(149,220 + 102,032) = 125,626 m^3). About 60 to 80 percent of the material is fluvial load while the remaining 20 to 40 percent is longshore drift. The quantity of river load may be high during a year of if high rainfall, or if there is a big storm. A substantial quantity of material may be transported into the surf zone by fresh water floods, having a high concentration of suspended material perhaps exceeding 600 ppm. However, this will be offset by the smaller quantities transported at low flows.

6.6 Delta Formation

Fluvial sediments transported to the sea by river flow are distributed and deposited seaward of the river mouth in accordance with the marine forces on which the orientation and pattern of the delta depends. Depending on the relative strength of fluvial versus marine forces, deltas may assume a spectrum of configurations ranging from those which are river dominated to those which are marine dominated. By using

Coleman's work as a reference (see section 2.8), the formation of the Kali Garang Delta can be described as follows

Table 6.10 Discharge Effectiveness Index at the Kali Garang Delta, Based on Data in 1989.

Months	Nearshore Wave Power (P) (J/s-m)	Average Discharge (Q_f) (m^3/s)	$\frac{P}{P_{max}}$	$\frac{Q}{Q_{max}}$	Discharge Effectiveness Index
January	4.309	9.89	0.789	0.204	0.029
February	5.464	48.39	1.000	1.000	0.105
March	4.137	15.12	0.757	0.312	0.044
April	3.489	13.16	0.639	0.272	0.044
May	2.177	5.91	0.398	0.122	0.031
June	2 593	8.56	0.475	0.177	0.039
July	2.017	2.82	0.369	0.058	0.016
August	1.915	2.26	0.351	0.047	0.015
September	2.762	1.94	0.506	0.040	0.009
October	2.840	3.32	0.520	0.069	0.015
November	3.263	3.52	0.597	0.073	0.012
December	3.883	6.34	0.711	0.131	0.019
Average	3.237	10.10	0.593	0.209	0.032

The wave climate of the Kali Garang Estuary (Figure 6.8) exhibits seasonal variability. Similarly, discharge also exhibits high seasonal variability with a peak in February. The period of maximum river discharge is approximately coincident with the time of maximum wave power. The discharge effectiveness index is thus small during most of the year (Table 6.10). Sediments that reach the sea are sorted by waves, and coarser fractions are worked back onshore. Wave-induced longshore drift apparently

has been responsible for the development of the relatively straight shoreline with bar building at the left-hand side. Only in the immediate vicinity of the West Channel river mouth has the river been able to build a slight protrusion. The waves generated by the east monsoon during low river discharges are sufficient to generate appreciable longshore drift toward the west. Hence the greatest accumulation of material lies west of the river mouth.

6.7 Discussion

The patterns of the movement and deposition of sediment at the area of the Kali Garang delta occur in seasonal cycle, with riverborne sediment dominating the supply during the rainy season and sediment resuspension and deposition dominating during the dry season. These seasonal differences, combined with the difference in longshore rates between western and eastern drifts make the delta a complicated system to evaluate. From limited existing and observation data, however, a simple concept of the basic patterns of movement and deposition of sediment can be presented. As the processes are seasonally modulated, they are separated into two parts.

The river sediment load is high during the rainy season (Fig.6.9a). The strong river flow is slightly shifted to the right side by waves generated by the west monsoon. The waves encountering the river flow are liable to break. This promotes extensive mixing of sea-water and fresh-water, and causes a breakdown in density

stratification. Vigorous mixing of sea-water and river water leads to the rapid deceleration of the fresh water flow, and equally rapid deposition of sediment. The coarser grained fractions are deposited at the zone of mixing near the river mouth as a crescent shaped bar. Some of the finer-grained fractions escape deposition and are carried seawards to be deposited further offshore.

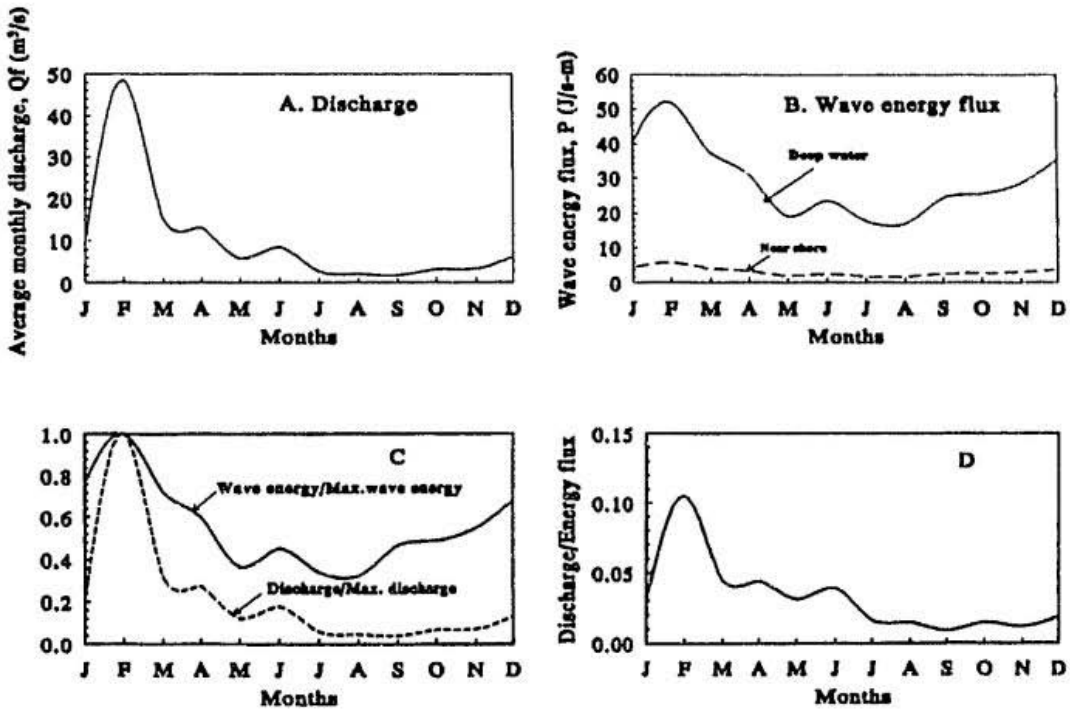

Figure 6.8 Discharge/wave climate at the Kali Garang Delta.

During low river flow in the dry season, the deposited material (the bar) is reworked rapidly by waves generated by the east monsoon. Under these conditions the bedload is moved back landwards and is deposited west of the river mouth (Fig.6.9b).

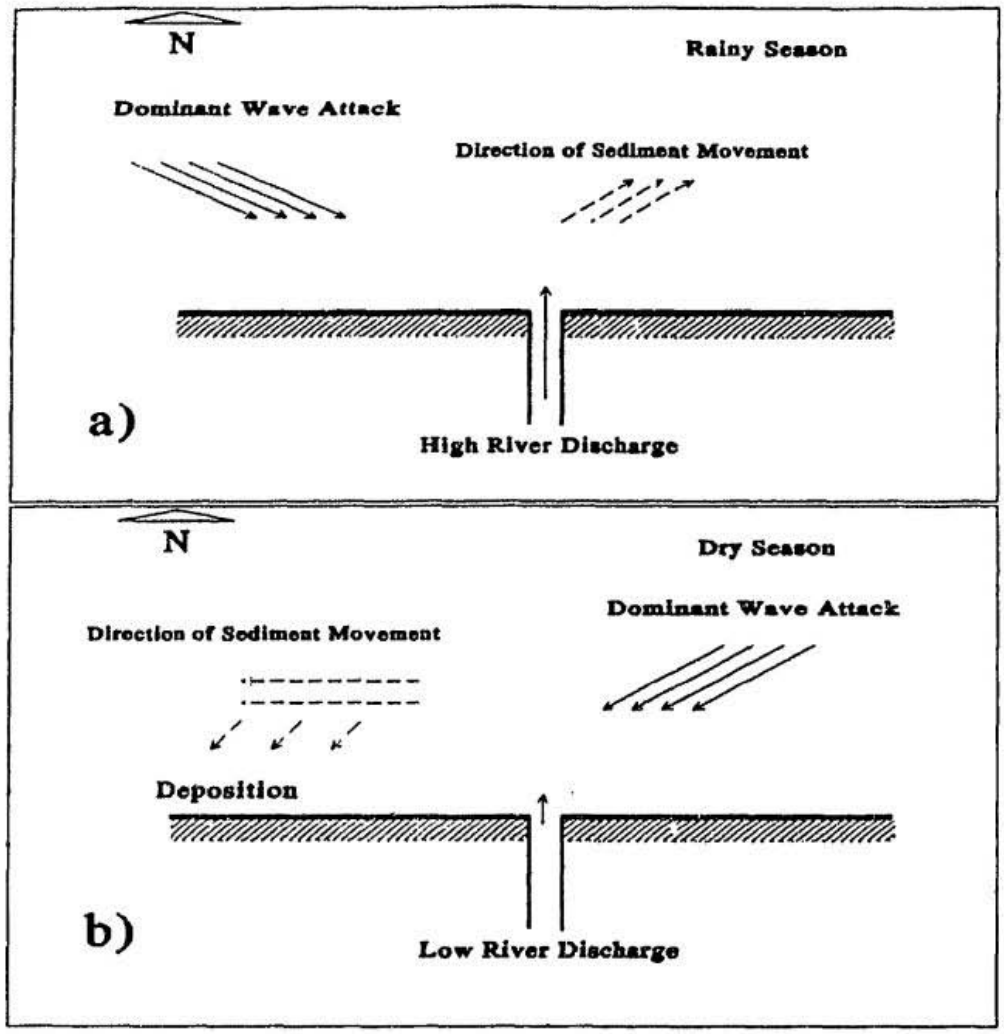

Figure 6.9 Schematic Chart of Processes of the Development of the Kali Garang Delta

As a measure of the relative strength of wind power over river discharge in the Kali Garang Delta, table 2.4 has been repeated as Table 6.11. It must again be stressed that these values are only based on data in 1989 that may vary significantly from other years or periods.

Table 6.11 Mean Annual Summaries of Discharge/Wave Power Climate and Attenuation Ratios of Seven Deltas and of the Kali Garang Delta

Delta	Mean Annual Wave Power (J/s-m)		Mean Discharge 10^3 m^3/s	Mean Annual Discharge Effectiveness Index	Mean Annual Attenuation Ratio
	Deep water	Near shore			
Mississippi	106.0	0.013	17.69	5477.0	7913.3
Danube	23.0	0.014	6.29	1171.0	2585.0
Ebro	72.8	0.051	0.55	267.8	1299.5
Niger	67.6	0.659	10.90	4.4	102.8
Nile	136.0	3.210	1.47	3.2	42.5
Sao Francisco	371.0	9.970	3.12	1.3	37.2
Senegal	156.0	37.700	0.77	0.3	4.2
Kali Garang	**27.1**	**3.237**	**0.01**	**0.03**	**8.4**

It is difficult to give a perfectly valid comparison between the Kali Garang Delta and the other seven deltas listed in Table 6.11 since the Kali Garang River system is small compared to the others. However some statements can be made in relation to the table above. The wave attenuation in the Kali Garang delta is higher than that in the Senegal Delta, but is far lower than in the Mississippi Delta. These attenuation ratios depend more strongly on the subaqueous profile rather than on the deep water wave power. The slope of the subaqueous nearshore of the Kali Garang (2.35×10^{-3} m/m) is gentler than of the Senegal (4.7×10^{-3}) but steeper than of the Mississippi (5.8×10^{-4}) (Wright, and Coleman, 1972). Therefore the discharge effectiveness index in the Kali Garang is lower than that of the Senegal. Consequently, the coastline of the Kali Garang is totally wave dominated. The delta shows little river produced irregularity.

Chapter 7

Discussion on Water Pollution in Estuaries

Estuaries have been considered ideal places for industrial and commercial businesses. Their proximity to the sea makes them beneficial locations for easy access to maritime transport. They are usually used as a supply of industrial and drinking water and, in addition they are frequently used as a waste disposal site. On the other hand, estuarine ecosystems provide an environment of considerable importance to numerous aquatic organisms. They serve as a refuge not only for various freshwater species but also for many marine populations.

With the rapid growth of industry and population in the last century, the estuarine loads are becoming unbalanced and perhaps even overtaxed and the water quality is being degraded. When the natural ecological balance is disturbed the water is termed polluted, and the substances that cause pollution are called pollutants.

The Kali Garang Estuary flows through an urban area and is not free from pollution problems. The pollutants originate mainly from domestic sewage. The degree of pollution in the Kali Garang Estuary can be seen from the water samples taken in both the West Channel and the Kali Semarang. Testing determined the magnitude of the biochemical oxygen demand (BOD) and the dissolved oxygen

concentration (DO). Results are presented in Figures 7.1 and 7.2 for the West Channel and the Kali Semarang, respectively.

Before discussing this further, it is relevant to briefly review the meaning of BOD, DO and their relation to pollution in estuaries. *Biochemical oxygen demand (BOD)* is the amount of oxygen required by microorganisms to biologically degrade the organic matter in the water. The higher the BOD, the greater the organic matter

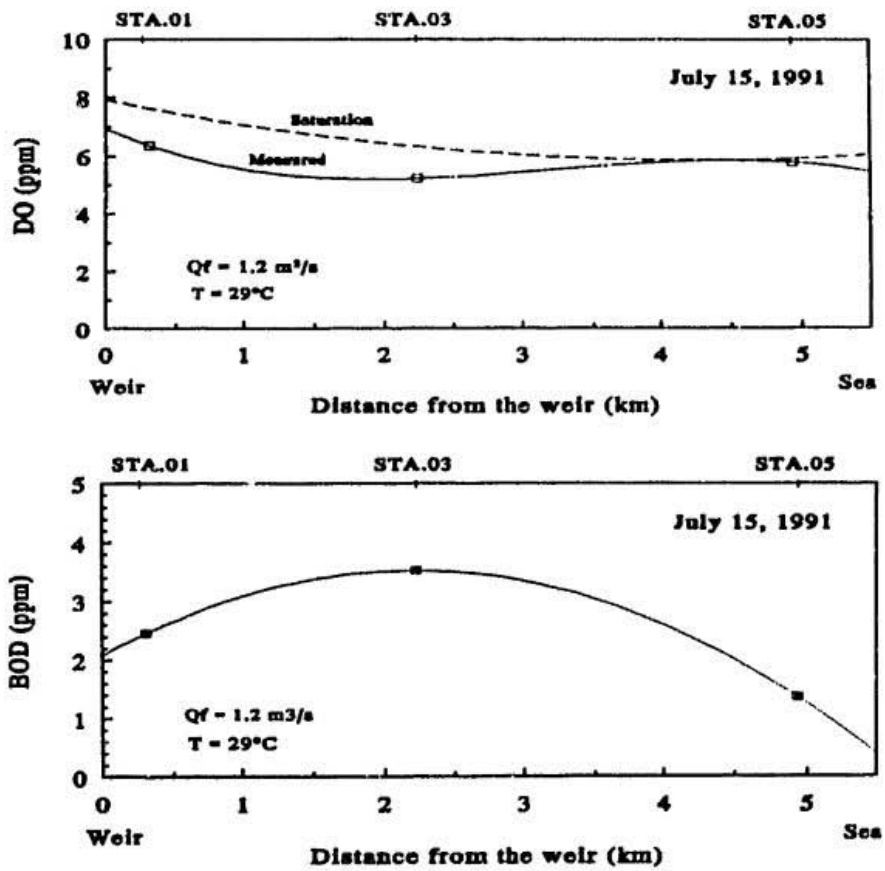

Figure 7.1 DO (above) and BOD (below) Curves at the West Channel, Based on Observations of July 15, 1991.

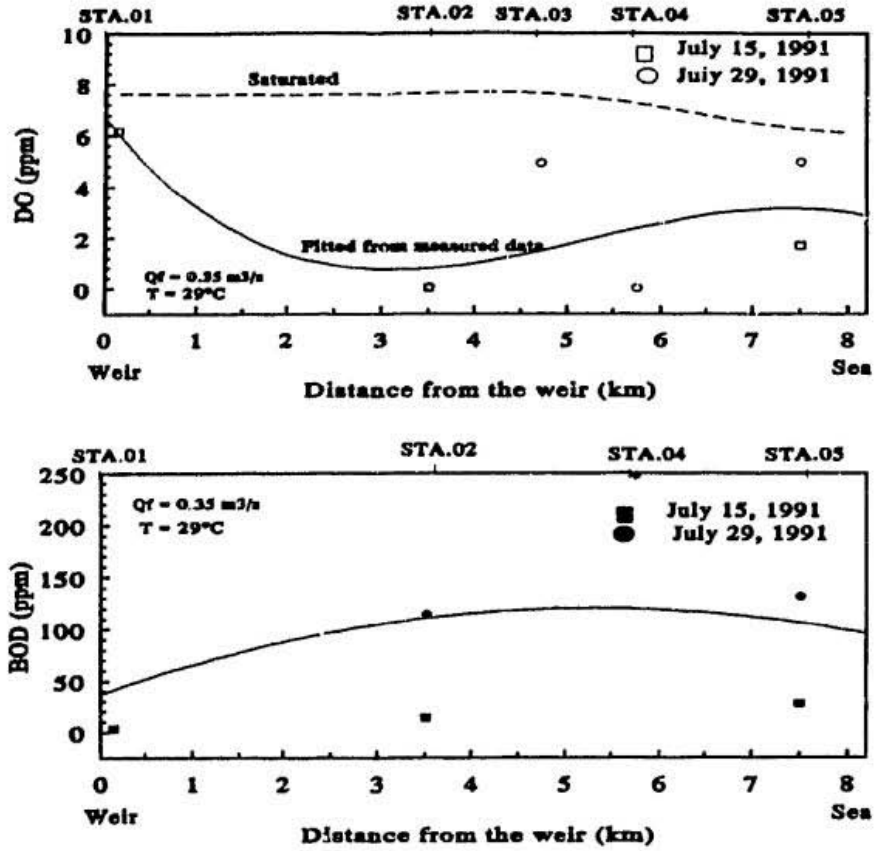

Figure 7.2 DO (above) and BOD (below) Curves at the Kali Semarang, Based on Observations of July 15, 1991 and July 29, 1991.

existing in the water, and the greater the problem created by the decomposition of that matter. Microbial activity by bacteria requires oxygen to decompose the organic matter. This activity reduces the dissolved oxygen (DO) concentration in the estuary. Decreasing DO to less than 4 mg/l causes most fish to die or move away. The relationships between DO concentration and water pollution in estuaries are usually determined by comparing the available DO with the saturation level. The DO at

saturation is the maximum concentration of oxygen within the water. The DO concentration at saturation is a function of salinity, temperature, and pressure. At atmospheric pressure, increasing the salinity and temperature decreases the DO saturation. Table 7.1 contains oxygen saturation values at different salinities and temperatures. The difference between DO saturation and available DO is called the DO deficit. The higher the DO deficit the higher the pollution.

Table 7.1 Saturation Values for Dissolved Oxygen in ppm at Different Temperatures and Salinities under Atmospheric Pressure (*From Davis, J.M., and Cornwell, D.A., 1986*)

Temperature °C	Salinity = 0 ppt	Salinity = 16 ppt	Salinity = 28 ppt	Salinity = 35 ppt
0	14.62	12.94	11.77	11.13
5	12.68	11.26	10.35	9.83
10	11.26	10.09	9.19	8.80
15	10.09	9.06	8.80	7.89
20	9.06	8.15	7.50	6.47
25	8.41	7.63	6.99	6.73
30	7.50	6.86	6.34	6.08

Dissolved Oxygen concentration in estuaries varies due to the variation of sources and sinks of DO along the estuary. Sources of DO are : (1) Reaeration from the atmosphere, (2) Photosynthetic oxygen production, and (3) DO in incoming tributaries and effluent. The sinks of DO include : (1) Oxidation of oxidizable waste material, (2) Oxygen demand of sediments, and (3) Use of oxygen for respiration by aquatic plants.

Oxygen transfer in estuaries through reaeration depends on internal mixing and turbulence due to velocity gradients and fluctuations, temperature, wind mixing, hydraulic structures, and surface films. The presence of aquatic plants in estuaries can have a profound effect on the DO resources because of their ability to photosynthesize, converting water and carbon dioxide into glucose, and releasing oxygen.

Discharge of settleable waste components in estuaries may result in the formation of sludge banks, particularly during the dry season in which the flow is low. When this deposit is thick enough, anaerobic decomposition of the organic material begins and several kinds of gases are produced. If the gas production is high this leads to some aesthetic problems as well as DO depletion.

The water tests presented in Figures 7.1 and 7.2 above show that the DO in the upstream part (near the weir) of both branches (the West Channel and the Kali Semarang) is the same (7 mg/l), and almost as high as the DO saturation. In the West Channel the DO below the weir decreases slightly due to increasing salinity. At the same time the DO saturation also decreases for the same reason. Overall the DO deficit decreases seaward. Near the mouth the DO deficit is almost zero. This phenomenon is believed to be due to aeration generated by winds blowing from the sea.

Below the weir the DO at the Kali Semarang decreases markedly until almost zero at STA.02 (3.5 km downstream of the weir). At this point the DO deficit is a maximum (7.5 mg/l). Below this point the DO increases due to the effect of salt water that intrudes upstream to that point. The polluted upstream water is diluted by

less polluted sea water. Although there is no information concerning the nature and quantity of domestic sewage discharging into the Kali Garang estuary, it is likely that the Kali Semarang receives more sewage than the West Channel does. The DO in the Kali Semarang is below the low limit of the DO required for aquatic life.

The high pollution of the Kali Semarang is believed to contribute to a acceleration of the deposition of sediment. This is because pollutants which originate from domestic sewage consist not only of liquid but also of solid and settleable material. The weak currents in the shallow water of the Kali Semarang Channel are unable to flush down the solid material. As result, the material settles and accumulates within the channel, particularly at the inner-bends where the flow is very weak. As domestic sewage contains organic material, it has a positive charge and significantly enhances flocculation.

Chapter 8

Conclusion

River systems in Indonesia are mainly influenced by the geology and morphology of the systems, the climate, and the condition of the receiving basin. The humid, mountainous, tropical basins provide a high volume of sediment that originates both from volcanic ashes and basin erosion. Monsoon seasons lead to the fluctuation of run off. Floods may occur during high runoff in the rainy season and droughts occur during low runoff in the dry season. The high volume of river loads leads to delta formations in most river systems. The deltas vary from river dominated to wave dominated depending on the marine forces against which the rivers are emptied.

Floods which inundate the low, flat, lower basin and sedimentation at the lower reaches are the most common problems. A number of construction projects in some river systems has altered the natural movement of water and sediment.

Limited observations which have been carried out in the Kali Garang estuary and have been discussed in the preceding chapters, give an illustration of the characteristics and phenomena faced in Indonesian river systems. Despite the limited data, some conclusions can be made. These are presented in the following paragraphs.

The construction of the Simongan Weir and the West Channel in the Kali Garang have shifted the main channel from its original lower course, the Kali Semarang, to the West Channel. Currently, the Kali Semarang is as narrow as 10 m to 40 m, and is highly polluted and is filled with sediment.

In section 4.3.1 the tidal wave in the West Channel was shown to be reflected by the weir as it progresses upstream from the sea. Boundary dissipation has a stronger effect than convergency, and the presence of some bridge piers along the channel reduces tidal energy. Tidal range, therefore, decreases in a landward direction. The water surface gradient at low slack water is about three times higher than that at the high water. The time of high water varies very little throughout the channel.

Observations of the tidal level throughout the Channel and tidal data at the coast have enabled the tidal volume at various tidal ranges to be calculated. In section 4.3.1 the tidal volume has been calculated for three different ranges: spring, mean, and neap tides. During a spring tide the tidal volume is about one third of the volume of high water (total volume). During neap tide this value decreases to about one eighth of the volume of high water (see Table 5.5).

Observations of salinity, temperature, and currents at STA.03, in the West Channel (see section 5.2.3), showed that the water in the upper one fourth of the depth has a net movement downstream. The remaining three fourths have a net movement in an upstream direction after a period of about one tidal cycle. Throughout the depth, however, the net movement is in a downstream direction throughout a tidal cycle.

The actual conditions and water movement during low fresh water flow in the West Channel have been described in section 4.3.2, and have been discussed in section 6.2. The river discharge has a very pronounced effect on the water movement in the channel. Although there is a low fresh water flow, surface currents always flow downstream throughout the tidal cycle. The surface layer is thinner at the seaward end due to widening of the channel and because of mixing with the salt water through a diffusion process. The surface layer may increase with increasing river flow, and the salt water may be swept completely out of the estuary during a very high river flow. In section 5.2.5 it was shown that a discharge of 75 m^3/s would push the saline wedge down to a point 125 m upstream of the mouth. Theoretical values of flow ratio, K, indicate without doubt that the channel is highly stratified throughout the entire year.

Material entering the West Channel comes mainly from the fresh water river system as suspended load and bedload. Grain size analysis of bed material along the West Channel shows that the particles vary in size from sand (2 mm) to clay (0.5 μm). The mean diameter (M_d) decreases seawards from 72 μm at just below the weir to 33 μm near the mouth. This is contrary to the theoretical assumption that particle diameter increases in a seaward direction after about the middle of the estuary. It implies that marine forces have little effect on returning sediment material upstream in the estuary.

Direct observations of tidal currents in the middle of the West Channel (STA.03) indicate that tidal currents are very weak and cannot initiate particle movement or increase sediment concentration. The maximum current is less than 10

cm/s. These extremely low tidal currents suggest that settled particles in the saline bottom layer are unaffected by them.

The effect of wave action on the inner estuary is also likely to be insignificant in returning sediment back landwards. Wave energy is dissipated by the river banks as the waves enter the narrow channel just upstream of the mouth. Wave action has an effect only until the river mouth. Indeed, the percentage of sand at the mouth is slightly higher than that at the middle.

Data relating to the change of bed elevation along the Kali Semarang during the period 1984 to 1990 has enabled the annual amount of deposited material within the channel to be estimated. In section 6.3 the values have been calculated. The annual deposited material during that period was 7,458 m^3. This material was deposited in the lower reaches and shows that the velocity slows down after the tidal limit is reached. Sediment carried down by the upper river starts to settle in this area, especially since the pollution from domestic sewage may take effect.

A theoretical annual sediment budget given in section 6.5 suggests that the amount of deposition is 126,000 m^3 per annum. About 60 to 80 percent is supplied by the river and another 20 to 40 percent by longshore drift. This value, although derived from theoretical considerations, compares well with the work of Burns and Mc Donnell (1976) which shows that the theoretical value given here is reasonable.

The receiving basin into which the Kali Garang debouches is a microtidal sea (mean tidal range = 0.65 m) with a very moderate wave energy climate. The maximum river discharge coincides with the maximum wave energy. Consequently, the

value of the discharge effectiveness index is low throughout the year. Based on data in 1989, the index ranges from a minimum at 0.009 to a maximum of 0.105 (average 0.032). The high volume of riverine sediment carried down during the rainy season is reworked by the west monsoon. This material is brought back near shore by the east monsoon during the low water flow of the dry season. As result, the coastline of the Kali Garang Delta is totally wave-dominated. The coastline is relatively straight with only a small protrusion at the West Channel mouth and some bar islands west of the mouth.

Pollution, which is experienced in most river systems in Indonesia, is likely, either directly or indirectly, to accelerate deposition processes in the inner estuary. This is particularly true if the pollutants consists of settleable material and organic matter.

After this study several problems remain evident, and several have been revealed which require further study and investigation. Total solids supplied by the fresh water river system should be carefully monitored during a one year period, or at least during the high river discharge of the rainy season. These results would confirm the actual fluvial load entering both estuary and surf zone. A long term study of wave climate is needed to determine the rate of littoral drift. Finally, a strict regulation of domestic sewage should be applied in order to reduce its effect on sedimentation and its hazard to aquatic and human life.

References

Bappeda Kotamadya Dati II Semarang. (1989). *Perencanaan Induk Drainase Kodya Dati II Semarang 1988/1989*, CV Nesaco, Semarang, Indonesia, 109 p.

Bearman, G., ed. (1989). *Waves, Tides and Shallow Water Processes*, Pergamon Press, Oxford, 107 p.

Bogardi, J.L. (1978). *Sediment Transport in Alluvial Streams*, Akademiai Kiado, Budapest., 774 p.

Bretschneider, C.L., and Reid, R.O. (1954). "Change in Wave Height Due to Bottom Friction, Percolation, and Refraction," *U.S. Army Corps of Engr: Beach Erosion Board Tech*, Memo 45, 36 p.

Burns, A.J, and Mc Donnell, D. (1976). *Stormwater Drainage Masterplan for the City of Semarang*, Trans - Asia, 324 p.

Cameron, W.M., and Pritchard, D.W. (1963). "Estuaries," *The Sea, Vol. 2*, ed. Hill, M.L., Wiley International, New York, 306 p.

Chadwick, A.J., and Morfett, J.C., (1986). *Hydraulics in Civil Engineering*, Allen & Unwin Ltd., London., 492 p.

Coleman, J.M. (1982). *Deltas : The Processes of Deposition and Models for Exploration*, 2nd ed., International Human Resources Development Corporation, Boston, MA., 124 p.

Davies, J.L. (1958). "Wave Refraction and the Evolution of Shoreline Curves," *Geographical Studies*, Vol. 5, no. 2, pp. 51-52.

Davis, M.L., and Cornwell, D.A., (1986). *Introduction to Environmental Engineering*, PWS Publishers, Boston, Massachusetts, 591 p.

Department of Public Work, Indonesia. (1961). *Comprehensive Report on the Brantas River Overall Project*, Nippon Koei Co. Ltd., Tokyo, Japan., 132 p.

Department of Public Works, Indonesia. (1966). *Design Calculation on Kali Porong Project*, Nippon Koei Co. Ltd., Tokyo, Japan, 107 p.

Department of Public Works, Indonesia. (1982). *Semarang Drainage Project*, PT. Deserco, Semarang, Indonesia, 65 p.

Dronkers, J.J. (1986). "Tide-Induced Residual Transport of Fine Sediment," *Lecture Note on Coastal and Estuarine Studies: Physics of Shallow Estuaries and Bays*, Springer-Verlag, Berlin, pp 228-258.

Dutrieux, E. (1990). "Study of the Ecological Functioning of the Mahakam Delta (East Kalimantan, Indonesia)," *Estuarine, Coastal and Self Science*, no.32, pp. 415-420.

Dyer, K.R. (1979). *Estuarine Hydrography and Sedimentation*, Cambridge University Press, Cambridge, 229 p.

Dyer, K.R. (1986). *Coastal and Estuarine Sediment Dynamics*, John Wiley and Sons, Chichester, Sussex (UK), 342 p.

Farmer, H.G., and Morgan, G.W. (1953) "The Salt Wedge," *Proc. 3rd Conf. Coastal Eng.*, pp 54-64.

Galvin, C.J. Jr. (1972). "Wave Breaking in Shallow Water," *Waves on Beaches and Resulting Sediment Transport*, Academic Press, New York.

Helder, W., and Ruardij P., (1982). "A One-dimensional Mixing and Flushing Model of The Ems-Dollard Estuary: Calculation of Time Scale at Different River Flows," *Netherlands Journal of Sea Research*, no. 52, pp. 293-312.

Inman, D.L. (1952). "Measures for Describing the Size Distribution of Sediments'" *Journal of Sedimentary Petrology*, Vol. 22, no. 3, pp. 125-145

Ippen, A.T., and Harleman, D.R.F. (1966). "Tidal Dynamics in Estuaries," *Estuary and Coastline Hydrodynamics*, ed. A.T. Ippen, McGraw-Hill Book Company, pp. 493-545.

Jennings, J.N. (1955). "The Influence of Wave Action on Coastal Outline in Plan," *Australian Geographer*, Vol. 6, pp. 36-44.

Kennish, M.J. (1986). *Ecology of Estuaries : Physical and Chemical Aspects*, CRC Press, Inc.,Boca Raton, Florida, 254 p.

Keulegan, G.H. (1966). "The Mechanism of an Arrested Saline Wedge," *Estuary and Coastline Hydrodynamics*, ed. A.T. Ippen, McGraw-Hill Book Company, pp.545-573.

Krumbein, W.C. (1936). "Application of Logaritmic Moments to Size Frequency Distribution of Sediments," *Journal of Sedimentary Petrology*, Vol. 6, no. 1., pp. 35-47

Lauff, G.H. (1967). *Estuaries*, American Association for the Advancement of Science, Publication No. 83, Washington DC, 757 p.

Milliman, J.D., and Meade, R.H. (1983). "World Wide Delivery of River Sediment to the Ocean," *Journal Geology*, Vol. 91, pp. 1-21.

Pickard, G.L. (1975). *Descriptive Physical Oceanography*, 2nd ed. Pergamon Press, Inc., Oxford, U.K. 214 p.

Pritchard, D.W. (1955) "Estuarine Circulation Pattern," *Proc.* Am. Soc. Civil Engs., Vol.81, Paper no. 717, pp. 1-11.

Roberson, J.A., Cassidy, J.J., and Chaudhry M.H. (1988). *Hydraulic Engineering*, Houghton Mifflin Company, Boston, 662 p.

Silvester, R. (1974). *Coastal Engineering, 2 : Sedimentation, Estuaries, Tides, Effluents, and Modelling*, Elsevier Scientific Publishing Co., Amsterdam, 338 p.

Thomann, R.V., and Mueller, J.A. (1987). *Principles of Surface Water Quality Modelling and Control*, Harper & Row, Publishers, New York, NY., 644 p.

Ucles, R.J., and Stephens, J.A. (1990). "The structure of Vertical Current Profiles in a Macrotidal, Partly-Mixed Estuary," *Estuaries*, Vol. 13, no. 4, pp. 349-361.

U.S. Army Coastal Engineering Research Centre, (1984). *Shore Protection Manual*, Vol. I and II, Government Printing Office, Washington DC.

Wiegel, R.L. (1964). *Oceanographic Engineering*, Prentice Hall, Englewood Cliffs, New Jersey, 522 p.

Wright, L.D. (1977). "Sediment Transport and Deposition at River Mouths : a Synthesis," *The American Association of Geologists Bulletin*, Vol. 82, pp 857-858.

Wright, L.D., and Coleman, J.M. (1971). "The Discharge/Wave Power Climate and the Morphology of Delta Coasts," *Assoc. American Geographer Proc.*, Vol.3., pp. 186-189.

Wright, L.D., and Coleman, J.M. (1972). "River Delta Morphology, Wave Climate and the Role of the Subaqueous Profile," *Science*, No. 176, pp. 282-284.

Wright, L.D., and Coleman, J.M. (1973). "Variation in Morphology of Major Deltas as Functions of Ocean Wave and River Discharge Regimes," *The American Association of Petroleum Geologists Bulletin*, Vol. 57, no. 2, pp 370-398.

Wright, L.D., and Coleman, J.M. (1974). "Mississippi River Mouth Processes : Effluent Dynamics and Morphologic Development," *Journal of Geology*, Vol. 82, pp 751-778.

Wright, L.D., Coleman, J.M., and Thom, B.G. (1973). "Process of Channel Development in a high-tide-range Environment: Cambridge Gulf-Ord River Delta, Western Australia," *Journal Geology*, Vol. 81, pp 15-41.

Wright, L.D., Coleman, J.M., and Thorn, B.G. (1975). "Sediment Transport and Deposition in a Microtidal River Channel : Ord River, Western Australia," *Estuarine Research*, Vol.2, Geology and Engineering, New York, Academic Press, pp. 309-321. 57, no. 2, pp 370-398.

Appendix A

Data Sheets of the Field Observations

Table A.1-1

Tidal Record

Location : West Channel
Date : June 26, 1991

Time	Water Level (cm)				Remarks
	Harbour	STA.05	STA.03	STA.01	
00.00	31.0	49.5	53.5	66.3	LW
01.00	37.0	55.0	59.0	67.8	0.00
02.00	47.0	62.9	68.0	71.2	Midnight
03.00	63.0	76.5	78.9	77.2	
04.00	74.0	84.6	87.3	84.0	
05.00	82.0	89.5	90.5	90.3	
06.00	90.0	91.8	94.7	97.0	
07.00	99.0	103.5	106.0	103.3	
08.00	103.0	107.0	107.1	109.9	HW at
09.00	102.0	102.5	103.8	111.8	Harbour
10.00	98.0	97.5	102.5	109.3	8.00 AM
11.00	93.0	90.5	91.5	98.8	
12.00	88.0	88.2	87.5	94.3	
13.00	83.0	82.5	83.9	90.8	
14.00	80.0	80.5	82.5	88.8	
15.00	77.0	78.0	81.0	83.8	
16.00	73.0	72.5	72.5	77.9	
17.00	68.0	67.5	68.5	74.8	
18.00	63.0	63.5	64.5	72.8	
19.00	57.0	60.7	60.5	69.3	
20.00	49.0	59.5	59.5	67.8	
21.00	41.0	54.5	57.0	66.3	
22.00	35.0	52.5	55.5	65.8	
23.00	32.0	49.8	54.0	64.8	LW at
24.00	32.0	49.1	52.5	64.8	Harbour
01.00	34.0	50.5	54.5	64.8	0.00
02.00	43.0	56.5	58.5	69.4	Midnight
Range	71.0	57.9	54.6	45.1	

Table A.1-2

Tidal Record

Location : West Channel
Date : July 04,1991

Time	Water Level (cm)				Remarks
	Harbour	STA.05	STA.03	STA.01	
00.00	39.0	49.5	55.5	68.8	
01.00	39.0	51.5	58.5	69.8	
02.00	45.0	54.5	60.5	70.3	
03.00	51.0	59.5	63.5	70.8	
04.00	56.0	67.0	67.1	71.5	HW at
05.00	62.0	71.5	71.5	75.3	Harbour
06.00	69.0	73.5	74.5	77.4	1.00 PM
07.00	78.0	84.5	86.5	91.1	
08.00	88.0	89.5	97.9	99.2	
09.00	91.0	91.9	96.5	102.1	
10.00	92.0	94.7	99.5	102.4	
11.00	99.0	103.7	100.5	103.1	
12.00	100.0	102.5	101.5	105.8	
13.00	102.0	104.0	105.0	106.8	
14.00	101.0	100.0	105.5	106.3	
15.00	100.0	97.7	102.5	105.1	
16.00	96.0	92.3	99.5	102.3	
17.00	89.0	82.5	85.5	91.5	
18.00	79.0	78.5	80.5	88.7	
19.00	67.0	73.5	76.7	82.2	
20.00	55.0	67.6	71.8	77.5	
21.00	45.0	59.5	65.5	73.8	
22.00	39.0	55.5	60.5	71.8	LW at
23.00	37.0	54.5	58.5	71.3	Harbour
24.00	40.0	54.5	58.5	70.8	11.00 PM
Range	65.0	49.5	47.0	35.5	

Table A.1-3

Tidal Record

Location : West Channel
Date : July 18, 1991

Time	Water Level (cm)				Remarks
	Harbour	STA.05	STA.03	STA.01	
00.00	32.0	40.7	43.3	66.3	
01.00	39.0	40.6	43.4	66.3	
02.00	51.0	43.2	45.3	68.0	
03.00	65.0	59.5	59.5	76.9	
04.00	70.0	69.7	72.5	79.5	
05.00	74.0	73.5	74.0	81.2	
06.00	85.0	76.5	82.9	89.0	
07.00	88.0	84.6	87.9	93.7	
08.00	88.0	89.7	94.1	95.1	
09.00	88.0	91.0	94.5	100.1	
10.00	87.0	88.3	94.1	98.9	
11.00	89.0	86.9	91.2	98.0	HW at
12.00	90.0	89.2	91.8	99.2	Harbour
13.00	94.0	90.5	92.7	97.3	0.45 PM
14.00	92.0	91.7	92.9	98.5	
15.00	91.0	88.6	90.7	94.1	
16.00	89.0	87.7	89.9	89.6	
17.00	81.0	84.6	87.2	87.0	
18.00	71.0	80.4	81.7	85.0	
19.00	60.0	75.2	77.6	84.6	
20.00	49.0	69.5	70.0	81.4	LW at
21.00	38.0	51.1	56.8	76.2	Harbour
22.00	33.0	45.1	49.1	69.8	10.30 PM
23.00	31.0	43.5	45.5	67.3	
24.00	35.0	45.2	48.0	68.8	
Range	63.0	48.2	49.0	32.8	

Table A.1-4

Tidal Record

Location : West Channel
Date : July 26, 1991

Time	Water Level (cm)				Remarks
	Harbour	STA.05	STA.03	STA.01	
00.00	29.0	38.5	43.5	65.8	
01.00	32.0	42.5	44.5	66.3	
02.00	40.0	50.5	53.5	68.2	
03.00	55.0	57.5	59.5	69.8	
04.00	67.0	67.0	67.1	71.5	
05.00	77.0	71.5	71.5	75.3	
06.00	84.0	73.5	74.5	77.4	HW at
07.00	91.0	84.5	86.5	91.1	Harbour
08.00	92.0	89.5	97.9	99.2	8.40 AM
09.00	93.0	96.5	99.5	102.1	
10.00	91.0	96.4	99.5	102.4	
11.00	83.0	94.7	99.0	101.3	
12.00	80.0	94.3	98.5	100.8	
13.00	77.0	91.1	96.0	100.1	
14.00	72.0	88.0	92.5	98.8	
15.00	67.0	83.8	89.5	95.3	
16.00	66.0	82.5	89.5	91.8	
17.00	66.0	82.5	85.5	91.5	
18.00	60.0	78.5	80.5	88.7	
19.00	53.0	73.5	76.7	82.2	LW at
20.00	49.0	67.6	71.8	77.5	Harbour
21.00	39.0	54.3	58.3	74.2	11.00 PM
22.00	32.0	48.5	49.5	68.8	
23.00	31.0	42.5	45.5	67.3	
24.00	31.0	41.5	45.5	67.8	
Range	71.0	57.9	54.6	45.1	

Table A.2-1

Tidal Record

Location : Kali Semarang
Date : July 04, 1991

Time	Water Level (cm)				Remarks
	Harbour	STA.05	STA.04	STA.02	
00.00	39.0	42.0	45.0	160.5	
01.00	39.0	42.0	45.0	160.5	
02.00	45.0	44.0	45.0	160.5	
03.00	51.0	50.0	49.0	160.5	
04.00	56.0	55.9	55.0	160.5	
05.00	62.0	59.1	57.0	160.5	
06.00	69.0	68.2	65.3	160.5	
07.00	78.0	77.9	76.8	160.5	
08.00	88.0	86.3	82.6	160.5	
09.00	91.0	88.1	87.6	160.5	
10.00	92.0	91.3	91.1	160.5	
11.00	99.0	98.3	97.2	160.5	
12.00	100.0	99.0	100.6	160.5	HW at
13.00	102.0	100.0	101.9	160.5	Harbour
14.00	101.0	101.5	102.0	160.5	1.00 PM
15.00	100.0	100.6	101.0	160.5	
16.00	96.0	97.2	98.5	160.5	
17.00	89.0	90.1	92.2	160.5	
18.00	79.0	82.2	83.8	160.5	
19.00	67.0	72.2	76.6	160.5	
20.00	55.0	65.3	69.2	160.5	
21.00	45.0	51.0	52.0	160.5	LW at
22.00	39.0	47.0	48.0	160.5	Harbour
23.00	37.0	43.0	45.0	160.5	11.00 PM
24.00	40.0	42.0	45.0	160.5	
Range	65.0	58.5	57.0	0.0	

Table A.2-2

Tidal Record

Location : Kali Semarang
Date : July 18, 1991

Time	Water Level (cm)				Remarks
	Harbour	STA.05	STA.04	STA.02	
00.00	32.0	40.5	45.0	160.5	
01.00	39.0	43.2	45.0	160.5	
02.00	51.0	49.7	47.0	160.5	
03.00	65.0	57.3	49.0	160.5	
04.00	70.0	68.6	67.5	160.5	
05.00	74.0	72.6	73.3	160.5	
06.00	85.0	83.5	83.6	160.5	
07.00	88.0	86.7	86.1	160.5	
08.00	88.0	87.9	89.2	160.5	
09.00	88.0	88.0	89.9	160.5	
10.00	87.0	87.6	90.1	160.5	
11.00	89.0	88.3	91.3	160.5	
12.00	90.0	90.9	95.5	160.5	HW at
13.00	94.0	95.8	98.3	160.5	Harbour
14.00	92.0	95.9	99.0	160.5	0.40 PM
15.00	91.0	91.3	94.5	160.5	
16.00	89.0	89.4	90.2	160.5	
17.00	81.0	82.5	85.6	160.5	
18.00	71.0	77.1	79.1	160.5	
19.00	60.0	69.0	70.2	160.5	
20.00	49.0	57.0	58.0	160.5	
21.00	38.0	48.0	51.0	160.5	LW at
22.00	33.0	42.0	47.0	160.5	Harbour
23.00	31.0	40.0	45.0	160.5	11.00 PM
24.00	35.0	41.0	45.0	160.5	
Range	63.0	50.9	54.0	0.0	

Table A.2-3

Tidal Record

Location : Kali Semarang
Date : July 20, 1991

Time	Water Level (cm)				Remarks
	Harbour	STA.05	STA.04	STA.02	
00.00	31.0	42.0	45.0	160.5	
01.00	37.0	42.0	45.0	160.5	
02.00	48.0	44.0	45.0	160.5	
03.00	59.0	57.0	56.0	160.5	
04.00	71.0	68.1	66.3	160.5	HW at
05.00	81.0	78.5	76.6	160.5	Harbour
06.00	83.0	84.2	83.5	160.5	6.00 AM
07.00	82.0	84.3	85.2	160.5	
08.00	79.0	77.6	79.8	160.5	
09.00	71.0	69.5	72.2	160.5	
10.00	66.0	67.0	68.2	160.5	LW
11.00	61.0	61.1	63.3	160.5	11.30 AM
12.00	61.0	63.0	63.9	160.5	
13.00	64.0	63.3	64.8	160.5	
14.00	68.0	65.4	68.6	160.5	
15.00	70.0	69.6	71.7	160.5	HW
16.00	74.0	73.8	73.8	160.5	4.00 PM
17.00	72.0	76.6	76.3	160.5	
18.00	70.0	74.3	75.4	160.5	
19.00	63.0	68.8	72.1	160.5	
20.00	55.0	65.6	70.3	160.5	
21.00	49.0	62.0	63.0	160.5	
22.00	44.0	52.0	53.0	160.5	LW
23.00	35.0	45.0	47.0	160.5	0.00 AM
24.00	29.0	42.0	45.0	160.5	Midnight
Range	22.0	23.2	21.9	0.0	

Table A.3-1

Longitudinal Survey Data

Location : West Channel
Date : June 15, 1991 (flood tide)

Time	Depth cm.	Counts Rev/60s	Velocity m/s.	Salinity ppt	Temperature °C	Density g/cm³	Remark Elevation
8.00 AM	10	53	0.229	0.00	27.20	1.0000	STA. 01
	50	12	0.064	0.90	27.30	1.0000	
	100	6	0.040	1.21	27.90	1.0000	rise
	150	0	0.000	20.20	28.50	1.0122	
	200	0	0.000	29.00	29.00	1.0186	
9.00 AM	10	66	0.284	0.10	27.50		STA. 02
	50	11	0.060	1.30	27.60	1.0000	
	100	3	0.028	7.20	28.00	1.0027	rise
	150	0	0.000	23.60	28.50	1.0148	
	200	4	-0.032	29.10	29.00	1.0187	
	250	12	-0.064	30.10	29.00	1.0195	
	300	0	0.000	31.30	29.00	1.0204	
10.00 AM	10	71	0.305	0.70	27.80	1.0000	STA. 03
	50	24	0.111	5.50	27.90	1.0014	
	100	8	0.048	15.30	28.10	1.0087	rise
	150	0	0.000	25.80	28.60	1.0164	
	200	17	-0.083	30.30	29.00	1.0196	
11.00 AM	10	73	0.313	5.30	28.40	1.0012	STA. 04
	50	5	0.036	15.70	28.90	1.0088	
	100	12	0.064	25.30	29.00	1.0159	rise
	150	0	0.000	28.80	29.00	1.0185	
	200	0	0.000	30.30	29.00	1.0196	
	250	10	-0.056	30.90	29.00	1.0201	
	300	5	-0.036	31.00	29.00	1.0201	
12.00 AM	10	89	0.381	10.25	29.20	1.0046	STA. 05
	50	32	0.143	25.10	29.30	1.0157	
	100	4	0.032	27.90	29.00	1.0178	maximum
	150	0	0.000	29.80	29.00	1.0192	
	200	0	0.000	31.10	29.00	1.0202	water
	250	0	0.000	31.20	29.00	1.0203	
	300	0	0.000	31.50	29.00	1.0205	level

Table A.3-2

Longitudinal Survey Data

Location : West Channel
Date : June 15, 1991 (ebb tide)

Time	Depth cm.	Counts Rev/60s	Velocity m/s.	Salinity ppt	Temperature °C	Density g/cm³	Remark Elevation
4.00 PM	10	46	0.199	0.15	30.70	1.0000	STA. 01
	50	2	0.024	0.95	30.60	1.0000	
	100	5	0.036	2.25	30.50	1.0000	fall
	150	0	0.000	23.30	30.20	1.0141	
	200	0	0.000	29.20	30.10	1.0185	
3.00 PM	[illegible]	62	0.267	1.15	30.80	1.0000	STA. 02
	50	8	0.048	2.70	30.50	1.0000	
	100	0	0.000	10.90	30.50	1.0048	fall
	150	4	0.032	25.60	30.10	1.0158	
	200	0	0.000	29.40	29.50	1.0188	
	250	0	0.000	30.20	29.40	1.0194	
	300	0	0.000	31.20	29.20	1.0202	
2.00 PM	10	52	0.225	2.15	30.10	1.0000	STA. 03
	50	23	0.107	6.35	30.00	1.0015	
	100	3	0.028	17.70	29.30	1.0102	fall
	150	0	0.000	26.60	29.20	1.0168	
	200	0	0.000	30.20	29.00	1.0195	
1.00 PM	10	52	0.225	6.75	30.00	1.0018	STA. 04
	50	26	0.119	17.30	29.80	1.0097	
	100	0	0.000	26.60	29.50	1.0167	fall
	150	6	0.040	29.00	29.10	1.0186	
	200	0	0.000	29.90	29.00	1.0193	
	250	0	0.000	30.95	29.00	1.0201	
	300	0	0.000	31.10	29.00	1.0202	
12.00 AM	10	89	0.381	10.25	29.20	1.0046	STA. 05
	50	32	0.143	25.10	29.30	1.0157	
	100	4	0.032	27.90	29.00	1.0178	maximum
	150	0	0.000	29.80	29.00	1.0192	
	200	0	0.000	31.10	29.00	1.0202	water
	250	0	0.000	31.20	29.00	1.0203	
	300	0	0.000	31.50	29.00	1.0205	level

Table A.3-3

Longitudinal Survey Data

Location : West Channel
Date : June 19, 1991 (flood tide)

Time	Depth cm.	Counts Rev/60s	Velocity m/s.	Salinity ppt	Temperature °C	Density g/cm³	Remark Elevation
9.00 AM	10	63	0.271	0.00	28.40	1.0000	STA. 01
	50	10	0.056	0.10	28.60	1.0000	
	100	2	0.024	10.50	29.00	1.0049	rise
	150	0	0.000	24.90	29.00	1.0156	
	200	0	0.000	28.50	29.00	1.0183	
10.00 AM	10	65	0.280	0.90	28.50	1.0000	STA. 02
	50	28	0.127	2.10	29.00	1.0000	
	100	7	0.044	11.50	29.00	1.0056	rise
	150	4	0.032	25.60	29.00	1.0161	
	200	0	0.000	29.30	29.00	1.0189	
	250	12	-0.064	30.20	29.00	1.0195	
	300	4	-0.032	31.00	29.00	1.0201	
11.00 AM	10	68	0.292	1.10	29.80	1.0000	STA. 03
	50	31	0.139	5.70	29.00	1.0013	
	100	9	0.052	16.30	29.00	1.0092	rise
	150	0	0.000	27.10	29.00	1.0172	
	200	16	-0.079	29.80	29.00	1.0192	
12.00 AM	10	72	0.309	13.50	29.80	1.0069	STA. 04
	50	29	0.131	19.30	29.80	1.0112	
	100	9	0.052	24.50	29.20	1.0152	rise
	150	0	0.000	28.20	29.00	1.0180	
	200	0	0.000	30.10	29.00	1.0195	
	250	15	-0.075	30.60	29.00	1.0198	
	300	4	-0.032	30.90	29.00	1.0201	
1.00 PM	10	86	0.368	18.30	29.80	1.0105	STA. 05
	50	52	0.225	27.50	29.50	1.0174	
	100	14	0.071	28.80	29.00	1.0185	rise
	150	0	0.000	30.20	29.00	1.0195	
	200	0	0.000	30.50	29.00	1.0198	
	250	10	-0.056	30.50	29.00	1.0198	
	300	5	-0.036	30.80	29.00	1.0200	

Table A.3-4

Longitudinal Survey Data

Location : West Channel
Date : June 26, 1991 (ebb tide)

Time	Depth cm.	Counts Rev/60s.	Velocity m/s.	Salinity ppt	Temperature °C	Density g/cm³	Remark Elevation
9.00 AM	10	55	0.237	0.00	28.40	1.0000	STA. 01
	50	0	0.000	0.50	28.60	1.0000	
	100	2	0.024	13.70	29.00	1.0073	112 cm
	150	0	0.000	25.60	29.00	1.0161	
	200	0	0.000	29.00	29.00	1.0186	
9.45 AM	10	55	0.237	0.00	28.50	1.0000	STA. 02
	50	28	0.127	1.60	29.00	1.0000	
	100	0	0.000	18.20	29.00	1.0106	106 cm
	150	4	0.032	27.10	29.00	1.0172	
	200	0	0.000	29.20	29.00	1.0188	
	250	0	0.000	30.30	29.00	1.0196	
	300	0	0.000	31.00	29.00	1.0201	
10.45 AM	10	38	0.166	1.00	29.80	1.0000	STA. 03
	50	31	0.139	10.30	29.00	1.0047	
	100	2	0.024	21.30	29.00	1.0129	92 cm
	150	0	0.000	28.00	29.00	1.0179	
	200	0	0.000	29.80	29.00	1.0192	
11.45 AM	10	49	0.212	15.30	29.80	1.0082	STA. 04
	50	31	0.139	22.30	29.80	1.0134	
	100	8	0.048	25.50	29.20	1.0163	88 cm
	150	0	0.000	28.10	29.00	1.0180	
	200	0	0.000	29.50	29.00	1.0190	
	250	0	0.000	30.90	29.00	1.0201	
	300	0	0.000	30.50	29.00	1.0198	
12.45 AM	10	90	0.385	19.60	29.80	1.0114	STA. 05
	50	24	0.111	27.80	29.50	1.0176	
	100	2	0.024	28.00	29.00	1.0179	83 cm
	150	9	0.052	28.50	29.00	1.0183	
	200	0	0.000	29.70	29.00	1.0192	
	250	0	0.000	30.70	29.00	1.0199	
	300	0	0.000	30.80	29.00	1.0200	

Table A.4-1

Sectional Survey Data

Location : STA.03, West Channel
Date : July 04, 1991

Time (WL)	Depth cm.	Counts Rev/60s	Velocity m/s.	Salinity ppt	Temperature °C	Density g/cm³
8.00 AM	10	79	0.329	0.01	28.10	1.0000
	25	36	0.159	10.00	28.30	1.0047
90 cm	50	0	0.000	20.50	28.50	1.0125
	100	3	-0.028	29.50	28.80	1.0191
	150	10	-0.056	29.80	29.00	1.0192
	190	0	0.000	29.50	29.50	1.0189
9.00 AM	10	55	0.234	1.90	28.10	1.0000
	25	32	0.143	9.90	28.30	1.0046
92 cm	50	0	0.000	20.50	28.50	1.0125
	100	0	0.000	29.80	28.90	1.0193
	150	9	-0.052	29.80	29.00	1.0192
	190	0	0.000	29.50	29.10	1.0190
10.00 PM	10	46	0.198	1.90	29.00	1.0000
	25	38	0.166	7.90	29.00	1.0029
95 cm	50	0	0.000	17.00	29.80	1.0095
	100	0	0.000	29.50	29.80	1.0188
	150	6	-0.040	29.80	29.50	1.0191
	190	0	0.000	29.90	29.40	1.0192
11.00 PM	10	72	0.301	1.65	30.10	1.0000
	25	40	0.174	10.50	30.20	1.0046
104 cm	50	0	0.000	22.10	30.40	1.0131
	100	3	-0.028	26.50	29.80	1.0165
	150	9	-0.052	28.20	29.80	1.0178
	190	0	0.000	29.20	29.80	1.0186

Table A.4-2

Sectional Survey Data

Location : STA.03, West Channel
Date : July 04, 1991

Time (WL)	Depth cm.	Counts Rev/60s	Velocity m/s.	Salinity ppt	Temperature °C	Density g/cm³
12.00 AM	10	78	0.325	2.30	30.40	1.0000
	25	48	0.206	10.30	30.70	1.0043
103 cm	50	0	0.000	22.10	30.80	1.0130
	100	16	-0.079	25.00	30.10	1.0153
	150	5	-0.036	27.10	29.80	1.0170
	190	0	0.000	29.90	29.80	1.0191
1.00 PM	10	105	0.432	1.75	31.00	1.0000
	25	113	0.463	11.60	31.20	1.0051
104 cm	50	0	0.000	22.70	31.40	1.0132
	100	0	0.000	28.00	30.40	1.0175
	150	0	0.000	29.80	29.80	1.0190
	190	0	0.000	29.90	29.80	1.0191
2.00 PM	10	117	0.479	1.75	31.10	1.0000
	25	53	0.226	11.90	31.20	1.0053
100 cm	50	0	0.000	23.20	31.20	1.0137
	100	0	0.000	28.50	30.20	1.0179
	150	0	0.000	29.80	30.00	1.0189
	190	0	0.000	29.80	29.80	1.0190
3.00 PM	10	67	0.281	1.50	31.10	1.0000
	25	51	0.218	13.20	31.10	1.0063
98 cm	50	0	0.000	25.00	31.00	1.0151
	100	0	0.000	29.00	29.90	1.0184
	150	0	0.000	29.80	29.80	1.0190
	190	0	0.000	29.80	29.80	1.0190

Table A.4-3

Sectional Survey Data

Location : Sta.03, West Channel
Date : July 18, 1991

Time (WL)	Depth cm.	Counts Rev/60s	Velocity m/s.	Salinity ppt	Temperature °C	Density g/cm³
6.00 AM	10	78	0.325	0.25	27.80	1.0000
	25	50	0.214	10.25	27.80	1.0050
88 cm	50	0	0.000	21.10	27.90	1.0131
	100	2	-0.024	27.60	28.50	1.0177
	150	5	-0.036	29.10	29.00	1.0187
	190	0	0.000	30.00	29.10	1.0194
7.00 AM	10	100	0.412	3.20	27.80	1.0000
	25	61	0.257	9.70	27.80	1.0046
94 cm	50	0	0.000	21.60	28.00	1.0134
	100	7	-0.044	28.80	28.50	1.0186
	150	2	-0.024	29.00	29.00	1.0186
	190	0	0.000	30.10	29.10	1.0194
8.00 AM	10	65	0.273	3.10	27.80	1.0000
	25	42	0.182	9.10	27.80	1.0041
95 cm	50	3	0.028	22.70	28.00	1.0142
	100	0	0.000	28.90	28.40	1.0137
	150	0	0.000	29.10	29.00	1.0187
	190	0	0.000	30.30	29.00	1.0196
9.00 AM	10	60	0.254	2.20	27.80	1.0000
	25	43	0.186	10.30	27.80	1.0050
94 cm	50	0	0.000	22.90	28.00	1.0144
	100	0	0.000	29.00	28.50	1.0188
	150	0	0.000	29.30	29.10	1.0188
	190	0	0.000	29.90	29.10	1.0193
10.00 AM	10	85	0.352	1.90	28.00	1.0000
	25	63	0.265	11.00	28.00	1.0055
91 cm	50	0	0.000	24.10	28.10	1.0153
	100	5	-0.036	28.90	28.60	1.0187
	150	2	-0.024	29.40	29.10	1.0189
	190	0	0.000	30.10	29.10	1.0194
11 00 AM	10	93	0.384	2.20	29.10	1.0000
	25	51	0.218	11.20	28.40	1.0056
92 cm	50	3	0.028	24.40	28.20	1.0154
	100	3	-0.028	27.90	28.50	1.0180
	150	6	-0.040	28.90	29.10	1.0185
	190	0	0.000	29.50	29.10	1.0190

Table A.4-4

Sectional Survey Data

Location : STA.03, West Channel
Date : July 18, 1991

Time (WL)	Depth cm	Counts Rev/60s	Velocity m/s	Salinity ppt	Temperature °C	Density g/cm³
12.00 AM	10	98	0.404	3.20	29.50	1.0000
	25	36	0.159	9.80	29.30	1.0043
93 cm	50	0	0.000	23.30	29.00	1.0144
	100	0	0.000	28.30	28.70	1.0182
	150	9	-0.052	28.80	29.20	1.0184
	190	0	0.000	29.80	29.10	1.0192
1.00 PM	10	107	0.440	2.70	30.10	1.0000
	25	89	0.368	8.90	30.00	1.0034
92 cm	50	0	0.000	20.90	30.00	1.0123
	100	0	0.000	27.80	29.00	1.0178
	150	0	0.000	29.10	29.30	1.0186
	190	0	0.000	29.30	29.20	1.0188
2.00 PM	10	99	0.408	1.20	31.00	1.0000
	25	39	0.170	9.10	30.80	1.0034
91 cm	50	0	0.000	21.30	30.50	1.0125
	100	0	0.000	26.50	29.20	1.0167
	150	0	0.000	28.10	29.50	1.0178
	190	0	0.000	29.80	29.10	1.0192
3.00 PM	10	65	0.273	0.95	31.30	1.0000
	25	41	0.178	8.50	31.20	1.0028
90 cm	50	0	0.000	21.20	31.20	1.0122
	100	0	0.000	27.20	30.00	1.0170
	150	0	0.000	29.20	29.30	1.0187
	190	0	0.000	30.00	29.40	1.0193
4.00 PM	10	56	0.238	0.80	31.40	1.0000
	25	31	0.139	8.70	31.20	1.0030
87 cm	50	0	0.000	20.30	31.10	1.0116
	100	0	0.000	26.60	30.20	1.0165
	150	0	0.000	29.20	30.00	1.0185
	190	0	0.000	30.30	29.60	1.0194
5.00 PM	10	44	0.190	0.75	31.00	1.0000
	25	32	0.143	9.30	31.10	1.0034
82 cm	50	0	0.000	20.95	31.20	1.0120
	100	0	0.000	25.20	30.60	1.0153
	150	0	0.000	28.90	30.10	1.0182
	190	0	0.000	30.20	29.80	1.0193

Table A.5-1

Float Test

Location : STA.03, West Channel
Date : July 19, 1991

Time		Distance (m)	Water Elev. (m,RBW)	Remarks
Start	Finish			
00.00	-	-	0.31	- flood tide starts about
01.00	01.11	20.0	0.32	midnight
02.00	02.07	20.0	0.48	- the float was released
02.30	02.35	20.0	0.52	at mid of the channel
03.00	03.11	20.0	0.59	- the float moves up-estuary
03.30	03.44	20.0	0.66	until 06.00 AM
04.00	04.20	20.0	0.71	- the position of float always
04.30	04.49	20.0	0.75	at the middle of the channel
05.00	05.17	20.0	0.81	
05.30	05.47	20.0	0.82	- from 6.00 to 7.30 AM, the
06.00	-	-	0.83	float moves up and down
.	-	-	.	
.	-	-	.	- HW at 6.15 AM
.	-	-	.	
07.30	07.47	20.0	0.79	- at 7.30, the float moves down
08.00	08.15	20.0	0.78	
08.30	08.41	20.0	0.74	- at 10.30 to 12.00 (Nooon), the
09.00	09.17	20.0	0.71	float moves up and down very
09.30	09.50	20.0	0.68	slowly
10.00	10.25	20.0	0.66	
11.00	11.30	20.0	0.61	- LW at 11.30 AM float moves
.	-	-	.	up
.	-	-	.	
.	-	-	.	
12.00	12.25	20.0	0.61	
13.00	13.20	20.0	0.64	- at 4.00 to 5.00 PM, the float
14.00	14.21	20.0	0.68	moves up and down slowly
15.00	15.24	20.0	0.70	
.	-	-	0.72	- at 5.00 PM, the float moves
17.00	-	-		down

Table A.5-2

Float Test

Location : STA.03, West Channel
Date : July 25, 1991

Time		Distance (m)	Water Elev. (m,RBW)	Remarks
Start	Finish			
00.00	-	-	0.31	- flood tide starts about midnight
01.00	01.18	20.0	0.32	
02.00	02.12	20.0	0.40	
02.30	02.36	20.0	0.49	- the float was released at mid at the channel
03.00	03.05	20.0	0.55	
03.30	03.37	20.0	0.62	
04.00	04.08	20.0	0.67	- the float moves up-estuary until 7.00 AM.
04.30	04.45	20.0	0.72	
05.00	05.20	20.0	0.76	
05.30	05.50	20.0	0.81	- the float remains about the mid of the channel
06.00	06.22	20.0	0.84	
07.00	-	-	0.90	- from 7.00 to 9.30 AM, the float moves up and down slowly
.	-	-	.	
.	-	-	.	
09.00	-	-	0.94	- HW at 8.45 AM
09.30	09.50	20.0	0.92	
10.00	10.19	20.0	0.91	- at 9.30 AM the float starts to move down
10.30	10.42	20.0	0.89	
11.00	11.12	20.0	0.85	
12.00	12.14	20.0	0.80	
13.00	13.16	20.0	0.77	- at 3.00 to 5.30 PM, the float moves up and down slowly
14.00	14.20	20.0	0.72	
15.00	-	-	0.67	
.	-	-	0.66	
17.00	-	-	0.64	- the float moves down at 5.30 PM.
17.30	17.49	20.0		

Table A.6-1

Float Test

Location : STA.05, Kali Semarang
Date : July 20, 1991

Time		Distance	Water Elev.	Remarks
Start	Finish	(m)	(m,RBW)	
00.30	00.49	20.0	0.49	- the float was released at the mid at the channel
01.00	01.17	20.0	0.52	
02.00	02.12	20.0	0.63	
02.30	02.41	20.0	0.70	- the float moves up-estuary until 7.00 am
03.00	03.10	20.0	0.77	
03.30	03.39	20.0	0.83	
04.00	04.08	20.0	0.88	- the float remains at about the middle of the channel
04.30	04.49	20.0	0.92	
05.00	05.20	20.0	0.93	
05.30	05.50	20.0	0.95	- from 6.00 to 8.30 AM, the float moves up and down
06.00	06.25	20.0	0.97	
06.30	-	-	0.98	
.	-	-	0.99	- HW at 7.15 AM
.	-	-	0.95	
08.30	08.55	20.0	0.91	- at 8.30 AM, the float starts to move down
09.00	09.30	20.0	.	
09.30	-	-	.	- at 10.30 to 12.00 (Noon), the float moves up and down very slowly.
.	-	-	.	
.	-	-	.	
.	-	-	.	- Water level almost constant from 10.00 AM to 1.00 PM, the float moves up and down slowly
.	-	-	0.90	
14.00	-	-	0.89	
15.00	-	-	0.90	
16.00	15.20	20.0	0.89	- at 3.00 PM, the float moves up again
17.00	16.28	20.0		
	-	-		- at 4.00 to 5.00 PM, the float stops.

Table A.6-2

Float Test

Location : STA.05, Kali Semarang
Date : July 26, 1991

Time		Distance (m)	Water Elev. (m,RBW)	Remarks
Start	Finish			
00.00	00.19	20.0	0.30	- the float was released at mid of the channel
03.00	00.46	20.0	0.31	
01.00	01.15	20.0	0.32	
02.00	02.11	20.0	0.40	- the float moves up-estuary until about 7.00 AM
02.30	02.40	20.0	0.45	
03.00	03.07	20.0	0.52	
03.30	03.38	20.0	0.59	- the float moves about the middle of the channel
04.00	04.13	20.0	0.68	
04.30	04.47	20.0	0.73	
05.00	05.20	20.0	0.78	- from 07.00 to 10.30 AM, the float moves up and down very slowly
05.30	05.50	20.0	0.82	
06.00	06.28	20.0	0.85	
07.00	-	-	0.89	
.	-	-	.	- HW at 8.30 AM
.	-	-	.	
.	-	-	.	
10.00	-	-	0.89	- at 10.30 AM, the float starts to move down very slowly
10.30	10.49	20.0	0.86	
11.00	11.25	20.0	0.83	
12.00	12.29	20.0	0.77	
13.00	-	-	0.73	
.	-	-	0.61	- at 1.00 PM, the float moves up and down until the test finished at 5.00 PM
.	-	-		
17.00	-	-		

Appendix B

Offshore Wave Energy Flux

Table B.1 Angle Between Wind Direction and Normal of Shoreline (α_o)

Direction	α_o	$\text{Cos}\alpha_o$	Avg ($\text{Cos}\alpha_o$)	$\text{Sin}\alpha_o$	Avg $\text{Sin}\alpha_o$	$\text{Cos}\alpha_o$ x $\text{Sin}\alpha_o$	Avg.(7)
(1).	(2)	(3)	(4)	(5)	(6)	(7)	(8)
Shoreline	-90.00	0.00		-1.00		0.00	
ENE	-76.25	0.24	0.12	-0.97	-0.99	-0.23	-0.12
NE	-53.25	0.60	0.42	-0.80	-0.89	-0.48	-0.36
NNE	-31.25	0.85	0.73	-0.52	-0.66	-0.44	-0.46
N	-8.75	0.99	0.92	-0.15	-0.34	-0.15	-0.30
NNW	13.75	0.97	0.98	0.24	0.04	0.23	0.04
NW	36.25	0.81	0.89	0.59	0.41	0.48	0.35
WNW	58.75	0.52	0.66	0.85	0.72	0.44	0.46
W	81.25	0.15	0.34	0.99	0.92	0.15	0.30
WSW/Shore-line	90.00	0.00	0.08	1.00	0.99	0.00	0.08

Table B.2 Determination of wave-group celerity (C_g)

T (sec.)	$L_o = 1.56T^2$ (m)	$\frac{d}{L_o}$	$\frac{H}{H_o}$	$\frac{d}{L}$	$L = \frac{d}{(d/L)}$	$\frac{C_g}{C}$	C_g
2.5	9.75	0.9231	0.9999	0.9231	9.75	0.5001	1.9503
3.5	19.11	0.4710	0.9874	0.4735	19.01	0.5128	2.7849
4.5	31.59	0.2849	0.9440	0.2987	30.13	0.5611	3.7569
5.5	47.19	0.1907	0.9162	0.2174	41.40	0.5956	4.4831
6.5	65.91	0.1365	0.9153	0.1720	52.33	0.5968	4.8043
7.5	87.75	0.1026	0.9307	0.1431	62.89	0.5771	4.8394

Table B.3 Offshore Wave Energy Flux for T = 2.5 Seconds

H_s (m)	H_o' (m)	Pct of occur. (%)	Frequency, f (%)								
			ENE 2.5	NE 2.3	NNE 1.2	N 7.0	NNW 3.8	NW 8.0	WNW 6.2	W 8.2	WSW 3.5
0.25	0.230	30.930	0.773	0.711	0.371	2.165	1.175	2.474	1.918	2.536	1.083
0.75	0.692	0.860	0.022	0.020	0.010	0.060	0.033	0.069	0.053	0.071	0.030
H_s (m)	H_o' (m)	H_f (m)	Energy flux (J/m-s)								
			ENE	NE	NNE	N	NNW	NW	WNW	W	WSW
0.25	0.230	0.231	1.005	0.924	0.482	2.813	1.527	3.215	2.491	3.295	1.406
0.75	0.692	0.692	0.251	0.231	0.121	0.704	0.382	0.804	0.623	0.825	0.352
Total I			1.256	1.155	0.603	3.517	1.909	4.019	3.115	4.120	1.758

Table B.4 Offshore Wave Energy Flux for T = 3.5 Seconds

H_s (m)	H_o' (m)	Pct of occur. (%)	Frequency, f								
			ENE 2.5	NE 2.3	NNE 1.2	N 7.0	NNW 3.8	NW 8.0	WNW 6.2	W 8.2	WSW 3.5
0.25	0.25	22.750	0.569	0.523	0.273	1.593	0.865	1.820	1.411	1.866	0.000
0.75	0.74	4.420	0.111	0.102	0.053	0.309	0.168	0.354	0.274	0.362	0.000
1.25	1.23	0.350	0.009	0.008	0.004	0.025	0.013	0.028	0.022	0.029	0.000
H_s (m)	H_o' (m)	H_f (m)	Energy flux (J/m-s)								
			ENE	NE	NNE	N	NNW	NW	WNW	W	WSW
0.25	0.25	0.247	1.207	1.111	0.579	3.380	1.835	3.863	2.994	3.960	0.000
0.75	0.74	0.741	2.111	1.942	1.013	5.910	3.209	6.755	5.235	6.924	0.000
1.25	1.23	1.234	0.464	0.427	0.223	1.300	0.706	1.486	1.151	1.523	0.000
Total II			3.782	3.480	1.816	10.59	5.749	12.104	9.380	12.406	0.000

Table B.5 Offshore Wave Energy Flux for T = 4.5 Seconds

H_s (m)	H_o' (m)	Pct of occur. (%)	Frequency, f (%)								
			ENE 2.5	NE 2.3	NNE 1.2	N 7.0	NNW 3.8	NW 8.0	WNW 6.2	W 8.2	WSW 3.5
0.25	0.24	9.910	0.248	0.228	0.119	0.694	0.377	0.793	0.614	0.813	0.000
0.75	0.71	6.080	0.152	0.001	0.001	0.004	0.002	0.005	0.004	0.005	0.000
1.25	1.18	2.400	0.060	0.001	0.000	0.002	0.001	0.002	0.001	0.002	0.000
1.75	1.65	0.300	0.008	0.000	0.000	0.000	0.000	0.000	0.000	0.000	0.000
H_s (m)	H_o' (m)	H_f (m)	Energy flux (J/m-s)								
			ENE	NE	NNE	N	NNW	NW	WNW	W	WSW
0.25	0.24	0.236	0.648	0.597	0.311	1.816	0.986	2.075	1.608	2.127	0.000
0.75	0.71	0.708	3.580	0.033	0.017	0.100	0.054	0.115	0 089	0.117	0.000
1.25	1.18	1.180	3.926	0.036	0.019	0.110	0.060	0.126	0.097	0.129	0.000
1.75	1.65	1.652	0.962	0.009	0.005	0.027	0.015	0.031	0.024	0.032	0.000
Total III			9.116	0.674	0.352	2.053	1.114	2.346	1.818	2.405	0.000

Table B.6 Offshore Wave Energy Flux for T = 5.5 Seconds

H_s (m)	H_o' (m)	Pct of occur. (%)	Frequency, f (%)								
			ENE 2.5	NE 2.3	NNE 1.2	N 7.0	NNW 3.8	NW 8.0	WNW 6.2	W 8.2	WSW 3.5
0.25	0.23	2.740	0.069	0.063	0.033	0.192	0.104	0.219	0.170	0.225	0.000
0.75	0.69	2.170	0.054	0.050	0.026	0.152	0.082	0.174	0.135	0.178	0.000
1.25	1.15	1.670	0.042	0.038	0.020	0.117	0.063	0.134	0.104	0.137	0.000
1.75	1.60	0.320	0.008	0.007	0.004	0.022	0.012	0.026	0.020	0.026	0.000
H_s (m)	H_o' (m)	H_f (m)	Energy flux (J/m-s)								
			ENE	NE	NNE	N	NNW	NW	WNW	W	WSW
0.25	0.23	0.229	0.202	0.185	0.097	0.564	0.306	0.645	0.500	0.661	0.000
0.75	0.69	0.687	1.436	1.321	0.689	4.022	2.183	4.596	3.562	4.711	0.000
1.25	1.15	1.145	3.071	2.825	1.474	8.598	4.667	9.826	7.615	10.071	0.000
1.75	1.60	1.603	1.153	1.061	0.554	3.229	1.753	3.690	2.860	3.782	0.000
Total IV			5.862	5.393	2.814	16.412	8.910	18.757	14.537	19.226	0.000

Table B.7 Offshore Wave Energy Flux for T = 6.5 Seconds

H_s (m)	H_o' (m)	Pct of occur. (%)	Frequency, f (%)								
			ENE 2.5	NE 2.3	NNE 1.2	N 7.0	NNW 3.8	NW 8.0	WNW 6.2	W 8.2	WSW 3.5
0.25	0.23	0.450	0.011	0.010	0.005	0.032	0.017	0.036	0.028	0.037	0.000
0.75	0.69	0.220	0.006	0.005	0.003	0.015	0.008	0.018	0.014	0.018	0.000
1.25	1.14	0.120	0.003	0.003	0.001	0.008	0.005	0.010	0.007	0.010	0.000
2.25	2.06	0.020	0.001	0.000	0.000	0.001	0.001	0.002	0.001	0.002	0.000
H_s (m)	H_o' (m)	H_f (m)	Energy flux (J/m-s)								
			ENE	NE	NNE	N	NNW	NW	WNW	W	WSW
0.25	0.23	0.229	0.035	0.033	0.017	0.099	0.054	0.113	0.088	0.116	0.000
0.75	0.69	0.686	0.156	0.143	0.075	0.436	0.237	0.498	0.386	0.511	0.000
1.25	1.14	1.144	0.236	0.217	0.113	0.661	0.359	0.755	0.585	0.774	0.000
2.25	2.06	2.059	0.127	0.117	0.061	0.357	0.194	0.408	0.316	0.418	0.000
Total V			0.555	0.510	0.266	1.553	0.843	1.775	1.375	1.819	0.000

Table B.8 Offshore Wave Energy Flux for T = 7.5 Seconds

H_s (m)	H_o' (m)	Pct of occur. (%)	Frequency, f (%)								
			ENE 2.5	NE 2.3	NNE 1.2	N 7.0	NNW 3.8	NW 8.0	WNW 6.2	W 8.2	WSW 3.5
0.25	0.23	0.020	0.001	0.000	0.000	0.001	0.001	0.002	0.001	0.002	0.000
0.75	0.70	0.000	0.000	0.000	0.000	0.000	0.000	0.000	0.000	0.000	0.000
1.25	1.16	0.020	0.001	0.000	0.000	0.001	0.001	0.002	0.001	0.002	0.000
1.75	1.63	0.000	0.000	0.000	0.000	0.000	0.000	0.000	0.000	0.000	0.000
H_s (m)	H_o' (m)	H_f (m)	Energy flux (J/m-s)								
			ENE	NE	NNE	N	NNW	NW	WNW	W	WSW
0.25	0.23	0.233	0.002	0.002	0.001	0.005	0.002	0.005	0.004	0.005	0.000
0.75	0.70	0.698	0.000	0.000	0.000	0.000	0.000	0.000	0.000	0.000	0.000
1.25	1.16	1.163	0.041	0.038	0.020	0.115	0.062	0.131	0.102	0.134	0.000
1.75	1.63	1.629	0.000	0.000	0.000	0.000	0.000	0.000	0.000	0.000	0.000
Total VI			0.043	0.039	0.020	0.119	0.065	0.136	0.106	0.140	0.000
Total(I+...+VI)			20.613	11.252	5.870	34.244	18.590	39.136	30.331	40.115	1.758

Table B.9 Monthly Distribution of Offshore Wave Energy Flux (P) During 1989

Months	Wave energy flux (P) per direction per month (J/m-s)									Total per month
	ENE	NE	NNE	N	NNW	NW	WNW	W	WSW	
January	0.675	0.745	0.162	1.971	1.325	3.606	5.777	6.860	0.292	21.4119
February	0.750	0.261	0.364	0.246	0.166	3.930	7.623	12.716	0.525	26.5808
March	1.424	0.969	0.526	2.423	1.656	4.254	4.855	4.854	0.196	21.1561
April	1.349	1.751	0.769	2.464	1.822	5.307	2.528	1.966	0.117	18.0721
May	2.399	1.267	0.445	4.752	1.987	0.932	0.120	0.521	0.029	12.0533
June	2.099	1.304	1.012	3.408	2.029	2.026	0.762	0.963	0.129	13.7316
July	2.324	0.596	0.607	2.464	0.994	1.864	1.204	1.123	0.029	11.2040
August	2.549	0.708	0.486	3.244	1.076	1.215	0.321	1.123	0.033	10.7555
September	2.174	0.931	0.405	3.983	1.573	2.876	1.605	1.284	0.054	14.8854
October	1.649	0.745	0.202	3.038	2.401	3.970	1.123	1.685	0.100	14.9150
November	1.724	1.080	0.526	4.517	2.443	4.619	1.444	0.923	0.042	17.3174
December	1.499	0.894	0.364	2.135	1.118	4.538	2.969	6.097	0.212	19.827?
Total per direction	20.613	11.252	5.870	34.244	18.590	39.136	30.331	40.115	1.758	201.910

Table B.10 Monthly Distribution of Longshore Component of Offshore Wave Energy Flux (P_{ls}) During 1989

Months	Longshore component of wave energy flux (P_{ls}) per direction per month (J/m-s)									Net P_{ls} per month	Gross P_{ls} per month
	ENE	NE	NNE	N	NNW	NW	WNW	W	WSW		
January	-0.078	-0.265	-0.075	-0.585	0.053	1.276	2.659	2.037	0.022	5.0444	7.0491
February	-0.087	-0.093	-0.168	-0.073	0.007	1.391	3.508	3.776	0.039	8.3000	9.1409
March	-0.164	-0.344	-0.243	-0.719	0.067	1.505	2.234	1.441	0.015	3.7916	6.7326
April	-0.156	-0.622	-0.355	-0.731	0.073	1.878	1.163	0.584	0.009	1.8433	5.5712
May	-0.277	-0.450	-0.206	-1.292	0.080	0.330	0.055	0.155	0.002	-1.6021	2.8467
June	-0.242	-0.463	-0.467	-1.012	0.082	0.717	0.351	0.286	0.010	-0.7392	3.6292
July	-0.268	-0.212	-0.280	-0.731	0.040	0.660	0.554	0.333	0.002	0.0976	3.0807
August	-0.294	-0.251	-0.224	-0.963	0.043	0.430	0.148	0.333	0.003	-0.7756	2.6900
September	-0.251	-0.331	-0.187	-1.183	0.063	1.018	0.739	0.381	0.004	0.2542	4.1561
October	-0.190	-0.265	-0.093	-0.902	0.097	1.405	0.517	0.500	0.008	1.0762	3.9771
November	-0.199	-0.384	-0.240	-1.341	0.098	1.635	0.665	0.274	0.003	0.5082	4.8412
December	-0.173	-0.318	-0.168	-0.634	0.045	1.606	1.366	1.810	0.016	3.5509	6.1361
Total	-2.379	-3.995	-2.709	-10.167	0.749	13.85	13.95	11.910	0.132	21.3495	59.850

Appendix C

Nearshore Wave Energy Flux

Table C.1 Angle Between Wind Direction and Normal of the Shoreline

Direction	α_o	$\text{Cos}\alpha_o$	Avg(3)	$\text{Sin}\alpha_o$	Avg.(5)	$\text{Cos}\alpha_o$ x $\text{Sin}\alpha_o$	Avg.(7)
(1)	(2)	(3)	(4)	(5)	(6)	(7)	(8)
S-line	-90.00	0.000		-1.000		0.000	
ENE	-76.25	0.238	0.119	-0.971	-0.986	-0.231	-0.115
NE	-53.25	0.598	0.418	-0.801	-0.886	-0.479	-0.355
NNE	-31.25	0.855	0.727	-0.519	-0.660	-0.444	-0.461
N	-8.75	0.988	0.922	-0.152	-0.335	-0.150	-0.297
NNW	13.75	0.971	0.980	0.238	0.043	0.231	0.040
NW	36.25	0.806	0.889	0.591	0.414	0.477	0.354
WNW	58.75	0.519	0.663	0.855	0.723	0.444	0.460
W	81.25	0.152	0.335	0.988	0.922	0.150	0.297
WSW/SL	90.00	0.000	0.076	1.000	0.994	0.000	0.075

Table C.2 Determination of Wave Group Celerity (C_g)

T (sec)	$L_o=1.56T^2$ (m)	$\frac{d}{Lo}$	$\frac{H}{Ho}$	$\frac{d}{L}$	$L=\frac{d}{(d/L)}$	$\frac{C_g}{C}$	C_g (m/s)	$\text{Sin}(2\pi d/L)$	ϕ	ϕ'
2.5	9.75	0.1754	0.914	0.205	8.362	0.599	2.002	1.669	1.130	2.531
3.5	19.11	0.0895	0.943	0.132	12.974	0.563	2.085	0.926	7.257	4.104
4.5	31.59	0.0541	1.010	0.098	17.397	0.490	1.896	0.658	24.914	4.812
5.5	47.19	0.0362	1.085	0.079	21.673	0.425	1.675	0.516	63.753	5.137
6.5	65.91	0.0259	1.159	0.066	25.858	0.372	1.481	0.428	136.871	5.293
7.5	87.75	0.0195	1.233	0.057	30.069	0.329	1.319	0.365	264.962	5.433

Table C.3 Nearshore Wave Energy Flux for T = 2.5 Seconds

H_s (m)	H_o' (m)	Pct of occur. (%)	Frequency, f (%)								
			ENE 2.5	NE 2.3	NNE 1.2	N 7.0	NNW 3.8	NW 8.0	WNW 6.2	W 8.2	WSW 3.5
0.250	0.273	30.930	0.773	0.711	0.371	2.165	1.175	2.474	1.918	2.536	1.083
0.750	0.820	0.860	0.022	0.020	0.010	0.060	0.033	0.069	0.053	0.071	0.030
H_s (m)	H_o' (m)	H_f (m)	Energy flux (J/m-s)								
			ENE	NE	NNE	N	NNW	NW	WNW	W	WSW
0.250	0.273	0.230	1.024	0.942	0.491	2.866	1.556	3.276	2.539	3.358	1.433
0.750	0.820	0.303	0.050	0.046	0.024	0.139	0.075	0.159	0.123	0.163	0.069
Total I			1.073	0.987	0.515	3.005	1.631	3.434	2.662	3.520	1.503

Table C.4 Nearshore Wave Energy Flux for T = 3.5 Seconds

H_s (m)	H_o' (m)	Pct of occur. (%)	Frequency, f (%)								
			ENE 2.5	NE 2.3	NNE 1.2	N 7.0	NNW 3.8	NW 8.0	WNW 6.2	W 8.2	WSW 3.5
0.250	0.270	22.750	0.569	0.523	0.273	1.593	0.865	1.820	1.411	1.866	0.000
0.750	0.811	4.420	0.111	0.102	0.053	0.309	0.168	0.354	0.274	0.362	0.000
1.250	1.352	0.350	0.009	0.008	0.004	0.025	0.013	0.028	0.022	0.029	0.000
H_s (m)	H_o' (m)	H_f (m)	Energy flux (J/m-s)								
			ENE	NE	NNE	N	NNW	NW	WNW	W	WSW
0.250	0.270	0.208	0.642	0.590	0.308	1.796	0.975	2.053	1.591	2.104	0.000
0.750	0.811	0.219	0.139	0.127	0.066	0.388	0.211	0.443	0.343	0.454	0.000
1.250	1.352	0.159	0.006	0.005	0.003	0.016	0.009	0.018	0.014	0.019	0.000
Total II			0.786	0.723	0.377	2.200	1.194	2.515	1.949	2.578	0.000

Table C.5 Nearshore Wave Energy Flux for T = 4.5 Seconds

H_s (m)	H_o' (m)	Pct of occur. (%)	Frequency, f (%)								
			ENE 2.5	NE 2.3	NNE 1.2	N 7.0	NNW 3.8	NW 8.0	WNW 6.2	W 8.2	WSW 3.5
0.250	0.248	9.910	0.248	0.228	0.119	0.694	0.377	0.793	0.614	0.813	0.000
0.750	0.743	6.080	0.152	0.140	0.073	0.426	0.231	0.486	0.377	0.499	0.000
1.250	1.238	2.400	0.060	0.055	0.029	0.168	0.091	0.192	0.149	0.197	0.000
1.750	1.733	0.300	0.008	0.007	0.004	0.021	0.011	0.024	0.019	0.025	0.000
H_s (m)	H_o' (m)	H_f (m)	Energy flux (J/m-s)								
			ENE	NE	NNE	N	NNW	NW	WNW	W	WSW
0.250	0.248	0.191	0.215	0.197	0.103	0.601	0.326	0.687	0.532	0.704	0.000
0.750	0.743	0.203	0.149	0.137	0.071	0.417	0.226	0.476	0.369	0.488	0.000
1.250	1.238	0.148	0.031	0.029	0.015	0.087	0.047	0.099	0.077	0.102	0.000
1.750	1.733	0.112	0.002	0.002	0.001	0.006	0.003	0.007	0.006	0.007	0.000
Total III			0.397	0.365	0.190	1.111	0.603	1.270	0.984	1.302	0.000

Table C.6 Nearshore Wave Energy Flux for T = 5.5 Seconds

H_s (m)	H_o' (m)	Pct of occur. (%)	Frequency, f (%)								
			ENE 2.5	NE 2.3	NNE 1.2	N 7.0	NNW 3.8	NW 8.0	WNW 6.2	W 8.2	WSW 3.5
0.250	0.230	2.740	0.069	0.063	0.033	0.192	0.104	0.219	0.170	0.225	0.000
0.750	0.691	2.170	0.054	0.050	0.026	0.152	0.082	0.174	0.135	0.178	0.000
1.250	1.152	1.670	0.042	0.038	0.020	0.117	0.063	0.134	0.104	0.137	0.000
1.750	1.613	0.320	0.008	0.007	0.004	0.022	0.012	0.026	0.020	0.026	0.000
H_s (m)	H_o' (m)	H_f (m)	Energy flux (J/m-s)								
			ENE	NE	NNE	N	NNW	NW	WNW	W	WSW
0.250	0.230	0.181	0.047	0.043	0.023	0.132	0.071	0.151	0.117	0.154	0.000
0.750	0.691	0.200	0.046	0.042	0.022	0.127	0.069	0.146	0.113	0.149	0.000
1.250	1.152	0.147	0.019	0.017	0.009	0.053	0.029	0.061	0.047	0.062	0.000
1.750	1.613	0.112	0.002	0.002	0.001	0.006	0.003	0.007	0.005	0.007	0.000
Total IV			0.114	0.105	0.055	0.318	0.173	0.364	0.282	0.373	0.000

Table C.7 Nearshore Wave Energy Flux for T = 6.5 Seconds

H_s (m)	H_o' (m)	Pct of occur. (%)	Frequency, f (%)								
			ENE 2.5	NE 2.3	NNE 1.2	N 7.0	NNW 3.8	NW 8.0	WNW 6.2	W 8.2	WSW 3.5
0.250	0.229	0.450	0.011	0.010	0.005	0.032	0.017	0.036	0.028	0.037	0.000
0.750	0.686	0.220	0.006	0.005	0.003	0.015	0.008	0.018	0.014	0.018	0.000
1.250	1.144	0.120	0.003	0.003	0.001	0.008	0.005	0.010	0.007	0.010	0.000
2.250	2.059	0.020	0.001	0.000	0.000	0.001	0.001	0.002	0.001	0.002	0.000

H_s (m)	H_o' (m)	H_f (m)	Energy flux (J/m-s)								
			ENE	NE	NNE	N	NNW	NW	WNW	W	WSW
0.250	0.216	0.173	0.006	0.006	0.003	0.017	0.009	0.020	0.015	0.020	0.000
0.750	0.647	0.201	0.004	0.004	0.002	0.012	0.006	0.013	0.010	0.014	0.000
1.250	1.079	0.151	0.001	0.001	0.001	0.004	0.002	0.004	0.003	0.004	0.000
2.250	1.941	0.093	0.000	0.000	0.000	0.000	0.000	0.000	0.000	0.000	0.000
Total V			0.011	0.011	0.006	0.033	0.018	0.037	0.029	0.038	0.000

Table C.8 Nearshore Wave Energy Flux for T = 7.5 Seconds

H_s (m)	H_o' (m)	Pct of occur. (%)	Frequency, f (%)								
			ENE 2.5	NE 2.3	NNE 1.2	N 7.0	NNW 3.8	NW 8.0	WNW 6.2	W 8.2	WSW 3.5
0.250	0.233	0.020	0.001	0.000	0.000	0.001	0.001	0.002	0.001	0.002	0.001
0.750	0.698	0.000	0.000	0.000	0.000	0.000	0.000	0.000	0.000	0.000	0.000
1.250	1.163	0.020	0.001	0.000	0.000	0.001	0.001	0.002	0.001	0.002	0.001
1.750	1.629	0.000	0.000	0.000	0.000	0.000	0.000	0.000	0.000	0.000	0.000

H_s (m)	H_o' (m)	H_f (m)	Energy flux (J/m-s)								
			ENE	NE	NNE	N	NNW	NW	WNW	W	WSW
0.250	0.203	0.166	0.000	0.000	0.000	0.001	0.000	0.001	0.001	0.001	0.000
0.750	0.608	0.202	0.000	0.000	0.000	0.000	0.000	0.000	0.000	0.000	0.000
1.250	1.014	0.154	0.000	0.000	0.000	0.001	0.000	0.001	0.000	0.001	0.000
1.750	1.419	0.119	0.000	0.000	0.000	0.000	0.000	0.000	0.000	0.000	0.000
Total VI			0.000	0.000	0.000	0.001	0.001	0.001	0.001	0.001	0.001
Total(I+..+VI)			2.381	2.191	1.143	6.669	3.620	7.622	5.907	7.812	1.503

Table C.9 Monthly Distribution of Nearshore Wave Energy Flux (P) During 1989

Months	Wave energy flux (P) per direction per month (J/m-s)									Total per month
	ENE	NE	NNE	N	NNW	NW	WNW	W	WSW	
January	0.078	0.145	0.032	0.384	0.258	0.702	1.125	1.336	0.249	4.309
February	0.087	0.051	0.071	0.048	0.032	0.765	1.485	2.476	0.449	5.464
March	0.165	0.189	0.102	0.472	0.323	0.828	0.945	0.945	0.167	4.136
April	0.156	0.341	0.150	0.480	0.355	1.034	0.492	0.383	0.100	3.490
May	0.277	0.247	0.087	0.848	0.387	0.181	0.023	0.102	0.025	2.177
June	0.242	0.254	0.197	0.664	0.395	0.394	0.148	0.187	0.110	2.593
July	0.268	0.116	0.118	0.480	0.194	0.363	0.234	0.219	0.025	2.017
August	0.294	0.138	0.095	0.632	0.210	0.237	0.063	0.219	0.028	1.915
September	0.251	0.181	0.079	0.776	0.306	0.560	0.313	0.250	0.046	2.762
October	0.191	0.145	0.039	0.592	0.468	0.773	0.219	0.328	0.085	2.840
November	0.199	0.210	0.102	0.880	0.476	0.899	0.281	0.180	0.036	3.263
December	0.173	0.174	0.071	0.416	0.218	0.884	0.578	1.187	0.182	3.883
Total/dir	2.381	2.191	1.143	6.669	3.620	7.622	5.907	7.812	1.503	38.849

Table C.10 Monthly Distribution of Longshore Component of Nearshore Wave Energy Flux (P_{ls}) During 1989

Months	Longshore component of wave energy flux (P_{ls}) per direction per month (J/m-s)									Net P_{ls} per month	Gross P_{ls} per month
	ENE	NE	NNE	N	NNW	NW	WNW	W	WSW		
January	-0.009	-0.052	-0.015	-0.114	0.010	0.249	0.518	0.397	0.019	1.003	1.381
February	-0.010	-0.018	-0.033	-0.014	0.001	0.271	0.683	0.735	0.034	1.649	1.799
March	-0.019	-0.067	-0.047	-0.140	0.013	0.293	0.435	0.281	0.013	0.761	1.308
April	-0.018	-0.121	-0.069	-0.142	0.014	0.366	0.227	0.114	0.008	0.377	1.078
May	-0.032	-0.088	-0.040	-0.252	0.016	0.064	0.011	0.030	0.002	-0.289	0.534
June	-0.028	-0.090	-0.091	-0.197	0.016	0.140	0.068	0.056	0.008	-0.118	0.694
July	-0.031	-0.041	-0.055	-0.142	0.008	0.128	0.108	0.065	0.002	0.042	0.580
August	-0.034	-0.049	-0.044	-0.188	0.008	0.084	0.029	0.065	0.002	-0.126	0.502
September	-0.029	-0.064	-0.036	-0.230	0.012	0.198	0.144	0.074	0.003	0.072	0.792
October	-0.022	-0.052	-0.018	-0.176	0.019	0.274	0.101	0.097	0.006	0.230	0.764
November	-0.023	-0.075	-0.047	-0.261	0.019	0.318	0.129	0.053	0.003	0.117	0.929
December	-0.020	-0.062	-0.033	-0.123	0.009	0.313	0.266	0.353	0.014	0.716	1.192
Total	-0.275	-0.778	-0.528	-1.980	0.146	2.697	2.718	2.319	0.113	4.433	11.555

Appendix D

Calculation of Water Profiles

Table D.1 Water Profiles

Subject : West Channel — Initial Water Elevation : + 0.42 m

(1)	(2)	(3)	(4)	(5)	(6)	(7)	(8)	(9)	(10)
Station	Q_f (m^3/s)	y (m)	A (m^2)	R (m)	E (m)	S_f (m/m)	ΔE_s (m)	L (m)	E (m)
STA.05	5	0.420	382.62	2.05	0.420	$4.11\ 10^{-8}$		0	
							0.00057		
STA.04		0.421	79.31	2.16	0.421	$8.87\ 10^{-7}$		1225	0.421
							0.00348		
STA.03		0.425	56.30	1.19	0.425	$3.92\ 10^{-6}$		1450	0.425
							0.00182		
STA.02		0.427	88.12	2.53	0.427	$5.84\ 10^{-7}$		810	0.427
							0.00571		
STA.01		0.432	38.50	1.06	0.433	$9.69\ 10^{-6}$		1112	0.433
STA.05	10	0.420	382.62	2.05	0.420	$1.64\ 10^{-7}$		0	
							0.00227		
STA.04		0.421	79.31	2.16	0.422	$3.55\ 10^{-6}$		1225	0.422
							0.01369		
STA.03		0.433	56.69	1.20	0.435	$1.53\ 10^{-5}$		1450	0.435
							0.00714		
STA.02		0.441	88.51	2.54	0.442	$2.31\ 10^{-6}$		810	0.442
							0.02124		
STA.01		0.460	39.40	1.09	0.463	$3.59\ 10^{-5}$		1112	0.463
STA.05	15	0.420	382.62	2.05	0.420	$3.70\ 10^{-7}$		0	
							0.00511		
STA.04		0.423	79.37	2.16	0.425	$7.97\ 10^{-6}$		1225	0.425
							0.02962		
STA.03		0.451	57.57	1.21	0.454	$3.29\ 10^{-5}$		1450	0.454
							0.01536		
STA.02		0.469	89.31	2.55	0.470	$5.05\ 10^{-6}$		810	0.470
							0.04251		
STA.01		0.506	40.88	1.13	0.513	$7.14\ 10^{-5}$		1112	0.513
STA.05	20	0.420	382.62	2.05	0.420	$6.58\ 10^{-7}$		0	
							0.00906		
STA.04		0.426	79.46	2.16	0.429	$1.41\ 10^{-5}$		1225	0.429
							0.05024		
STA.03		0.473	58.66	1.23	0.479	$5.52\ 10^{-5}$		1450	0.479
							0.02586		
STA.02		0.502	90.26	2.57	0.505	$8.71\ 10^{-6}$		810	0.505
							0.06622		
STA.01		0.560	42.63	1.18	0.571	$1.10\ 10^{-4}$		1112	0.571

Table D.1 (Continued)

(1)	(2)	(3)	(4)	(5)	(6)	(7)	(8)	(9)	(10)
STA.05	25	0.420	382.62	2.05	0.420	$1.03\ 10^{-8}$		0	
							0.01413		
STA.04		0.429	79.55	2.16	0.434	$2.20\ 10^{-5}$		1225	0.434
							0.07436		
STA.03		0.499	59.95	1.25	0.508	$8.05\ 10^{-5}$		1450	0.508
							0.03792		
STA.02		0.542	91.41	2.59	0.546	$1.31\ 10^{-5}$		810	0.546
							0.08989		
STA.01		0.620	44.59	1.23	0.636	$1.49\ 10^{-4}$		1112	0.636
STA.05	50	0.420	382.62	2.05	0.421	$4.11\ 10^{-6}$		0	
							0.05527		
STA.04		0.456	80.42	2.17	0.476	$8.61\ 10^{-5}$		1225	0.476
							0.21711		
STA.03		0.666	68.53	1.40	0.693	$2.13\ 10^{-4}$		1450	0.693
							0.10344		
STA.02		0.784	98.64	2.73	0.797	$4.21\ 10^{-5}$		810	0.797
							0.18585		
STA.01		0.941	55.41	1.52	0.983	$2.92\ 10^{-4}$		1112	0.983
STA.05	75	0.420	382.62	2.05	0.422	$9.25\ 10^{-6}$		0	
							0.11969		
STA.04		0.499	81.86	2.17	0.542	$1.86\ 10^{-4}$		1225	0.542
							0.36155		
STA.03		0.858	79.01	1.56	0.904	$3.13\ 10^{-4}$		1450	0.903
							0.15726		
STA.02		1.036	106.64	2.87	1.061	$7.58\ 10^{-5}$		810	1.061
							0.24973		
STA.01		1.246	66.24	1.77	1.311	$3.73\ 10^{-4}$		1112	1.311
STA.05	100	0.420	382.62	2.05	0.423	$1.64\ 10^{-5}$		0	
							0.20178		
STA.04		0.553	83.83	2.19	0.626	$3.13\ 10^{-4}$		1225	0.625
							0.49587		
STA.03		1.059	90.69	1.71	1.121	$3.71\ 10^{-4}$		1450	1.121
							0.19459		
STA.02		1.277	114.83	3.00	1.316	$1.10\ 10^{-4}$		810	1.316
							0.29670		
STA.01		1.525	76.68	1.99	1.612	$4.24\ 10^{-4}$		1112	1.612

Table D.2 Water Profiles

Subject : West Channel — Initial Water Elevation : + 0.74 cm

(1)	(2)	(3)	(4)	(5)	(6)	(7)	(8)	(9)	(10)
Station	Q_f (m^3/s)	y (m)	A (m^2)	R (m)	E (m)	S_f (m/m)	ΔEs (m)	L (m)	E (m)
STA.05	5	0.740	439.73	2.08	0.740	$3.03\ 10^{-8}$		0	
							0.00039		
STA.04		0.740	92.10	2.29	0.740	$6.10\ 10^{-7}$		1225	0.740
							0.00174		
STA.03		0.742	72.60	1.46	0.742	$1.79\ 10^{-6}$		1450	0.742
							0.00090		
STA.02		0.743	97.53	2.71	0.743	$4.35\ 10^{-7}$		810	0.743
							0.00271		
STA.01		0.745	48.74	1.34	0.746	$4.43\ 10^{-6}$		1112	0.746
STA.05	10	0.740	439.73	2.08	0.740	$1.21\ 10^{-7}$		0	
							0.00157		
STA.04		0.741	92.15	2.29	0.742	$2.44\ 10^{-6}$		1225	0.742
							0.00690		
STA.03		0.747	72.87	1.46	0.748	$7.08\ 10^{-6}$		1450	0.749
							0.00357		
STA.02		0.751	97.77	2.71	0.752	$1.73\ 10^{-6}$		810	0.752
							0.01049		
STA.01		0.760	49.24	1.36	0.762	$1.71\ 10^{-5}$		1112	0.762
STA.05	15	0.740	439.73	2.08	0.740	$2.73\ 10^{-7}$		0	
							0.00351		
STA.04		0.743	92.25	2.29	0.744	$5.46\ 10^{-6}$		1225	0.744
							0.01523		
STA.03		0.758	73.47	1.47	0.760	$1.55\ 10^{-5}$		1450	0.760
							0.00785		
STA.02		0.767	98.27	2.72	0.768	$3.83\ 10^{-6}$		810	0.768
							0.02238		
STA.01		0.786	50.11	1.38	0.791	$3.64\ 10^{-5}$		1112	0.791
STA.05	20	0.740	439.73	2.08	0.740	$4.85\ 10^{-7}$		0	
							0.00624		
STA.04		0.744	92.31	2.29	0.746	$9.70\ 10^{-6}$		1225	0.746
							0.02658		
STA.03		0.769	74.07	1.48	0.773	$2.70\ 10^{-5}$		1450	0.773
							0.01364		
STA.02		0.784	98.79	2.73	0.786	$6.71\ 10^{-6}$		810	0.786
							0.03745		
STA.01		0.816	51.13	1.41	0.824	$6.07\ 10^{-5}$		1112	0.824

Table D.2 (Continued)

(1)	(2)	(3)	(4)	(5)	(6)	(7)	(8)	(9)	(10)
STA.05	25	0.740	439.73	2.08	0.740	$7.58\ 10^{-7}$		0	
							0.00972		
STA.04		0.746	92.41	2.30	0.750	$1.51\ 10^{-5}$		1225	0.750
							0.04050		
STA.03		0.784	74.89	1.49	0.790	$4.08\ 10^{-5}$		1450	0.790
							0.02067		
STA.02		0.807	99.51	2.74	0.810	$1.03\ 10^{-5}$		810	0.810
							0.05440		
STA.01		0.853	52.38	1.44	0.865	$8.76\ 10^{-5}$		1112	0.865
STA.05	50	0.740	439.73	2.08	0.741	$3.03\ 10^{-6}$		0	
							0.03779		
STA.04		0.764	93.35	2.31	0.779	$5.87\ 10^{-5}$		1225	0.778
							0.13571		
STA.03		0.895	81.11	1.59	0.914	$1.29\ 10^{-4}$		1450	0.914
							0.06646		
STA.02		0.969	104.65	2.83	0.981	$3.56\ 10^{-5}$		810	0.981
							0.14209		
STA.01		1.088	60.56	1.64	1.123	$2.20\ 10^{-4}$		1112	1.123
STA.05	75	0.740	439.73	2.08	0.741	$6.83\ 10^{-6}$		0	
							0.08140		
STA.04		0.791	94.82	2.34	0.823	$1.26\ 10^{-4}$		1225	0.823
							0.24950		
STA.03		1.036	89.32	1.70	1.072	$2.18\ 10^{-4}$		1450	1.072
							0.11567		
STA.02		1.165	111.16	2.94	1.188	$6.75\ 10^{-5}$		810	1.188
							0.21403		
STA.01		1.343	69.81	1.85	1.402	$3.17\ 10^{-4}$		1112	1.402
STA.05	100	0.740	439.73	2.08	0.743	$1.21\ 10^{-5}$		0	
							0.13661		
STA.04		0.825	96.77	2.37	0.879	$2.11\ 10^{-4}$		1225	0.879
							0.36399		
STA.03		1.191	98.74	1.81	1.243	$2.91\ 10^{-4}$		1450	1.243
							0.15891		
STA.02		1.366	118.20	3.05	1.402	$1.01\ 10^{-4}$		810	1.402
							0.26978		
STA.01		1.592	79.26	2.04	1.673	$3.84\ 10^{-4}$		1112	1.672

Table D.3 Water Profiles

Subject : West Channel Initial Water Depth : +1.06 m

(1)	(2)	(3)	(4)	(5)	(6)	(7)	(8)	(9)	(10)
Station	Q_f (m^3/s)	Y (m)	A (m^2)	R (m)	E (m)	S_f (m/m)	ΔEs (m)	L (m)	E (m)
STA.05	5	1.060	496.79	2.14	1.060	$2.29\ 10^{-8}$		0	
							0.00021		
STA.04		1.060	113.45	2.76	1.060	$3.14\ 10^{-7}$		1225	1.060
							0.00090		
STA.03		1.061	90.81	1.71	1.061	$9.24\ 10^{-7}$		1450	1.061
							0.00051		
STA.02		1.062	107.99	2.88	1.062	$3.26\ 10^{-7}$		810	1.062
							0.00146		
STA.01		1.064	59.71	1.62	1.064	$2.30\ 10^{-6}$		1112	1.064
STA.05	10	1.060	496.79	2.14	1.060	$9.18\ 10^{-8}$		0	
							0.00082		
STA.04		1.061	113.54	2.76	1.061	$1.25\ 10^{-6}$		1225	1.061
							0.00357		
STA.03		1.064	90.99	1.72	1.065	$3.67\ 10^{-6}$		1450	1.065
							0.00201		
STA.02		1.067	108.15	2.89	1.067	$1.30\ 10^{-6}$		810	1.067
							0.00576		
STA.01		1.072	59.99	1.63	1.073	$9.07\ 10^{-6}$		1112	1.073
STA.05	15	1.060	496.79	2.14	1.060	$2.07\ 10^{-7}$		0	
							0.00185		
STA.04		1.061	113.54	2.76	1.062	$2.82\ 10^{-6}$		1225	1.062
							0.00798		
STA.03		1.069	91.29	1.72	1.070	$8.19\ 10^{-6}$		1450	1.070
							0.00449		
STA.02		1.074	108.39	2.89	1.075	$2.91\ 10^{-6}$		810	1.075
							0.01268		
STA.01		1.085	60.45	1.64	1.088	$1.99\ 10^{-5}$		1112	1.088
STA.05	20	1.060	496.79	2.14	1.060	$3.67\ 10^{-7}$		0	
							0.00329		
STA.04		1.061	113.54	2.76	1.063	$5.01\ 10^{-6}$		1225	1.063
							0.01407		
STA.03		1.075	91.65	1.72	1.077	$1.44\ 10^{-5}$		1450	1.077
							0.00791		
STA.02		1.083	108.69	2.90	1.085	$5.13\ 10^{-6}$		810	1.085
							0.02192		
STA.01		1.102	61.05	1.65	1.107	$3.43\ 10^{-5}$		1112	1.107

Table D.3 (continued)

(1)	(2)	(3)	(4)	(5)	(6)	(7)	(8)	(9)	(10)
STA.05	25	1.060	496.79	2.14	1.060	$5.74\ 10^{-7}$		0	
							0.00512		
STA.04		1.063	113.71	2.76	1.065	$7.79\ 10^{-6}$		1225	1.065
							0.02171		
STA.03		1.083	92.13	1.72	1.087	$2.22\ 10^{-5}$		1450	1.087
							0.01218		
STA.02		1.096	109.12	2.90	1.099	$7.92\ 10^{-6}$		810	1.099
							0.03302		
STA.01		1.124	61.84	1.65	1.132	$5.15\ 10^{-5}$		1112	1.132
STA.05	50	1.060	496.79	2.14	1.061	$2.29\ 10^{-6}$		0	
							0.02010		
STA.04		1.071	114.39	2.78	1.081	$3.05\ 10^{-5}$		1225	1.081
							0.07934		
STA.03		1.146	95.96	1.78	1.160	$.89\ 10^{-5}$		1450	1.160
							0.04375		
STA.02		1.194	112.45	2.96	1.204	$2.91\ 10^{-5}$		810	1.204
							0.10040		
STA.01		1.300	68.22	1.82	1.327	$1.51\ 10^{-4}$		1112	1.304
STA.05	75	1.060	496.79	2.14	1.061	$5.16\ 10^{-6}$		0	
							0.04394		
STA.04		1.083	115.43	2.81	1.105	$6.66\ 10^{-5}$		1225	1.105
							0.15821		
STA.03		1.235	101.49	1.84	1.263	$1.52\ 10^{-4}$		1450	1.263
							0.08512		
STA.02		1.327	117.11	3.03	1.348	$5.85\ 10^{-5}$		810	1.348
							0.17612		
STA.01		1.473	74.69	1.96	1.524	$2.58\ 10^{-4}$		1112	1.524
STA.05	100	1.060	496.79	2.14	1.062	$9.18\ 10^{-6}$			
							0.07491		
STA.04		1.100	116.94	2.86	1.137	$1.13\ 10^{-4}$		1225	1.137
							0.24620		
STA.03		1.339	108.14	1.90	1.383	$2.26\ 10^{-4}$		1450	1.383
							0.12890		
STA.02		1.477	122.55	3.11	1.511	$9.18\ 10^{-5}$		810	1.511
							0.24031		
STA.01		1.676	82.55	2.10	1.751	$3.40\ 10^{-4}$		1112	1.751

Appendix E

Estimation of Suspended Load

Table E Estiamtion of Suspended Load Rate (Kalinske's Formula)

Section	Q_f (m^3/s)	I_c (m)	y (m)	R (m)	U_* (m/s)	q_s (10^{-3} m^3/s)	Q_s ($10^{-3}m^3/s$)
	5	0.296	0.746	2.025	0.00767	0.00000	0.00008
Section I	10	1.120	0.759	2.035	0.01495	0.00008	0.00268
	15	2.330	0.781	2.053	0.02166	0.00059	0.01889
STA.01	20	3.760	0.808	2.073	0.02765	0.00214	0.06840
to	25	5.320	0.840	2.098	0.03309	0.00550	0.17616
STA.02	50	12.800	1.046	2.249	0.05314	0.06684	2.13875
	75	19.200	1.265	2.402	0.06726	0.23138	7.40418
	100	24.200	1.486	2.549	0.07779	0.49792	15.93333
	5	0.133	0.743	2.081	0.00521	0.00000	0.00002
Section II	10	0.524	0.751	2.085	0.01035	0.00002	0.00081
	15	1.140	0.765	2.095	0.01531	0.00015	0.00640
STA.02	20	1.950	0.781	2.106	0.02007	0.00062	0.02669
to	25	2.910	0.802	2.120	0.02460	0.00181	0.07800
STA.03	50	8.790	0.942	2.213	0.04368	0.03739	1.60797
	75	14.700	1.110	2.321	0.05785	0.16436	7.06769
	100	19.900	1.285	2.430	0.06888	0.41203	17.71710
	5	0.141	0.742	1.929	0.00517	0.00000	0.00005
Section III	10	0.555	0.745	1.932	0.01026	0.00004	0.00181
	15	1.210	0.751	1.937	0.01516	0.00032	0.01420
STA.03	20	2.090	0.758	1.942	0.01995	0.00134	0.06035
to	25	3.140	0.767	1.950	0.02451	0.00396	0.17834
STA.04	50	9.930	0.833	2.003	0.04417	0.08836	3.97630
	75	17.700	0.917	2.068	0.05992	0.44082	19.83690
	100	25.400	1.011	2.139	0.07301	1.24801	56.16049
	5	0.032	0.740	2.247	0.00265	0.00000	0.00000
Section IV	10	0.127	0.741	2.248	0.00529	0.00000	0.00012
	15	0.285	0.741	2.248	0.00793	0.00001	0.00100
STA.04	20	0.506	0.742	2.248	0.01056	0.00005	0.00454
to	25	0.788	0.743	2.249	0.01319	0.00016	0.01459
STA.05	50	3.080	0.752	2.255	0.02610	0.00577	0.53353
	75	6.670	0.766	2.265	0.03850	0.04470	4.13486
	100	11.200	0.783	2.280	0.05005	0.17823	16.48664

Appendix F

Estimation of Bedload Rate

Table F Estimation of Bedload Rate (Sato-Kikawa-Ashida Formula)

Section	Q_f (m^3/s)	I_e	y (m)	R (m)	Shear stress τ_o (N/m^2)	τ_o/τ_c	$F(\tau_c/\tau_o)$	U_* (m/s)	q_b (10^{-3} $m^3/s.m$)	Q_b (10^{-3} m^3/s)
	5	0.296	0.746	2.025	0.0588	0.62	0.00	0.00767	0.00000	0.00000
Section I	10	1.120	0.759	2.035	0.2236	2.35	0.75	0.01495	0.00010	0.00309
	15	2.330	0.781	2.053	0.4693	4.93	0.97	0.02166	0.00038	0.01214
STA.01	20	3.760	0.808	2.073	0.7646	8.03	0.99	0.02765	0.00081	0.02578
to	25	5.320	0.840	2.098	1.0949	11.50	1.00	0.03309	0.00139	0.04462
STA.02	50	12.800	1.046	2.249	2.8240	29.66	1.00	0.05314	0.00578	0.18484
	75	19.200	1.265	2.402	4.5242	47.52	1.00	0.06726	0.01171	0.37480
	100	24.200	1.486	2.549	6.0514	63.56	1.00	0.07779	0.01812	0.57978
	5	0.133	0.743	2.081	0.0272	0.42	0.00	0.00521	0.00000	0.00000
Section II	10	0.524	0.751	2.085	0.1072	1.68	0.50	0.01035	0.00002	0.00092
	15	1.140	0.765	2.095	0.2343	3.67	0.94	0.01531	0.00013	0.00558
STA.02	20	1.950	0.781	2.106	0.4029	6.30	0.98	0.02007	0.00031	0.01312
to	25	2.910	0.802	2.120	0.6052	9.47	0.99	0.02460	0.00057	0.02439
STA.03	50	8.790	0.942	2.213	1.9083	29.86	1.00	0.04368	0.00321	0.13796
	75	14.700	1.110	2.321	3.3470	52.38	1.00	0.05785	0.00745	0.32048
	100	19.900	1.285	2.430	4.7438	74.24	1.00	0.06888	0.01258	0.54075
	5	0.141	0.742	1.929	0.0267	0.85	0.01	0.00517	0.00000	0.00000
Section	10	0.550	0.745	1.932	0.1052	3.34	0.91	0.01026	0.00004	0.00170
III	15	1.210	0.751	1.937	0.2299	7.30	0.99	0.01516	0.00013	0.00598
	20	2.090	0.758	1.942	0.3982	12.64	1.00	0.01995	0.00031	0.01376
STA.03	25	3.140	0.767	1.950	0.6007	19.07	1.00	0.02451	0.00057	0.02550
to	50	9.930	0.833	2.003	1.9512	61.94	1.00	0.04417	0.00332	0.14928
STA.04	75	17.700	0.917	2.068	3.5908	113.99	1.00	0.05992	0.00828	0.37268
	100	25.400	1.011	2.139	5.3298	169.20	1.00	0.07301	0.01498	0.67393
	5	0.032	0.740	2.247	0.0070	0.23	0.00	0.00265	0.00000	0.00000
Section	10	0.127	0.741	2.248	0.0280	0.92	0.02	0.00529	0.00000	0.00001
IV	15	0.285	0.741	2.248	0.0629	2.07	0.71	0.00793	0.00001	0.00126
	20	0.506	0.742	2.248	0.1116	3.67	0.93	0.01056	0.00004	0.00390
STA.04	25	0.788	0.743	2.249	0.1739	5.72	0.97	0.01319	0.00009	0.00792
to	50	3.080	0.752	2.255	0.6813	22.43	1.00	0.02610	0.00068	0.06332
STA.05	75	6.670	0.766	2.265	1.4821	48.80	1.00	0.03850	0.00220	0.20313
	100	11.200	0.783	2.280	2.5051	82.49	1.00	0.05005	0.00483	0.44639

Appendix G

Calculation of Longshore Transport

Table G.1 Determination of α_o

Direction	α_o	Sector	α_{o1}	$F(\alpha_{o1})$	$F(\alpha_o)$
			-90.00	-0.0000	
ENE	-87.5	13.75			-0.1612
			-76.25	-0.3224	
NE	-65.0	22.50			-0.5828
			-53.75	-0.8363	
NNE	-42.5	22.50			-0.8481
			-31.25	-0.8529	
N	-20.0	22.50			-0.5764
			-8.75	-0.2998	
NNW	2.5	22.50			0.0793
			13.75	0.4584	
NW	25.0	22.50			0.6811
			36.25	0.9038	
WNW	47.5	22.50			0.8283
			58.75	0.7528	
W	70.0	22.50			0.4703
			81.25	0.1878	
WSW	92.5	8.75			0.0939
			90.00	0.0000	

Table G.2 Determination of Shoaling coefficient (H/H_o')

T	$L_o=1.56T^2$	$\frac{d}{L_o}$	$\frac{H}{H_o'}$	$\frac{d}{L}$	$L=\frac{d}{(d/L)}$
2.5	9.75	0.5128	0.9916	0.5144	9.72
3.5	19.11	0.2616	0.9362	0.2780	17.99
4.5	31.59	0.1583	0.9130	0.1901	26.30
5.5	47.19	0.1060	0.9282	0.1462	34.20
6.5	65.91	0.0759	0.9609	0.1194	41.88
7.5	87.75	0.0570	1.0010	0.1013	49.36

Table G.3 Longshore Transport for T = 2.5 Seconds

H_s (m)	H_o' (m)	pct of occur	Frequency of occurrence (%)							
			ENE 2.5	NE 2.3	NNE 1.2	N 7.0	NNW 3.8	NW 8.0	WNW 6.2	W 8.2
0.25	0.2479	30.93	0.773	0.711	0.371	2.165	1.175	2.474	1.918	2.536
0.75	0.7437	0.86	0.022	0.020	0.010	0.060	0.033	0.069	0.053	0.071
H_s (m)	H_o' (m)	pct of occur	Longshore transport (m^3/year)							
			ENE -0.161	NE -0.583	NNE -0.848	N -0.576	NNW 0.079	NW 0.681	WNW 0.828	W 0.470
0.25	0.2479	30.93	-77.4	-257.5	-195.5	-775.2	57.9	1046.8	986.6	740.9
0.75	0.7437	0.86	-33.6	-111.6	-84.7	-336.0	25.1	453.7	427.6	321.1
Total I			-111.0	-369.1	-280.3	-1111.1	83.0	1500.5	1414.2	1062.0

Table G.4 Longshore Transport for T = 3.5 Seconds

H_s (m)	H_o' (m)	pct of occur	Frequency of occurrence (%)							
			ENE 2.5	NE 2.3	NNE 1.2	N 7.0	NNW 3.8	NW 8.0	WNW 6.2	W 8.2
0.25	0.232	22.75	0.569	0.523	0.273	1.593	0.865	1.820	1.411	1.866
0.75	0.697	4.42	0.111	0.102	0.053	0.309	0.168	0.354	0.274	0.362
1.25	1.162	0.35	0.009	0.008	0.004	0.025	0.013	0.028	0.022	0.029
H_s (m)	H_o' (m)	pct. of occur	Longshore transport (m^3/year)							
			ENE -0.161	NE -0.583	NNE -0.848	N -0.576	NNW 0.079	NW 0.681	WNW 0.828	W 0.470
0.25	0.232	22.75	-48.5	-161.4	-122.6	-485.9	36.3	656.2	618.5	464.5
0.75	0.697	4.42	-147.0	-488.9	-371.2	-1471.8	109.9	1987.5	1873.2	1406.7
1.25	1.162	0.35	-41.7	-138.8	-105.4	-417.9	31.2	564.4	531.9	399.5
Total II			-237.3	-789.2	-599.2	-2375.6	177.4	3208.2	3023.7	2270.6

Table G.5 Longshore Transport for T = 4.5 Seconds

H_s (m)	H_o' (m)	pct of occur	Frequency of occurrence (%)							
			ENE 2.5	NE 2.3	NNE 1.2	N 7.0	NNW 3.8	NW 8.0	WNW 6.2	W 8.2
0.25	0.228	9.91	0.248	0.228	0.119	0.694	0.377	0.793	0.614	0.81[illegible]
0.75	0.685	6.08	0.152	0.140	0.073	0.428	0.231	0.488	0.377	0.499
1.25	1.141	2.40	0.060	0.055	0.029	0.166	0.091	0.192	0.149	0.197
1.75	1.598	0.30	0.008	0.007	0.004	0.021	0.011	0.024	0.019	0.025
H_s (m)	H_o' (m)	pct of occur	Longshore transport (m^3/year)							
			ENE -0.161	NE -0.583	NNE -0.848	N -0.576	NNW 0.079	NW 0.681	WNW 0.828	W 0.470
0.25	0.228	9.91	-20.2	-67.1	-51.0	-202.0	15.1	272.8	257.1	193.1
0.75	0.685	6.08	-193.0	-641.9	-487.4	-1932.2	144.3	2609.3	2609.3	1846.8
1.25	1.141	2.40	-273.2	-908.7	-689.9	-2735.2	204.3	3693.7	3481.3	2614.3
1.75	1.598	0.30	79.2	-263.4	-200.0	-792.9	59.2	1070.6	1009.2	757.6
Total II			-565.6	-1881.1	-1428.2	-5662.3	422.9	7646.6	7206.9	5412.0

Table G.6 Longshore Transport for T = 5.5 Seconds

H_s (m)	H_o' (m)	pct of occur	Frequency of occurrence (%)							
			ENE 2.5	NE 2.3	NNE 1.2	N 7.0	NNW 3.8	NW 8.0	WNW 6.2	W 8.2
0.25	0.232	2.74	0.069	0.063	0.033	0.192	0.104	0.219	0.170	0.225
0.75	0.696	2.17	0.054	0.050	0.028	0.152	0.082	0.174	0.135	0.178
1.25	1.141	1.67	0.042	0.038	0.020	0.117	0.063	0.134	0.104	0.137
1.75	1.624	0.32	0.008	0.007	0.004	0.022	0.012	0.028	0.020	0.028
H_s (m)	H_o' (m)	pct. of occur	Longshore transport (m^3/year)							
			ENE -0.161	NE -0.583	NNE -0.848	N -0.576	NNW 0.079	NW 0.681	WNW 0.828	W 0.470
0.25	0.232	2.74	-5.8	-19.3	-14.7	-58.2	4.3	78.6	74.1	55.6
0.75	0.696	2.17	-71.8	-238.8	-181.3	-718.7	53.7	970.5	914.7	686.9
1.25	1.141	1.67	-196.1	-658.9	-500.3	-1983.4	148.1	2878.5	2524.5	1895.7
1.75	1.624	0.32	-88.0	-292.8	-22.34	-881.4	65.8	1190.3	1121.8	842.4
Total IV			-363.7	-1209.8	-918.6	-3641.7	272.0	4917.9	4635.1	3480.7

Table G.7 Longshore Transport for T = 6.5 Seconds

H_s (m)	H_o' (m)	pct of occur	Frequency of occurrence (%)							
			ENE 2.5	NE 2.3	NNE 1.2	N 7.0	NNW 3.8	NW 8.0	WNW 6.2	W 8.2
0.25	0.240	0.45	0.011	0.010	0.005	0.032	0.017	0.036	0.028	0.037
0.75	0.721	0.22	0.008	0.005	0.003	0.015	0.008	0.018	0.014	0.018
1.25	1.201	0.12	0.003	0.003	0.001	0.008	0.005	0.010	0.007	0.010
1.75	2.162	0.02	0.001	0.000	0.000	0.001	0.001	0.002	0.001	0.002
H_s (m)	H_o' (m)	pct. of occur	Longshore transport (m^3/year)							
			ENE -0.161	NE -0.583	NNE -0.848	N -0.576	NNW 0.079	NW 0.681	WNW 0.828	W 0.470
0.25	0.240	0.45	-1.0	-3.5	-2.6	-10.4	0.8	14.1	13.3	10.0
0.75	0.721	0.22	-7.9	-26.4	-20.0	-79.4	5.9	107.3	101.1	75.9
1.25	1.201	0.12	-15.5	-51.6	-39.2	-155.4	11.6	209.9	197.8	148.5
1.75	2.162	0.02	-37.4	-37.4	-28.4	-112.6	8.4	152.0	143.3	107.6
Total II			-35.7	-118.9	-90.3	-357.9	26.7	483.3	455.5	342.1

Table G.8 Longshore Transport for T = 7.5 Seconds

H_s (m)	H_o' (m)	pct of occur	Frequency of occurrence (%)							
			ENE 2.5	NE 2.3	NNE 1.2	N 7.0	NNW 3.8	NW 8.0	WNW 6.2	W 8.2
0.25	0.250	0.02	0.001	0.000	0.000	0.001	0.001	0.002	0.170	0.002
0.75	0.751	0.00	0.000	0.000	0.000	0.000	0.000	0.000	0.135	0.000
1.25	1.251	0.02	0.001	0.000	0.000	0.001	0.001	0.002	0.104	0.002
1.75	1.752	0.00	0.000	0.000	0.000	0.000	0.000	0.000	0.020	0.000
H_s (m)	Ho. (m)	pct of occur	Longshore transport (m^3/year)							
			ENE -0.161	NE -0.583	NNE -0.848	N -0.576	NNW 0.079	NW 0.681	WNW 0.828	W 0.470
0.25	0.250	0.02	-0.1	-0.2	-0.1	-0.5	0.0	0.7	0.7	0.5
0.75	0.751	0.00	0.0	0.0	0.0	0.0	0.0	0.0	0.0	0.0
1.25	1.251	0.02	-2.9	-9.5	-7.2	-28.7	2.1	36.7	36.5	27.4
1.75	1.752	0.00	0.0	0.0	0.0	0.0	0.0	0.0	0.0	0.0
Total IV			-3.0	-9.7	-7.3	-29.2	2.2	39.4	37.2	27.9
Total (I+...+VI)			-1316	-4378	-3324	-13178	984	17796	16773	12595
Q_l , Q_r			-22196 m^3/year				48148 m^3/year			

Appendix H

Table H Function of d/L_o (*Source : U.S. Army CERC, 1984*)

$\frac{d}{L_o}$	$\frac{d}{L}$	$\frac{2\pi d}{L}$	Tanh $\frac{2\pi d}{L}$	Sinh $\frac{2\pi d}{L}$	Cosh $\frac{2\pi d}{L}$	$\frac{H}{H_o'}$	$\frac{C_g}{C}$
0.0000	0.0000	0.0000	0.0000	0.0000	1.0000	∞	0.0000
0.0001	0.0040	0.0251	0.0251	0.0251	1.0003	4.467	0.0251
0.0002	0.0056	0.0355	0.0354	0.0355	1.0006	3.757	0.0354
0.0003	0.0069	0.0434	0.0434	0.0434	1.0009	3.395	0.0433
0.0004	0.0080	0.0501	0.0501	0.0502	1.0013	3.160	0.0501
0.0005	0.0089	0.0561	0.0560	0.0561	1.0016	2.989	0.0559
0.0006	0.0098	0.0614	0.0614	0.0615	1.0019	2.856	0.0613
0.0007	0.0106	0.0664	0.0663	0.0664	1.0022	2.749	0.0662
0.0008	0.0113	0.0710	0.0708	0.0710	1.0025	2.659	0.0707
0.0009	0.0120	0.0753	0.0751	0.0753	1.0028	2.582	0.0750
0.0010	0.0126	0.0794	0.0792	0.0794	1.0032	2.515	0.0790
0.0020	0.0179	0.1123	0.1119	0.1125	1.0063	2.119	0.1114
0.0030	0.0219	0.1377	0.1369	0.1382	1.0095	1.917	0.1360
0.0040	0.0254	0.1592	0.1579	0.1599	1.0127	1.788	0.1565
0.0050	0.0284	0.1782	0.1764	0.1791	1.0159	1.692	0.1746
0.0060	0.0311	0.1954	0.1929	0.1967	1.0192	1.620	0.1905
0.0070	0.0336	0.2113	0.2682	0.2128	1.0224	1.561	0.2051
0.0080	0.0359	0.2261	0.2223	0.2280	1.0257	1.512	0.2186
0.0090	0.0382	0.2401	0.2356	0.2424	1.0290	1.471	0.2312
0.0100	0.0403	0.2533	0.2480	0.2560	1.0322	1.435	0.2429
0.0200	0.0576	0.3621	0.3470	0.3701	1.0660	1.226	0.3327
0.0300	0.0714	0.4483	0.4205	0.4634	1.1021	1.125	0.3947
0.0400	0.0833	0.5233	0.4802	0.5475	1.1401	1.064	0.4414
0.0500	0.0942	0.5916	0.5310	0.6267	1.1802	1.023	0.4779
0.0600	0.1043	0.6553	0.5753	0.7033	1.2225	0.993	0.5068
0.0700	0.1139	0.7157	0.6144	0.7783	1.2672	0.9713	0.5300
0.0800	0.1232	0.7741	0.6493	0.8538	1.3149	0.9548	0.5485
0.0900	0.1322	0.8306	0.6808	0.9295	1.3653	0.9422	0.5632
0.1000	0.1410	0.8858	0.7093	1.006	1.4187	0.9327	0.5747
0.2000	0.2251	1.4140	0.8884	1.935	2.1780	0.9181	0.5932
0.3000	0.3121	1.961	0.9611	3.483	3.624	0.9490	0.5552
0.4000	0.4050	2.544	0.9877	6.329	6.407	0.9761	0.5248
0.5000	0.5018	3.153	0.9964	11.68	11.72	0.9905	0.5096
0.6000	0.6006	3.774	0.9990	21.76	21.78	0.9965	0.5035
0.7000	0.7002	4.400	0.9997	40.71	40.72	0.9988	0.5012
0.8000	0.8001	5.027	0.9999	76.24	76.24	0.9996	0.5004
0.9000	0.9000	5.655	1.0000	142.9	142.9	0.9999	0.5010
1.0000	1.0000	6.283	1.0000	267.7	267.7	1.0000	0.5000